

South Dakota
Department of Transportation
Office of Research



U.S. Department
of Transportation
Federal Highway
Administration

SD2002-01-F
TPF-5(042)-F



The Deleterious Chemical Effects of Concentrated Deicing Solutions on Portland Cement Concrete

Study SD2002-01
Final Report

Prepared by
Michigan Tech Transportation Institute
1400 Townsend Drive
Houghton, MI

April 2008

DISCLAIMER

The contents of this report reflect the views of the authors who are responsible for the facts and accuracy of the data presented herein. The contents do not necessarily reflect the official views or policies of the South Dakota Department of Transportation, the State Transportation Commission, or the Federal Highway Administration. This report does not constitute a standard, specification, or regulation.

ACKNOWLEDGEMENTS

This work was performed under the supervision of the SD2002-01 Technical Panel:

Bob Dawson.....	Iowa DOT	Bob Reis	Caltrans
Roberto de Dios	Colorado DOT	Chris Romo.....	Wyoming DOT
Brett Hestdalen	FHWA	Craig Smith.....	SDDOT Sioux Falls Area
Dennis Johnson.....	SDDOT Research	Roger Surdahl	FHWA
Dan Johnston	SDDOT Research	Paul Virmani.....	FHWA
Mike Lynch.....	Montana DOT	Richard Williammee.....	Texas DOT
Kelley Morse	Illinois DOT	Ron Wright	Idaho DOT

The work was performed in cooperation with the United States Department of Transportation Federal Highway Administration. The work was accomplished as Transportation Pooled Fund Study TPF-5(042).

TECHNICAL REPORT STANDARD TITLE PAGE

1. Report No. SD2002-01-F	2. Government Accession No.	3. Recipient's Catalog No.	
4. Title and Subtitle The Deleterious Chemical Effects of Concentrated Deicing Solutions on Portland Cement Concrete		5. Report Date April 30, 2008	
		6. Performing Organization Code	
7. Author(s) Lawrence Sutter (Michigan Tech), Karl Peterson (Michigan Tech), Gustavo Julio-Betancourt (Univ. of Toronto), Doug Hooton (Univ. of Toronto), Tom Van Dam (Applied Pavement Technology), Kurt Smith (Applied Pavement Technology)		8. Performing Organization Report No.	
9. Performing Organization Name and Address Michigan Tech Transportation Institute 1400 Townsend Dr. Houghton, MI 49931		10. Work Unit No.	
		11. Contract or Grant No. 310802	
12. Sponsoring Agency Name and Address South Dakota Department of Transportation Office of Research 700 East Broadway Avenue Pierre, SD 57501-2586		13. Type of Report and Period Covered Final Report September 2002 to April 2008	
		14. Sponsoring Agency Code HRZ201(01), TPF-5(042)	
15. Supplementary Notes Additional published documents: Executive (SD2002-01-X), Literature Review (SD2002-01-L), Implementation Guidelines (SD2002-01-G) and Technical Appendices (SD2002-01-A)			
16. Abstract <p>This research project investigated the effects of concentrated brines of magnesium chloride, calcium chloride, sodium chloride, and calcium magnesium acetate on portland cement concrete. Although known to be effective at deicing and anti-icing, the deleterious effects these chemicals may have on concrete have not been well documented. As a result of this research, it was determined that there is significant evidence that magnesium chloride and calcium chloride chemically interact with hardened portland cement paste in concrete resulting in expansive cracking, increased permeability, and a significant loss in compressive strength. Although the same effects were not seen with sodium chloride brines, it was shown that sodium chloride brines have the highest rate of ingress into hardened concrete. This latter fact is significant with respect to corrosion of embedded steel. The mechanism for attack of hardened cement paste varies with deicer chemical but in general, a chemical reaction between chlorides and cement hydration products results in the dissolution of the hardened cement paste and formation of oxychloride phases, which are expansive. The chemical attack of the hardened cement paste is significantly reduced if supplementary cementitious materials are included in the concrete mixture. Both coal fly ash and ground granulated blast furnace slag were found to be effective at mitigating the chemical attack caused by the deicers tested. In the tests performed, ground granulated blast furnace slag performed better as a mitigation strategy as compared to coal fly ash. Additionally, siloxane and silane sealants were effective at slowing the ingress of deicing chemicals into the concrete and thereby reducing the observed distress. In general, the siloxane sealant appeared to be more effective than the silane, but both were effective and should be considered as a maintenance strategy.</p>			
17. Keywords deicing chemicals, anti-icing chemicals, concrete distress, petrography, oxychloride		18. Distribution Statement No restrictions. This document is available to the public from the sponsoring agency.	
19. Security Classification (of this report) Unclassified	20. Security Classification (of this page) Unclassified	21. No. of Pages 216	22. Price

TABLE OF CONTENTS

DISCLAIMER	II
ACKNOWLEDGEMENTS	II
TECHNICAL REPORT STANDARD TITLE PAGE	III
TABLE OF CONTENTS	V
LIST OF FIGURES	IX
LIST OF TABLES	XVI
TABLE OF ACRONYMS	XVII
SECTION 1 - INTRODUCTION	1
1.0 Problem Statement	1
1.1 Summary of Project Tasks	2
1.2 Report Organization and Distribution	2
SECTION 2 - BACKGROUND	3
2.1. Concrete Properties that Affect Freeze-Thaw and Chemical Resistance	3
2.1.1 Cement Chemistry	3
2.1.2 Permeability	3
2.1.3 Air Content	4
2.1.4 Aggregate Properties	4
2.1.5 Cracking	5
2.2. Types of Interactions	5
2.2.1. Physical Mechanisms of Paste Freeze-Thaw Attack	5
2.2.2 Chemical Mechanisms of Paste Freeze-Thaw Attack	6
2.2.2.1 Effects of Magnesium Chloride	6
2.2.2.2 Effects of Calcium Chloride	7
2.2.2.3 Effects of Calcium Magnesium Acetate	8
2.2.2.4 Background and Effects of MgCl ₂ -Based Agricultural Products.....	9
2.3 Pavement Construction Practices – Effects on Deicer Scaling/Deterioration	9
2.3.1 Materials.....	9
2.3.1.1 Cementitious and Supplementary Cementitious Materials	9
2.3.1.2 Ground Granulated Blast Furnace Slag.....	9
2.3.2 Construction Considerations for Preventing Deicer Distress	9
2.3.2.1 Ambient and Seasonal Construction Conditions.....	10
2.3.2.2 Consolidation	10
2.3.2.3 Steel Placement	10
2.3.2.4 Finishing.....	11
2.3.2.5 Curing	11
2.3.3 Preventive Strategies for Controlling Specific Types of Materials-Related Distress.....	12
2.3.3.1 Deicer Scaling/Deterioration.....	12
2.4 Literature Review Summary	13
SECTION 3. EXPERIMENTAL APPROACH	15
3.1. Overview	15
3.2. Analytical Methods	15

3.2.1. Visual Inspection.....	15
3.2.2. Stereo Optical Microscope Examination.....	15
3.2.3. Staining Tests	16
3.2.4. Petrographic Optical Microscope Examination.....	16
3.2.4.1. General Information.....	16
3.2.5. Scanning Electron Microscopy.....	16
3.2.6. X-ray Microscope.....	17
3.2.7. X-ray Diffraction Analysis.....	17
3.2.8. Profile Grinding to Determine Chloride Profiles	18
3.2.9. Bulk Diffusion/Sorptivity.....	18
3.2.10. Rapid Chloride Permeability Testing	18
3.2.11. Other Test Methods	19
3.2.11.1. Length Change	19
3.2.11.2. Mass Change.....	19
3.2.11.3. Solution pH	19
3.2.11.4. Compressive Strength	19
3.2.11.5. Mercury Intrusion Porosimetry (MIP)	19
3.2.11.6. Exposure Solution Chemical Analysis.....	19
3.3. Characterization of Field Specimens	20
3.3.1. Identification of Field Sites for Task 5.....	20
3.4. Phase I Experimental Approach: Laboratory Testing of Portland Cement Mortar.....	20
3.4.1. Overview	20
3.4.2. Phase I Work Conducted at Michigan Tech.....	20
3.4.2.1. Mixture Design and Preparation	20
3.4.2.2. Deicer Solutions.....	21
3.4.2.3. Experimental Approach	23
3.4.3 Phase I Work Conducted at the University of Toronto	24
3.4.3.1. Mixture Design and Preparation	24
3.4.3.2. Deicer Solutions.....	24
3.4.3.3. Experimental Approach	24
3.5. Phase II Experimental Approach: Laboratory Testing of Portland Cement Concrete	25
3.5.1. Overview	25
3.5.2. Phase II Work Conducted at Michigan Tech.....	25
3.5.2.1. Mixture Design and Preparation	25
3.5.2.2. Deicing Solutions.....	25
3.5.2.3. Experimental Approach	26
3.5.3 Phase II Work Conducted at the University of Toronto.....	27
3.5.3.1 Mixture Design and Preparation	27
3.5.3.2 Deicer Solutions.....	28
3.5.3.3 Experimental Approach	28
SECTION 4. CHARACTERIZATION OF FIELD SPECIMENS.....	29
4.1 Approach	29
4.2 Petrographic Analysis of Identified Sites.....	30
4.2.1 South Dakota, Sioux Falls, eastbound 26th Street left-turn lane onto northbound, Interstate Highway 29	30
4.2.2 Montana, eastbound Interstate Highway 90 bridge deck, near milepost 61.8, Tarkio interchange.....	57

CHAPTER 5 - LABORATORY RESULTS.....	73
5.1 Overview.....	73
5.2 Phase I Laboratory Experiment Results	73
5.2.1 Results of Phase I Experiments Conducted at Michigan Tech.....	73
5.2.1.1 Low Temperature Experiment	73
5.2.1.2 Additional Phase I Experiment	92
5.2.2 Results of Phase I Experiments Conducted at the University of Toronto	93
5.2.2.1 Compressive Strength	93
5.2.2.2 Expansion.....	93
5.2.2.3 Mass Change.....	93
5.2.2.4 Visual Observations	95
5.2.2.5 Mercury Intrusion Porosimetry (MIP)	95
5.2.2.6 Solution pH.....	96
5.2.2.7 Determination of Pessimum Concentration for MgCl ₂ and CaCl ₂	98
5.3 Phase II Laboratory Experiment Results	99
5.3.1 Results of Phase II Experiments Jointly Conducted at Michigan Tech and the University of Toronto	99
5.3.1.1 Physical Characterization of Mortar and Concrete Mixtures.....	99
5.3.1.2. Rapid Chloride Permeability Test.....	100
5.3.1.3. Bulk Diffusion.....	100
5.3.1.4. Sorptivity.....	100
5.3.2 Results of Phase II Experiments Conducted at the Michigan Tech.....	103
5.3.2.1 Macroscopic Observations.....	103
5.3.2.2. X-ray Diffraction.....	116
5.3.2.3 Optical Microscopy.....	126
5.3.2.4. Scanning Electron Microscopy	147
5.3.3 Results of Phase II Experiments Conducted at the University of Toronto.....	156
5.3.3.1 ASTM C 666 Freeze Thaw Testing	156
5.3.3.2 Scaling Resistance.....	158
SECTION 6. DISCUSSION.....	162
6.1. Overview	162
6.2. Effects of Various Deicing/Anti-Icing Chemicals.....	162
6.2.1. Effects of Sodium Chloride (NaCl) on Concrete Pavements and Bridge Decks.....	162
6.2.1.1. Visible Deterioration After Exposure to Deicers	162
6.2.1.2. Petrographic Evidence of Chemical Interaction Resulting in Distress	163
6.2.1.3. Expansion After Exposure	163
6.2.1.4. Loss of Compressive Strength After Exposure	163
6.2.1.5. Mass Change after Exposure.....	163
6.2.1.6. Freeze-Thaw Performance (ASTM C666 and ASTM C672)).....	163
6.2.1.7. Assessment of the Effects of NaCl.....	164
6.2.2. Effects of Magnesium Chloride (MgCl ₂) on Concrete Pavements and Bridge Decks	164
6.2.2.1. Visible Deterioration After Exposure to Deicers	164
6.2.2.2. Petrographic Evidence of Chemical Interaction Resulting in Distress	164
6.2.2.3. Expansion After Exposure	165
6.2.2.4. Loss of Compressive Strength After Exposure	165
6.2.2.5. Mass Change after Exposure.....	166
6.2.2.6. Freeze-Thaw Performance (ASTM C666 and ASTM 672).....	166
6.2.2.7. Assessment of the Effects of MgCl ₂	166

6.2.3. Effects of Calcium Chloride (CaCl ₂) on Concrete Pavements and Bridge Decks.....	166
6.2.3.1. Visible Deterioration After Exposure to Deicers	166
6.2.3.2. Petrographic Evidence of Chemical Interaction Resulting in Distress	166
6.2.3.3. Expansion After Exposure	167
6.2.3.4. Loss of Compressive Strength After Exposure	167
6.2.3.5. Mass Change after Exposure.....	167
6.2.3.6. Freeze-Thaw Performance (ASTM C666 and ASTM 672).....	167
6.2.3.7. Assessment of the Effects of CaCl ₂	167
6.2.4. Effects of Calcium Magnesium Acetate (CMA) on Concrete Pavements and Bridge Decks.....	168
6.2.4.1. Visible Deterioration After Exposure to Deicers	168
6.2.4.2. Petrographic Evidence of Chemical Interaction Resulting in Distress	168
6.2.4.3. Expansion After Exposure	168
6.2.4.4. Loss of Compressive Strength After Exposure	168
6.2.4.5. Mass Change after Exposure.....	169
6.2.4.6. Freeze-Thaw Performance (ASTM C666 and ASTM 672).....	169
6.2.4.7. Assessment of the Effects of CMA.....	169
6.2.5. Effects of Magnesium Chloride Based Agricultural Product (MBAP) on Concrete Pavements and Bridge Decks	169
6.2.5.1. Visible Deterioration After Exposure to Deicers	169
6.2.5.2. Petrographic Evidence of Chemical Interaction Resulting in Distress	169
6.2.5.3. Expansion After Exposure	169
6.2.5.4. Loss of Compressive Strength After Exposure	169
6.2.5.5. Mass Change after Exposure.....	170
6.2.5.6. Freeze-Thaw Performance (ASTM C666 and ASTM 672).....	170
6.2.5.7. Assessment of the Effects of MBAP.....	170
6.3. Assessing and Minimizing the Impact of Deicing/Anti-Icing Chemicals.....	170
6.4. Life Cycle Cost Analysis.....	171
SECTION 7. MITIGATION STRATEGIES	173
7.1. Mitigation Strategies – Maintenance	173
7.2. Mitigation Strategies – Engineering.....	173
SECTION 8. CONCLUSIONS.....	174
SECTION 9. RECOMMENDATIONS.....	185
SECTION 10. BIBLIOGRAPHY.....	187

LIST OF FIGURES

Figure 3.1. The partial phase diagrams for the deicer solutions tested showing the eutectic points for each solution.	22
Figure 3.2. Cyclic temperature test procedure for one cycle for cylinders exposed to deicer solutions and a control solution.	23
Figure 4.1. Diagram to show core locations based on submitted field information.	31
Figure 4.2. Photograph of core site.	31
Figure 4.3. Photographs of the joints sampled, and of the holes after the coring operation.	32
Figure 4.4. Cores taken at joint.	33
Figure 4.4. Cores taken away from joint.	34
Figure 4.6. Polished slabs to show complete cross-section through core SD-1 both before (left) and after application of phenolphthalein stain (right) tic marks every cm.	35
Figure 4.7. Polished slabs to show complete cross-section through core SD-1 after treatment to enhance appearance of air voids and cracks, tic marks every cm.	36
Figure 4.8. Polished slabs to show complete cross-section through core SD-4 both before (left) and after application of phenolphthalein stain (right) tic marks every cm.	37
Figure 4.9. Polished slabs to show complete cross-section through core SD-4 after treatment to enhance appearance of air voids and cracks, tic marks every cm.	38
Figure 4.10. Stereo microscope images to show air void structure on polished slab from core SD-4. .	40
Figure 4.11. Mosaic of 12 frames collected from thin section prepared from billet cut from top portion of core SD-1 (each individual frame measures 2.612 x 1.959 mm).	41
Figure 4.12. Mosaic of 12 frames collected from thin section prepared from billet cut from top portion of core SD-1 after masking out air voids, fine aggregate, and micro-cracks to isolate cement paste (each individual frame measures 2.612 x 1.959 mm).	42
Figure 4.13. Mosaic of 12 frames collected from thin section prepared from a second billet cut from top portion of core SD-1 (each individual frame measures 2.612 x 1.959 mm).	44
Figure 4.14. Mosaic of 12 frames collected from thin section prepared from billet cut from top portion of core SD-7 (each individual frame measures 2.612 x 1.959 mm).	45
Figure 4.15. Mosaic of 12 frames collected from thin section prepared from billet cut from top portion of core SD-7 after masking out air voids, fine aggregate, and micro-cracks to isolate cement paste (each individual frame measures 2.612 x 1.959 mm).	46
Figure 4.16. Mosaic of 12 frames collected from thin section prepared from billet cut from top portion of core SD-4 (each individual frame measures 2.612 x 1.959 mm).	48
Figure 4.17. Mosaic of 12 frames collected from thin section prepared from billet cut from top portion of core SD-4 after masking out air voids, fine aggregate, and micro-cracks to isolate cement paste (each individual frame measures 2.612 x 1.959 mm).	49
Figure 4.18. Mosaic of 12 frames collected from thin section prepared from a second billet cut from top portion of core SD-4 (each individual frame measures 2.612 x 1.959 mm).	51
Figure 4.19. Mosaic of 12 frames collected from thin section prepared from billet cut from top portion of core SD-5 (each individual frame measures 2.612 x 1.959 mm).	52
Figure 4.20. Mosaic of 12 frames collected from thin section prepared from billet cut from top portion of core SD-5 after masking out air voids, fine aggregate, and micro-cracks to isolate cement paste (each individual frame measures 2.612 x 1.959 mm).	53
Figure 4.21. Histogram comparing cement paste pixel intensities using all 12 frames as collected from thin sections prepared from cores taken at the joint versus cores taken mid-panel.	54

Figure 4.22. Chloride profile from billet prepared from core SD-3, panel corner.....	55
Figure 4.23. Duplicate chloride profile from additional billet prepared from core SD-3, panel corner.....	55
Figure 4.24. Chloride profile from billet prepared from core SD-7, mid-panel.	56
Figure 4.25. Duplicate chloride profile from additional billet prepared from core SD-7, mid-panel....	56
Figure 4.26. Diagram to show location of cores according to field notes.	58
Figure 4.27. Photograph of core site.....	58
Figure 4.28. Photograph from beneath bridge deck after coring operation.	59
Figure 4.29. Cores retrieved from site, core T-1 (top), core T-2 (bottom).	60
Figure 4.30. Polished slabs to show complete cross-section through core T-2 both before (left) and after application of phenolphthalein stain (right) tic marks every cm.	61
Figure 4.31. Polished slabs to show complete cross-section through core T-2 after treatment to enhance appearance of air voids and cracks, tic marks every cm.	62
Figure 4.32. Stereo microscope images to show air void structure on polished slab from core T-2.	64
Figure 4.33. Mosaic of 12 frames collected from thin section prepared from billet cut from top portion of core T-2 (each individual frame measures 2.612 x 1.959 mm).	65
Figure 4.34. Mosaic of 12 frames collected from thin section prepared from billet cut from top portion of core T-2 after masking out air voids, fine aggregate, and micro-cracks to isolate cement paste (each individual frame measures 2.612 x 1.959 mm).	66
Figure 4.35. Chloride profile from billet prepared from core T-2.	67
Figure 4.36. Duplicate chloride profile from additional billet prepared from core T-2.....	68
Figure 4.37. Duplicate chloride profile from additional billet prepared from core T-2.....	68
Figure 4.38. Transmitted light scanned image of thin section to show location of elemental maps shown in Figure 4.40. The top of the thin section represents the wear surface of the pavement, (tic marks every mm).	69
Figure 4.39. Transmitted light scanned image of thin section to show location of elemental maps shown in Figure 4.41. The large crack, sub-parallel to the pavement surface, is at a depth of about 40 mm, (tic marks every mm).	70
Figure 4.40. Elemental maps from pavement surface, darker regions indicate higher concentrations..	71
Figure 4.41. Elemental maps from crack at depth, darker regions indicate higher concentrations.	72
Figure 5.1. Cylinders exposed to NaCl solution after 84 days of constant low temperature test. From left to right: 0.40, 0.50, and 0.60 w/c mortar cylinders.	73
Figure 5.2. Cylinders exposed to MgCl ₂ solution after 84 days of constant low temperature test. From left to right: 0.40, 0.50, and 0.60 w/c mortar cylinders.	73
Figure 5.3. Cylinders exposed to CaCl ₂ solution after 84 days of constant low temperature test. From left to right: 0.40, 0.50, and 0.60 w/c mortar cylinders.	74
Figure 5.4. Cylinders exposed to CMA solution after 84 days of constant low temperature test. From left to right: 0.40, 0.50, and 0.60 w/c mortar cylinders.	74
Figure 5.5. Control cylinders exposed to limewater solution after 84 days of constant low temperature test. From left to right: 0.40, 0.50, and 0.60 w/c mortar cylinders.	74
Figure 5.6. Back-scattered electron images of thin sections prepared from mortar cylinders immersed in chemical solutions.....	76
Figure 5.7. Cross-polarized light images of thin sections prepared from mortar cylinders immersed in chemical solutions.....	77

Figure 5.8. Cracks and air voids filled with remnant calcium oxychloride crystals in $MgCl_2$ solution immersed sample. From left to right, epifluorescent and crossed polars.	78
Figure 5.9. Cracks and air voids filled with remnant calcium oxychloride crystals in $CaCl_2$ solution immersed sample. From left to right, epifluorescent and crossed polars.	78
Figure 5.10. Remnant calcium oxychloride crystals that are pseudomorphs of secondary calcium hydroxide crystals formed in an air void from $MgCl_2$ solution immersed sample.	78
Figure 5.11. Elemental map for magnesium collected from thin sections prepared from mortar cylinders immersed in chemical solutions.	79
Figure 5.12. Brucite, (magnesium hydroxide) crystals in air void and seam beneath sand grain near exterior in cylinder immersed in $MgCl_2$ solution.	80
Figure 5.13. Magnesium chloride hydrate crystals in air voids near exterior in thin section prepared from cylinder immersed in $MgCl_2$ solution.	80
Figure 5.14. Elemental map for chlorine collected from thin sections prepared from mortar cylinders immersed in chemical solutions.	81
Figure 5.15. From left to right: back scattered electron image, cross polarized light, and epifluorescent mode images of a thin section prepared from a cylinder immersed in magnesium chloride solution.	82
Figure 5.16. Elemental maps, from left to right: calcium, chlorine, and magnesium.	83
Figure 5.17. From left to right: back scattered electron image, cross polarized light, and epifluorescent mode images of a thin section prepared from a cylinder immersed in calcium chloride solution.	84
Figure 5.18. Elemental maps, from left to right: calcium, chloride, and magnesium.	85
Figure 5.19. From left to right: back scattered electron image, cross polarized light, and epifluorescent mode images of a thin section prepared from a cylinder immersed in sodium chloride solution.	86
Figure 5.20. Elemental maps, from left to right: calcium, sodium, and chlorine.	87
Figure 5.21. From left to right: back scattered electron image, cross polarized light, and epifluorescent mode images of a thin section prepared from a cylinder immersed in calcium magnesium acetate solution.	88
Figure 5.22. Elemental maps, from left to right: calcium, magnesium, and chlorine.	89
Figure 5.23. From left to right: back scattered electron image, cross polarized light, and epifluorescent mode images of a thin section prepared from a cylinder immersed in limewater.	90
Figure 5.24. Elemental maps, from left to right: calcium, magnesium, and chlorine.	91
Figure 5.25. Cylinders exposed to 3% $CaCl_2$ solution after 56 days of constant low temperature test.	92
Figure 5.26. Cylinders exposed to 7% $CaCl_2$ solution after 56 days of constant low temperature test.	92
Figure 5.27. Cylinders exposed to 10% $CaCl_2$ solution after 56 days of constant low temperature test.	92
Figure 5.28. Cylinders exposed to 14% $CaCl_2$ solution after 56 days of constant low temperature test.	92
Figure 5.29. Cylinders exposed to 17% $CaCl_2$ solution after 56 days of constant low temperature test.	93
Figure 5.30. Compressive strength evolution with time of mortar cubes exposed to different deicers.	94
Figure 5.31. Length change of mortar bars with time for mortar bars exposed to different deicers.	94
Figure 5.32. Mass change of mortar bars with time of mortar bars exposed to different deicers.	95
Figure 5.33. Measured pH change during deicer exposure period.	96
Figure 5.34. Disintegration of mortar cubes during exposure to CMA at 73.4 °F [23 °C].	97

Figure 5.35. Effect of $MgCl_2$ and $CaCl_2$ on compressive strength after 30 days of exposure.	98
Figure 5.36. Sorptivity of portland cement concrete - w/c - 0.55	101
Figure 5.37. Sorptivity of portland cement concrete - w/c - 0.45	101
Figure 5.38. Sorptivity - fly ash concrete - w/cm - 0.55	102
Figure 5.39. Sorptivity - fly ash concrete - w/cm - 0.45	102
Figure 5.40. Sorptivity - GGBFS concrete - w/cm - 0.55	102
Figure 5.41. Sorptivity - GGBFS concrete - w/cm - 0.45	102
Figure 5.42. Sorptivity - concrete w/cm - 0.55 - $CaCl_2$	102
Figure 5.43. Sorptivity - concrete w/cm - 0.45 - $CaCl_2$	102
Figure 5.44. Sorptivity - concrete w/cm - 0.55 - $MgCl_2$	103
Figure 5.45. Sorptivity - concrete w/cm - 0.45 - $MgCl_2$	103
Figure 5.46. Sorptivity - concrete w/cm - 0.55 - $NaCl$	103
Figure 5.47. Sorptivity - concrete w/cm - 0.45 - $NaCl$	103
Figure 5.48. Sorptivity - concrete w/cm - 0.55 - water	103
Figure 5.49. Sorptivity - concrete w/cm - 0.45 - water	103
Figure 5.50. Photographs of 4 inch [100 mm] diameter 0.45 w/c ordinary portland cement (OPC) concrete specimens after 500 days in high concentration brines.	104
Figure 5.51. Crystals on exterior of concrete specimen after 500 days immersion in high-concentration $CaCl_2$ solution.	104
Figure 5.52. White precipitate on exterior of 4 inch [100 mm] diameter concrete specimen after 500 days immersion in low-concentration CMA solution.	105
Figure 5.53. Visible alteration on saw-cut plane through 0.45 w/c mortar specimens.	107
Figure 5.54. Average visible alteration versus time for high concentration brines with 0.45 and 0.55 w/c portland cement concrete specimens and mortar specimens	108
Figure 5.55. Average visible alteration versus time for low concentration brines with 0.45 and 0.55 w/c portland cement concrete specimens and mortar specimens.....	108
Figure 5.56. Fitted chloride profiles for 0.45 w/c straight portland cement concrete specimens immersed in high-concentration brines at 60 days.....	111
Figure 5.57. Fitted chloride profiles for 0.45 w/cm fly ash concrete specimens immersed in high- concentration brines at 60 days.	111
Figure 5.58. Fitted chloride profiles for 0.45 w/cm GGBFS concrete specimens immersed in high- concentration brines at 60 days.	112
Figure 5.59. Fitted chloride profiles for 0.45 w/c straight portland cement concrete specimens immersed in low-concentration brines at 60 days.....	112
Figure 5.60. Fitted chloride profiles for 0.55 w/c straight portland cement concrete specimens immersed in high-concentration brines at 60 days.....	113
Figure 5.61. Fitted chloride profiles for 0.55 w/c straight portland cement mortar specimens immersed in high-concentration brines at 60 days.....	113
Figure 5.62. Fitted chloride profiles for 0.55 w/c straight portland cement concrete specimens sealed with silane and immersed in high-concentration brines at 60 days.....	114
Figure 5.63. Fitted chloride profiles for 0.55 w/c straight portland cement concrete specimens sealed with siloxane and immersed in high-concentration brines at 60 days.....	114
Figure 5.64. Scanned image, (left) and elemental map, (right) from billet cross-section through the near-surface of a 0.45 w/cm fly ash concrete specimen immersed 60 days in 15 % $MgCl_2$	115

Figure 5.65. Scanned image, (left) and elemental map, (right) from billet cross-section through the near-surface of a 0.45 <i>w/cm</i> fly ash mortar specimen immersed 60 days in 15% MgCl ₂	115
Figure 5.66. XRD patterns from the wet extracted paste and the wet exterior precipitate collected from concrete exposed to CaCl ₂ brine for 500 days compared to the reference 8.34, 4.13, 2.76 angstrom peaks for Monosi and Collepari's calcium oxychloride phase.....	117
Figure 5.67. XRD pattern from the wet precipitate collected from the exterior of concrete exposed to CaCl ₂ brine for 500 days compared to 3CaO•CaCl ₂ •15H ₂ O reference peaks.....	118
Figure 5.68. XRD patterns from the wet and oven-dried external precipitate collected from concrete exposed to CaCl ₂ brine for 500 days compared to reference patterns for calcium oxychloride and CaCl ₂ •Ca(OH) ₂ •2H ₂ O.	118
Figure 5.69. Fresh calcium oxychloride crystals before, (top) and after oven drying and conversion to CaCl ₂ •Ca(OH) ₂ •2H ₂ O.	119
Figure 5.70. CaCl ₂ •Ca(OH) ₂ •2H ₂ O crystals before, (top) and after immersion in distilled water in atmospheric equilibrium with CO ₂ at room temperature and subsequent alteration.....	120
Figure 5.71. XRD patterns from oven-dried external precipitate crystals, and the resultant remnant material after immersion in room temperature water, as compared to a reference patterns for calcite and CaCl ₂ •Ca(OH) ₂ •2H ₂ O.	121
Figure 5.72. Fresh calcium oxychloride crystals before, (top) and after immersion in a sealed container of hot CaCl ₂ brine.....	122
Figure 5.73. XRD patterns from wet external precipitate, and the resultant remnant material after curing in hot CaCl ₂ brine, with reference patterns for calcium oxychloride and portlandite.....	123
Figure 5.74. XRD patterns from the wet and air-dried extracted paste collected from concrete specimens exposed to CaCl ₂ brine for 500 days, with reference patterns for calcite and quartz.	123
Figure 5.75. XRD patterns from the wet extracted paste and wet external precipitate collected from concrete exposed to MgCl ₂ brine for 500 days, with reference pattern for Mg ₃ (OH) ₅ Cl•4H ₂ O.	124
Figure 5.76. XRD patterns from the wet and oven dried external precipitate collected from concrete exposed to MgCl ₂ brine for 500 days, with reference patterns for Mg ₃ (OH) ₅ Cl•4H ₂ O and MgCl ₂ •6H ₂ O.....	124
Figure 5.77. XRD patterns from the wet and air-dried extracted paste collected from concrete exposed to MgCl ₂ brine for 500 days.	125
Figure 5.78. XRD pattern from the external precipitate collected from concrete exposed to MBAP solution for 500 days, with reference pattern for Mg ₃ (OH) ₅ Cl•4H ₂ O.....	125
Figure 5.79. XRD pattern from the external precipitate collected from concrete exposed to CMA solution for 500 days, with reference pattern for calcite.	126
Figure 5.80. Epifluorescent thin section views of the 0.45 <i>w/c</i> concrete specimens immersed in solution for 500 days, exterior surfaces to the right.	128
Figure 5.81. Close-up views of regions outlined in pink in Figure 5.183, but with exterior surfaces oriented towards the top. Cross-sectional epifluorescent mode images of the 0.45 <i>w/c</i> concrete specimens after 500 days of immersion in solution.	129
Figure 5.82. Close-up view of deteriorated portion from 0.45 <i>w/c</i> straight portland concrete exposed to CaCl ₂ brine. From left to right: epifluorescent and crossed polars.	130
Figure 5.83. Close-up view of deteriorated portion from 0.45 <i>w/c</i> straight portland concrete exposed to MgCl ₂ brine. From left to right: epifluorescent and crossed polars.	130
Figure 5.84. Close-up view of deteriorated portion from 0.45 <i>w/c</i> straight portland concrete exposed to MBAP brine. From left to right: epifluorescent and crossed polars.	130

Figure 5.85. Cement paste just below the surface from 0.45 w/c straight portland cement concrete exposed to NaCl brine. From left to right: epifluorescent and crossed polars.	131
Figure 5.86. Cement paste just below the surface from 0.45 w/c straight portland cement concrete exposed to CMA brine.	131
Figure 5.87. Cement paste just below the surface from 0.45 w/c straight portland cement concrete exposed to limewater. Ca(OH) ₂ deposits in air voids.	131
Figure 5.88. Epifluorescent thin section views of the 0.45 w/cm concrete specimens immersed in CaCl ₂ solution for 500 days, exterior surfaces to the right.	133
Figure 5.89. Close-up views of regions outlined in pink in Figure 5.88, but with exterior surfaces oriented towards the top. Cross-sectional epifluorescent mode images of the 0.45 w/cm concrete specimens after 500 days of immersion in CaCl ₂ solution.	134
Figure 5.90. Regions of cement paste in 0.45 w/c straight portland cement concrete exposed to CaCl ₂ brine where Ca(OH) ₂ is depleted, (right) and still present, (left).	135
Figure 5.91. Regions of cement paste in 0.45 w/cm fly ash concrete exposed to CaCl ₂ brine where Ca(OH) ₂ is depleted, (right) and still present, (left).	136
Figure 5.92. Regions of cement paste in 0.45 w/cm GGBFS concrete exposed to CaCl ₂ brine where Ca(OH) ₂ is depleted, (right) and still present, (left).	137
Figure 5.93. Deteriorated portion from 0.45 w/c straight portland cement concrete exposed to CaCl ₂ brine with blocky Ca(OH) ₂ crystals.	138
Figure 5.94. Deteriorated portion from 0.45 w/cm fly ash concrete exposed to CaCl ₂ brine with blocky Ca(OH) ₂ crystals.	138
Figure 5.95. Secondary blocky calcium hydroxide crystals in air voids of 0.45 w/cm GGBFS concrete exposed to CaCl ₂	138
Figure 5.96. Epifluorescent thin section views of 0.45 w/cm concrete specimens, and a 0.55 w/c concrete silane-sealed specimen, all immersed in MgCl ₂ solution for 500 days, exterior surfaces to the right.	140
Figure 5.97. Close-up views of regions outlined in pink in Figure 5.96, but with exterior surfaces oriented towards the top. Cross-sectional epifluorescent mode images of 0.45 w/cm concrete specimens, and a 0.55 w/c concrete specimen after 500 days of immersion in MgCl ₂ solution.	141
Figure 5.98. Regions of cement paste in 0.45 w/c straight portland cement concrete exposed to MgCl ₂ brine where Ca(OH) ₂ is depleted, (right) and still present, (left).	142
Figure 5.99. Regions of cement paste in 0.45 w/cm fly ash concrete exposed to MgCl ₂ brine where Ca(OH) ₂ is depleted, (right) and still present, (left).	143
Figure 5.100. Regions of cement paste in 0.45 w/cm GGBFS concrete exposed to MgCl ₂ brine where Ca(OH) ₂ is depleted, (right) and still present, (left).	144
Figure 5.101. Deteriorated 0.45 w/c straight portland cement concrete exposed to MgCl ₂ brine with blocky Ca(OH) ₂ crystals.	145
Figure 5.102. Secondary blocky Ca(OH) ₂ crystals in air voids of 0.45 w/cm fly ash concrete exposed to MgCl ₂	145
Figure 5.103. Deteriorated 0.45 w/cm GGBFS concrete exposed to MgCl ₂ brine with blocky Ca(OH) ₂ crystals in air voids. From left to right: epifluorescent and crossed polars.	145
Figure 5.104. Fibrous crystals at surface of 0.45 w/c straight portland cement concrete exposed to MgCl ₂ brine.	146
Figure 5.105. Fibrous crystals in voids near surface of 0.45 w/c straight portland cement concrete exposed to MgCl ₂ brine.	146

Figure 5.106. Cement paste just below surface, 0.45 w/c straight portland cement concrete, silane-sealed, exposed to MgCl ₂ brine.....	146
Figure 5.107. BSE images from 0.45 w/c concrete specimens exposed to high concentration brines and the limewater control after 500 days.....	148
Figure 5.108. Elemental maps collected from 0.45 w/c concrete specimen immersed in CaCl ₂ brine at 500 days.....	149
Figure 5.109. Elemental maps collected from 0.45 w/c concrete specimen immersed in MgCl ₂ brine at 500 days.....	150
Figure 5.110. Elemental maps collected from 0.45 w/c concrete specimen immersed in MBAP brine at 500 days.....	151
Brighter regions correspond to higher counts for characteristic elemental X-rays.....	151
Figure 5.111. BSE image of magnesium chloride hydroxide hydrate (lighter) and brucite (darker) crystals at surface of 0.45 w/c concrete specimen exposed to MgCl ₂ brine.....	153
Figure 5.112. BSE images comparing bladed crystals observed near the top of the specimen exposed to CaCl ₂ brine, (upper images) to secondary blocky calcium hydroxide crystals observed at depth (lower images).....	155
Figure 5.113. Length change of concrete prisms exposed to deicers under freezing and thawing cycles.....	156
Figure 5.114. Mass change of concrete prisms exposed to deicers under freezing and thawing cycles.....	157
Figure 5.115. Relative dynamic modulus of elasticity of concrete prisms exposed to deicers under freezing and thawing cycles.....	157
Figure 5.116. Durability factor of concrete prisms exposed to deicers under freezing and thawing cycles.....	158
Figure 5.117. Scaled material of concrete slabs exposed to 22% CaCl ₂ in comparison with those exposed to 23% NaCl before the start of the salt scaling test.....	159
Figure 5.118. Photographs of concrete surfaces at cycle 0 (a) pretreated with 23% NaCl and tested with 3% NaCl and (b) pretreated with 22% CaCl ₂ and tested with 4% CaCl ₂	160
Figure 5.119. Photographs of concrete surfaces at cycle 50 (a) pretreated with 23% NaCl and tested with 3% NaCl and (b) pretreated with 22% CaCl ₂ and tested with 4% CaCl ₂	160
Figure 5.120. Photographs of concrete surfaces at cycle 100 (a) pretreated with 23% NaCl and tested with 3% NaCl and (b) pretreated with 22% CaCl ₂ and tested with 4% CaCl ₂	161

LIST OF TABLES

Table 3.1. Mix design proportions for the 0.40, 0.50, and 0.60 <i>w/c</i> mixtures.	20
Table 3.2. Deicer solids used to make deicer solutions.	21
Table 3.3. Saturation concentrations of salt solutions at two temperatures.	22
Table 3.4. Exposure solution chemical analysis by ICP.	24
Table 3.5. Deicer concentrations used for testing in Phase II.	26
Table 3.6. Experimental design for cylindrical specimens tested at 40 °F [4.4 °C].	27
Table 4.1 Pavement sites identified in cooperation with the technical advisory panel for examination as part of Task 5.	29
Table 4.2 Bridge decks identified as additional field sites for examination as part of Task 5.	29
Table 4.3. Air void parameters.	39
Table 4.4. Average cement paste pixel intensities per frame, and equivalent <i>w/c</i> values (as compared to 28-day moist cured mortar samples) for core SD-1.	43
Table 4.5. Average cement paste pixel intensities per frame, and equivalent <i>w/c</i> values (as compared to 28-day moist cured mortar samples) for core SD-7.	47
Table 4.6. Average cement paste pixel intensities per frame, and equivalent <i>w/c</i> values (as compared to 28-day moist cured mortar samples) from core SD-4.	50
Table 4.7. Average cement paste pixel intensities per frame, and equivalent <i>w/c</i> values (as compared to 28-day moist cured mortar samples) core SD-5.	54
Table 4.8. Air void parameters.	63
Table 4.9. Average cement paste pixel intensities per frame, and equivalent <i>w/c</i> values (as compared to 28-day moist cured mortar samples).	67
Table 5.1. List of visual ratings for all mortar cylinders from the low temperature tests.	74
Table 5.2. Mortar samples tested for rapid chloride permeability, bulk diffusion, and sorptivity.	99
Table 5.3. Concrete samples tested for rapid chloride permeability, bulk diffusion, and sorptivity.	99
Table 5.4. Sorptivity results for concrete samples.	101
Table 5.5. Typical EDS measurements from crystals in magnesium-enriched near-surface zone of specimens immersed in high concentration MBAP or MgCl ₂ brines, compared to ideal mineral compositions for brucite and magnesium chloride hydroxide hydrate.	152
Table 5.6. Typical EDS measurements from blocky crystals in cracks and voids at depth in specimens immersed in high concentration CaCl ₂ , MgCl ₂ and MBAP brines, compared to ideal mineral compositions for calcium hydroxide and calcite.	154
Table 5.7. Typical EDS measurements from bladed crystals observed in cracks and voids in near- surface zone of specimen immersed in high concentration CaCl ₂ brine, compared to ideal mineral composition for calcium chloride hydroxide hydrate.	154

TABLE OF ACRONYMS

Acronym	Definition
AASHTO	American Association of State Highway and Transportation Officials
ACI	American Concrete Institute
ACR	Alkali Carbonate Reaction
ASR	Alkali Silica Reaction
ASTM	American Society for Testing and Materials
AVA	Air Void Analyzer
BSE	Back-Scattered Electron
C ₂ S	Dicalcium Silicate
C ₃ A	Tricalcium Aluminate
C ₃ S	Tricalcium Silicate
C ₄ AF	Tetracalcium Aluminoferrite
Ca(OH) ₂	Calcium Hydroxide
Ca ²⁺	Calcium Ion
CaCl ₂	Calcium Chloride
CaCO ₃	Calcite
(CaMg)CO ₃	Dolomite
CANMET	Canada Center for Mineral and Energy Technology
CCD	Charge Coupled Device
CH	Calcium Hydroxide
Cl	Chlorine
Cl ⁻	Chloride Ion
CMA	Calcium Magnesium Acetate
C-N(K)-S-H	Calcium-Alkali-Silicate-Hydrate
CO ₂	Carbon Dioxide
COV	Coefficient of Variation
CSH	Calcium Silicate Hydrate
DC	Direct Current
DOT	Department of Transportation
EDS	Energy Dispersive Spectrometry
EMPA	Electron Micro-Probe Analysis
ESEM	Environmental Scanning Electron Microscope
F-T	Freeze-Thaw
GGBFS	Ground Granulated Blast Furnace Slag
dpi	Dots per Inch
dpm	Dots per Millimeter

Acronym	Definition
HPC	High Performance Concretes
ICP	Inductively Coupled Plasma Spectroscopy
ICP-OES	Inductively Coupled Plasma Optical Emission Spectroscopy
K	Potassium
LVSEM	Low-Vacuum Scanning Electron Microscope
MBAP	Magnesium Chloride Based Agricultural Product
MDOT	Michigan Department of Transportation
Mg	Magnesium
Mg(OH) ₂	Brucite
Mg ²⁺	Magnesium Ion
MgCl ₂	Magnesium Chloride
MIP	Mercury Intrusion Porosimetry
MSH	Magnesium-Silicate-Hydrate
N(K)-S-H	Alkali-Silicate-Hydrate
NaCl	Sodium Chloride
ODOT	Ohio Department of Transportation
OH ⁻	Hydroxide Ion
psi	Pounds per Square Inch
psia	Pounds per Square Inch Absolute
RCPT	Rapid Chloride Permeability Test
RGB	Red-Green-Blue
SCM	Supplementary Cementitious Materials
SDDOT	South Dakota Department of Transportation
SEM	Scanning Electron Microscopy
SHA	State Highway Agency
SHRP	Strategic Highway Research Program
UV	Ultra-Violet
vpm	Vibrations per Minute
w/c	Water-to-Cement Ratio
w/cm	Water-to-Cementitious Ratio
XRD	X-ray Diffraction
XRF	X-ray Fluorescence

SECTION 1 - INTRODUCTION

1.0 PROBLEM STATEMENT

Keeping roads safe and passable is a key concern for any State Highway Agency (SHA), especially during the winter season when ice and snow accumulation on roads and bridges can create hazardous driving conditions. To accomplish this, SHAs are constantly seeking out, evaluating, and adapting new winter maintenance strategies that are cost effective and environmentally friendly. One such area where new strategies are being employed is the broad area of deicing and anti-icing. Deicing is defined as any effort to remove ice from road and bridge surfaces after ice deposition has occurred. This is in contrast to anti-icing, which is defined as a surface treatment applied prior to ice formation that eliminates ice accumulation or facilitates ice removal by lessening the bond between the ice and the riding surface. In general, deicing and anti-icing are accomplished through the use of various chemicals including aqueous solutions of chlorides (e.g. magnesium chloride, sodium chloride, and calcium chloride) or other chemicals such as calcium magnesium acetate and urea. Although the efficacy of these chemicals for deicing and anti-icing has been clearly demonstrated, possible detrimental effects to concrete in transportation structures have not been fully examined and documented. In this sense, the true cost effectiveness has not been determined as chemical attack on concrete is a possibility and in turn, the resulting deterioration of the structures from chemical attack may lead to costly rehabilitation or replacement. Based upon published research, the most problematic chemicals appear to be the chlorides of magnesium, calcium, and sodium and other chemicals containing calcium and magnesium (e.g. calcium magnesium acetate). Use of these chemicals has increased given their relatively low cost, ease of use, and effectiveness for deicing and anti-icing, in certain applications. Use of alternative chemicals such as propylene glycol and ethylene glycol have seen limited use given concerns about their environmental impact, whereas potassium acetate, sodium acetate, potassium formate, and sodium formate are used almost exclusively on airports (with some use in automated bridge deicing systems) due to high cost. In the end, chloride-based deicers appear to be the best choice for highway applications if they can be used in such a way as to minimize possible chemical attack to concrete.

The degradation of concrete used in pavements and bridges that may occur as a result of attack by chemical deicers/anti-icers is the result of an increased concentration of dissociated calcium and magnesium ions in the concrete pore water. In theory, these free ions are available to combine with materials in the concrete to form expansive or weak reaction products such as brucite or magnesium silicate hydrates, respectively. Of course, the dissociation of chlorides into ionic species also increases the concentration of chloride in the pore water solution, which has been well documented as a primary cause of scaling and corrosion of reinforcing steel. These possible and known effects must be fully understood if these chemicals are to be used as a mainstay of any deicing or anti-icing strategy. The goal of this research was to examine the effects of deicing and anti-icing chemicals on portland cement concrete and to recommend changes to concrete mixture designs, construction practices, and winter maintenance procedures that will make these solutions non-detrimental to concrete durability.

1.1 SUMMARY OF PROJECT TASKS

- Task 1: Literature Review
- Task 2: Conduct Survey
- Task 3: Site Selection
- Task 4: Meeting with Technical Panel
- Task 5: Characterization of Field Specimens
- Task 6: Laboratory Experiment
- Task 7: Assessing and Minimizing the Impact of Deicing/Anti-Icing Chemicals
- Task 8: Effects of Various Deicing/Anti-Icing Chemicals
- Task 9: Life Cycle Cost Analyses
- Task 10: Development of Guidelines
- Task 11: Submit Interim Report
- Task 12: Meeting With Technical Panel at Michigan Tech
- Task 13: Prepare and Submit Final Report
- Task 14: Executive Presentation to Research Panel
- Task 15: Executive Presentation to SDDOT Executive Review Board

1.2 REPORT ORGANIZATION AND DISTRIBUTION

The final report for this project is extensive. To facilitate distribution, the report has been broken down into a number of separate volumes and these are listed below.

- **Executive Summary** – Provides a concise overview of the entire project.
- **Final Report** – The final technical report organized into nine sections.
 - Section 1:* A brief introduction
 - Section 2:* An abridged background for the project based on the Task 1 literature review
 - Section 3:* Presents the experimental approach for the entire project
 - Section 4:* An abridged summary of the Task 5 results
 - Section 5:* An abridged summary of Task 6 laboratory results for Phase I and Phase II
 - Section 6:* Presents a discussion of the results of Tasks 5, 6, 7, 8 and 9
 - Section 7:* Presents suggested mitigation strategies based upon the results of this study
 - Section 8:* Conclusions based upon the results of this study
 - Section 9:* Recommendations based upon the results of this study
 - Section 10:* Bibliography used as the basis for Section 2
- **Technical Appendices** – The appendices contain details on specific analytical methods used in the study and an unabridged summary of results for the characterization of field specimens and for all laboratory experiments.
- **Full Literature Review** – Provides the unabridged version of the literature review.
- **Implementation Guidelines** – A practical guideline document to assist DOT personnel in implementing this research.

SECTION 2 - BACKGROUND

Traditionally, winter maintenance entails plowing snow and applying chemicals and/or abrasives to melt the ice cover. In the past, many SHAs favored the use of rock salt (NaCl), although methods of snow and ice removal may vary across the States that practice winter maintenance. Over the years, traditional snow and ice removal methods have been modified in order to comply with environmental regulations, reduce corrosive damage to vehicles, and provide a more economical method to maintain safe roads. Current methods of snow and ice removal include deicing, pre-wetting salt or abrasive material, and anti-icing.

The purpose of this background section is to summarize past research efforts regarding damage resulting from the use of various deicing agents on concrete transportation structures.

2.1. CONCRETE PROPERTIES THAT AFFECT FREEZE-THAW AND CHEMICAL RESISTANCE

To better understand the effects that freeze-thaw cycles and deicing chemicals have on concrete, it is important to have a working knowledge of the basic properties of concrete. The most prominent characteristics to control are: cement chemistry; permeability; air content; aggregate properties; and cracking. In addition, it is necessary to understand the physical and chemical interactions that take place on the surface and within the hardened cement paste.

2.1.1 CEMENT CHEMISTRY

The major constituents present in cement are impure phases of the four compounds: tricalcium silicate (C_3S), dicalcium silicate (C_2S), tricalcium aluminate (C_3A), and tetracalcium aluminoferrite (C_4AF). These chemical compounds form at high temperatures within the cement kiln as part of the cement production process. The calcium silicates make up approximately “three-fourths of the cement and are responsible for the cementing qualities” (Mindess et al. 2003). When mixed with water, the cement undergoes a series of chemical reactions that ultimately hardens the cement into hydrated cement paste. These reactions are commonly referred to as hydration reactions and the hardened cement paste as hydration products (Mindess et al. 2003), also referred to as calcium silicate hydrate (CSH). In addition to CSH, the other abundant reaction product is calcium hydroxide ($Ca(OH)_2$).

One way to mitigate problems with deicing chemicals is to partially replace portland cement with supplementary cementitious materials (SCMs) such as fly ash, silica fume or ground granulated blast furnace slag (GGBFS). The use of SCMs has many benefits, including their influence on lowering the heat of hydration and improved strength gain over time. More importantly, they aid in the resistance of concrete to chemical attack by improving the chemical nature and microstructure of the hydrated cement paste, and by decreasing the amount of $Ca(OH)_2$ and decreasing permeability (Neville 1997).

2.1.2 PERMEABILITY

It is widely understood that the water-to-cement (w/c) ratio has the largest influence on the durability of concrete. When SCMs are used this is referred to as the water-to-cementitious (w/cm) ratio (*Note*: unless otherwise specified, the terms w/c and w/cm may be used interchangeably in this discussion). By having a relatively low w/c ratio, the porosity of the hardened concrete will decrease and in turn, be stronger and have lower permeability. Porosity is a “measure of the proportion of the total volume of concrete occupied by pores” (Neville 1997). Concrete having lower permeability is the more durable because permeability of concrete “controls the rate of entry of moisture that may contain aggressive chemicals (i.e. chlorides) and the movement of water during heating or freezing” (Mindess et al.

2003). Therefore, a lower w/c ratio increases strength and improves resistance to cracking from the internal stresses generated by adverse reactions.

In addition, the w/c ratio affects the volume of capillary pores that form as the cement paste hydrates (i.e. volume increases significantly for w/c ratio > 0.42). Permeability is therefore controlled by an interconnecting network of capillary pores. During hydration, the capillary network becomes increasingly tortuous as interconnected pores are blocked by the formation of hydration products, most notably CSH. Calcium hydroxide also continues to grow within the residual pores, forming impermeable regions. At a given degree of hydration, “the time at which complete discontinuity of the capillary pores occurs is a function of the w/c ratio,” (Mindess et al. 2003). Furthermore, permeability decreases as the cement continues to hydrate over time.

Although the bulk hardened cement paste has the largest influence on permeability, it is also significantly influenced by the paste-aggregate interface. Cracking at the paste-aggregate interface increases permeability, creating pathways for the flow of water. In order to ensure the resistance of newly placed concrete to alternating freezing and thawing cycles, it is desirable to allow the concrete to cure completely before exposing it to harsh winter conditions. In certain cases even after complying with all these requirements, the leaching of calcium hydroxide (which constitutes up to 20% of the concrete matrix) due to concrete exposure to acidic or highly concentrated salt solutions will decrease the strength and increase the porosity of the concrete, affecting the long term durability.

One important aspect of concrete permeability regarding the application of deicing chemicals is chloride diffusion. Diffusion is a process by which a fluid permeates a porous material such as soil or concrete. The surface concentration is the principal determinant of chloride diffusion in near-saturated concrete (Mindess 2003). However, the movement of chloride in concrete is also a function of several other variables. These include pore size and spacing, pore volume fraction, changes in pore size with respect to location within the cement paste, and structure of phases present in the pore system.

2.1.3 AIR CONTENT

Increasing the air content of concrete through air entrainment has been found to improve its resistance to freeze-thaw (F-T) damage (to a point), but at the expense of lowering its strength. In fact, “a strength loss of 10-20% occurs in air entrained concretes” (Mindess et al. 2003). However, to have good F-T protection, air entrainment is required.

The closely spaced entrained air voids “protect concrete during freezing by providing reservoirs for water that exits from the paste on freezing” (Mindess et al. 2003). Standards recommend a maximum value for bubble spacing and the minimum value of the specific surface of the air bubbles in concrete in order to ensure the presence of small, well-spaced air bubbles. This provides adequate protection from freezing and thawing with the least amount of strength loss.

2.1.4 AGGREGATE PROPERTIES

Concrete distress associated with the aggregate fraction has been reported in the literature but in general it is not considered to be a dominant mechanism.

One type of deleterious chemical reaction associated with the aggregate fraction of concrete was studied by Cody and Spry (1994), in which they examined a particular type of aggregate and its susceptibility to chemical attack, namely by magnesium ions. In their findings, Cody and Spry (1994) reported that dolomite coarse aggregate that undergoes dedolomitization would release magnesium ions, which then migrate to the cement paste and interact with the hydrated cement paste.

The reaction Cody and Spry identified within the non-durable concrete was referred to as alkali-carbonate reactivity (ACR) that occurs between the dolomite (i.e. $(\text{CaMg})\text{CO}_3$) coarse aggregate and cement pore solution. This reaction occurs when dolomite from the aggregate is attacked by alkali from the high pH concrete pore solution. Consequently, magnesium and carbonate ions are released into the pore solution and react to form new minerals that cause crystal growth pressures that lead to expansion of the concrete causing premature failure (Cody & Spry 1994).

Cody and Spry identified the ultimate cause of concrete deterioration as the alkali-dolomite reaction. However, they also concluded that “the reaction itself does not produce deterioration”. It is actually the environmental changes, such as slight volume expansions that cause weakening of the aggregate-paste bonding and micro-cracking.

2.1.5 CRACKING

Although cracking may not cause immediate structural failure, it may provide the onset for deterioration that ultimately leads to failure. As cracking spreads, it increases the permeability of concrete, leading to surface scaling and further internal stress-related cracking.

Cracking results from various contributing factors. One factor is the loss of water in fresh concrete; this leads to surface cracking due to evaporation and/or suction of water by the subbase or formwork materials. This type of cracking is referred to as plastic shrinkage cracking. Other types of shrinkage include drying shrinkage, and autogenous shrinkage. Drying shrinkage is controlled by creating contraction joints in pavements and slabs. Autogenous shrinkage results due to water loss associated with the formation of hydration products themselves, and is generally thought to be of consequence only when the w/c ratio drops below 0.40.

The cracking discussed thus far is visible with the naked eye, and is therefore referred to as macrocracking. However all cracking initiates at a micro-level with microcracks, which cannot be seen without the aid of a microscope, coalescing into macrocracks as failure occurs. Microcracks are very fine cracks that can occur at the interface of the aggregate and cement paste or in the paste itself. This type of cracking may result from “differences in the mechanical properties between coarse aggregates and the hydrated cement paste” (Neville 1997). Microcracking has been known to result from freeze-thaw cycling, as hydraulic and osmotic pressures build up within the hydrated cement paste.

2.2. TYPES OF INTERACTIONS

Both physical and chemical interactions occur within concrete when it is exposed to freeze-thaw conditions and deicing chemicals. Physical interaction is initiated when the saturated concrete freezes, subjecting the concrete to volume change and the development of internal stresses that are amplified by the presence of deicer ions in the pore solution and the thermal shock that occurs as ice is melted. Chemical interaction results from the application of deicing chemicals, leading to possible degradation of the concrete structure. Combined, physical and chemical interactions disrupt the concrete properties previously discussed.

2.2.1. PHYSICAL MECHANISMS OF PASTE FREEZE-THAW ATTACK

Saturated concrete subjected to freeze-thaw conditions can undergo damaging internal physical alterations as pressure develops from ice formation within the pore system. Both the hydration products and aggregates can be vulnerable to freeze-thaw damage, which will produce microcracking and ultimately surface scaling and deterioration. The application of deicing chemicals tends to increase the magnitude of physical deterioration by increasing the development of internal pressures.

Another factor that contributes to the amplifying effect deicers have on physical freeze-thaw damage is that deicers increase the saturation level of concrete, increasing hydraulic pressures. This behavior causes concrete subjected to deicer salt application to remain in a critically saturated state for longer periods of time, increasing the likelihood of damage. Because deicers do not penetrate concrete in a pure state, but are instead in an aqueous solution, the diffusion of the deicers is said to be more efficient than the penetration of pure deicer into water saturated concrete (Setzer 1997).

Physical degradation caused by NaCl is usually in the form of severe scaling when concrete is subjected to freeze-thaw cycling (Mu et al. 2002). This type of degradation is primarily a result of the supercooling effect that occurs when NaCl reduces the freezing point of water in the concrete pores (Ghafoori and Mathis 1997). This reduces the immediate development of hydraulic pressures in the concrete as the water remains liquid as the temperature drops below the freezing point. However, when the supercooled pore water finally begins to freeze, it does so at a much faster rate, generating a “greater magnitude of hydraulic pressure” (Marchand et al. 1994). Another physical effect of NaCl in the pore solution near the concrete’s surface is the development of increased osmotic pressure that occurs after or during freezing (Marchand et al. 1994).

In addition to the theories already discussed another physical mechanism that can help explain the cause of concrete scaling from the application of deicing salts is that of salt crystallization within the pores (Hansen 1963). It is hypothesized that the pore solution can become supersaturated as wetting and drying cycles concentrate salts in the pores (Harnik 1980, Mindess et al. 2003). Once crystallization begins, salt molecules are drawn out of smaller pores into the larger pores, inducing potentially harmful crystallization pressures (Ghafoori 1997). An estimation of the magnitude of the crystallization pressure resulting from salt crystal formation has been provided by Winkler and Singer (1972). In their research, they indicated that gypsum and halite crystal growth may exert pressures exceeding 29,000 psi [200 MPa].

2.2.2 CHEMICAL MECHANISMS OF PASTE FREEZE-THAW ATTACK

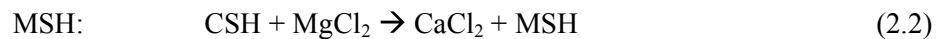
Although most research suggests that salt scaling is primarily a physical deterioration mechanism, some researchers feel strongly that chemical interactions may also be occurring. Marchand (1994) summarized this view stating that more attention should be paid to the chemical interaction between the deicing salts and cement paste hydration products. Recent research indicates that the chemical interaction between deicers and concrete may not be as benign as previously thought.

It is suggested that the Ca(OH)_2 dissolution process results in increased porosity at exposed surfaces, increasing the permeability of the concrete. This in turn increases the amount of water available to freeze due to increased pore volume (Marchand, 1994). One study conducted by the Michigan Department of Transportation (MDOT) adds credence to this theory. Muethel (1997) confirmed through laboratory analysis that depletion of calcium hydroxide led to an increase in permeability and reduced alkalinity of the concrete in the vicinity of cracks and joints. The reduction in the concrete pH contributed to corrosion of reinforcing mesh in the jointed reinforced pavements.

2.2.2.1 Effects of Magnesium Chloride

Like other deicers, MgCl_2 effectively reduces the temperature at which water freezes and will have similar physical effects on concrete as NaCl. However, when the MgCl_2 occurs in the melt water on the concrete surface, the subsequent chemical interactions that occur may have a negative impact as the solution ultimately penetrates into the concrete. This concern has also been raised in Canada where evidence of MgCl_2 having deleterious effects in concrete has been gathered from literature review and

presented in transportation association meetings (Hansson and Laurent 2000). Some interactions of magnesium and chloride ions with the cement hydration products in cement paste are known to cause damaging alterations to the cement paste structure, reducing concrete strength while increasing porosity. These changes result from the ability of magnesium and chloride ions to deplete $\text{Ca}(\text{OH})_2$ to form brucite ($\text{Mg}(\text{OH})_2$) and CaCl_2 . These ions also cause decalcification of the hydration product calcium-silicate-hydrate (CSH), making the paste very porous and converting it to the secondary product, magnesium-silicate-hydrate (MSH). MSH is non-cementitious and tends to develop shrinkage cracks, which lead to crumbling of the hydrated cement paste (Lee et al. 1998). Similar compounds are observed after exposing concrete samples to magnesium sulfate, which is a more aggressive solution than magnesium chloride (Frigione and Sersale 1989). The general reactions for the formation of brucite and MSH from MgCl_2 are as follows:



Other studies have investigated the impact of SCMs on minimizing degradation. The use of GGBFS cement has proven to be beneficial, when the level of replacement is kept between 45 to 80%, for mortar samples immersed in solutions with 25% MgCl_2 by mass compared with replacement outside this range and plain portland cement (Riedel et al. 1967, Smolczyk 1966). In these studies, no deterioration was observed even after two years of exposure while portland cement samples were destroyed after 6 months (Kleinlogel 1950). One of the reasons for this good performance has been attributed to the lower $\text{Ca}(\text{OH})_2$ content in the GGBFS blends at the start of exposure when compared with portland cement mixes (Tumidajski and Chan 1996) as well as the lower porosity of the paste and lower Ca/Si ratio of CSH (Ftikos and Parissakis 1995).

Hydrated magnesium oxychloride compounds such as $3\text{Mg}(\text{OH})_2 \cdot \text{MgCl}_2 \cdot 8\text{H}_2\text{O}$ and $5\text{Mg}(\text{OH})_2 \cdot \text{MgCl}_2 \cdot 8\text{H}_2\text{O}$ can be reaction products in concrete samples exposed to concentrated magnesium chloride solutions (Monosi and Collepardi 1993). Both forms are stable below 212°F [100°C], with $5\text{Mg}(\text{OH})_2 \cdot \text{MgCl}_2 \cdot 8\text{H}_2\text{O}$ being more stable than $3\text{Mg}(\text{OH})_2 \cdot \text{MgCl}_2 \cdot 8\text{H}_2\text{O}$ when exposed to CO_2 (Castellar et al. 1996). These two magnesium oxychloride compounds have been extensively studied in the $\text{MgO-MgCl}_2\text{-H}_2\text{O}$ system and are part of the hydrated products of magnesium oxychloride or Sorel's cement (Dehua and Chuanmei 1996).

Similar to many hydrated basic magnesium salts, these oxychlorides are needle-like crystals, up to 0.1 mm long (Wolff and Walter-Levy 1953, Tooper and Cartz 1966). The minimum concentration of magnesium chloride needed for the formation of magnesium oxychloride in the $\text{MgO-MgCl}_2\text{-H}_2\text{O}$ system has been reported as 1.96 M (Dehua and Chuanmei 1999). It is probable that brucite can transform into magnesium oxychloride after exposure to concentrated magnesium chloride solutions of 2 molal and above based on studies of the solubility of both compounds (Altmaier et al. 2003).

2.2.2.2 Effects of Calcium Chloride

Collepardi et al. (1994) cited a number of studies that have concluded that CaCl_2 , another common deicer, is associated with a deleterious chemical reaction with concrete. The chemical attack is accompanied by the formation of a hydrated calcium oxychloride according to the following reaction:



The reaction proceeds most efficiently at temperatures just above freezing (40 °F to 50 °F [4°C to 10°C]), with rapid formation of hydrated calcium oxychloride. This reaction is considered to be disruptive to the concrete matrix because of the hydraulic pressures generated. The destructive nature

of the formation of calcium oxychloride could also be explained by the crystal growth pressure theory in which the crystallization of solids occurs from a supersaturated solution contained in a porous material. High pressure develops during crystal growth due to restraint by the porous material as long as the supersaturated solution stays in a metastable state long enough for crystals to form (Chatterji and Thaulow 1997). Collepardi et al. (1994) speculates that the damaging nature of this reaction has been masked by corrosion of reinforcing steel and freeze-thaw deterioration of the paste, but states that the chemical degradation that occurs is very detrimental. Collepardi et al. cites experimental evidence, based on decreasing compressive strength, suggesting that severe deterioration occurred in non-air entrained concrete exposed to CaCl_2 deicers even though there was no steel to corrode nor was the concrete subjected to temperatures below freezing.

Collepardi has done other research on the chemical effects of CaCl_2 on cement paste using X-ray diffraction techniques. Analysis of degraded cement paste specimens revealed X-ray diffraction profiles characteristic of the hydrate monochloroaluminate ($\text{C}_3\text{A}\cdot\text{CaCl}_2\cdot 10\text{H}_2\text{O}$) and also of the hydrated calcium oxychloride $3\text{CaO}\cdot\text{CaCl}_2\cdot 15\text{H}_2\text{O}$. The X-ray diffraction profiles corresponding to the oxychloride presence were found only in specimens that were analyzed when moist. Similar analyses were performed with dried samples, but failed to reveal the oxychloride diffraction pattern. Calcium oxychloride has been found to be unstable at 68°F [20°C] and 20% relative humidity, which are normal laboratory conditions (Shi 2001). Therefore, it is believed that previous researchers had not connected CaCl_2 paste damage to the oxychloride presence because the oxychloride presence in dried cement paste is not discernable by X-ray diffraction (Monosi et al. 1990).

On the other hand, the presence of $\text{Ca}(\text{OH})_2$ seems to be necessary for the formation of calcium oxychloride. The exposure of cement paste samples to highly concentrated solutions of CaCl_2 (30% by mass) at 104°F [40°C] can cause $\text{Ca}(\text{OH})_2$ leaching such that no free $\text{Ca}(\text{OH})_2$ is available for calcium oxychlorides to form (Chatterji 1979).

There are also direct chemical effects of CaCl_2 on the cement paste. For example, when exposed to CaCl_2 deicer, chloride concentrations tend to increase within the paste causing discoloration. This may be due to the formation of CaCl_2 hydrate or to adsorption of chloride ions by the CSH. Iron released from calcium-alumino-ferrite-hydrate also contributes to discoloration (Lee et al. 1998). Also, significant discoloration of the cement paste has been observed in a previous study by Kosmatka et al. (2002). They attribute these effects to the formation of calcium chloride hydrate phases ($3\text{CaO}\cdot\text{CaCl}_2\cdot 12\text{H}_2\text{O}$; $\text{CaO}\cdot\text{CaCl}_2\cdot 2\text{H}_2\text{O}$), to adsorption of chloride ion by the CSH phase.

As stated previously, all chloride solutions will cause a transformation of hydration products from ettringite to chloroaluminate. Therefore, in the presence of CaCl_2 solutions, pre-existing ettringite will be transformed to calcium chloroaluminate or trichloroaluminate, which has a crystal structure similar to ettringite (Day 1992).

2.2.2.3 Effects of Calcium Magnesium Acetate

One study on the effects of calcium magnesium acetate (CMA) found that it was not as corrosive as NaCl (McCrum 1989). However, more recent studies have shown that CMA solutions may be the most deleterious deicing chemical. Concentrated solutions of CMA dissolved the cement paste in mortar samples during an exposure period of 15 months and the attack was more aggressive at 68°F [20°C] than at 41°F [5°C]. Reduction in compressive strength was considerable (e.g. up to 23%). The disintegration of the sample was faster in CMA with Ca/Mg ratio of 0.91 as compared to CMA solution with a Ca/Mg ratio of 1.26 (Peterson 1995).

2.2.2.4 Background and Effects of MgCl₂-Based Agricultural Products

Magnesium based agricultural product (MBAP) deicers contain agricultural by-products such as silage (condensed solubles from grain processors, brewers, and vintners), whey and steepwater (liquor from processing corn) in addition to MgCl₂. Developers of these products claim that they are environmentally friendly and non-toxic to vegetation due to their natural ingredients. It is also stated that another benefit of the natural components is that MBAP deicers tend to inhibit corrosion of concrete caused by chloride salts. Some appealing physical properties of MBAP deicers are that they freeze at lower temperatures than most other deicers, possess a high percentage of deicing solids, and mix readily with liquid chloride brines.

There is a downside, however, to using agricultural by-products in winter maintenance. A study conducted by Roosevelt and Fitch (2000) found the composition of the solutions varies from batch to batch due to the inconsistencies in the by-product. As a result of using agricultural by-products, many of the laboratory tests produced noticeable amounts of mold on the surfaces of the concrete specimens (Roosevelt and Fitch, 2000). Although, an inhibitor to control mold growth is available, the researchers note that they did not use it for this study.

2.3 PAVEMENT CONSTRUCTION PRACTICES – EFFECTS ON DEICER SCALING/DETERIORATION

2.3.1 MATERIALS

2.3.1.1 Cementitious and Supplementary Cementitious Materials

The selection of cement type and the use of supplementary cementitious materials (SCMs) are an extremely important element in designing durable concrete pavements. In many applications, the use of a standard ASTM C150 Type I cement will provide satisfactory results. But durability should not be taken for granted, and therefore the properties of the cement and supplementary cementitious/pozzolanic materials must be considered in the context of the long-term physical and chemical stability of the concrete pavement.

2.3.2.2 Ground Granulated Blast Furnace Slag

Ground granulated blast furnace slag (GGBFS) is a byproduct of the production of pig iron, in which the molten slag (at a temperature of 2700°F [1500°C]) is rapidly chilled by quenching in water. This forms a glassy, sand-like material that is then finely ground to less than 45 μm, producing a surface area of 400 to 600 m²/kg Blaine (PCA 1992). GGBFS is nonmetallic, consisting mostly of silicate glass containing calcium, magnesium, aluminum, and silicate with potentially small quantities of crystalline compounds of melilite (Mehta 1993). This rough textured material is cementitious in nature, meaning that it has hydraulic cementing properties on its own. When combined with portland cement, the NaOH or CaOH activates the GGBFS, which hydrates and sets in a manner similar to portland cement (PCA 1992). Specifications for GGBFS for use in concrete are provided in ASTM C989, “*Specification for Ground Granulated Blast-furnace Slag for Use in Concrete and Mortars*”.

2.3.2 CONSTRUCTION CONSIDERATIONS FOR PREVENTING DEICER DISTRESS

Construction can have a very important impact on the occurrence of deicer related distress. Durable concrete must be relatively watertight and non-reactive. From a construction perspective, this means that it must be well mixed, consolidated, and cured under conditions that will produce stable hydration products. Construction practices that have a direct impact on mixing, consolidation, and curing include ambient and seasonal construction conditions, duration of the mixing cycle, method of consolidation,

steel placement, finishing, and curing. The following discussion focuses exclusively on those elements of the construction sequence that have a direct bearing on concrete durability.

2.3.2.1 Ambient and Seasonal Construction Conditions

Ambient and seasonal conditions can play an important role in the durability of concrete through their influence on the development of drying shrinkage cracking, excessive heat of hydration, and inadequate curing prior to deicer application. Hot-weather and cold-weather construction practice as described in *Design and Control of Concrete Mixtures* (PCA 1992) and elsewhere must be followed. It is imperative that drying shrinkage cracking be avoided to maintain the integrity of the concrete surface. This can only be accomplished if an awareness of the relationship between relative humidity, temperature, and wind exists and is acted upon by the construction team.

2.3.2.2 Consolidation

The goal of consolidation of paving concrete is the removal of entrapped air while avoiding segregation and disruption to the entrained air system. Assuming that a high quality, well-graded, workable mixture is used, it should be easily consolidated through internal and/or external vibration. Internal vibration is applied through immersion-type vibrators typically located after the strike-off in the paver. Important factors to consider are the frequency of vibration, amplitude, and the speed of paving. Frequency is typically set between 7,000 and 12,000 vpm, although a recent study recommends fixing the frequency at 10,000 vpm (Gress 1997). This same study recommends weekly calibration checks on the vibrators, a negative (down from horizontal) vibrator slope of 30° or to one-half the pavement depth, and a fixed, uniform paver speed. Other sources state that 8,000 vpm is more typical. In any event, it is critical that the vibration is set to consolidate the concrete without segregation.

It is emphasized that undervibration can result in poor consolidation and overvibration may lead to segregation and the disruption of the air void system in the immediate vicinity of the internal vibrator. It has been noted on a number of projects affected by durability problems that the vibrator trails are visible on the pavement surface and appear to be an initiation point for cracking, spalling, and scaling (Gress 1997). In some instances, petrographic analysis has revealed that the air content in the path of vibration is significantly less than that between the vibrators.

When constructing concrete pavements, considerable attention must be directed to produce a mix that has consistent consolidation characteristics. A paving rate and vibrator frequency must be established early in the project that adequately consolidates the concrete without harmful segregation or disruption to the air void system. If the mix is found to be harsh and difficult to place, construction should be stopped until the problem is corrected. Too often, difficulties in placement are not discovered until a pavement begins to suffer early signs of deterioration at which point little can be done.

2.3.2.3 Steel Placement

The placement of embedded steel in concrete pavement has a direct bearing on the potential for corrosion. Steel used at joints, such as dowel and tie bars, is typically placed at mid-depth, thus concrete cover is not an issue. But in these applications, the joint provides a direct route for chloride ion and moisture ingress, and thus these bars must be protected with a durable coating to avoid corrosion. Epoxy is the most commonly used protective coating, although the cladding of dowels with plastic and stainless steel has also been used by some agencies.

For reinforcing steel, adequate concrete cover is essential to prevent corrosion. At least 2 inches [50 mm] of quality concrete cover is required in environments where chloride-based deicers are used. To

ensure that at least 90 to 95 percent of the reinforcing steel is adequately protected, it is recommended that a design cover of 2.5 inches [65 mm] be used. Thus, during construction, great care must be exercised to avoid “high steel” which is susceptible to corrosion.

2.3.2.4 Finishing

In slipform paving, mechanical floating is commonly used immediately following the vibrating pan to embed large aggregate particles, correct small surface imperfections, and “close the surface.” If the entire slipform paving operation proceeded smoothly, no other finishing other than texturing may be required. But in most cases, additional finishing is needed to correct surface imperfections.

After paving, the surface is checked using a 10- to 13-ft [3- to 4-meter] straight edge. Surface imperfections are commonly corrected using a hand-operated float. It is common that little bleed water occurs with stiff, slipformed concrete, but under certain conditions, it may be present. It is emphasized that finishing should not be conducted when bleed water is present, as there is a danger that either bleed water will become trapped beneath the concrete surface creating a plane of weakness or air content in the surface layer will be reduced. In either case, scaling of the surface may occur due to freeze-thaw damage, particularly if chemical deicers are used.

Finishers commonly desire to add more water to the surface to assist in the finishing operation. It is known that this practice must be resisted as working water into the concrete surface will increase the w/c ratio and reduce the air content, leading to scaling. If the mix is difficult to work without water being added during finishing, the entire construction operation should be reviewed.

On occasion, a paving edge may slump, requiring correction. In this case, it should be carefully rebuilt with added concrete, working against a bulkhead placed against the slab edge. Care must be taken to avoid over-working or over-finishing the repair.

2.3.2.5 Curing

Gowripalan (1993) found that improper curing resulted in the surface having a high rate of evaporation that produced a porous, permeable, and weak surface due to insufficient hydration. He also cited research that found that near the surface, the permeability of poorly cured concrete could be as much as ten times that of well-cured concrete.

Ideally, concrete would be cured in such a way that the presence of mixing water is maintained. This requires the continued application of water either through ponding, fogging, or covering the concrete with a saturated cloth such as burlap. Unfortunately, wet curing is not practical for most large paving projects. Instead, the most common curing method is to prevent the loss of mixing water through the application of a membrane-forming curing compound as specified under ASTM C309, “*Specification for Liquid Membrane-Forming Compounds for Curing Concrete*”. The effectiveness of curing compounds can be assessed through ASTM C156, “*Test Method for Water Retention by Liquid Membrane-Forming Curing Compounds for Concrete*”.

The curing compound should be applied immediately following texturing. Any delay, particularly during hot, windy conditions, can cause significant harm to the concrete resulting in plastic shrinkage cracking. Although these cracks are small and isolated to the concrete surface, they provide access for potentially deleterious compounds into the concrete structure.

Great care should be exercised in the application of curing compounds. The application must be uniform and of sufficient quantity to ensure that the surface is completely sealed. On large paving

projects, power-driven spray equipment should be used. It is highly recommended that two coats be applied to ensure complete coverage (PCA 1992).

There are concerns that some curing compounds are not effective. Highway agencies are highly encouraged to test curing compounds to verify their moisture-retention properties. Water-based curing compounds should not be “watered down” during construction. Also, the curing compound should be resistant to damage caused by construction traffic.

Different concrete mixtures will require different lengths of curing prior to opening to traffic. This must be carefully considered when concrete mixtures containing fly ash or GGBFS are used. Temperature also has a major effect on the required length of curing, and the use of maturity concepts to determine appropriate opening times is recommended. In addition to strength gain required for load carrying capacity, newly placed concrete also requires an air-drying period of 1 month before it is subjected to deicer applications. This will add to the scaling resistance of the concrete.

2.3.3 PREVENTIVE STRATEGIES FOR CONTROLLING SPECIFIC TYPES OF MATERIALS-RELATED DISTRESS

2.3.3.1 Deicer Scaling/Deterioration

In general, deicer scaling is not a concern for properly constructed, high quality portland cement concrete. But even if the concrete is properly constructed and cured, deicers may damage concrete with poor mix characteristics. Pigeon (1994) comments on this by stating that “air entrainment improves to a very large degree the resistance to deicer salt scaling...and as could be expected, scaling decreases with water-cement ratio, and finishing and curing operations are particularly important.” As indicated, the two primary mix design considerations for producing deicer scaling/deterioration resistant concrete are proper air entrainment and a relatively high cement content with corresponding low w/c ratio.

Air content is an important consideration when trying to prevent deicer scaling. Concrete adequately air-entrained for freeze-thaw may be susceptible to the development of salt scaling. Collepardi et al. (1994) concludes that air contents recommended by ACI for “severe exposure” should be followed if the concrete is to be exposed to calcium chloride deicers, finding that concrete with air contents meeting ACI “moderate exposure” requirements suffered severe degradation in laboratory testing even without being subjected to freeze-thaw action.

In addition to the use of entrained air, high cement content, and low w/c ratio, the use of fly ash has been proposed to enhance deicer scaling/deterioration resistance. The PCA (1992) reports that air-entrained concrete containing fly ash has similar freeze-thaw durability to concrete made with portland cement as the sole binder as long as the same compressive strength, air void system, and curing are obtained. The results of a study conducted by Malhotra (1991) agree with those by Malek (1988) in which it was found that the incorporation of fly ash appreciably reduced the permeability of concrete to chloride ions. This study was based on measuring chloride ion permeability using ASTM C1202 and not on a measure of scaling resistance. Bilodeau (1991) found that concrete containing up to 30 percent ASTM Type F fly ash generally performed well under the combined effect of freezing and thawing in the presence of salt deicer, although performance of the fly ash concrete was more variable. Although extended periods of moist-curing or drying periods did not seem to significantly affect performance, the use of membrane curing had a decided benefit, particularly for fly ash concrete. In a paper published a year later, Bilodeau (1992) reported on the properties of concrete containing ASTM Type F fly ash as 58 percent of the total cementitious materials content. He noted that in addition to acceptable mechanical properties, high volume fly ash concrete had excellent resistance to chloride ion

penetration as compared to plain concrete mixes. He mentioned that further testing is needed to demonstrate scaling resistance.

An experiment conducted by Byfors (1987) examined the influence of fly ash and silica fume addition on chloride ion penetration and pore solution alkalinity. It is reported that the additions of either fly ash or silica fume considerably reduces the rate of chloride ion diffusion. Malhotra (1991) cites a number of studies conducted by CANMET, which indicate the incorporation of low calcium fly ash (i.e. ASTM C618 Type F) in concrete significantly reduces chloride ion penetration.

2.4 LITERATURE REVIEW SUMMARY

Traditionally, winter maintenance entails plowing snow and applying chemicals and/or abrasives to melt the snow and ice cover. Over the years, traditional snow and ice removal methods have been modified in order to comply with environmental regulations, reduce corrosive damage to vehicles, and provide a more economical method to maintain safe roads. Current methods of snow and ice removal include deicing, pre-wetting salt or abrasive material, and anti-icing.

Concrete consists of coarse aggregate, fine aggregate (i.e. sand), portland cement, water, and typically, entrained air. The water and portland cement react to form hydration products, most notably calcium silicate hydrate (CSH) and calcium hydroxide ($\text{Ca}(\text{OH})_2$).

A number of concrete properties affect performance when the concrete is exposed to deicers. The most important characteristics to control are: permeability; air content; cement chemistry; aggregate properties; and cracking.

It is widely understood that the water to cement ratio (w/c) has the largest influence on the durability of concrete. By having a relatively low w/c ratio, the porosity of the hydration products will decrease and in turn, the concrete will be less permeable.

One important aspect of concrete permeability regarding the application of deicing chemicals is chloride diffusion. The movement of chloride ions in concrete is a function of several variables. These include the concentration of deicer solution at the concrete surface, pore size and spacing, pore volume fraction, changes in pore size with respect to location within the cement paste, and chemical composition of phases present in the hydrated cement paste.

Cracking in concrete significantly increases the permeability and makes the concrete more susceptible to ingress of fluids. Although cracking may not cause immediate structural failure, it may provide for the onset of deterioration that ultimately leads to failure. As cracking spreads, it increases the permeability of concrete, leading to surface scaling and further internal stress-related cracking.

Entrained air has been found to improve the freeze-thaw (F-T) resistance of concrete. It is also known that a disadvantage of increasing the entrained air content is that it lowers the strength and increases the permeability of concrete. However, to have good F-T protection, air entrainment is required.

Both physical and chemical interactions occur within concrete when it is exposed to freeze-thaw conditions and deicing chemicals. Physical interaction is initiated when the saturated concrete freezes, subjecting the concrete to expansion and internal stresses. Additionally, some researchers have reported that the crystallization of salts or other phases within the concrete pore system can also lead to expansive cracking. Chemical interaction results from the interaction of deicing chemicals with the hardened cement paste, leading to possible degradation of the concrete structure.

Deicer scaling/deterioration is typically characterized by scaling or crazing of the slab surface due to the repeated application of deicing chemicals. Although the exact causes of deicer scaling are not known, it is commonly thought to be primarily a form of physical attack, possibly resulting from a combination of factors. Some researchers have stated that the presence of deicing chemicals can magnify or amplify the mechanisms that lead to F-T deterioration of the paste.

Although most research suggests that physical deterioration is the dominant source of distress associated with deicers, some researchers feel strongly that chemical interactions may also be occurring. It is known that the calcium hydroxide dissolution process results in increased porosity at exposed surfaces, increasing the permeability of the concrete, and the dissolved calcium hydroxide reacts with deicers to form deleterious compounds.

Magnesium chloride ($MgCl_2$) effectively reduces the temperature at which water freezes and will have similar physical effects on concrete as NaCl. However, when the $MgCl_2$ occurs in the melt water on the concrete surface, the subsequent chemical interactions that occur may have a negative impact as the solution ultimately penetrates into the concrete. Some interactions of magnesium and chloride ions with the cement hydration products are known to cause damaging alterations to the cement paste structure, reducing concrete strength while increasing porosity. Magnesium oxychloride compounds can occur as reaction products in concrete samples exposed to concentrated chloride solutions

Other researchers have concluded that calcium chloride ($CaCl_2$), another common deicer, is associated with a deleterious chemical reaction with concrete where calcium oxychloride forms, causing cracks as it expands.

Magnesium based agricultural product (MBAP) deicers contain agricultural by-products in addition to $MgCl_2$. Some appealing physical properties of MBAP deicers are that they freeze at lower temperatures than most other deicers, they possess a high percentage of deicing solids, and mix readily with liquid chloride brines.

One reported way to mitigate problems with deicing chemicals is the partial replacement of portland cement in the concrete mixture with another cementitious material such as fly ash, silica fume, or GGBFS. The use of these industrial by-products has many benefits, including their influence on the heat of hydration and strength. More importantly, they aid in the resistance of concrete to chemical attack by improving the chemical nature and microstructure of the hydrated cement paste by decreasing the amount of calcium hydroxide present and decreasing permeability.

In general, physical attack associated with deicing chemicals is not a concern for properly constructed, high quality portland cement concrete. But even if the concrete is properly constructed and cured, deicers may damage concrete with poor mixture characteristics. The two primary mixture design considerations for producing deicer scaling resistant concrete are a relatively low w/c ratio (with corresponding high cement content) and air entrainment. State highway agencies standard specifications reflect this, although the specified maximum w/c ratio and minimum cement content vary greatly from state to state, indicating that consensus does not exist among the various agencies. It is not clear if chemical attack can be prevented through sound construction practices alone.

SECTION 3. EXPERIMENTAL APPROACH

3.1. OVERVIEW

To accomplish the work described in Tasks 5 through 9 of this project, a series of field explorations and laboratory experiments were performed, and the results of these form the basis of the conclusions presented in this report. The purpose of this section is to describe the experimental approach used in this study. In general, the explorations and experiments performed fall into three broad activities: *Characterization of Field Specimens*, *Phase I Laboratory Experiments on Portland Cement Mortar*, and *Phase II Laboratory Experiments on Portland Cement Concrete*. The analytical methods used in all three activities, the general approach to the characterization of field specimens, and the experimental design and approach used in the two laboratory experiments are presented in the remainder of this report section and also in Appendix A - Experimental Methods..

3.2. ANALYTICAL METHODS

For samples received from the field sites and samples resulting from the laboratory experiments, a number of analytical methods were used to accomplish a complete microstructural characterization. Techniques used included visual inspection, stereo optical microscope examination, staining, plus petrographic optical microscope, scanning electron microscope, and x-ray microscope examination. For the laboratory experiments, mortar and concrete specimens exposed to various deicers were examined by most of these same methods in addition to x-ray diffraction, profile grinding to determine chloride diffusion coefficients, sorptivity testing, and rapid chloride profile testing. Each of these techniques will be briefly introduced and discussed in the following sections. All tests were conducted following ASTM or other applicable standards where they exist.

3.2.1. VISUAL INSPECTION

Visual inspection entails observations made of the specimen with the naked eye or a hand lens. The general condition of the concrete was assessed in accordance ASTM C856 *Practice for Petrographic Examination of Hardened Concrete*.

Many of the features observed during the initial visual examination were examined more closely using various staining techniques, stereo optical microscopy, petrographic optical microscopy, and scanning electron microscopy. Qualitative observations made during visual inspection help to provide an overall assessment of the concrete as well as focus future investigation.

3.2.2. STEREO OPTICAL MICROSCOPE EXAMINATION

Of all the available microscopic methods, the stereo optical microscope is clearly the first analytical instrument to use when analyzing concrete. It provides a good depth of field image with sufficient magnification to see most key features in concrete microstructure. The most common types of concrete specimens observed in a stereo optical microscope are broken pieces, polished slabs, and thin sections. For this study, all observations were performed on polished slabs, which require preparation time but provide for more detailed analysis of the concrete.

Concrete can be evaluated for its susceptibility to damage by paste F-T damage by following ASTM C457 *Test Method for Microscopical Determination of Parameters of the Air-Void System in Hardened Concrete*. This test method uses a stereo optical microscope coupled with a movable stage to determine the volumetric fraction of the air voids and other phases in the concrete. From this

analysis, the key parameters of the air-void system can be determined including the Powers spacing factor, specific surface, and volumetric air content.

The microscopic examination of the air-void system in hardened concrete can be obtained from a point count, linear traverse, or an area traverse. All three methods rely on measurements obtained from a polished plane surface of concrete. For this work, air-void system parameters were determined by means of a point count (ASTM C457 Procedure B). For more details on the test method, the reader is directed to ASTM C457.

For normal strength concrete, entrained air-void systems with a Powers spacing factor of 0.008 inch (0.20 mm) or less have been shown to provide good F-T protection. While the Powers spacing factor is not considered a truly definitive measure of F-T protection, it is still used as the standard method of quantifying the distribution of entrained air in concrete.

3.2.3. STAINING TESTS

Staining is a relatively easy method for identifying large-scale chemical anomalies in concrete. Two staining methods were used in this study. They are the sodium cobaltinitrite method for diagnosing ASR (Guthrie 1997) and the phenolphthalein stain for determining depth of carbonation. In the sodium cobaltinitrite method, yellow stained regions indicate reaction products resulting from ASR. The use of phenolphthalein as a stain for determining the depth and extent of carbonation is based upon the pH of the cement paste. Any cement paste within the concrete that has a pH greater than 10 will be stained a magenta color. All other constituents including carbonated paste remain unchanged.

3.2.4. PETROGRAPHIC OPTICAL MICROSCOPE EXAMINATION

3.2.4.1. General Information

Using polarized light, the petrographic optical microscope can be used to identify subtle optical properties in different minerals that are characteristic and often unique to that mineral. The petrographic optical microscope was used in this study for evaluating mortar and concrete microstructure, and identifying the composition or mineralogical characteristics of phases within concrete. By this method, a more complete picture of the concrete microstructure is obtained.

All samples examined using the petrographic optical microscope were thin sections. Concrete thin sections were prepared on standard geological thin section slides using standard geological sample preparation methods. An ultimate thickness of 20 to 25 microns was obtained by first cutting and grinding the section to very near the desired thickness. Then, the section is thinned by hand until the desired thickness is achieved.

All thin sections used for this study were prepared by first impregnating the concrete with an epoxy containing an ultra-violet (UV) light-sensitive dye. Once prepared using this approach, cracks, voids, and areas of varying paste density can be readily identified. Also, estimations of the effective w/c ratio can be obtained. A more detailed discussion of determining the effective w/c ratio is provided in Appendix A – Experimental Methods.

3.2.5. SCANNING ELECTRON MICROSCOPY

The scanning electron microscope (SEM) forms an image by rastering a focused electron beam across a small rectangular area of a specimen. The electron beam and specimen interact, resulting in emission of two electron signals of interest and characteristic x-rays. As the electron beam strikes the specimen, electrons from the material are released. These are called secondary electrons, have a very low kinetic energy (<500 eV), and are used to form topographical images of a specimen. Electrons that originate

in the electron beam have a very high energy (15-25 keV) and these electrons scatter in proportion to the specimen density at the point of impact. These “backscattered electrons” are used to form images showing composition based contrast in the image. As the electron beam is scanning the specimen area, the electron yield from the specimen is monitored using an electron detector. This electron signal is used to modulate the brightness or intensity of a viewing display. This modulation/scanning process maps out an image on the viewing display that is an “electronic representation” of what the specimen surface looks like. By design, an SEM produces images with extraordinary depth of field allowing for examination of rough surfaces.

When a point on a specimen is excited with the incident electron beam, characteristic x-rays are emitted from the specimen that are unique identifiers of the elements present in the irradiated volume. By identifying the energy or wavelength of the characteristic x-rays produced using a spectrometer, the elements present are identified. For a given incident electron beam current, the rate of characteristic x-ray production for a given element will be proportional to that element’s concentration. This effect forms the basis of x-ray mapping and quantitative x-ray microanalysis.

The SEM allows for quantitative analysis of volumes on the order of one cubic micron. Secondary deposits in cracks and voids can be identified and mineral recalculations of the analysis results can be used to accurately identify the phase. X-ray mapping is a convenient way to illustrate the spatial distribution of elements in an area of the specimen.

For this study, the SEM was used for imaging, x-ray microanalysis, and x-ray mapping. In general, selected samples examined by the petrographic microscope were examined by SEM to obtain detailed quantitative analysis of phases observed and to obtain x-ray maps. All analyses for this study were conducted with a FEI XL-40 environmental SEM. X-ray analyses and mapping were performed using an EDAX Phoenix energy dispersive x-ray analyzer. Unless otherwise noted, all analyses were performed with a 15kV accelerating voltage.

3.2.6. X-RAY MICROSCOPE

The x-ray microscope is a relatively new instrument that provides innovative ways of analyzing materials. It uses a precisely shaped glass tube to “focus” x-rays to a user selectable spot source of 10 to 300 microns. The specimen is stepped under the focused x-ray flux in a regular grid pattern or a specific point on the specimen is analyzed by moving the point of interest to the focal point of the guide tube. The incident x-rays fluoresce characteristic x-rays from the specimen in a manner analogous to a SEM producing x-rays with a focused electron beam. These characteristic x-rays are used to perform a quantitative analysis of the analysis point or to produce an x-ray map of a scanned area.

The instrument used was a Horiba/Oxford XGT-2000W x-ray analytical microscope. In this study, the x-ray microscope was one method used to determine the chloride profiles from field and laboratory prepared specimens. The profiles were determined by developing a calibration curve for x-ray intensity versus chlorine concentration. For more information on this process, see Appendix A - Experimental Methods.

3.2.7. X-RAY DIFFRACTION ANALYSIS

X-ray diffraction (XRD) can be used to identify the type and abundance of crystalline phases within a concrete microstructure. In general, x-ray diffraction results in identification of the inter-atomic distances between all atoms in a crystalline structure. For any crystalline material, this arrangement of atoms in an ordered unit cell is unique and characteristic of that crystalline phase.

For a given diffraction scan over a specified angular range, a diffraction pattern is produced that is the combination of unique patterns generated from each constituent of the material. The pattern represents the diffracted intensity measured as the diffractometer scans through a range of angles, and consists of sharp diffraction peaks, or lines, superimposed on a slowly varying background. For a given crystalline material, a family of lines occurs because diffraction occurs in multiple angular directions. The angular occurrence and relative heights of the diffraction lines forming a family is unique to that crystalline material and serves as a “fingerprint” of the material.

X-ray diffraction was used in this study to identify secondary deposits observed in the laboratory specimens. The instrument used at Michigan Tech was a Scintag XDS-2000 automated diffractometer. At the University of Toronto, The x-ray diffractometer was a PANalytical instrument with a vertical goniometer.

3.2.8. PROFILE GRINDING TO DETERMINE CHLORIDE PROFILES

This test is described in more detail in either the ASTM C1556, *Determining the Apparent Chloride Diffusion Coefficient of Cementitious Mixtures by Bulk Diffusion*, or the NordTest NTBuild 443 Test Method. The specimen surface is carefully removed with a diamond tipped bit in a mill or lathe in 0.02 inch [0.5 mm] depth increments. The material removed is dust, which is carefully collected and analyzed for chloride content. The dust obtained from each layer is subsequently analyzed using inductively coupled plasma optical emission spectroscopy, or similar methods, to determine the chloride content of the layer. The concentration determined at each depth is plotted to determine the chloride profile in the sample. In this case a 2 inch [50 mm] diameter diamond bit mounted on a milling machine was used to take ~0.04 inch [1.0 mm] thick powder samples.

3.2.9. BULK DIFFUSION/SORPTIVITY

The bulk diffusion test (ASTM C1556 or NordTest NTBuild 443) is used to measure the apparent diffusivity of concrete (i.e. total penetration of both free and bound chlorides). A 2 inch [50 mm] thick specimen is saturated with limewater, coated with epoxy on all but one side, and immersed in a 2.8 M NaCl solution typically for 35 days. Profile grinding as described previously is then used to determine the chloride profile from the exposed surface. Apparent diffusion coefficients are then determined by fitting a curve to the chloride penetration profile using Crank’s numeric solution to Fick’s second law.

Sorptivity is a measurement of the unsaturated flow of a fluid into the concrete due to capillary forces that draw the fluids into the pores. Measuring this in the laboratory is simple once the specimen is properly conditioned to a standard moisture condition, as it is then a matter of measuring the mass gain due to water sorption into the concrete over a relatively short time frame (30 minutes). The method used essentially followed ASTM C1585, *Measurement of Rate of Absorption of Water by Hydraulic-Cement Concretes*.

3.2.10. RAPID CHLORIDE PERMEABILITY TESTING

The concrete and mortar’s resistance to chloride ion penetration was assessed using ASTM C1202 *Electrical Indication of Concrete’s Ability to Resist Chloride Ion Penetration*. This test is commonly referred to as the Rapid Chloride Permeability Test (RCPT), but this is inaccurate since it is not measuring concrete permeability per se, but the ionic movement through the concrete. The test method determines the electrical conductance of concrete by subjecting a saturated concrete specimen to 60 volts DC for six hours. One side of the specimen is exposed to a sodium chloride solution and the other side to a sodium hydroxide solution. The total charge passed, measured in coulombs, is used as a

measure of permeability. In this study, 2 inch [50 mm] thick laboratory specimens were tested to estimate the mixture permeability.

3.2.11. OTHER TEST METHODS

For other laboratory testing at the University of Toronto, a series of test methods were performed at specific ages before and after mortar and concrete specimens were exposed to deicer solutions to determine how the exposure of the specimens to the deicers could affect certain physical properties and their long-term durability performance.

3.2.11.1. Length Change

Mortar and concrete prisms were cast to determine the expansion or contraction caused by the exposure of these specimens to deicers. The length change was determined according to ASTM C157 “*Test Method for Length Change of Hardened of Hydraulic-Cement Mortar and Concrete.*” Mortar specimens were 1 x 1 x 1 1/4 inch [25 x 25 x 285 mm] prisms and concrete specimens were 3 x 3 x 1 1/4 inch [75 x 75 x 285 mm]. After 24 ± 2 hours and once each specimen had been stored in lime water for 30 minutes, an initial reading was taken using a length comparator, and after at 7, 14, 28 days as well. Additional readings were taken at specific ages after placing the specimens in the exposure solution.

3.2.11.2. Mass Change

Changes in the volume of the mortar and concrete prisms were measured by determining the changes in mass with time. The mass change was determined using a balance with a readability of 0.01 g at the same age the length of the specimens was measured. That is, at 7, 14 and 28 days and after exposure to the deicers at specific ages.

3.2.11.3. Solution pH

The pH of the exposure solution (deicer) was measured with time using a digital pH meter capable of measuring within the pH range of 0 to 14 and with an accuracy of ±0.02. An automatic temperature compensation probe was attached to the pH meter to compensate for temperature changes during measurements.

3.2.11.4. Compressive Strength

The determination of compressive strength in mortars was done using 2 inch [50 mm] cubes according to ASTM C109 *Test Method for Compressive Strength of Hydraulic Cement Mortars (Using 2-in. or [50-mm] Cube Specimens)*.

3.2.11.5. Mercury Intrusion Porosimetry (MIP)

The pore volume change of mortar specimens was determined after exposure to deicers using the Autoscan-60 mercury porosimeter manufactured by Quantachrome. In short, the pore volume is determined by pressurizing mercury into the pores of a mortar specimen up to 60,000 psia [414 MPa] and by using the Washburn equation, $P \cdot r = -2\gamma \cos\theta$, which correlates the applied pressure (P) with the intruded pore radius (r) of the mortar, where γ and θ are the mercury surface tension and the contact angle between the mercury and the pore wall, respectively.

3.2.11.6. Exposure Solution Chemical Analysis

After diluting the deicers to the desired concentrations, aliquots were sent for chemical analysis to an independent private laboratory. The elemental concentration of ions of interest was determined by

using ICP-OES. The ions analyzed were: Al, Ca, Fe, Mg, P, K, Na, Si and S. In addition, chloride concentration was determined by potentiometric titration using a Metrohm DMS 760 titrator.

3.3. CHARACTERIZATION OF FIELD SPECIMENS

3.3.1. IDENTIFICATION OF FIELD SITES FOR TASK 5

To accomplish project Task 5, Characterization of Field Specimens, the research team began by meeting with the technical advisory panel and discussing possible sites that 1) represent the range of deicers being currently used and 2) either exhibit some level of distress or represent new pavements that have been exposed only to one specific deicer. The intent of the study was to identify distress mechanisms that are visible in field concrete and study field concrete that has been exposed to a specific deicer, to assess how that one specific deicer is interacting with the concrete. Initially, five sites were identified for coring and analysis by petrographic methods. Later, two additional sites were sampled and core samples from these sites were also examined by petrographic methods.

After the sites were identified, coring was performed by the state DOT with jurisdiction over each site. The coring plan used was developed in previous research and published in *Guidelines for Detection, Analysis, and Treatment of Materials-Related Distress in Concrete Pavements, Volume 1: Final Report*. FHWA-RD-01-163 (Van Dam et. al 2002a).

Following procedures set forth in the referenced guidelines (Van Dam et. al. 2002a), the cores retrieved from the selected sites were packaged and shipped to Michigan Tech for analysis. For more information on this process, see Appendix A, Experimental Methods.

3.4. PHASE I EXPERIMENTAL APPROACH: LABORATORY TESTING OF PORTLAND CEMENT MORTAR

3.4.1. OVERVIEW

For Phase I, work was performed at Michigan Tech and at the University of Toronto. The Phase I approach will be described for each institution separately.

3.4.2. PHASE I WORK CONDUCTED AT MICHIGAN TECH

3.4.2.1. Mixture Design and Preparation

In Phase I, three different mortar mixtures were tested under various temperature regimes to examine how deicing chemicals interact with hardened portland cement paste. Also, the results of these tests were used to help select material parameters for Phase II where concrete was tested.

Three different mortar mixtures were prepared using 20-30 Ottawa sand (ASTM C778), Lafarge Alpena Type I/II cement, and water. The mix designs are presented in Table 3.1.

Table 3.1. Mix design proportions for the 0.40, 0.50, and 0.60 w/c mixtures.

	Mix Design (g)	Mix Design (g)	Mix Design (g)
w/c	0.40	0.50	0.60
Cement	500.0	500.0	500.0
Water	200.0	250.0	300.0
Sand	1462.5	1666.4	1870.2
Air entrainer	0.28 ml	0.28 ml	0.28 ml

The w/c was the independent variable with increments of 0.40, 0.50, and 0.60. The paste content was held constant for all mix designs. Approximately twenty five hundred 2 inch diameter by 4 inch high [50 mm by 100 mm] mortar cylinders were made, in addition to twelve 4 inch diameter by 8 inch high [100 mm by 200 mm] cylinders. The cylinders were cured in lime baths for 28 days, and then placed in a temperature control room at 40 °F [4.4 °C] until deicer exposure testing began. The approach was to have 30 samples, of each w/c , exposed to each of the four principal deicers and a control solution (lime water). The exposure would be under three different temperature regimes as described below. The large number of samples made was intended to provide extra samples accounting for poorly consolidated or damaged samples that could not be tested. The large number of samples tested provided multiple samples under each condition for replication, and samples to be removed from solution at various times to study the effect of time on diffusion or any observed deterioration. Samples were originally scheduled to be removed at 7, 14, 28, 56, 84, or 112 days. Specimens removed at each time period were to be examined using petrographic methods, tested for strength by means of split-tensile testing, and analyzed to determine the chloride ingress. As will be described in the Results section (Section 5), not all of these goals were obtained.

3.4.2.2. Deicer Solutions

The deicer solutions used in Phase I of his study were prepared by dissolving solid deicer salts in water. The one exception was the magnesium chloride based agricultural by-product (MBAP) deicer, which was prepared from a liquid. Table 3.2 below lists the sources of deicers used.

Table 3.2. Deicer solids used to make deicer solutions.

Deicing Chemical	Form
NaCl	Food Grade Crystalline
MgCl ₂	Hexahydrate Flake
CaCl ₂	Flake
Calcium Magnesium Acetate	Solid Pellet
MgCl ₂ based agricultural by-product (MBAP)	Liquid

For the three principal chlorides, the solution strengths were chosen by first selecting 15% by weight MgCl₂ as the basis for comparison. This concentration was chosen to represent the dilution that occurs when salt solutions are applied to a road surface (i.e. magnesium chloride brines are typically applied at concentrations much greater than 15% by weight). Then, to assess the effects of each deicer on hydrated portland cement paste on an equitable basis, the solutions were normalized on the basis of molal concentration of chloride ion. Molality offers the advantage of equal numbers of moles of each deicer cation per volume solution, which makes determination of diffusion coefficients more straightforward and gives a basis for comparison of deicer chemicals in terms of the chemical interaction only. A solution of 15% MgCl₂ and water has a molal concentration of 1.85 m Mg²⁺ and 3.7 m Cl⁻. Similarly, a solution of 17% CaCl₂ and water has a molal concentration of 1.85 m Ca²⁺ and 3.7 m Cl⁻. A solution of 17.8% NaCl has a molal concentration of 3.7 m Na⁺ and 3.7 m Cl⁻. In Phase I the CMA solution strength was used at the normal application concentration of 25% CMA by weight, which is a molal concentration. The MBAP deicer was not tested in Phase I.

Except for the NaCl solution, the concentrations chosen are all less than the eutectic composition for each system theoretically resulting in no solid salt in the solution. The MgCl₂, CaCl₂ and CMA solutions formed a “slush” that was ice and salt solution. In the case of the NaCl solution, below -5.8 °F [-21 °C] only ice and solid NaCl•2H₂O (hydrohalite) are present. The partial phase diagrams for the deicer solutions are shown in Figure 3.1. Table 3.3 shows the saturation concentration for each

solution. In addition to the four basic deicing solutions, in all testing regimes, specimens were tested in saturated limewater solutions as a control.

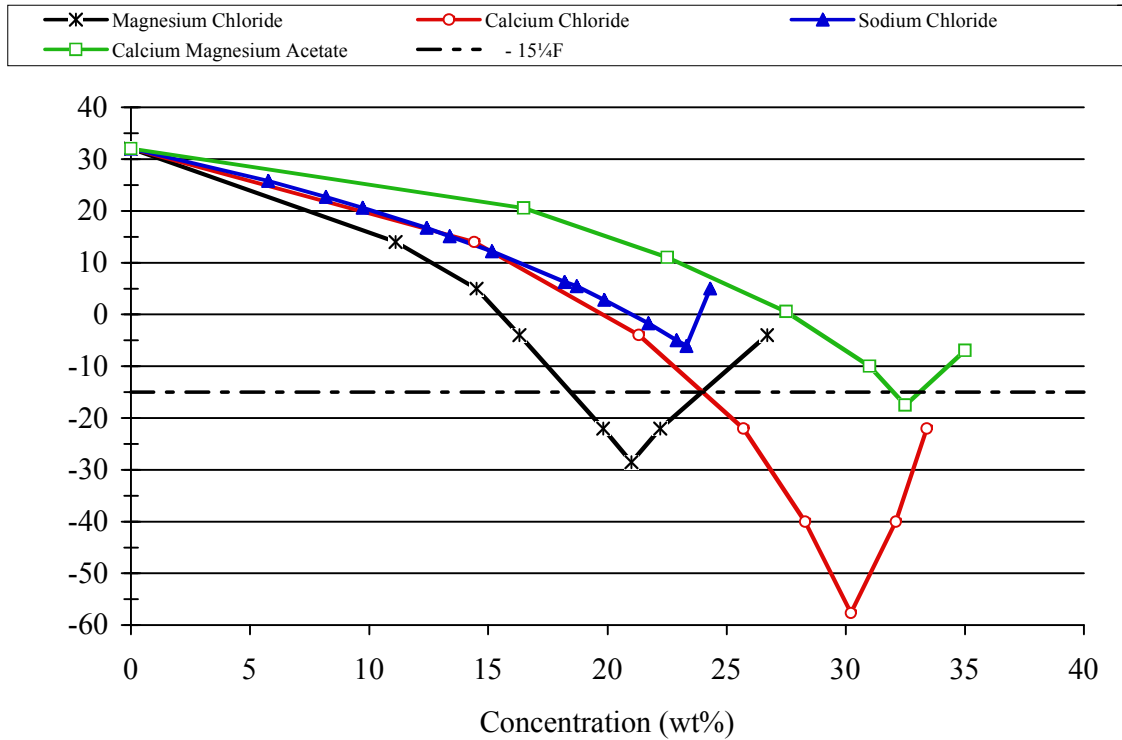


Figure 3.1. The partial phase diagrams for the deicer solutions tested showing the eutectic points for each solution. The temperature -15°F [-26°C] is shown as a dotted horizontal line.

Table 3.3. Saturation concentrations of salt solutions at two temperatures.

Deicer	Saturation Concentration at -15°F	Saturation Concentration at 32°F
	Weight Percent Salt (wt %)	Weight Percent Salt (wt %)
MgCl ₂	24% MgCl ₂	34.6% MgCl ₂
CaCl ₂	34% CaCl ₂	37.3% CaCl ₂
CMA	33% CMA	No Data
NaCl	-	26.3% NaCl

3.4.2.3. Experimental Approach

In Phase I, three distinct temperature regimes were used to test the samples.

Cyclical Temperature Test

In the first temperature regime, the specimens were cycled between being submerged in salt solution or a control solution at -15°F [-26°C] for 20 hours, to being in air at 135°F [57°C] for 20 hours. Figure 3.2 outlines the steps in the cyclic temperature test procedure.

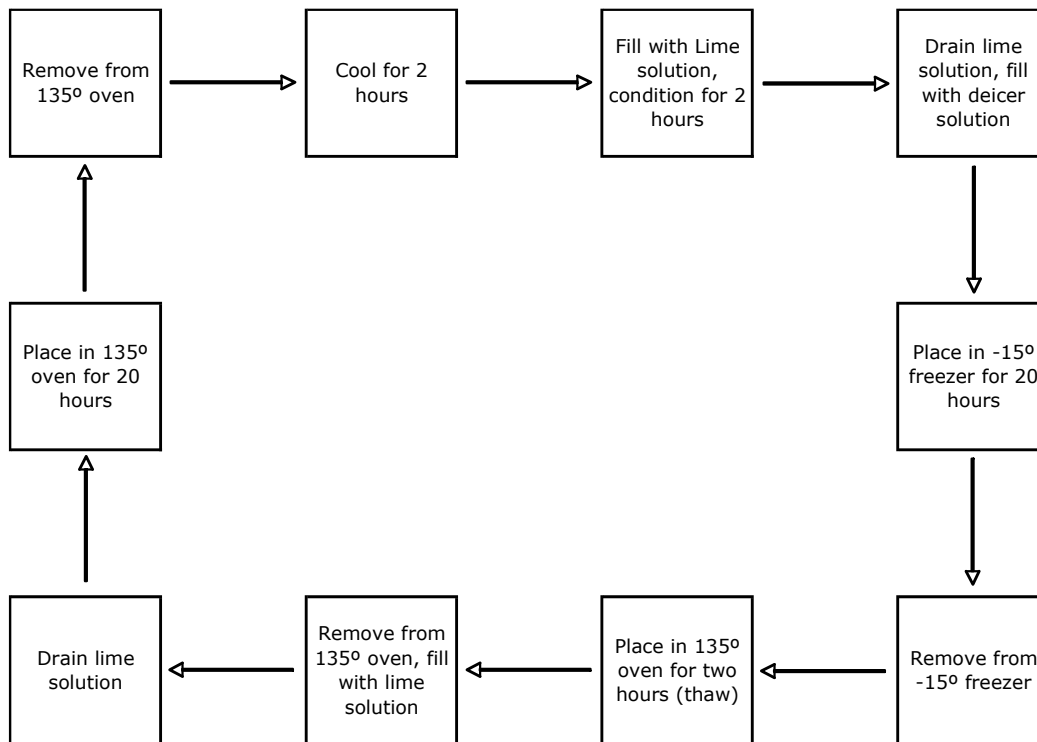


Figure 3.2. Cyclic temperature test procedure for one cycle for cylinders exposed to deicer solutions and a control solution.

Low Temperature Diffusion Test

In this regime, the specimens were submerged in the various deicer solutions and a control solution for a given amount of time (e.g. 0, 7, 14, 28, 56, 84, or 112 days) at a constant, specified temperature of 40°F [4.4°C]. Prior to testing, all the cylinders were conditioned by soaking in limewater for 72 hours at $68\text{-}70^{\circ}\text{F}$ [$20\text{-}21^{\circ}\text{C}$].

High Temperature Diffusion Test

In this regime, the specimens were submerged in the various deicer solutions and a control solution for a given amount of time (e.g. 0, 7, 14, 28, 56, 84, or 112 days) at a constant, specified temperature of 135°F [57°C]. Prior to testing, all the cylinders were conditioned by soaking in limewater for 72 hours at $68\text{-}70^{\circ}\text{F}$ [$20\text{-}21^{\circ}\text{C}$].

3.4.3 PHASE I WORK CONDUCTED AT THE UNIVERSITY OF TORONTO

3.4.3.1. Mixture Design and Preparation

For mortar specimens prepared at the University of Toronto, normal portland cement (Type I) from Lafarge was used for all mixtures. Mortar mixtures were prepared with standard graded Ottawa sand. The fine aggregate used to prepare concrete mixtures was glacial sand with a fineness modulus of 2.75. Mortar specimens were prepared using a mortar mixture with water-cement ratio of 0.485 and cement-sand ratio of 2.75 as per ASTM recommended mixture for mortar specimens (e.g. ASTM C1012-04, “*Test Method for Length Change of Hydraulic-Cement Mortars Exposed to a Sulfate Solution*”). After casting, fresh specimens were kept under moist conditions (100% relative humidity) at 73.5 °F [23 °C] for 24 ± 2 hours. Then, the molds were stripped and the specimens were removed, labeled and returned to containers filled with lime water where they were kept for 28 days.

3.4.3.2. Deicer Solutions

Five deicers were used in Phase I including NaCl, MgCl₂, calcium magnesium acetate (CMA), CaCl₂ and Caliber M1000. In addition, a reference solution of calcium hydroxide was used for comparison purposes. All experiments were done at 73.5 °F [23 °C] and the concentration of the deicers was fixed to 3 molar chloride concentration. In the case of the CMA deicer the concentration was based on the concentration of both calcium and magnesium in the solution. Table 3.4 shows the elemental composition for the exposure solutions including their pH.

Table 3.4. Exposure solution chemical analysis by ICP.

	Elemental Composition (part per million - ppm)										
	Al	Ca	Fe	Mg	P	K	Na	Si	S	Cl	pH
Ca(OH) ₂	<1	918	<1	20	<1	36	25	<1	10	26	12.7
NaCl	949	1635	1031	464	9	532	71815	7094	515	107722	7.6
Caliber M1000	<1	81	<1	54273	3	1150	1155	0.5	446	105016	7.8
MgCl ₂	110	1828	748	34604	91	346	927	222	49	107414	8.3
CaCl ₂	<2	59246	<3	<15	<2	<30	<60	<1	<10	106222	5.6
CMA	299	21999	237	27983	37	188	12296	779	159	0	8.8

3.4.3.3. Experimental Approach

For Phase I, 1 x 1 x 11¼ inch [25 x 25 x 285 mm] mortar bars and 2 inch [50 mm] cubes were cast as described above. At the end of the curing period, the specimens were removed from the container and transferred to another container filled with a deicer solution prepared using the concentrations described in Section 3.4.3.2. At specific ages various tests as described in Section 3.2.11 were performed to determine the effect of each deicer on the mortar specimens. These tests included length change, mass change, solution pH, compressive strength, and mercury intrusion porosimetry.

In addition, experiments were performed further evaluating MgCl₂ and CaCl₂ based on the fact that strong evidence was found in the literature regarding the chemical interaction between these two deicers and cement-based materials at low temperatures. The first experiment consisted of placing 2 inch [50 mm] mortar cubes in plastic containers filled with 10, 14, 20, 25 and 30% by mass of MgCl₂ solution and 5, 11, 15, 22 and 28% by mass of CaCl₂ solution at 41 °F [5 °C]. At 30 days of exposure time the mortar cubes were used to determine the changes in compressive strength. With respect to compressive strength after deicer exposure, specimens exposed to the pessimum concentration of MgCl₂ and CaCl₂ were analyzed by x-ray diffraction to identify the phase or phases involved in the chemical interaction.

For the second experiment, 1 x 1 x 11¼ inch [25 x 25 x 285 mm] mortar bars were exposed to 5, 10, 20 and 30% by mass MgCl₂ solution at 73.5 °F [23 °C] and at various exposure times the length, mass change and pH of the solution was measured.

3.5. PHASE II EXPERIMENTAL APPROACH: LABORATORY TESTING OF PORTLAND CEMENT CONCRETE

3.5.1. OVERVIEW

As will be discussed in the Section 5 of this report, the results of the Phase I experiments conducted at Michigan Tech and the University of Toronto identified that at least two of the deicing chemicals tested caused damage in portland cement mortar. Also, Phase I identified which testing regimes were ineffective at demonstrating the effects of deicing chemicals on mortar, and by implication, concrete. These ineffective tests were not continued from Phase I to Phase II. The low temperature experiment conducted at Michigan Tech had interesting results, clearly demonstrating that chemical attack by some deicers is a real possibility and this test was conducted in Phase II. Additionally, from the DOT survey, feedback from the panel members, and conversations with practitioners around the upper Midwest and western states, it is clear that scaling is a common manifestation of distress associated with deicers of all types. Therefore, Phase II of this research focused on two general areas: scaling and chemical attack to concrete in the presence of deicers. Tests were performed to assess scaling, the mechanisms of chemical attack, and the effects of sealers on preventing distress. Also, fundamental material parameters were determined including the relative diffusivity of the various deicers in concrete and the role of solution strength on concrete degradation. For Phase II, work was performed at Michigan Tech and at the University of Toronto. The Phase II approach will be described for each institution separately.

3.5.2. PHASE II WORK CONDUCTED AT MICHIGAN TECH

3.5.2.1. Mixture Design and Preparation

The concrete mixtures used in this experiment were made with a high quality, partially crushed gravel coarse aggregate (maximum aggregate size of 1 inch [25 mm]) from Superior Sand & Gravel, Hancock Michigan, natural sand (same source as coarse aggregate), 564 lb/yd³ [335 kg/m³] Lafarge Alpena Type I/II cement, Master Builders / BASF Admixtures VR-90 vinsol resin air entraining agent (air content of 6 ± 1 percent), and a w/c of 0.45 and 0.55. The slump was 3 ± 0.5 inch [76 ± 12 mm]. Two additional mixtures were prepared, one made with 15 percent replacement of cement with Class F fly ash provided by Boral Materials and another made with 35 percent replacement of cement with GGBFS provided as a blended cement product from Lafarge. The cement used in the blended product was also a Lafarge Type I/II from Alpena, Michigan. For quality control purposes, the concrete mixtures were sampled and tested to determine concrete fresh properties such as slump, air content, temperature, and unit weight. Specimens were moist cured at 100% humidity in the molds for one day, and then wet cured in lime saturated baths for 27 days. Specimens cast were standard 4 inch diameter by 8 inch high [100 mm by 200 mm] cylinders, which in turn were section to produce three 4 inch diameter by 2 inch high [100 mm by 50 mm] specimens per cylinder.

3.5.2.2. Deicing Solutions

A goal of Phase II was to determine the effect of deicer concentration on observed concrete degradation. To accomplish this, two concentration levels were established for deicer solutions and are referred to as Low and High. These concentrations are given in Table 3.6. The high concentrations were identical to the concentrations used for each deicer in Phase I with the exception of CMA. In

Phase I, CMA was tested at the typical application strength. This did not take into account the dilution that occurs as the deicer melts ice or snow. For Phase II, the CMA solution concentration was reduced to 15% CMA by weight. The MBAP concentration was chosen to provide approximately the same amount of Mg^{2+} ions in solution as compared to the standard $MgCl_2$ solution. The exact composition of the MBAP solution cannot be calculated on a gravimetric or volumetric basis as the exact composition of the product is unknown. The low concentration was chosen to be approximately 40% of the high concentration. The concentrations of deicer solutions used in Phase II are given in Table 3.5.

Table 3.5. Deicer concentrations used for testing in Phase II.

	Concentration (wt%)		Cl ⁻ Molality	
	Low	High	Low	High
NaCl	7.3	17.8	1.35	3.7
CaCl ₂	7.3	17.0	1.43	3.7
MgCl ₂	6.2	15.0	1.38	3.7
CMA	6.5	15.0		
MBAP	8.1	15.0		
Lime Water	Saturated Solution			

3.5.2.3. Experimental Approach

Low Temperature Testing

The low temperature testing conducted in Phase I at Michigan Tech revealed some interesting results, particularly with respect to the observations of chemical degradation observed in the specimens submerged in $CaCl_2$ and $MgCl_2$. To more fully understand these observations, 4 inch diameter by 2 inch high [100 mm by 50 mm] cylindrical concrete specimens were made and submerged in deicer solutions at the concentrations listed in Table 3.6. Each week, the solution was replaced, and mass change monitored, with the specimens being analyzed after 56 and 84 days of submersion, as indicated in Table 3.7.

Analytical Methods

For examining the specimens from the Phase II low temperature experiment, the same petrographic analysis were applied as was done in Phase I. Optical microscopy, electron, and x-ray microscopy was used to characterize the microstructure of the specimens. A thorough analysis of the specimens was performed to identify any possible signs of chemical or physical distress.

Table 3.6. Experimental design for cylindrical specimens tested at 40 °F [4.4 °C].

PC – portland cement only, Fly Ash – portland cement with fly ash substitution, GGBFS - portland cement with GGBFS substitution. Numbers in cells represent the number of two inch by four-inch specimens placed in each solution. High and Low concentrations are as described in Table 3.5.

Specimen Description	CaCl ₂		MgCl ₂		NaCl		CMA		MBAP		Lime Water
	High	Low	High	Low	High	Low	High	Low	High	Low	sat'd
0.45 w/c PC	2	2	2	2	2	2	2	2	2	2	2
0.55 w/c PC	2	2	2	2	2	2	2	2	2	2	2
0.55 w/c PC Silane Sealant	2	2	2	2	2	2	2	2	2	2	
0.55 w/c PC Siloxane Sealant	2	2	2	2	2	2	2	2	2	2	
0.45 w/cm Fly Ash	2	2	2	2	2	2	2	2	2	2	2
0.55 w/cm Fly Ash	2	2	2	2	2	2	2	2	2	2	2
0.55 w/cm Fly Ash Silane Sealant	2	2	2	2	2	2	2	2	2	2	
0.55 w/cm Fly Ash Siloxane Sealant	2	2	2	2	2	2	2	2	2	2	
0.45 w/cm GGBFS	2	2	2	2	2	2	2	2	2	2	2
0.55 w/cm GGBFS	2	2	2	2	2	2	2	2	2	2	2
0.55 w/cm GGBFS Silane Sealant	2	2	2	2	2	2	2	2	2	2	
0.55 w/cm GGBFS Siloxane Sealant	2	2	2	2	2	2	2	2	2	2	

3.5.3 PHASE II WORK CONDUCTED AT THE UNIVERSITY OF TORONTO

3.5.3.1 Mixture Design and Preparation

The concrete slabs and prisms used for testing were prepared along with 4 x 8 inch [100 x 200 mm] cylinder specimens cast for compressive strength testing at 28 days of age. The mixtures used were prepared with 615 lb/yd³ [365 kg/m³] Lafarge Type I portland cement and a w/c of 0.45. The coarse aggregate used was a durable crushed limestone with a nominal maximum size of 3/4 inch [19 mm]. A medium range water-reducing admixture (Master Builders / BASF Admixtures Pozzolith 200N) and air-entraining admixture (Master Builders / BASF Admixtures Micro Air) were added to the concrete mixtures with a target air content of 6 ± 1 percent. The concrete mixtures were sampled and tested to determine concrete fresh properties such as slump, air content, temperature, and unit weight.

After casting, the concrete specimens were covered with plastic sheets and wet burlap to avoid drying of the test surface (e.g. concrete slabs). On the next day, the forms were stripped and specimens were removed, labeled and stored in a moist room (100% relative humidity and 73.5 °F [23 °C]) for 28 days or until required for testing.

3.5.3.2 Deicer Solutions

Concrete slabs were exposed to the pessimum concentration found in the mortar experiments in Phase I for MgCl_2 and CaCl_2 . The concrete slabs were exposed to 22% CaCl_2 and 20% MgCl_2 at 41 °F [5 °C] for a year as a preconditioning period and then the salt scaling resistance was determined following the standard procedure; that is, exposing the concrete surface to either 4% CaCl_2 or 4% MgCl_2 for 50 cycles (one cycle consisted of 16 hours freezing and 8 hours thawing). At the same time, reference slabs were exposed to 23% NaCl for a year and then their salt scaling resistance was determined following the standard procedure. Concrete prisms were subjected to rapid cycles of freezing and thawing using water an exposure solution that was CaCl_2 , MgCl_2 and NaCl fixed to 3 molar by chloride concentration.

3.5.3.3 Experimental Approach

Salt Scaling Resistance

Concrete slabs 12 x 9 x 3 inch [305 x 230 x 75 mm] were cast and tested for salt scaling resistance in accordance with ASTM C672 *Test Method for Scaling Resistance of Concrete Surfaces Exposed to De-Icing Chemicals*. Styrofoam berms were attached and sealed with silicone around the perimeter of the slabs to create a dyke so the exposure solution could be ponded on the surface. The slabs were kept in the freezer for 16 hours at 0 °F [-18 °C] and then taken from the freezer to laboratory conditions (73.5 °F [23 °C], 45 to 55% relative humidity) for 8 hours. Some modifications were introduced to the standard so it could be used to differentiate any deterioration caused by the chemical interaction between the deicer and the concrete matrix. The concrete slabs were exposed to 22% CaCl_2 and 20% MgCl_2 at 41 °F [5 °C] for a year as a preconditioning period and then the salt scaling resistance was determined following the standard procedure; that is, exposing the concrete surface to either 4% CaCl_2 or 4% MgCl_2 for 50 cycles (one cycles consisted of 16 hours freezing and 8 hours thawing). At the same time, reference slabs were exposed to 23% NaCl for a year and then their salt scaling resistance was determined. X-ray diffraction was performed on the surface of the concrete at the end of the exposure period.

Freezing and Thawing Resistance

Concrete prisms 3 x 3 x 11¼ inch [75 x 75 x 285 mm] were subjected to freezing and thawing cycles in conformance with ASTM C666 *Test Method for Resistance of Concrete to Rapid Freezing and Thawing*. The Procedure A, rapid freezing and thawing in water was performed with one modification, deicers chemicals were used instead of water. In short, the specimens are subjected to a complete cycle when its temperature decreases from 40 to 0 °F [4.4 to -18 °C] and then increases from 0 to 40 °F [-18 to 4.4 °C] within 2 to 5 hours. During this test the length change is measured every week and the durability factor is calculated from the fundamental transverse frequency as well. A maximum number of 36 cycles are required for determination of these two properties every week. The determination of the fundamental transverse frequency was done according to ASTM C215, “*Test Method for Fundamental Transverse, Longitudinal, and Torsional Resonant Frequencies of Concrete Specimens.*”

SECTION 4. CHARACTERIZATION OF FIELD SPECIMENS

4.1 APPROACH

To approach Task 5, Characterization of Field Specimens, the research team began by meeting with the technical advisory panel and discussing possible sites that 1) represent the range of deicers being currently studied and 2) either exhibit some level of distress or represent new pavements that have been exposed only to one specific deicer. The intent of the study was to identify distress mechanisms that are visible in field concrete and study field concrete that has been exposed to a specific deicer, to assess how that one specific deicer is interacting with the concrete. The sites identified are listed below in Table 4.1.

Table 4.1 Pavement sites identified in cooperation with the technical advisory panel for examination as part of Task 5.

Colorado, State Highway 83, South of Denver near Milepost 57
Iowa, eastbound US Highway 34, western end of the Burlington Bridge.
Idaho, westbound Interstate Highway 184 west of Boise, near milepost 3
Montana, westbound Interstate Highway 90 bridge deck near milepost 117
South Dakota, Sioux Falls, eastbound 26th Street left turn lane

In general, the sites initially identified lacked unambiguous evidence of distress associated with deicers. To continue the field study, the research team obtained cores from a number of bridge decks in Montana that were exhibiting distress. Although these bridge decks are maintained using various non-NaCl deicers, they are all bridge decks that have been in service for numerous years and as a result, have been exposed to NaCl deicers for a significant portion of their service lives. Ultimately, because of this maintenance history, any distress identified would be difficult to associate with a specific deicing chemical. However, the team felt it was important to examine these bridge decks to determine if any visible mechanisms of chemical attack could be identified. The specific bridge decks sampled are listed below in Table 4.2.

Table 4.2 Bridge decks identified as additional field sites for examination as part of Task 5.

Montana, eastbound Interstate Highway 90 bridge deck, near milepost 61.8, Tarkio interchange
Montana, westbound Interstate Highway 90 bridge deck, near milepost 37.2, Sloway interchange

Presented in the remainder of this section are the results obtained from petrographic analyses of the samples representing two of the sites identified in Tables 4.1 and 4.2. A complete summary of the results of the characterization of all field sites is provided in the Appendix to this report.

4.2 PETROGRAPHIC ANALYSIS OF IDENTIFIED SITES

4.2.1 South Dakota, Sioux Falls, eastbound 26th Street left-turn lane onto northbound, Interstate Highway 29

This pavement was placed on November 1, 1996, and exposed to $MgCl_2$ brine shortly thereafter on November 15, 1996. A letter came with the cores that described the pavement surface to be in good condition, but stated that the cores taken near the joint looked like they had been eaten away. Figure 4.1 shows the locations of the cores, and Figure 4.2 shows an overview of the turn lane. Figure 4.3 shows the core holes from near the joint. What had been interpreted in the letter as deterioration was just the normal appearance of a concrete joint as exposed in cross section. Figures 4.4 and 4.4 show photographs of the individual cores. Two of the cores were cut into slabs and polished: core SD-1 (at a joint), and core SD-4 (mid-panel). Figures 4.6 through 4.9 show the slabs as polished, after staining with phenolphthalein, and after treatment to enhance air voids and cracks. The phenolphthalein stain showed normal carbonation depths. The black and white treatment did not reveal any macro-cracking in either of the cores. Table 4.3 summarizes the air void parameters. Both sets of slabs showed adequate entrained air, with spacing factors of 0.158 mm and 0.176 mm for cores SD-1 and SD-4 respectively. Figure 4.10 shows an example stereomicroscope image of the air void structure. Initially, water to cement ratio estimations were performed both on a thin section prepared from a core taken at the joint, (SD-1) and on a thin section prepared from a core taken at mid-panel, (SD-4). The w/c estimates were consistently higher for the core taken at the joint versus the core taken at mid-panel. To double-check the results, an additional thin section was prepared from the same pair of cores. To further investigate the trend, thin sections were also prepared from another pair of cores representing the joint, (SD-7) and the mid-panel, (SD-5). The same trend of higher w/c estimates near the joint was observed. Figures 4.11 and 4.12 show the images used to make the measurements from the first thin section prepared from the top of core SD-1 (at a joint). The results of the w/c estimation are summarized in Table 4.4, with an average w/c value of 0.47 as compared to the 28-day moist cured mortar sample standards. Figure 4.13 shows images collected from the second thin section prepared from core SD-1. These images were not masked and used for w/c measurement, but provided as a visual check on the first thin section. Figures 4.14 and 4.15 show the images used to make the measurements from the thin section prepared from the top of core SD-7 (also at a joint). The results of the w/c estimation are summarized in Table 4.5, with an average w/c value of 0.45. Figures 4.16 and 4.17 show the images used to make the measurements from the thin section prepared from the top of core SD-4 (from mid-panel). The results of the w/c estimation are summarized in Table 4.6, with an average w/c value of 0.38. Figure 4.18 shows images collected from the second thin section prepared from core SD-4. These images were not masked and used for w/c measurement, but provided as a visual check on the first thin section. Figures 4.19 and 4.20 show the images used to make the measurements from the thin section prepared from the top of core SD-5 (also from mid-panel). The results of the w/c estimation are summarized in Table 4.7, with an average w/c value of 0.35. Figure 4.21 compares cement paste fluorescence histograms from the four cores. The samples prepared from the joint fluoresced consistently brighter than the samples prepared from mid-panel. Figures 4.22 through 4.25 show chloride profiles from cores SD-3 and SD-7.

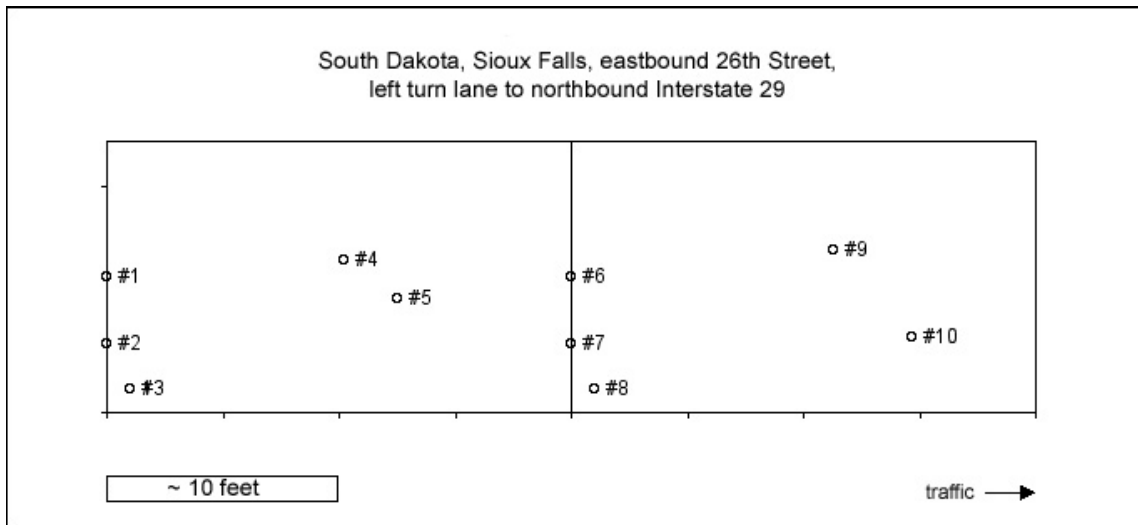


Figure 4.1. Diagram to show core locations based on submitted field information.



Figure 4.2. Photograph of core site.

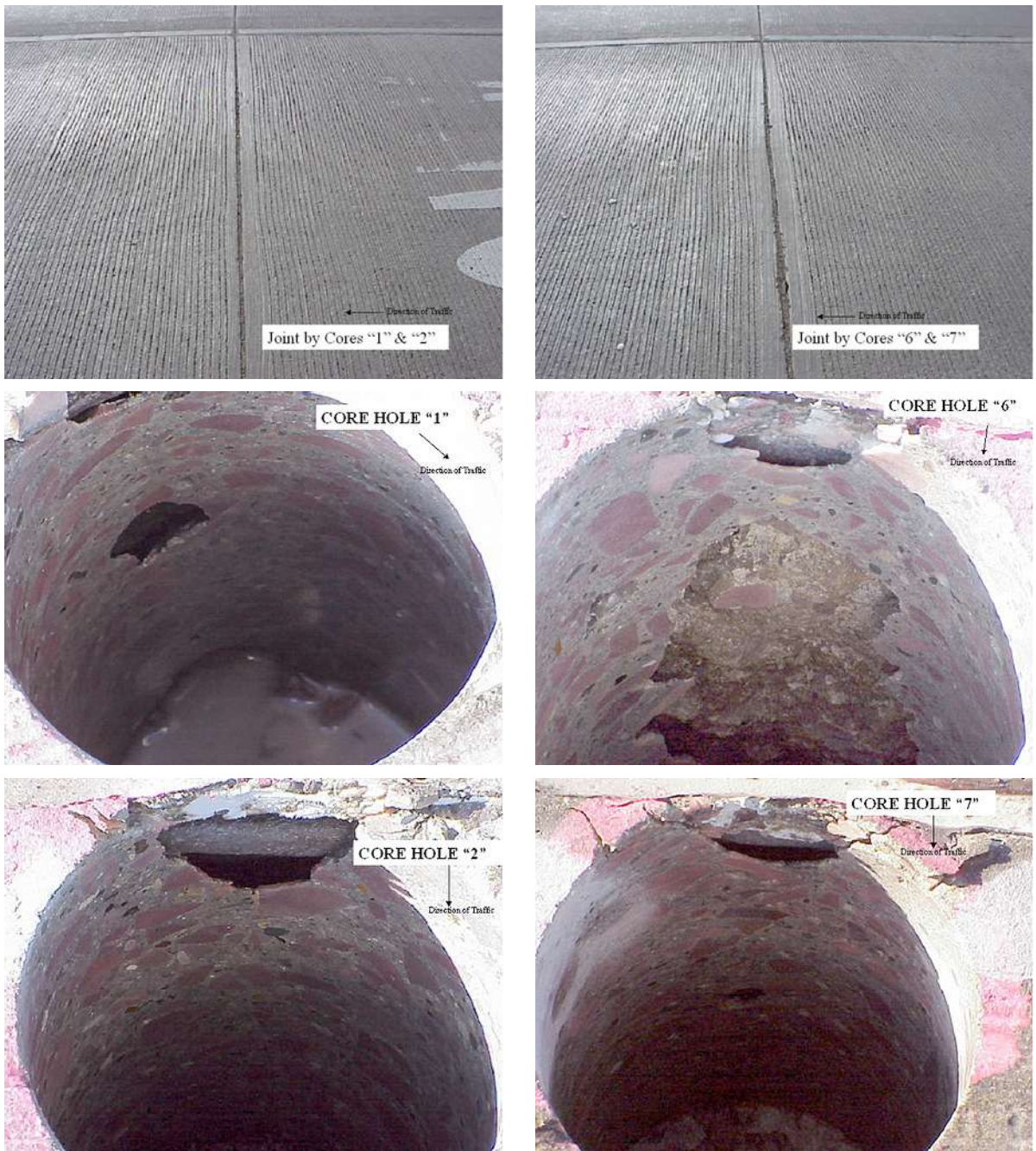


Figure 4.3. Photographs of the joints sampled, and of the holes after the coring operation.

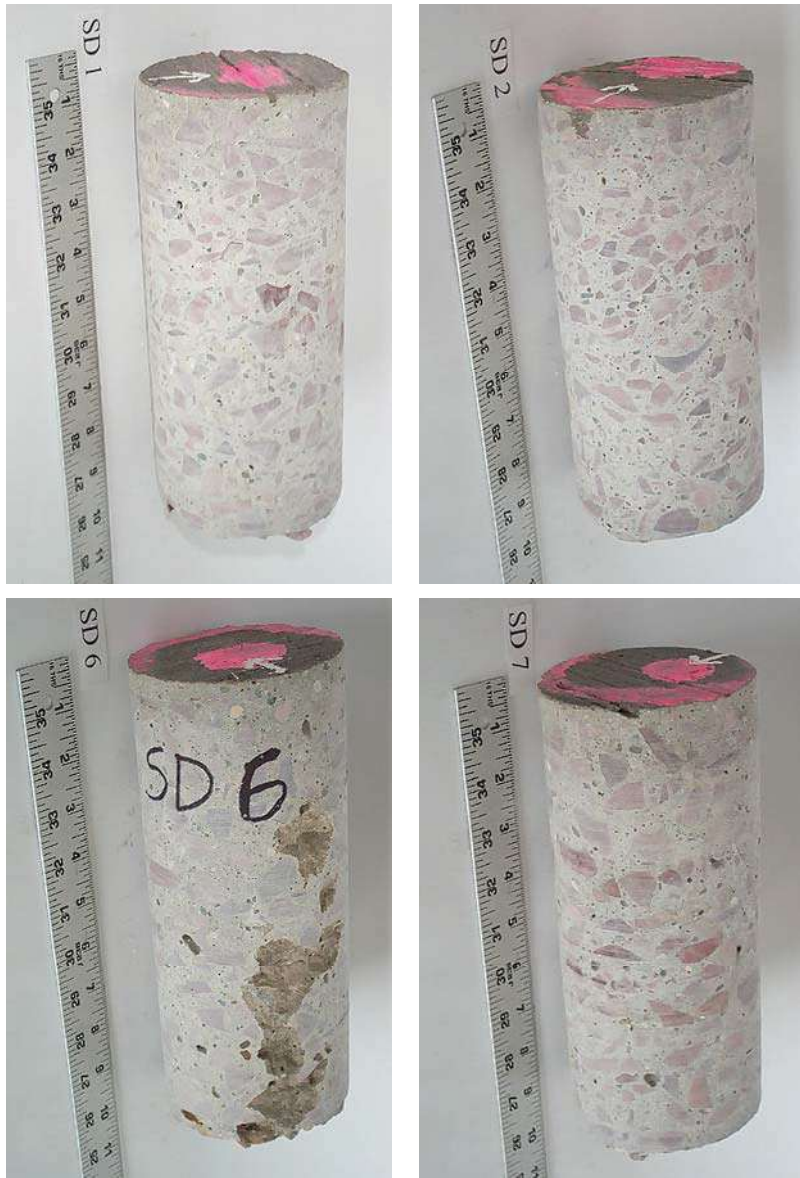


Figure 4.4. Cores taken at joint.

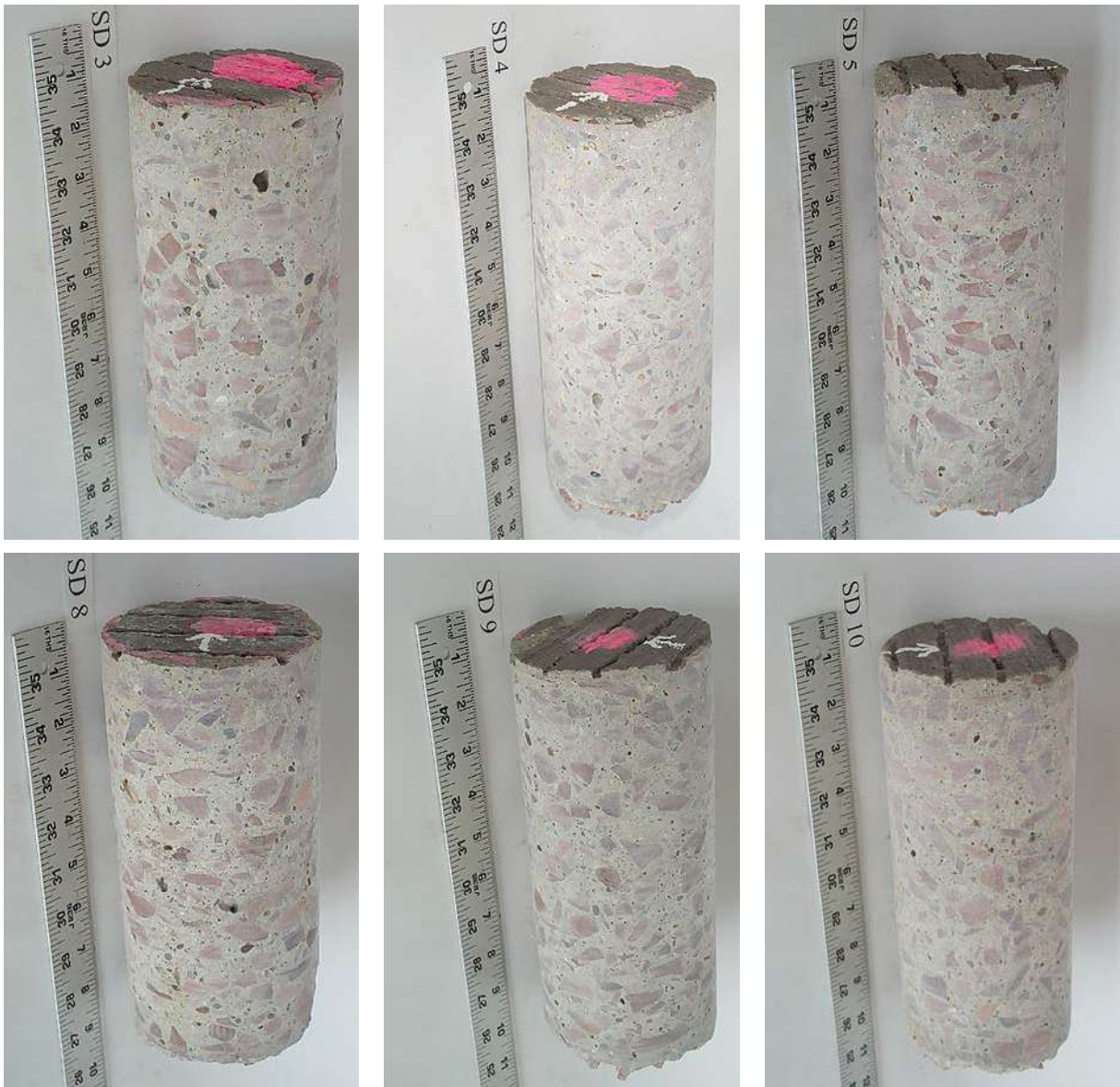


Figure 4.4. Cores taken away from joint.

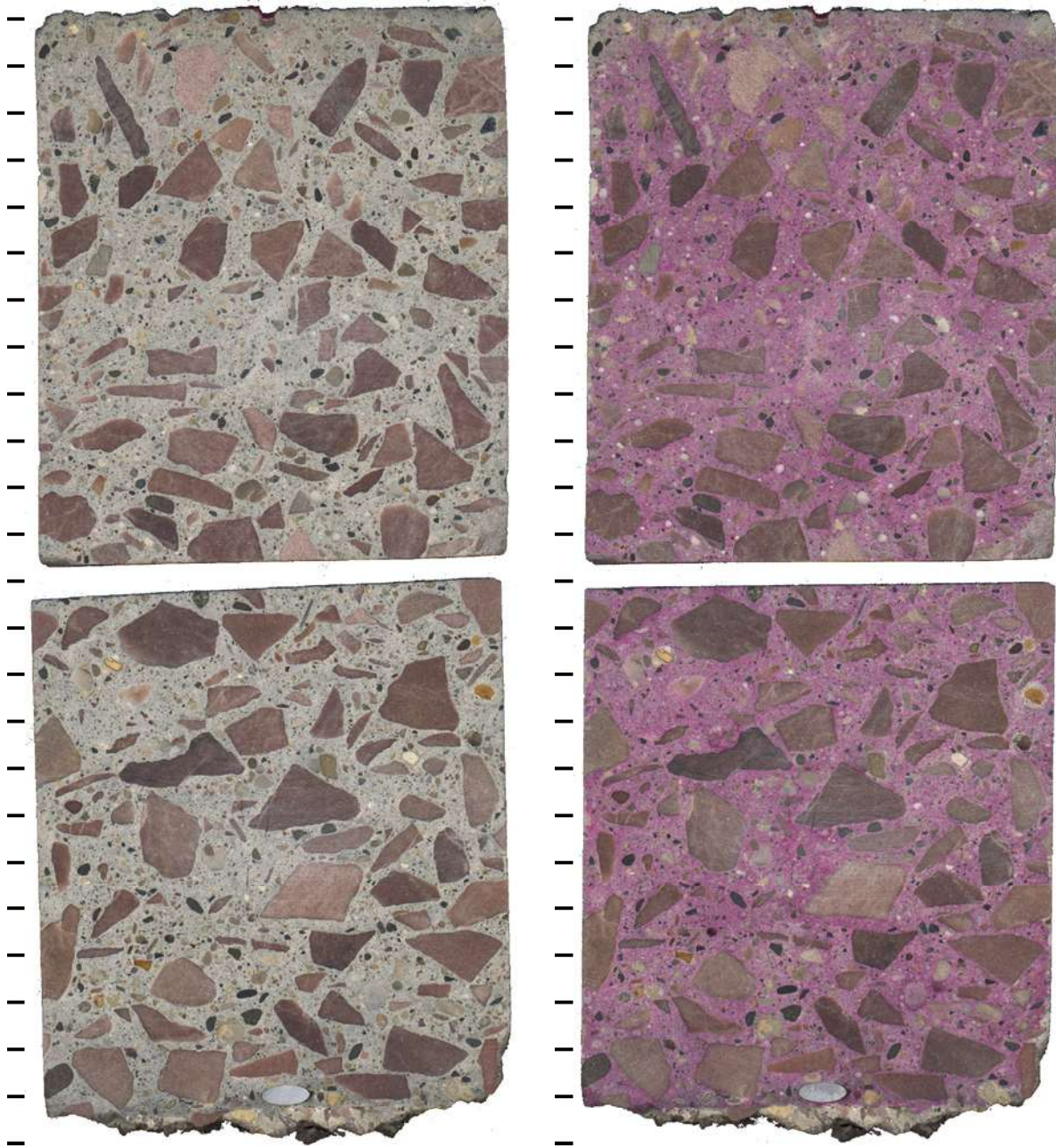


Figure 4.6. Polished slabs to show complete cross-section through core SD-1 both before (left) and after application of phenolphthalein stain (right) tic marks every cm.

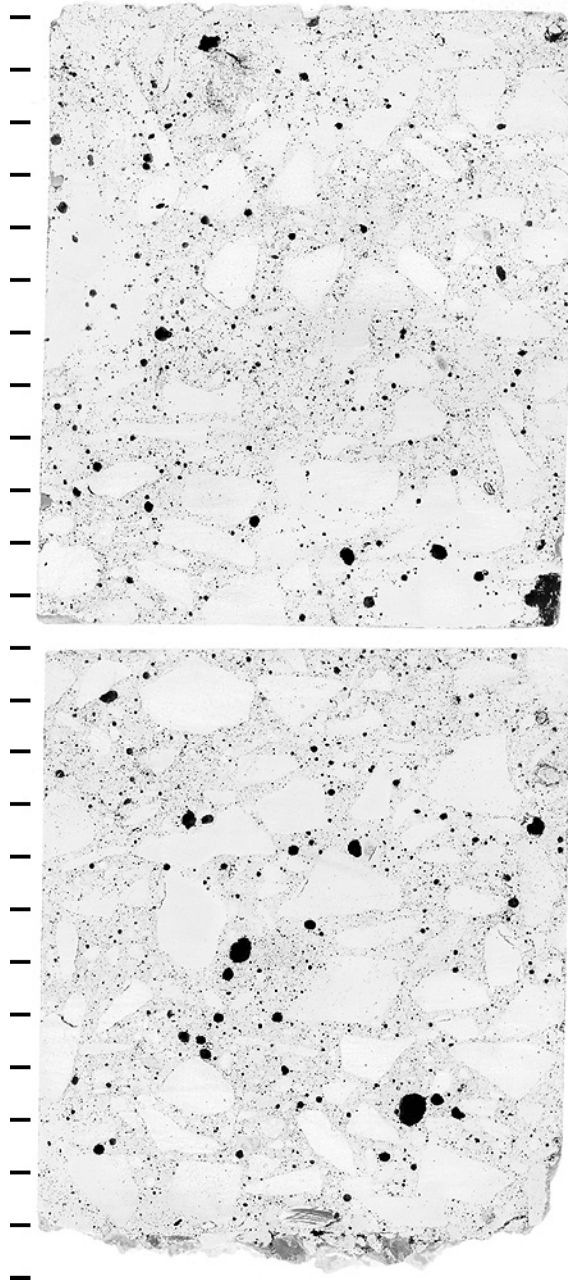


Figure 4.7. Polished slabs to show complete cross-section through core SD-1 after treatment to enhance appearance of air voids and cracks, tic marks every cm.

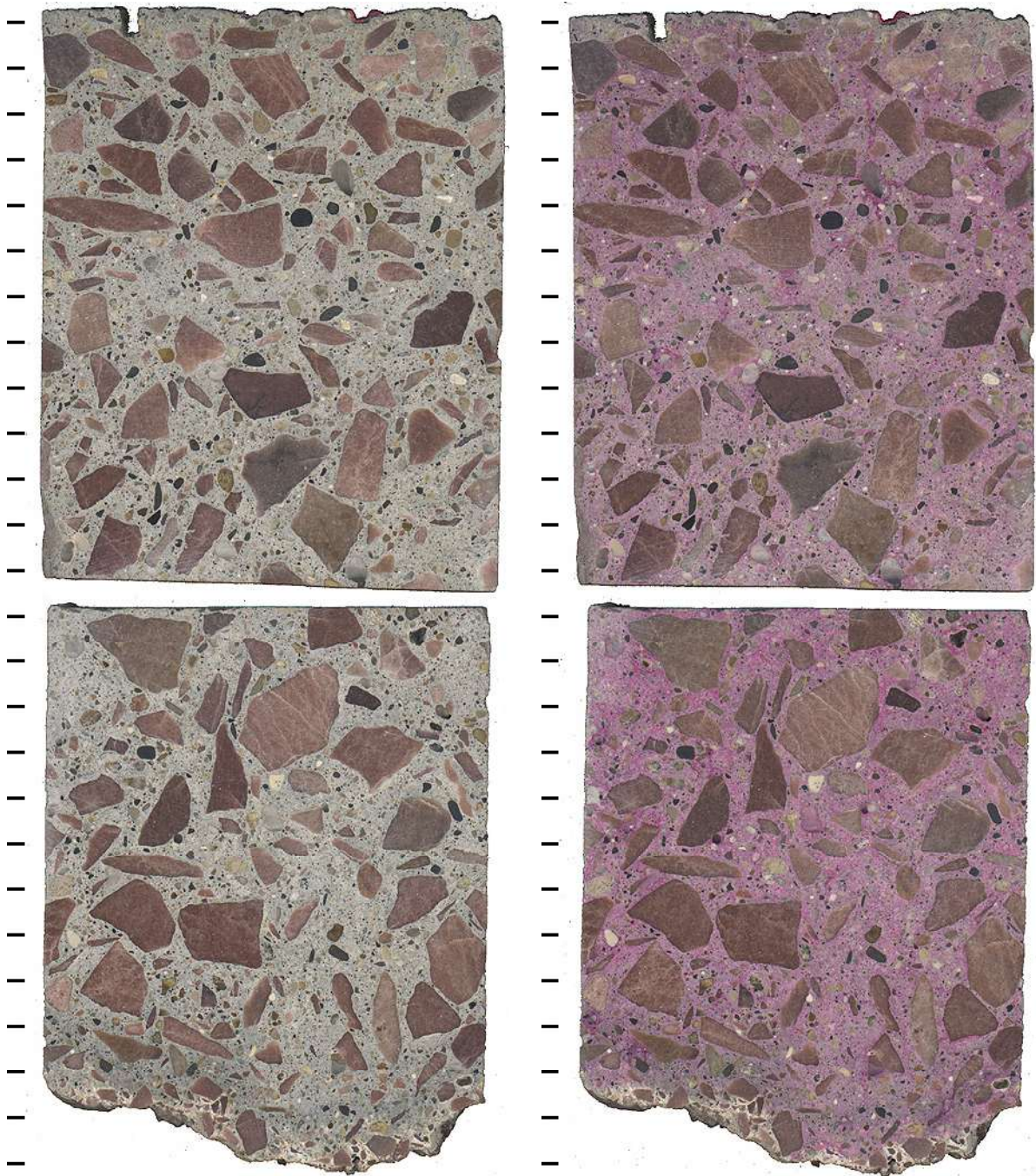


Figure 4.8. Polished slabs to show complete cross-section through core SD-4 both before (left) and after application of phenolphthalein stain (right) tic marks every cm.

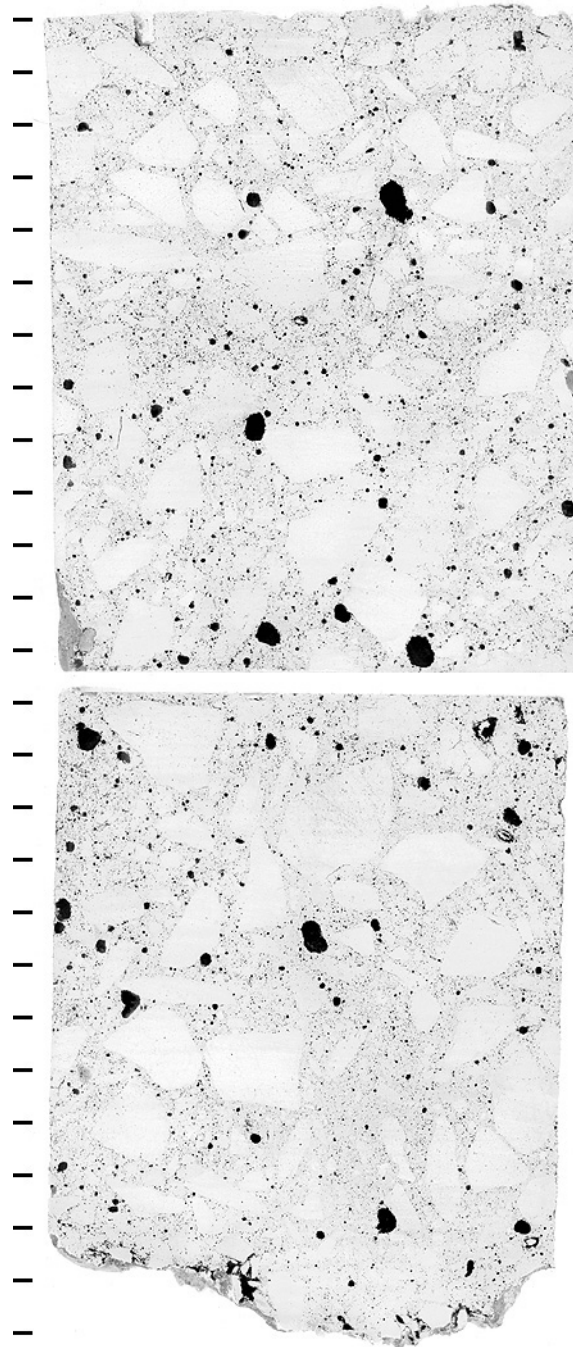


Figure 4.9. Polished slabs to show complete cross-section through core SD-4 after treatment to enhance appearance of air voids and cracks, tic marks every cm.

Table 4.3. Air void parameters

Sample ID	SD-01	SD-04
Location	At joint	Away from Joint
Raw data		
Total traverse length (mm)	3625.5	3625.5
Area analyzed (cm ²)	71.0	71.0
Air stops	85	91
Paste stops	396	382
Aggregate stops	907	915
Secondary deposit stops	0	0
Total stops	1388	1388
Number of air intercepts	1577	1420
Number of filled void intercepts	2	0
Results		
Air vol%	6.1	6.6
Paste vol%	28.5	27.5
Aggregate vol%	65.3	65.9
Secondary deposit vol%	0.0	0.0
Existing average chord length (mm)	0.141	0.167
Existing paste/air ratio	4.7	4.2
Existing air void specific surface (mm ⁻¹)	28.4	23.9
Existing air void frequency (voids/m)	435	392
Existing spacing factor (mm)	0.158	0.176
Original average chord length (mm)	0.141	0.167
Original paste/air ratio	4.7	4.2
Original air void specific surface (mm ⁻¹)	28.4	23.9
Original air void frequency (voids/m)	436	392
Original spacing factor (mm)	0.158	0.176

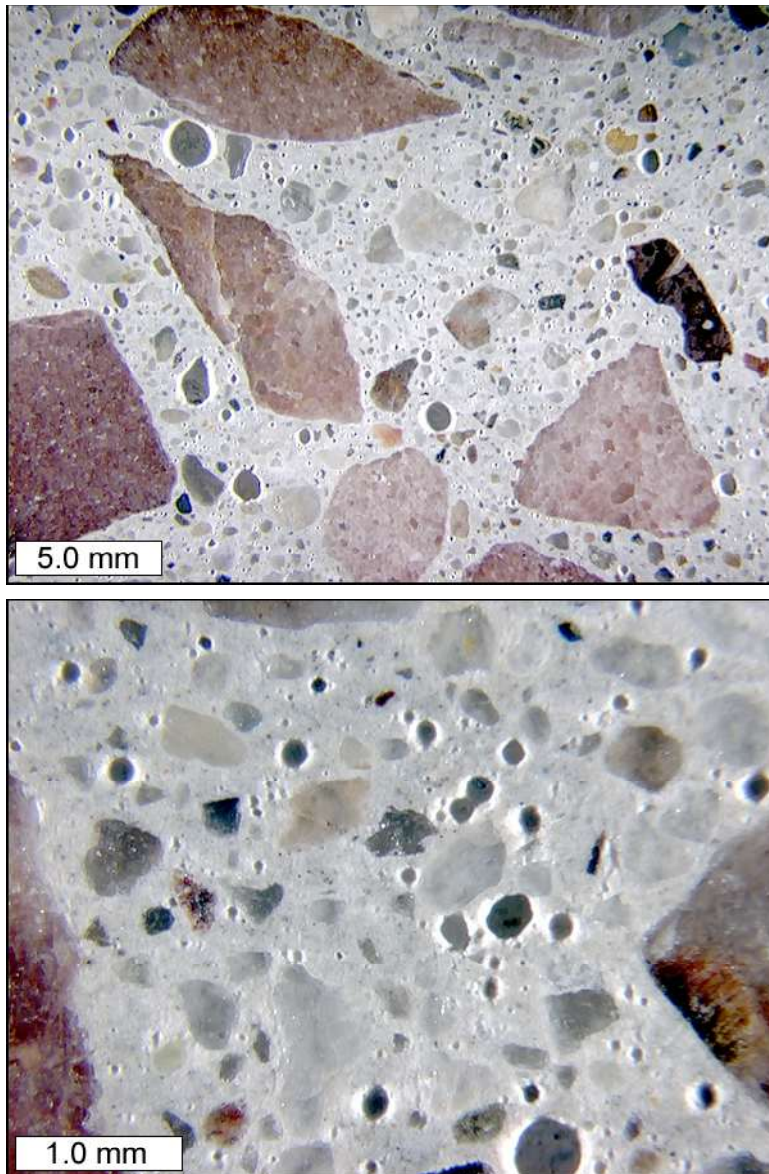


Figure 4.10. Stereo microscope images to show air void structure on polished slab from core SD-4.

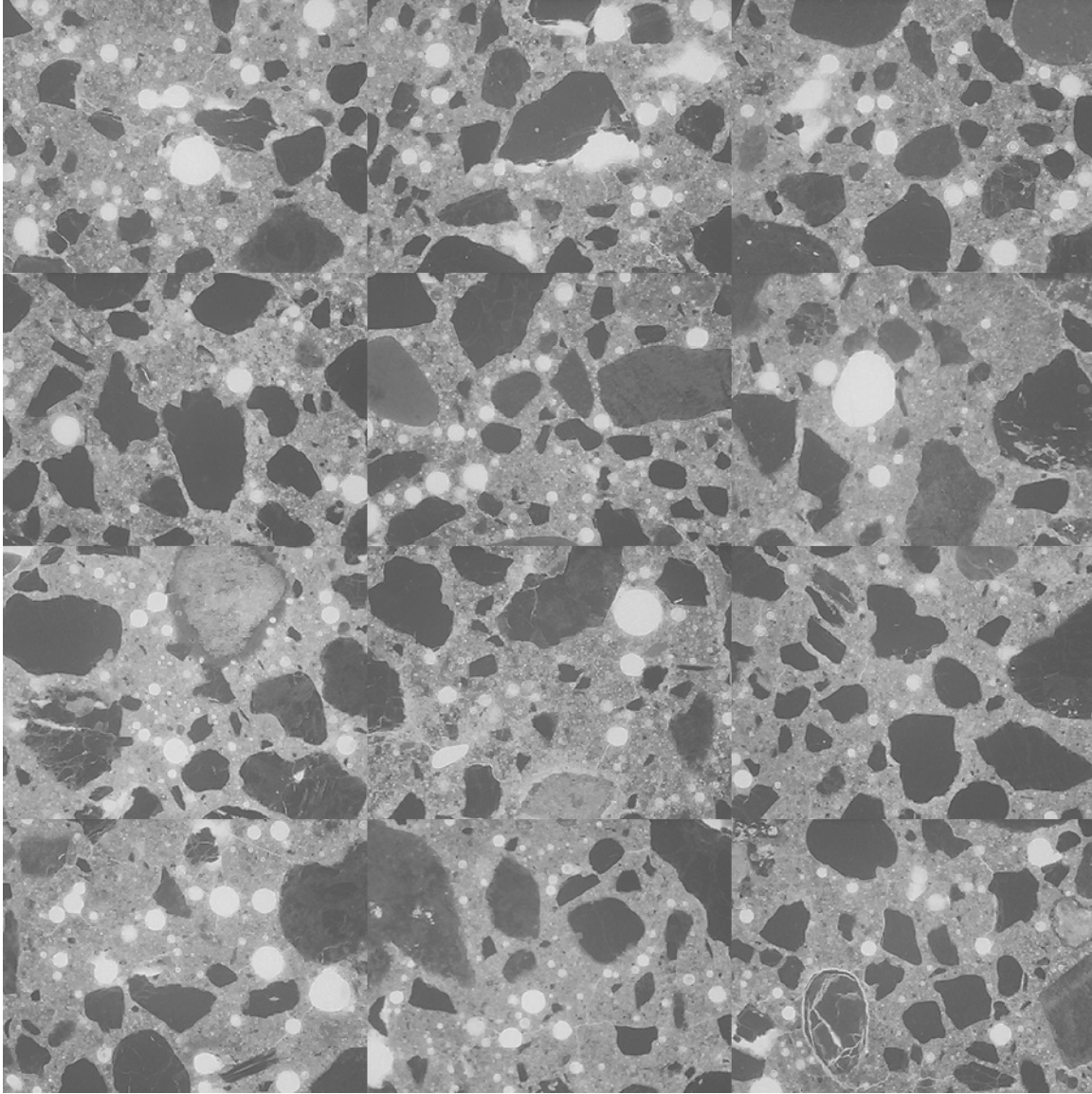


Figure 4.11. Mosaic of 12 frames collected from thin section prepared from billet cut from top portion of core SD-1 (each individual frame measures 2.612 x 1.959 mm).

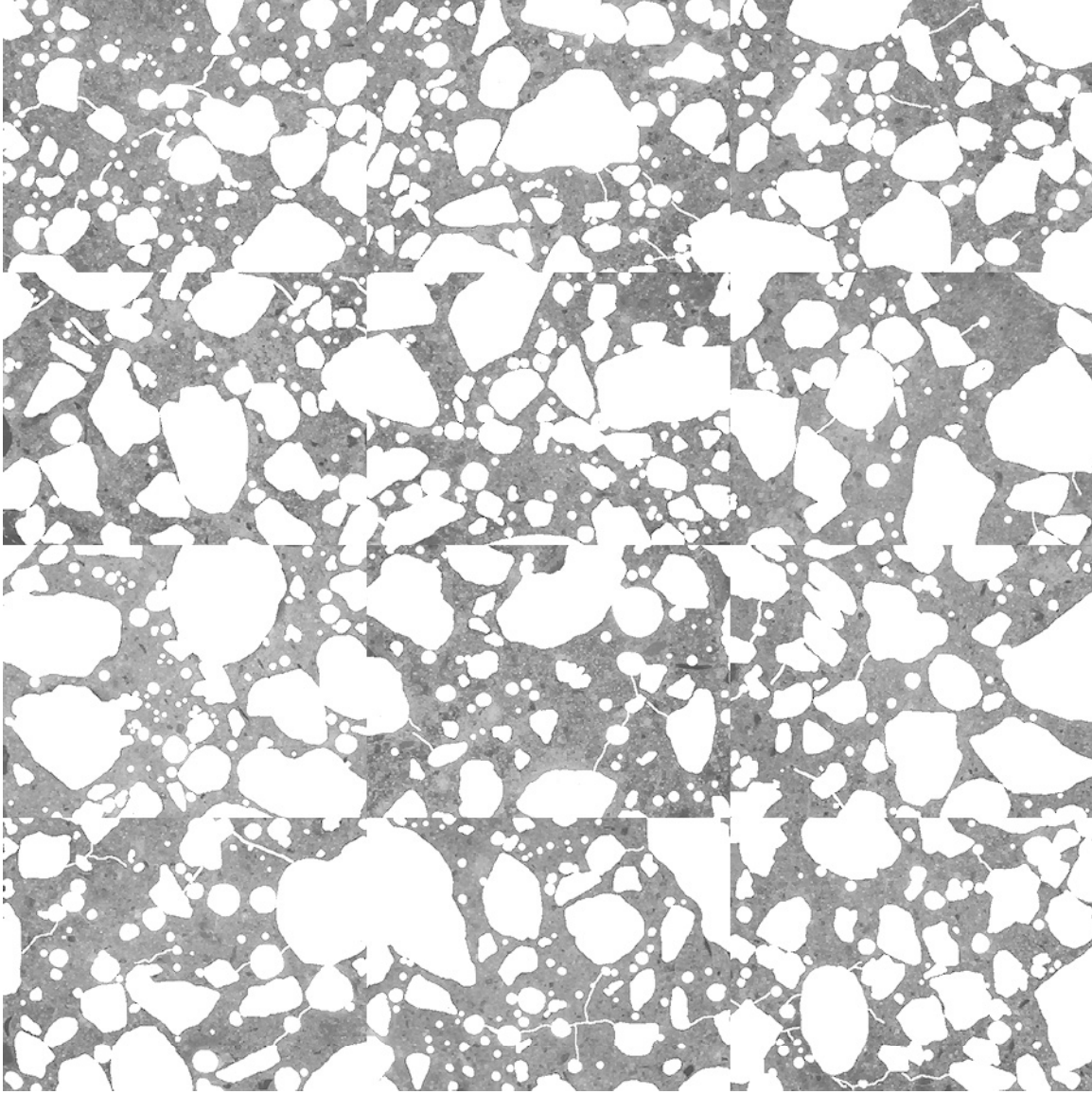


Figure 4.12. Mosaic of 12 frames collected from thin section prepared from billet cut from top portion of core SD-1 after masking out air voids, fine aggregate, and micro-cracks to isolate cement paste (each individual frame measures 2.612 x 1.959 mm).

Table 4.4. Average cement paste pixel intensities per frame, and equivalent w/c values (as compared to 28-day moist cured mortar samples) for core SD-1.

Cement Paste Pixel Fluorescence Measurements (average intensity per frame)			
101	101	95	95
93	98	120	97
101	102	101	97
equivalent w/c ($y = 0.0044x + 0.0329$)			
0.47	0.47	0.45	0.45
0.44	0.46	0.56	0.46
0.47	0.48	0.47	0.46

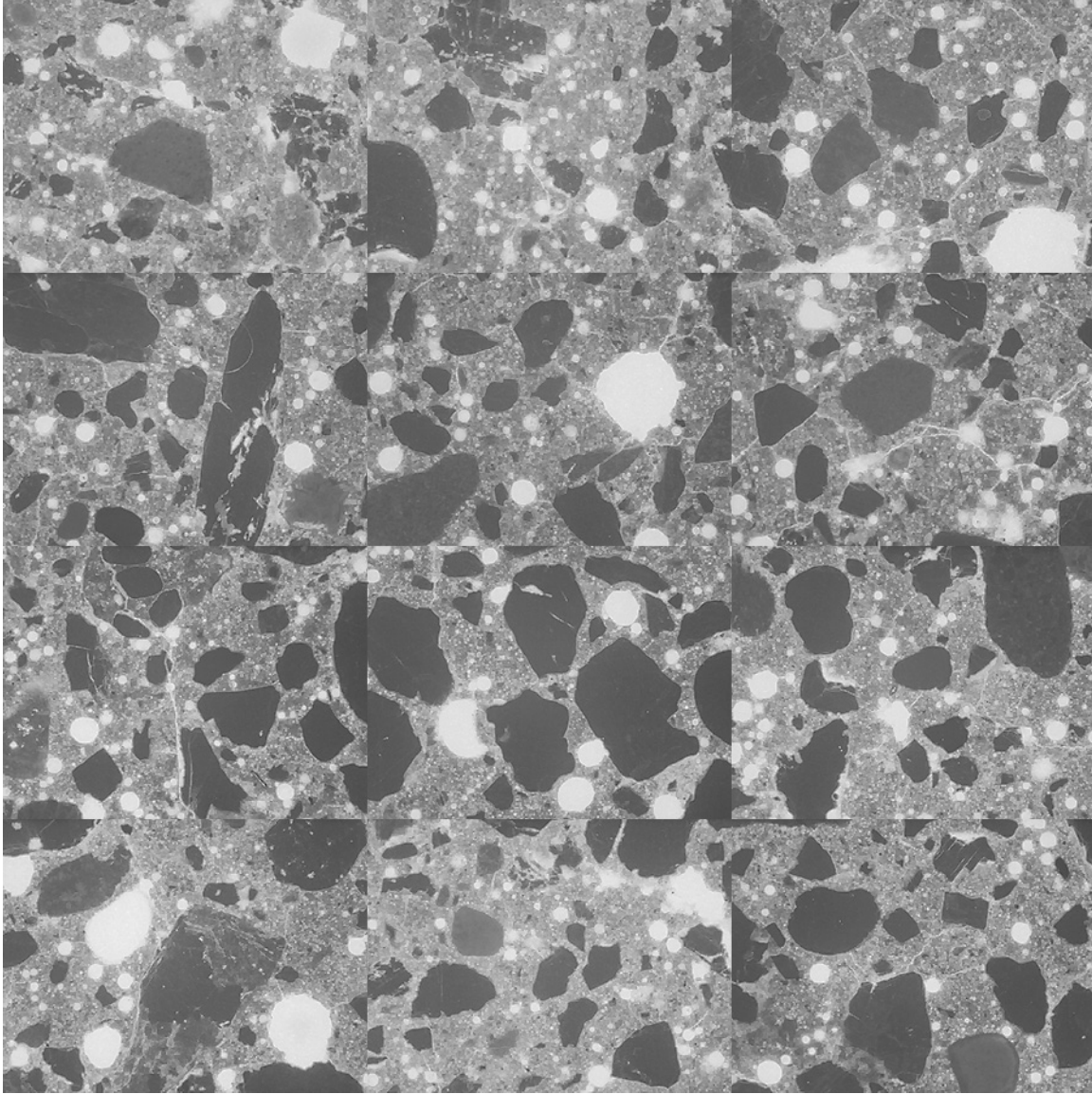


Figure 4.13. Mosaic of 12 frames collected from thin section prepared from a second billet cut from top portion of core SD-1 (each individual frame measures 2.612 x 1.959 mm). These frames were not masked and used for *w/c* determination, but recorded as visual check against the first section prepared from core SD-1.

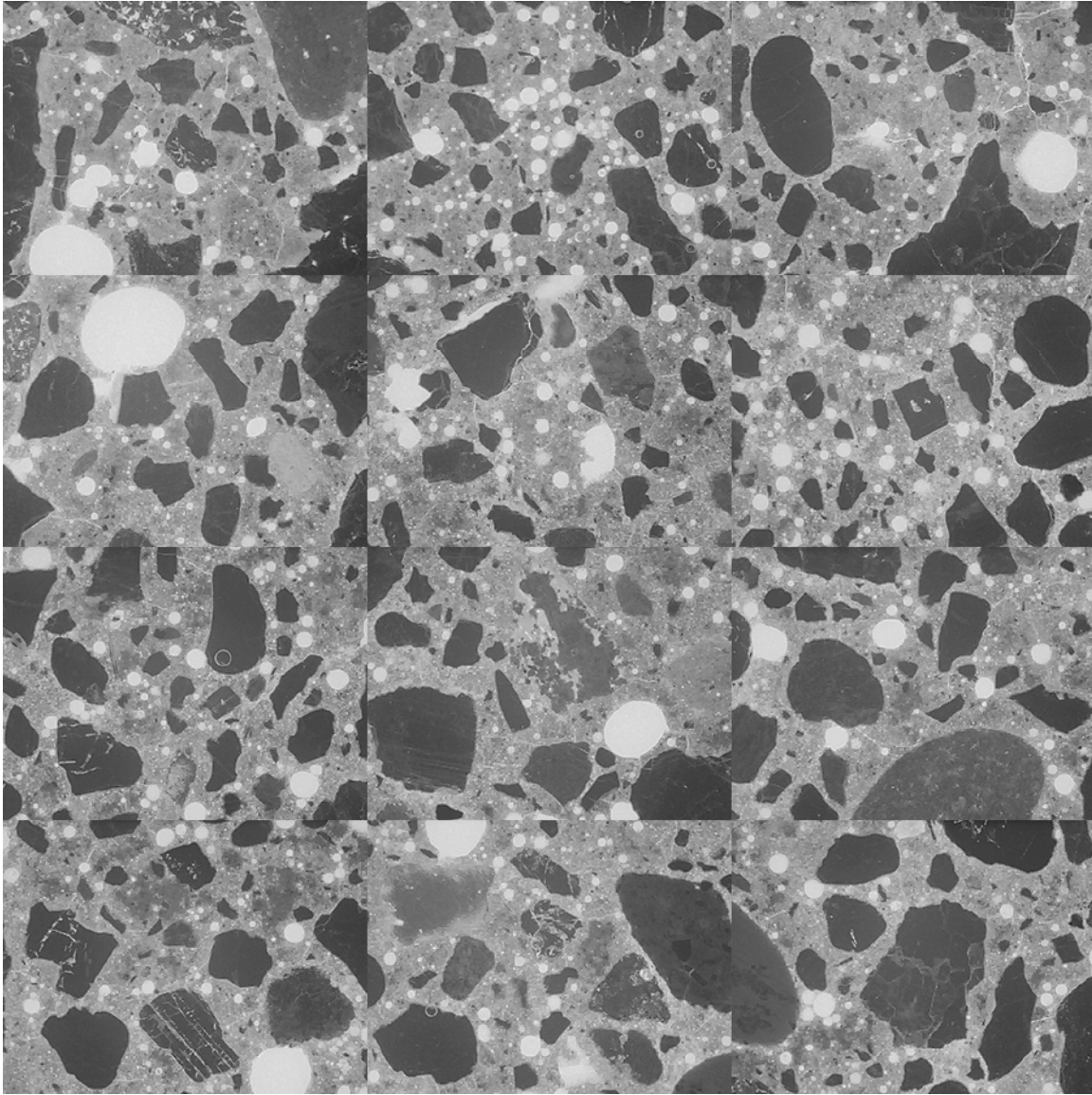


Figure 4.14. Mosaic of 12 frames collected from thin section prepared from billet cut from top portion of core SD-7 (each individual frame measures 2.612 x 1.959 mm).

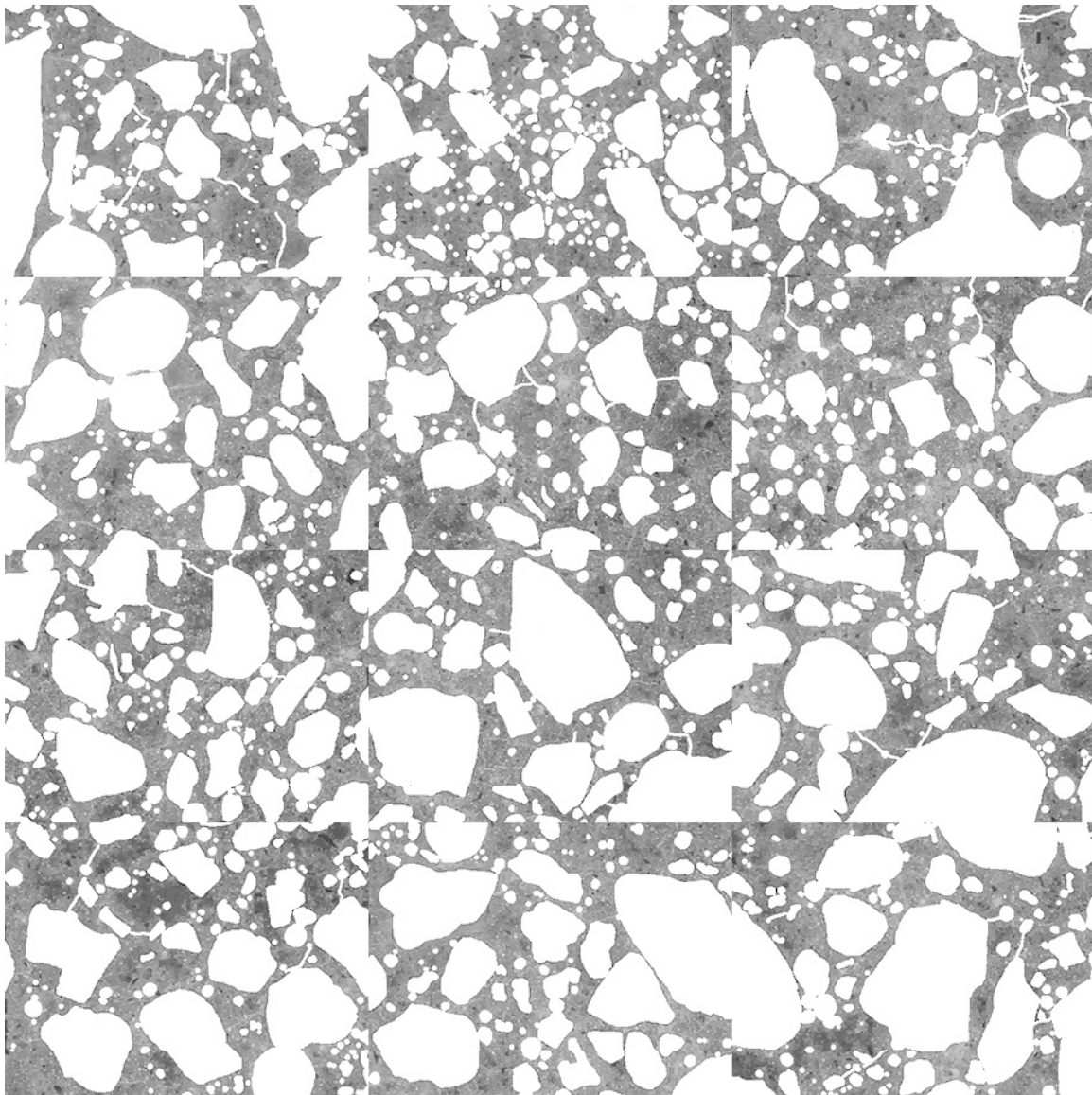


Figure 4.15. Mosaic of 12 frames collected from thin section prepared from billet cut from top portion of core SD-7 after masking out air voids, fine aggregate, and micro-cracks to isolate cement paste (each individual frame measures 2.612 x 1.959 mm).

Table 4.5. Average cement paste pixel intensities per frame, and equivalent w/c values (as compared to 28-day moist cured mortar samples) for core SD-7.

Cement Paste Pixel Fluorescence Measurements (average intensity per frame)			
97	97	96	103
92	102	91	95
95	89	103	95
equivalent w/c ($y = 0.0044x + 0.0329$)			
0.46	0.45	0.45	0.48
0.44	0.48	0.43	0.45
0.45	0.42	0.48	0.45

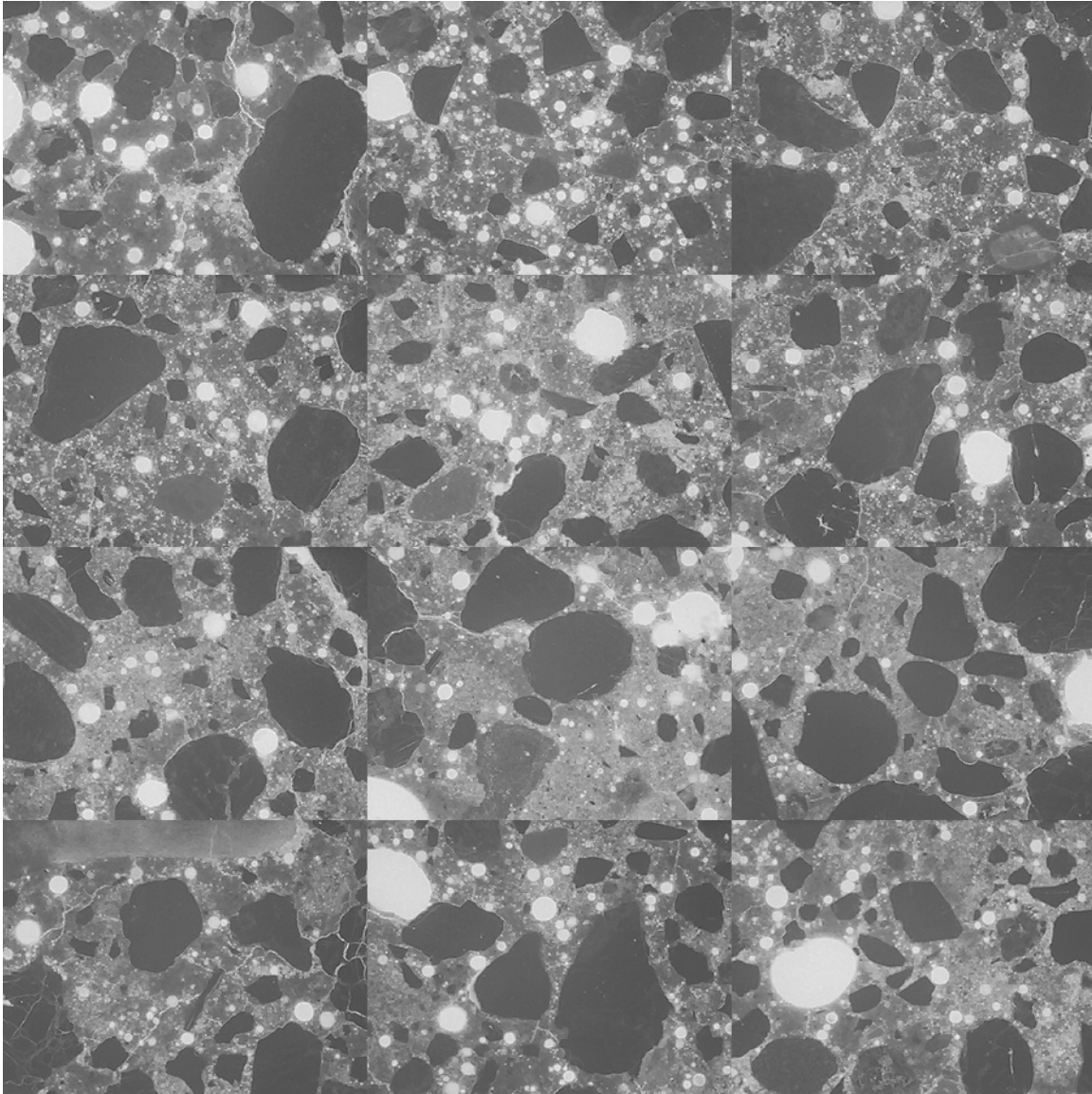


Figure 4.16. Mosaic of 12 frames collected from thin section prepared from billet cut from top portion of core SD-4 (each individual frame measures 2.612 x 1.959 mm).

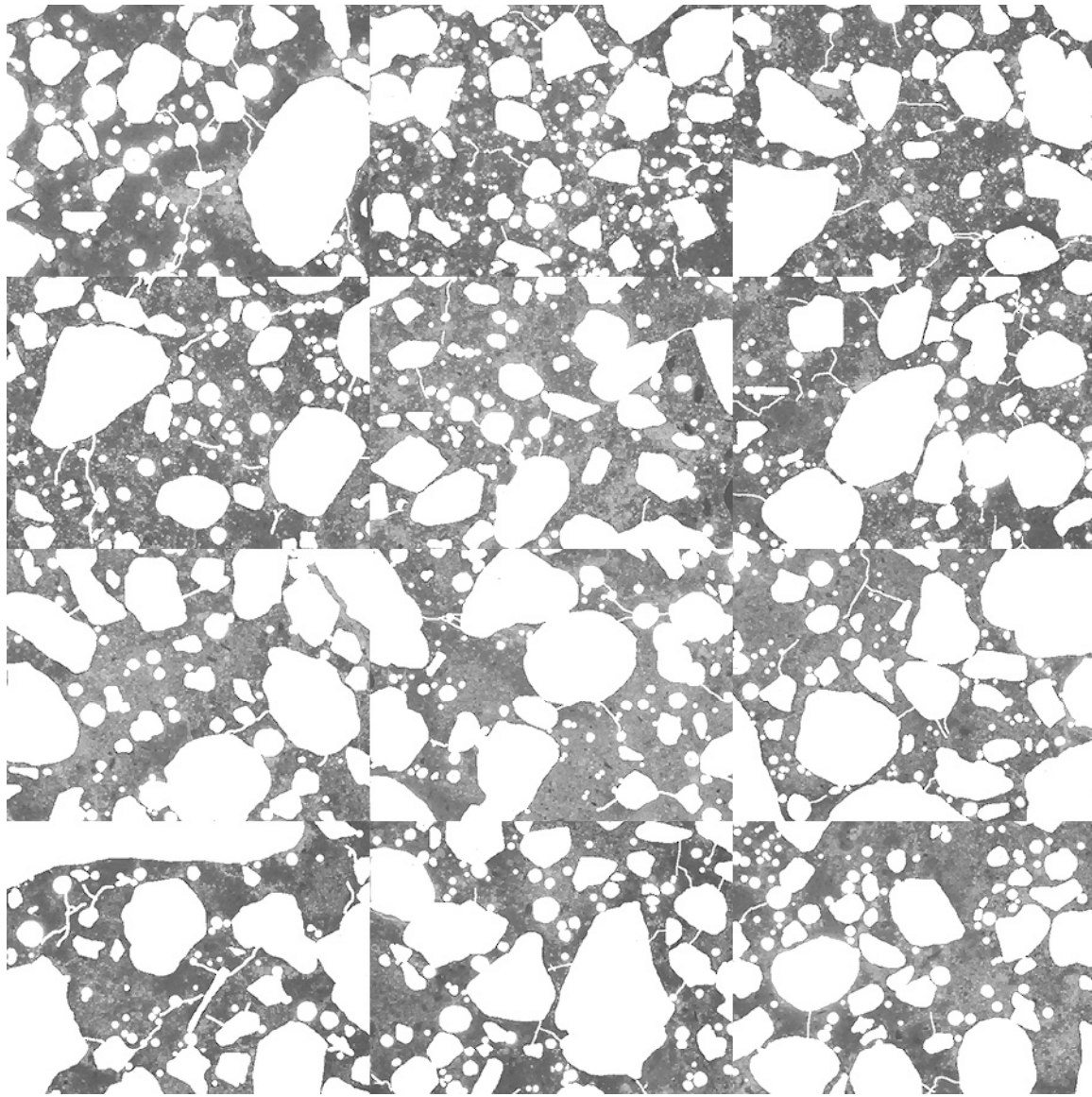


Figure 4.17. Mosaic of 12 frames collected from thin section prepared from billet cut from top portion of core SD-4 after masking out air voids, fine aggregate, and micro-cracks to isolate cement paste (each individual frame measures 2.612 x 1.959 mm).

Table 4.6. Average cement paste pixel intensities per frame, and equivalent w/c values (as compared to 28-day moist cured mortar samples) from core SD-4.

Cement Paste Pixel Fluorescence Measurements (average intensity per frame)			
78	78	71	76
93	90	94	85
85	68	70	70
equivalent w/c ($y = 0.0044x + 0.0329$)			
0.37	0.37	0.34	0.37
0.44	0.35	0.43	0.44
0.40	0.33	0.34	0.34

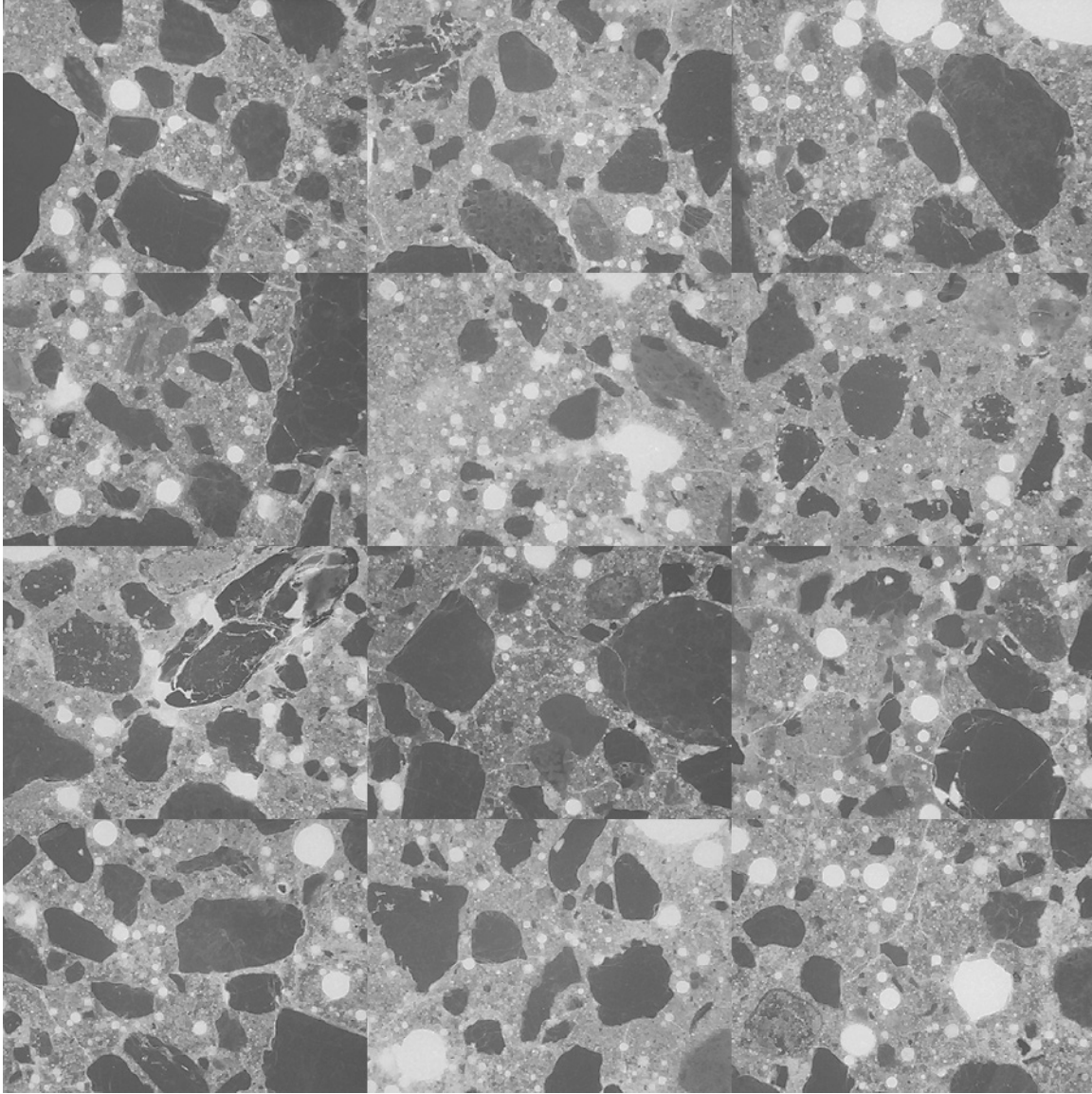


Figure 4.18. Mosaic of 12 frames collected from thin section prepared from a second billet cut from top portion of core SD-4 (each individual frame measures 2.612 x 1.959 mm). These frames were not masked and used for *w/c* determination, but recorded as visual check against the first section prepared from core SD-4.

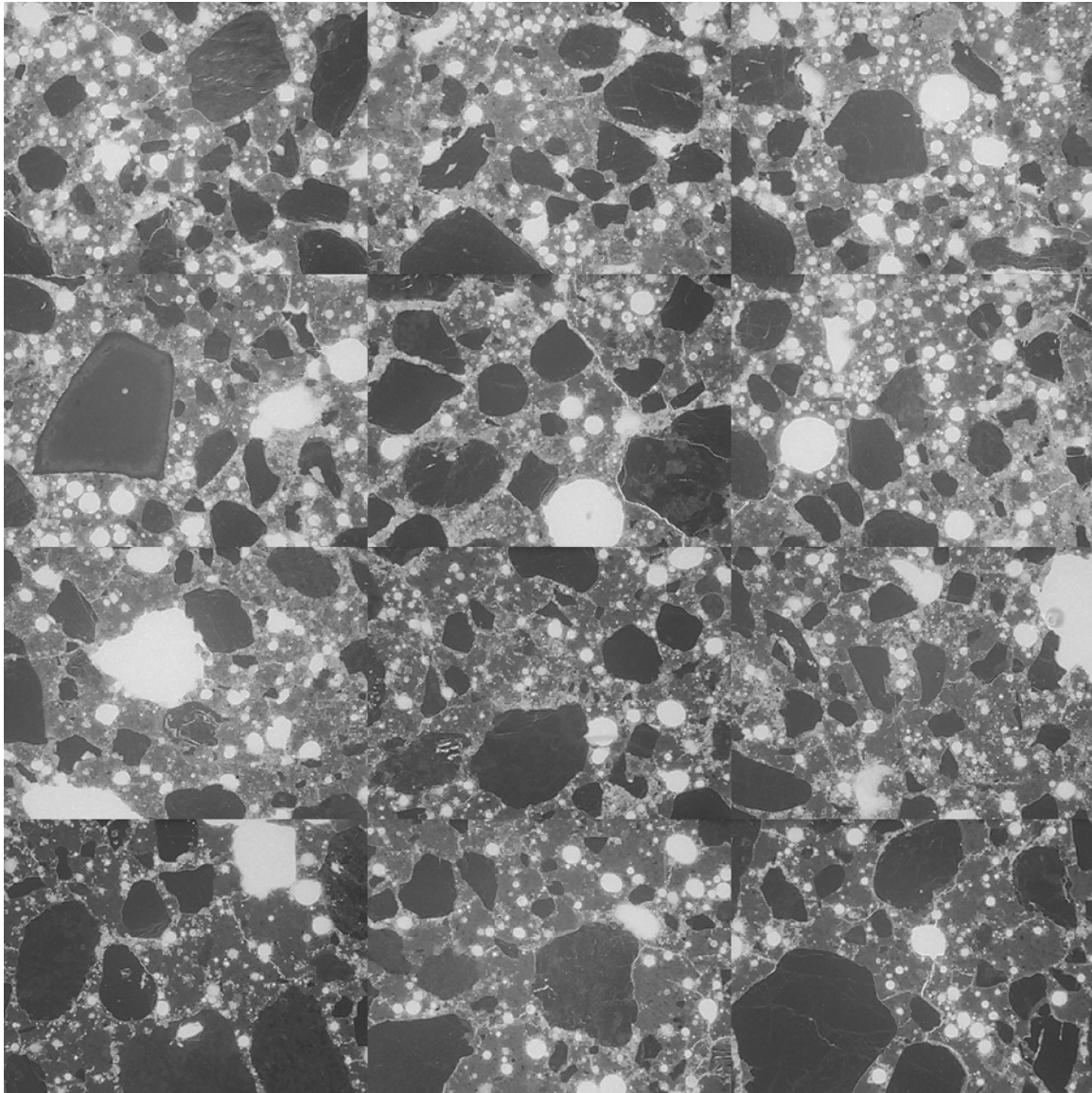


Figure 4.19. Mosaic of 12 frames collected from thin section prepared from billet cut from top portion of core SD-5 (each individual frame measures 2.612 x 1.959 mm).

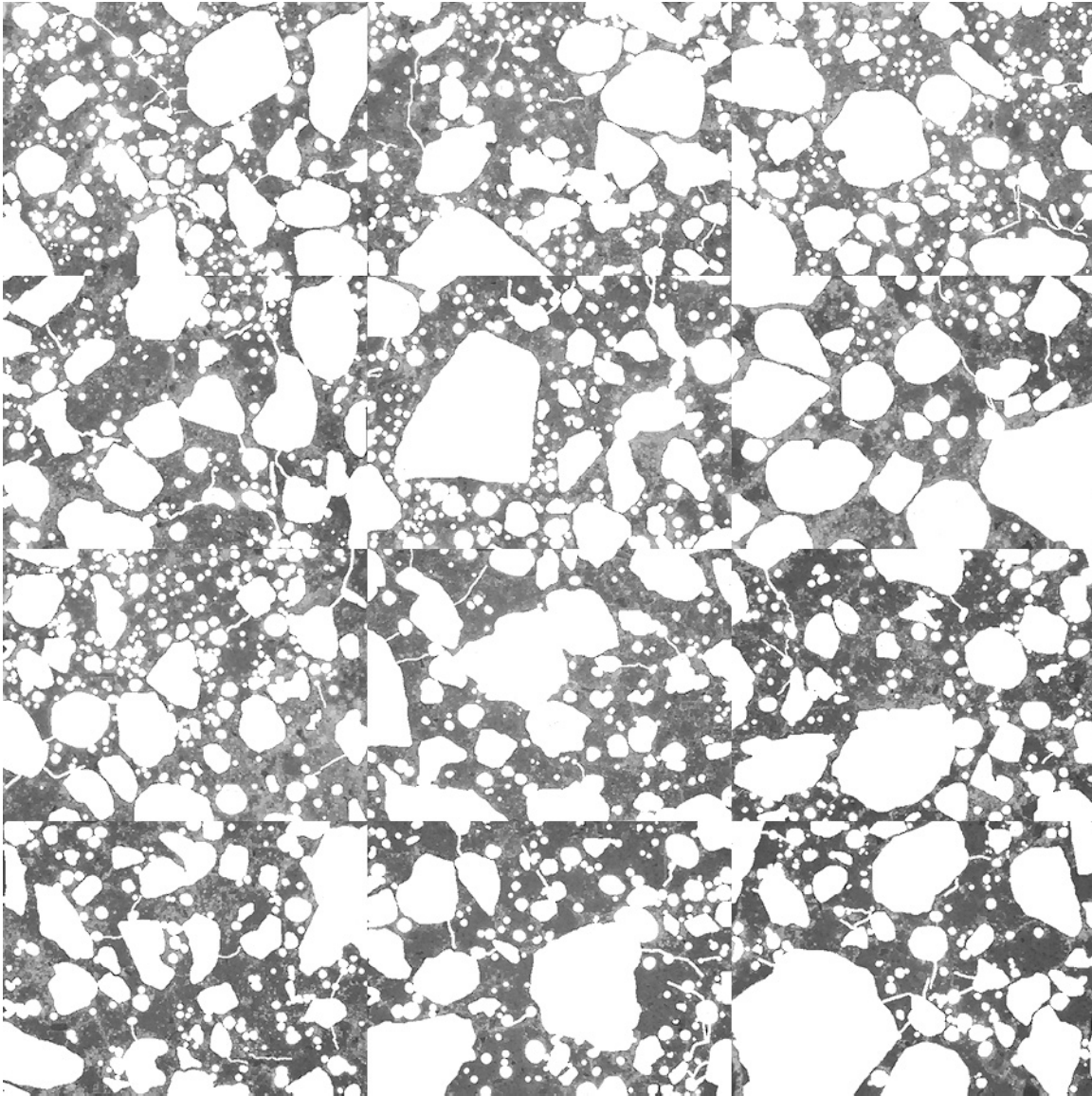


Figure 4.20. Mosaic of 12 frames collected from thin section prepared from billet cut from top portion of core SD-5 after masking out air voids, fine aggregate, and micro-cracks to isolate cement paste (each individual frame measures 2.612 x 1.959 mm).

Table 4.7. Average cement paste pixel intensities per frame, and equivalent w/c values (as compared to 28-day moist cured mortar samples) core SD-5.

Cement Paste Pixel Fluorescence Measurements (average intensity per frame)			
86	84	86	74
82	74	83	75
58	64	62	52
equivalent w/c ($y = 0.0044x + 0.0329$)			
0.41	0.40	0.41	0.36
0.39	0.36	0.39	0.36
0.29	0.31	0.30	0.26

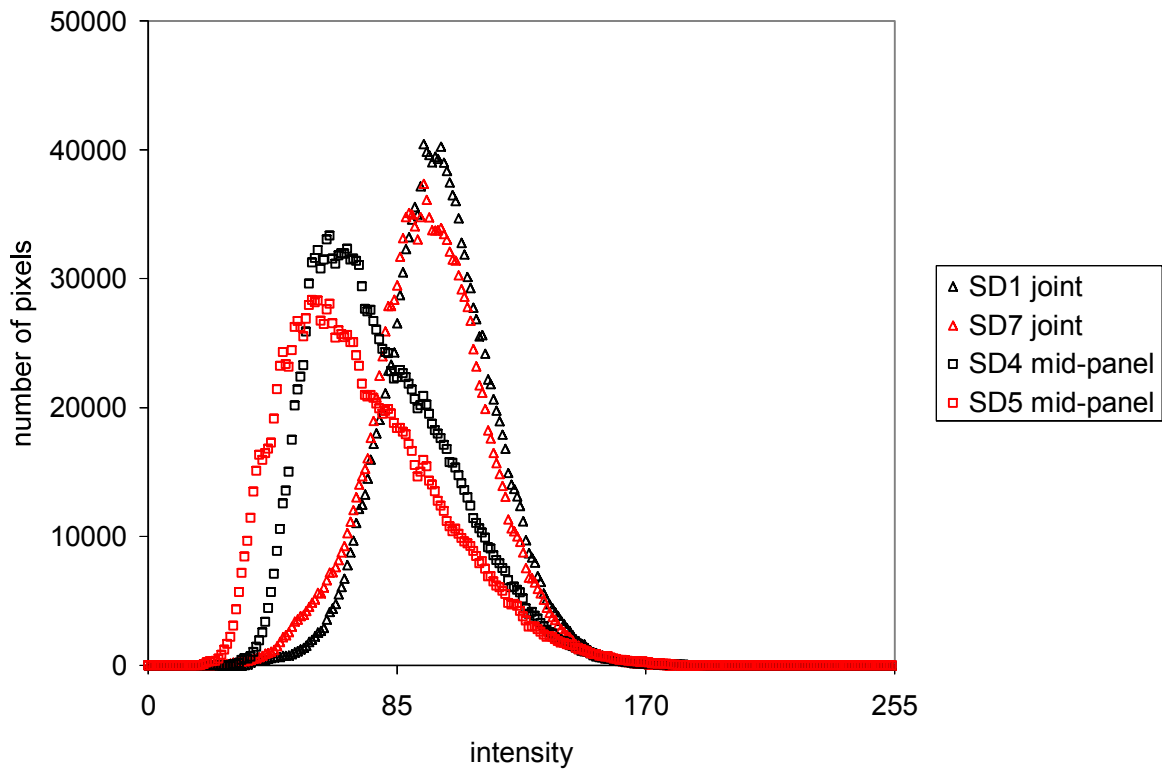


Figure 4.21. Histogram comparing cement paste pixel intensities using all 12 frames as collected from thin sections prepared from cores taken at the joint versus cores taken mid-panel.

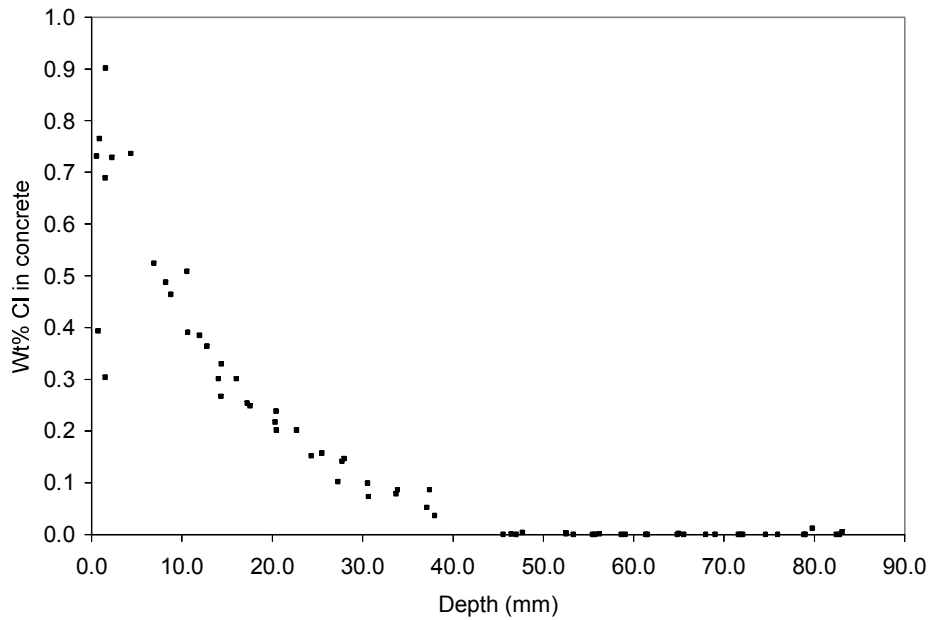


Figure 4.22. Chloride profile from billet prepared from core SD-3, panel corner.

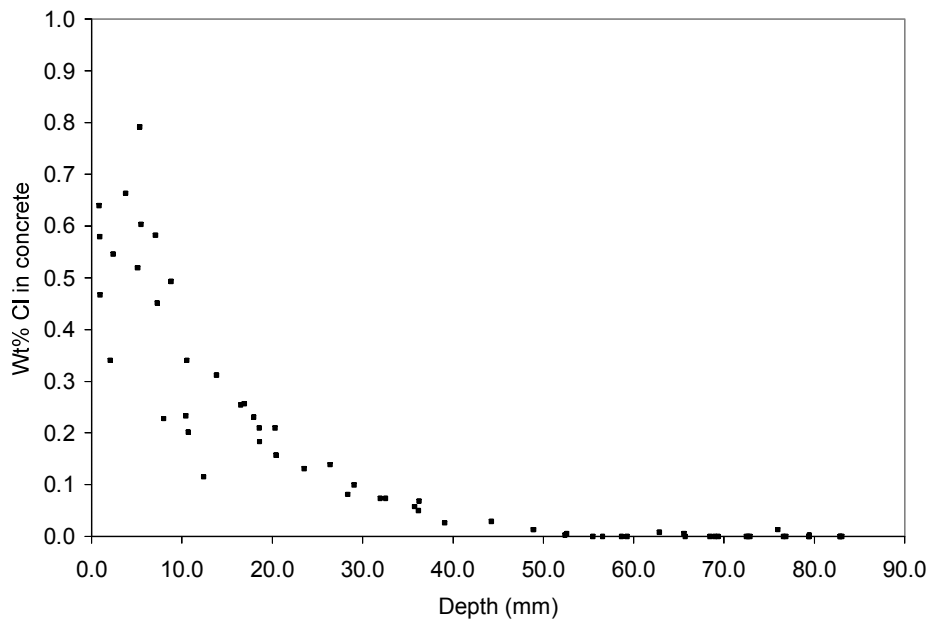


Figure 4.23. Duplicate chloride profile from additional billet prepared from core SD-3, panel corner.

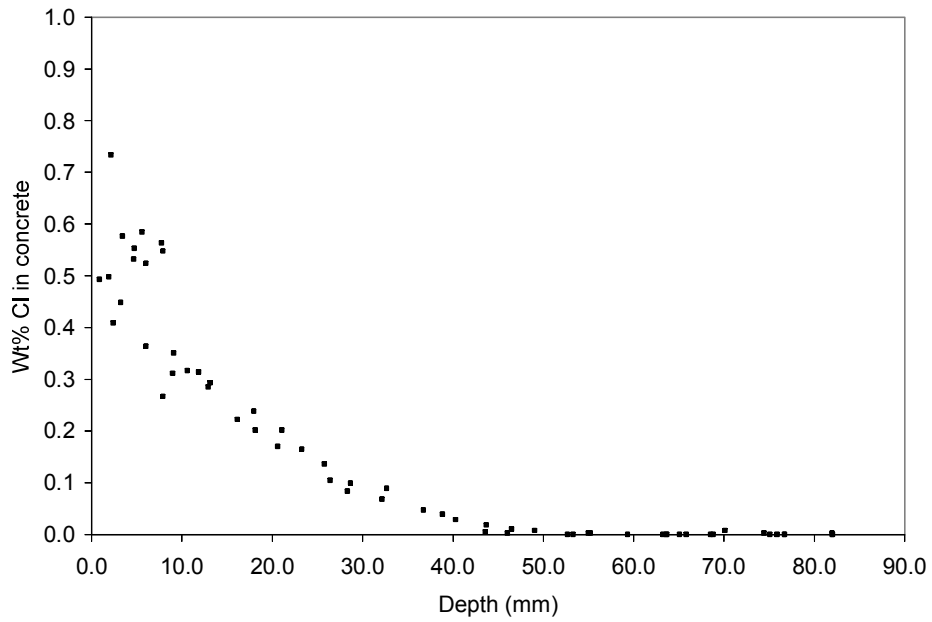


Figure 4.24. Chloride profile from billet prepared from core SD-7, mid-panel.

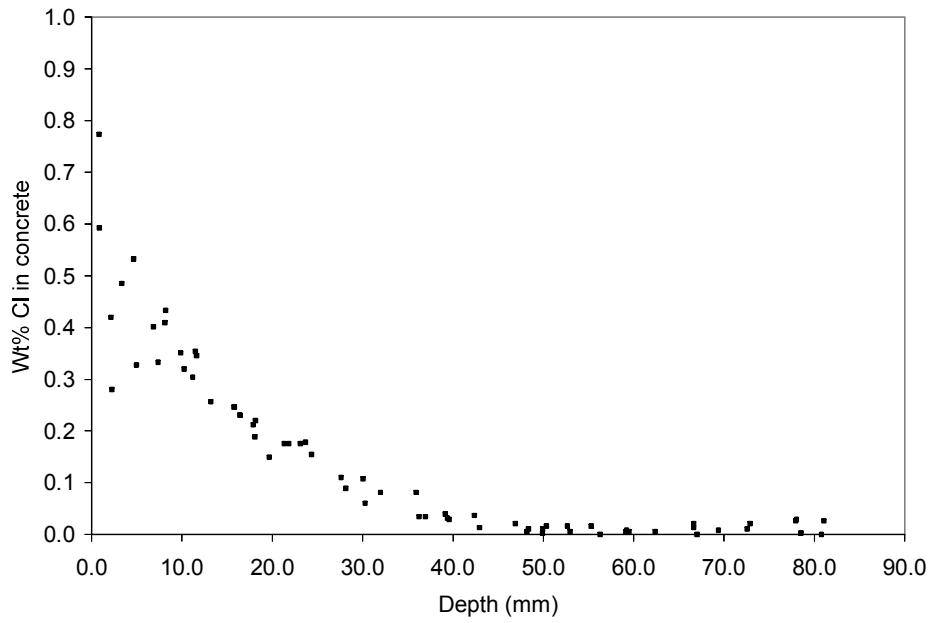


Figure 4.25. Duplicate chloride profile from additional billet prepared from core SD-7, mid-panel.

4.2.2 Montana, eastbound Interstate Highway 90 bridge deck, near milepost 61.8, Tarkio interchange

The Tarkio interchange was constructed in 1958, and lies at the border of two maintenance areas: 1113, and 1114. Maintenance personnel indicated they used both $MgCl_2$ brine, and a combination of $NaCl$ and sand on this bridge deck. Maintenance personnel described spalling at many of the bridge decks in the area that had been coated with a thick ($\sim 1/4"$) layer of epoxy and aggregate. In order to patch the spalls, they had to first scrape away the epoxy layer, which debonded and came off in sheets. It was never stated that this was the case at the Tarkio interchange, which appeared to be uncoated. Figure 4.26 shows the locations of the cores, and Figure 4.27 shows the condition of the bridge deck, covered with cold patch material. Figure 4.28 shows the underside of the bridge deck with pronounced efflorescence, especially in areas directly below regions covered with cold patch material. Figure 4.29 shows photographs of the cores. Core T-1 exhibited a crack plane at a depth of about 45 mm. The entire core was vacuum impregnated with epoxy and used only for thin section preparation. Core T-2 was intact, and cut into slabs and polished. Figures 4.30 and 4.31 show the slab as polished, after staining with phenolphthalein, and after treatment to enhance air voids and cracks. The phenolphthalein stain showed normal carbonation at the surface, but pronounced carbonation of over a centimeter thick at the base of the deck. The black and white treatment did not reveal any macro-cracking. Table 4.8 summarizes the air void parameters. The slab showed inadequate entrained air, with a spacing factor of 0.296 mm. Figure 4.32 shows an example stereomicroscope image of the air void structure. A w/c ratio estimation was performed on a thin section prepared from the top of core T-2. Figures 4.33 and 4.34 show the images used to make the measurements. The results of the w/c estimation are summarized in Table 4.9, with an average w/c value of 0.33 as compared to the 28-day moist cured mortar sample standards. Figures 4.35 through 4.37 show chloride profiles from cores T-2. Figures 4.38 and 4.39 show locations on the thin sections prepared from core T-1 that were used for elemental mapping. Regions were mapped to represent the pavement surface and the crack at depth. Figures 4.40 and 4.41 show the elemental maps from the two regions. Chloride profiles were not recorded from core T-1 because it had been epoxy impregnated; the epoxy contains chlorine. The most interesting feature of the elemental maps is the Mg map from Figure 4.41 that shows magnesium enrichment at the surface of the bridge deck.

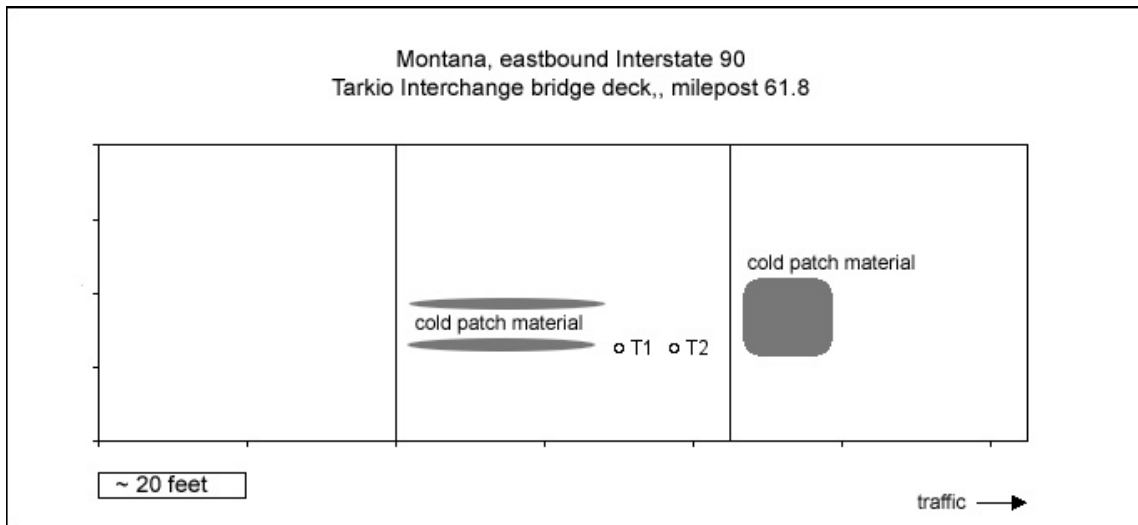


Figure 4.26. Diagram to show location of cores according to field notes.



Figure 4.27. Photograph of core site.



Figure 4.28. Photograph from beneath bridge deck after coring operation. Hole from core T-2 is visible. Dampness permeating through cracks visible beneath the area of core T-1. White efflorescence common in areas directly below regions covered with cold patch material.



Figure 4.29. Cores retrieved from site, core T-1 (top), core T-2 (bottom).

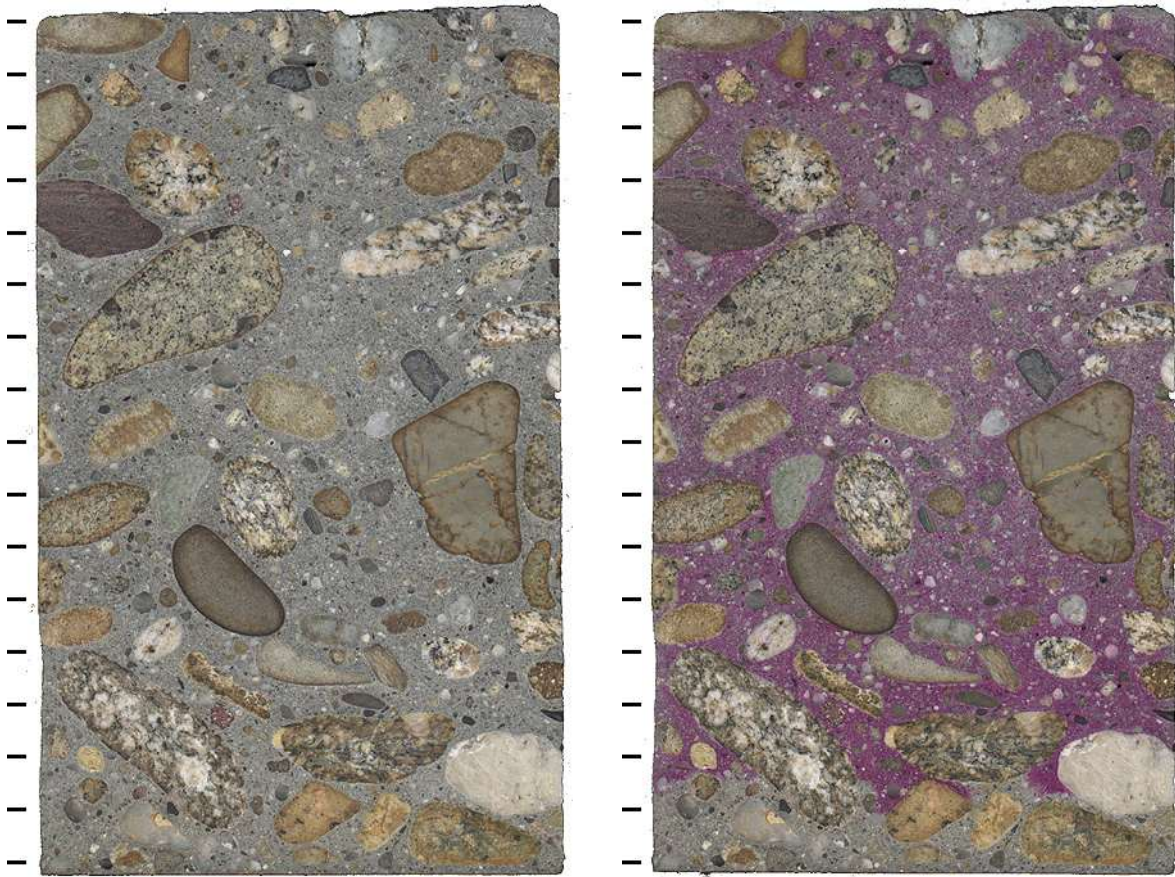


Figure 4.30. Polished slabs to show complete cross-section through core T-2 both before (left) and after application of phenolphthalein stain (right) tic marks every cm.

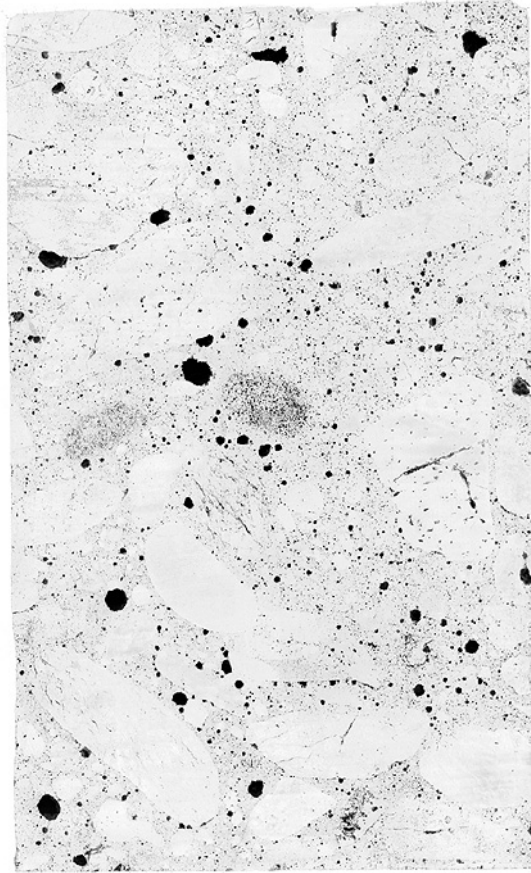


Figure 4.31. Polished slabs to show complete cross-section through core T-2 after treatment to enhance appearance of air voids and cracks, tic marks every cm.

Table 4.8. Air void parameters

Sample ID	T-2
Location	Area in Good Condition
Raw data	
Total traverse length (mm)	3772.1
Area analyzed (cm ²)	73.9
Air stops	70
Paste stops	413
Aggregate stops	961
Secondary deposit stops	0
Total stops	1444
Number of air intercepts	617
Number of filled void intercepts	0
Results	
Air vol%	4.9
Paste vol%	28.6
Aggregate vol%	66.6
Secondary deposit vol%	0.0
Existing average chord length (mm)	0.370
Existing paste/air ratio	5.9
Existing air void specific surface (mm ⁻¹)	13.5
Existing air void frequency (voids/m)	164
Existing spacing factor (mm)	0.296
Original average chord length (mm)	0.370
Original paste/air ratio	5.9
Original air void specific surface (mm ⁻¹)	13.5
Original air void frequency (voids/m)	164
Original spacing factor (mm)	0.296

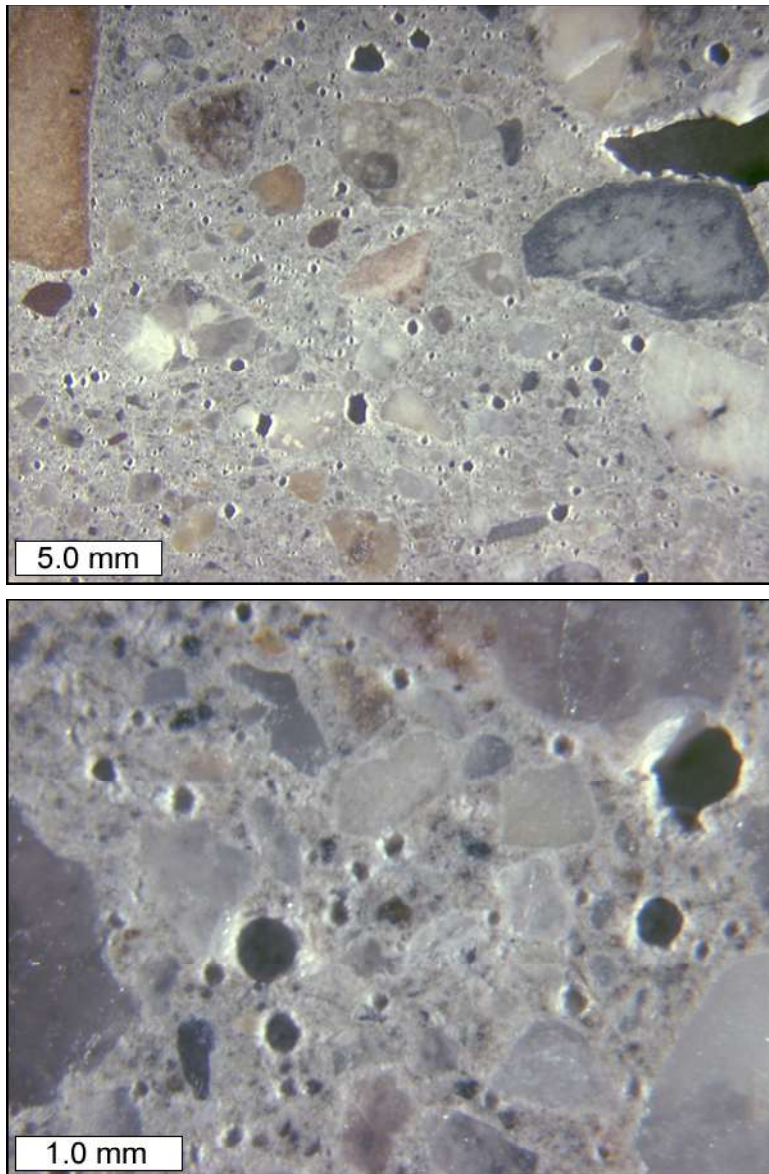


Figure 4.32. Stereo microscope images to show air void structure on polished slab from core T-2.

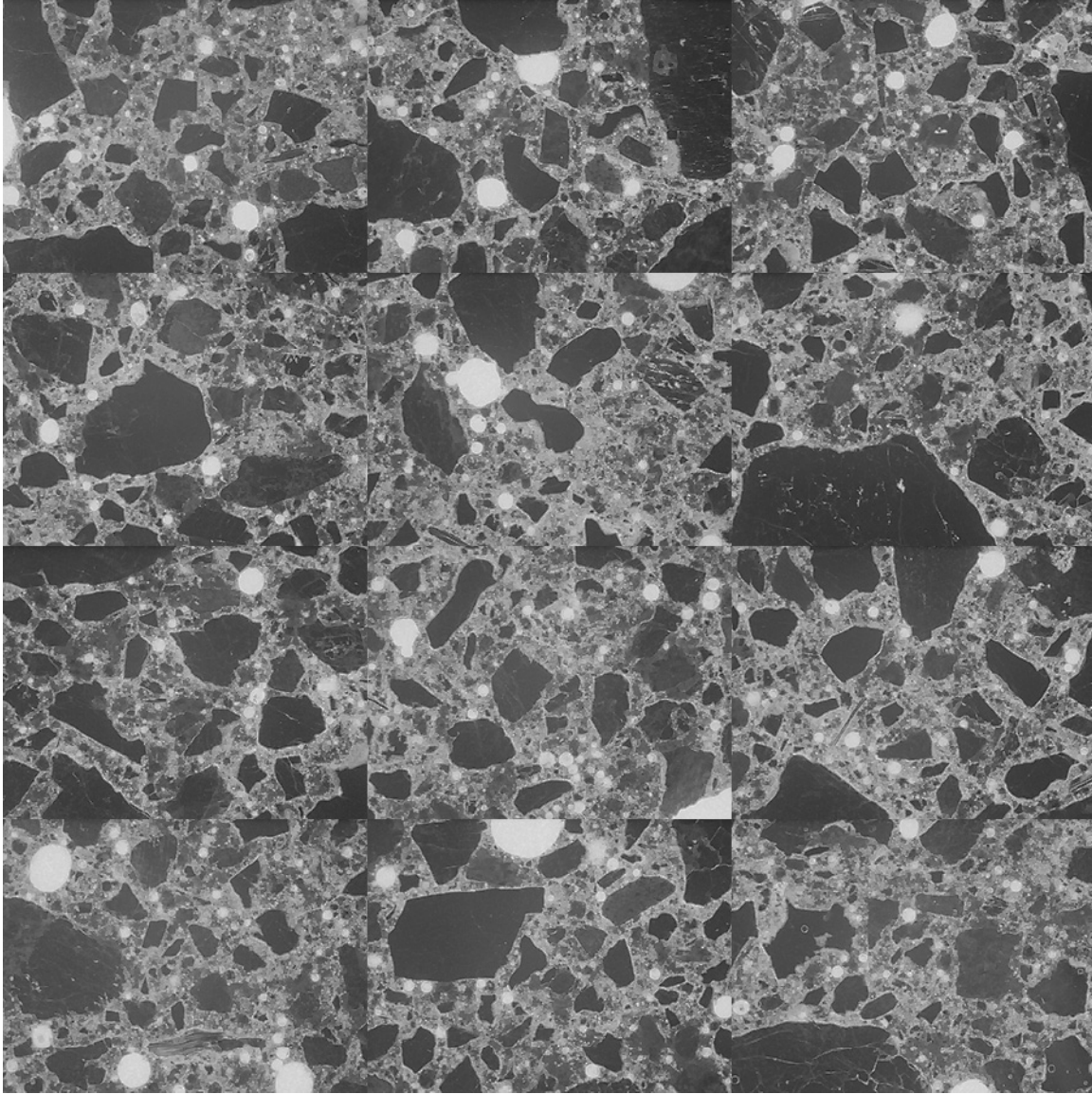


Figure 4.33. Mosaic of 12 frames collected from thin section prepared from billet cut from top portion of core T-2 (each individual frame measures 2.612 x 1.959 mm).

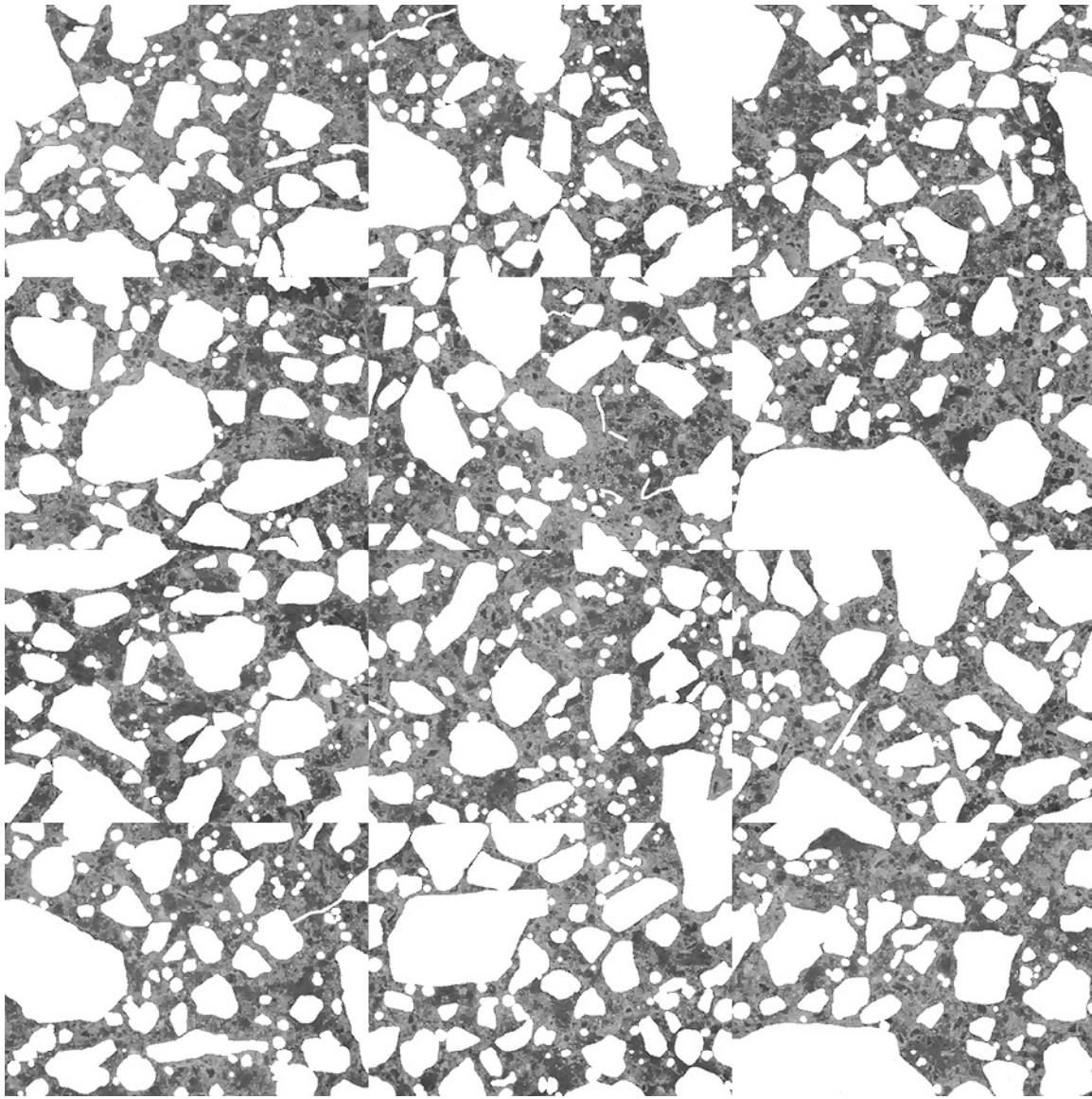


Figure 4.34. Mosaic of 12 frames collected from thin section prepared from billet cut from top portion of core T-2 after masking out air voids, fine aggregate, and micro-cracks to isolate cement paste (each individual frame measures 2.612 x 1.959 mm).

Table 4.9. Average cement paste pixel intensities per frame, and equivalent w/c values (as compared to 28-day moist cured mortar samples).

Cement Paste Pixel Fluorescence Measurements (average intensity per frame)			
71	67	63	68
72	67	62	72
75	68	69	72
equivalent w/c ($y = 0.0044x + 0.0329$)			
0.34	0.33	0.31	0.33
0.35	0.32	0.31	0.35
0.36	0.33	0.33	0.35

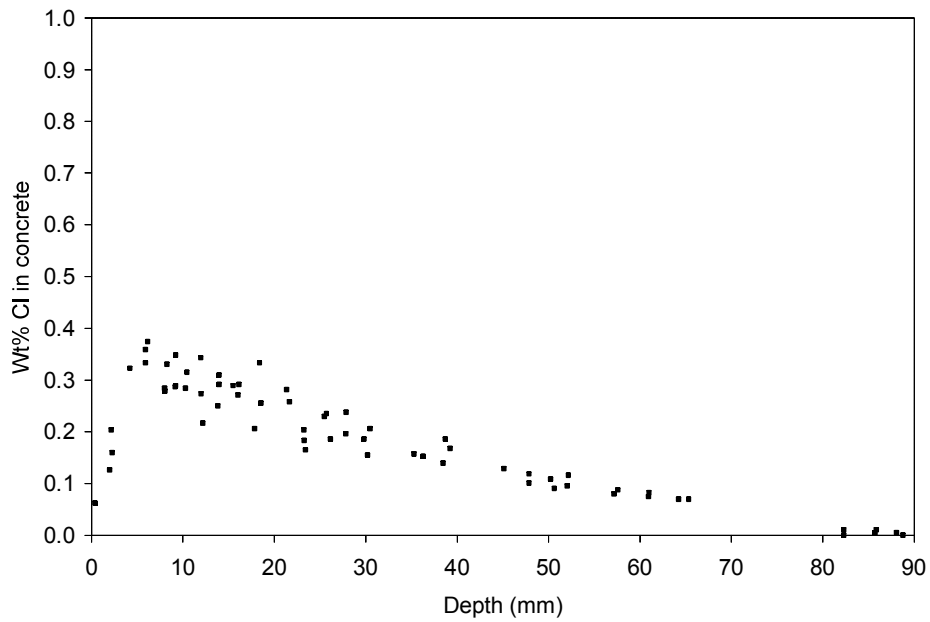


Figure 4.35. Chloride profile from billet prepared from core T-2.

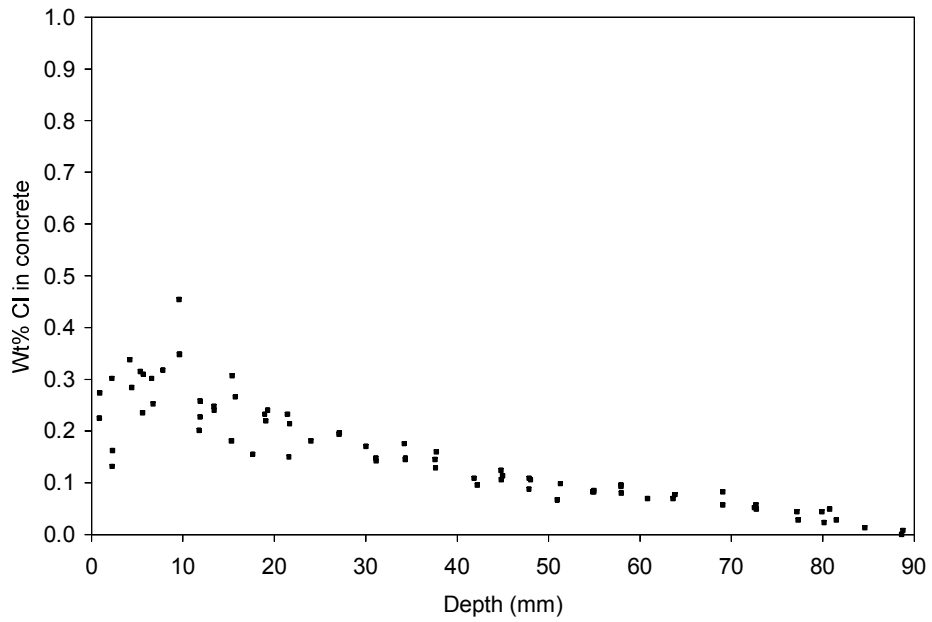


Figure 4.36. Duplicate chloride profile from additional billet prepared from core T-2.

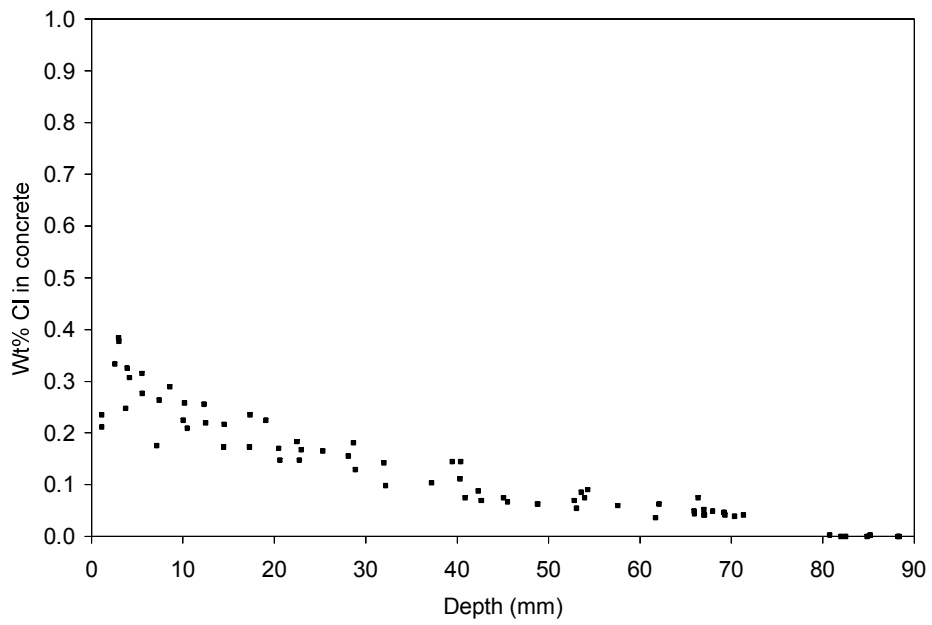


Figure 4.37. Duplicate chloride profile from additional billet prepared from core T-2.

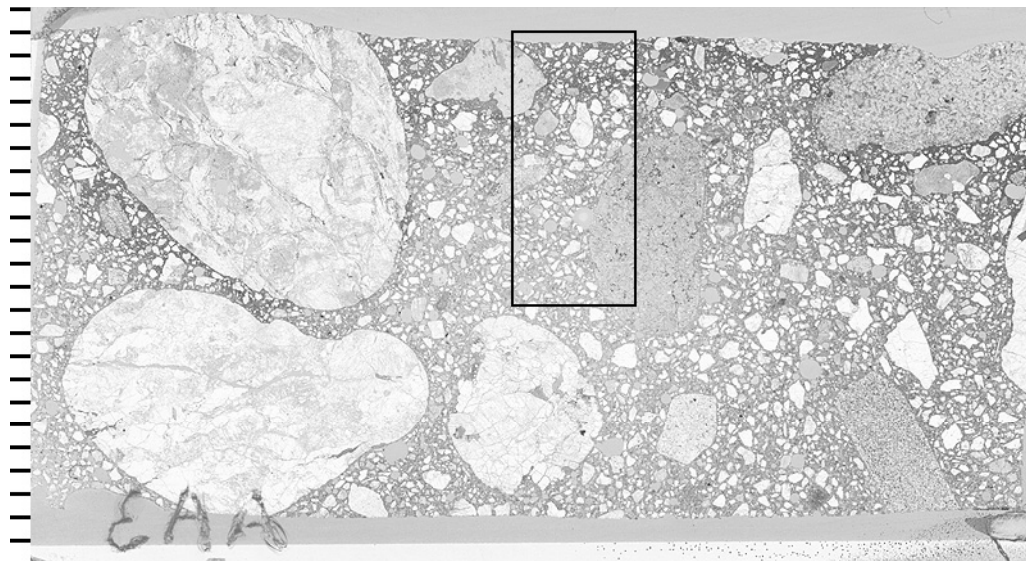


Figure 4.38. Transmitted light scanned image of thin section to show location of elemental maps shown in Figure 4.40. The top of the thin section represents the wear surface of the pavement, (tic marks every mm).

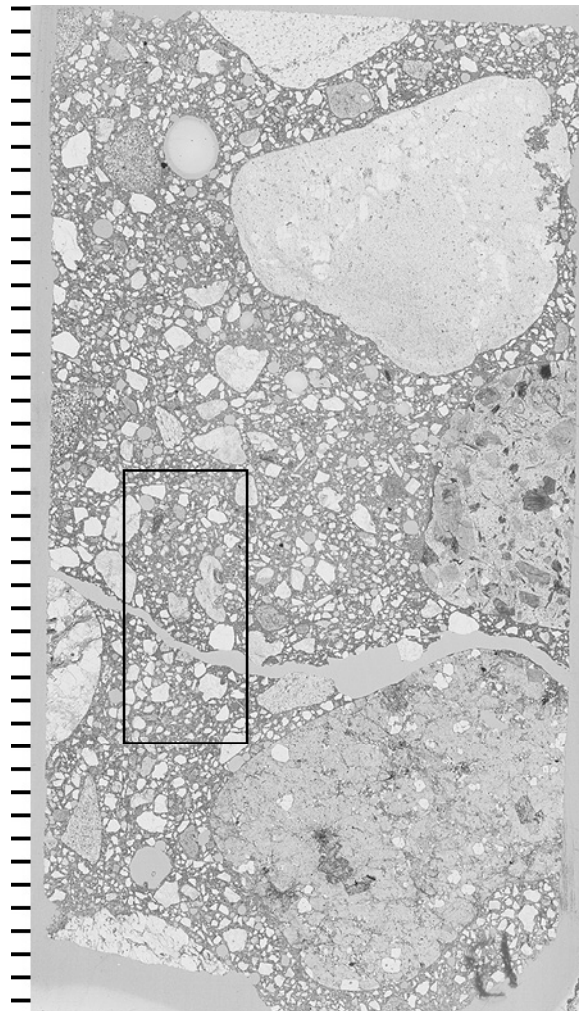


Figure 4.39. Transmitted light scanned image of thin section to show location of elemental maps shown in Figure 4.41. The large crack, sub-parallel to the pavement surface, is at a depth of about 40 mm, (tic marks every mm).

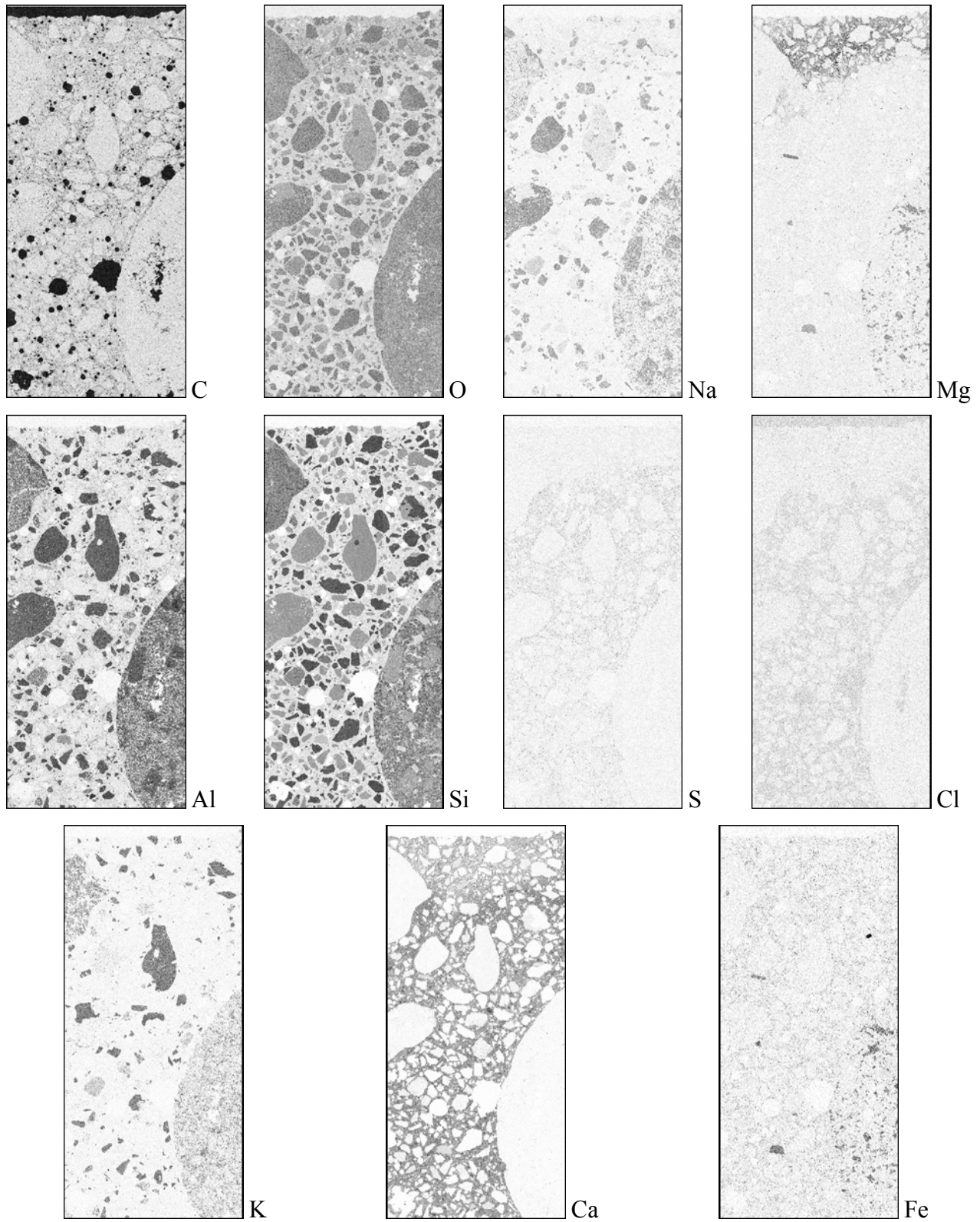


Figure 4.40. Elemental maps from pavement surface, darker regions indicate higher concentrations.

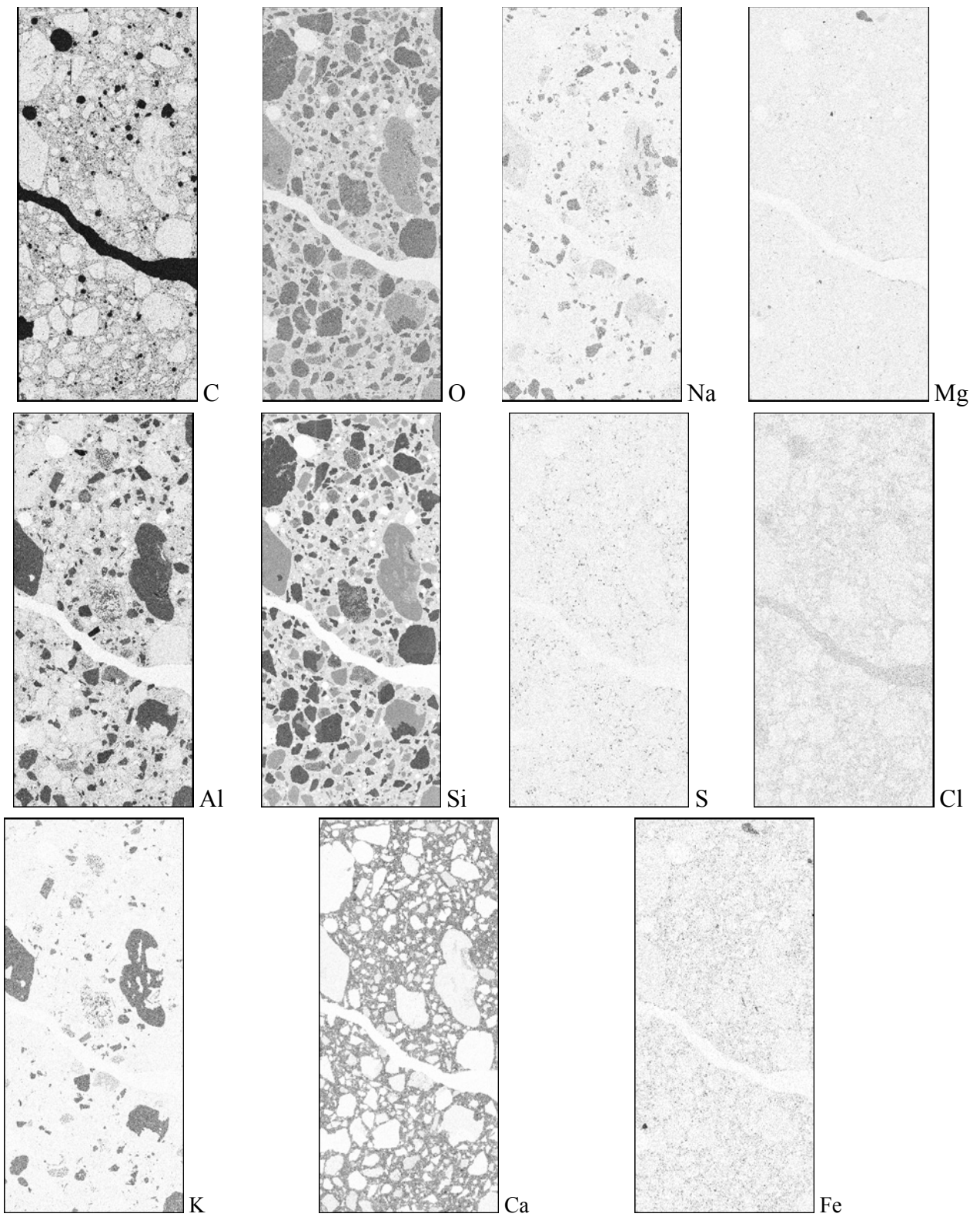


Figure 4.41. Elemental maps from crack at depth, darker regions indicate higher concentrations.

CHAPTER 5 - LABORATORY RESULTS

5.1 OVERVIEW

This section presents the key results of the Phase I and Phase II laboratory experiments. The complete results of all laboratory experiments are presented in the Appendix to this report in Section 3 - . The results of each phase will be presented separately and are organized based upon the work done at Michigan Tech and that done at the University of Toronto.

5.2 PHASE I LABORATORY EXPERIMENT RESULTS

5.2.1 RESULTS OF PHASE I EXPERIMENTS CONDUCTED AT MICHIGAN TECH

5.2.1.1 Low Temperature Experiment

Observations

The constant low temperature experiment was designed to monitor chloride ingress at 28, 56, and 112 days at a temperature of 40 °F [4.4 °C]. Some of the cylinders were coated with epoxy on all sides except for the top surface in order to monitor one-dimensional chloride diffusion. Other cylinders were not coated with epoxy, in order to monitor radial diffusion into the sides of the cylinders. As shown in Figure 5.1, the cylinders in the NaCl solution showed no deterioration after 84 days. Conversely, by 84 days, the cylinders in the MgCl₂ and CaCl₂ solutions were severely deteriorated, as shown in Figures 5.2 and 5.3. It was decided to end the constant temperature experiments for all cylinders at 84 days. The cylinders in the CMA solution showed little to no distress after 84 days as shown in Figure 5.18, although there was some staining evident in the 0.60 w/c cylinders. The control cylinders in the limewater solution, as shown in Figure 5.5, showed no signs of distress after 84 days. Table 5.1 summarizes the visual ratings for the cylinders over time for the low temperature exposure tests.



Figure 5.1. Cylinders exposed to NaCl solution after 84 days of constant low temperature test. From left to right: 0.40, 0.50, and 0.60 w/c mortar cylinders.



Figure 5.2. Cylinders exposed to MgCl₂ solution after 84 days of constant low temperature test. From left to right: 0.40, 0.50, and 0.60 w/c mortar cylinders.



Figure 5.3. Cylinders exposed to CaCl_2 solution after 84 days of constant low temperature test. From left to right: 0.40, 0.50, and 0.60 w/c mortar cylinders.



Figure 5.4. Cylinders exposed to CMA solution after 84 days of constant low temperature test. From left to right: 0.40, 0.50, and 0.60 w/c mortar cylinders.



Figure 5.5. Control cylinders exposed to limewater solution after 84 days of constant low temperature test. From left to right: 0.40, 0.50, and 0.60 w/c mortar cylinders.

Table 5.1. List of visual ratings for all mortar cylinders from the low temperature tests.

Rating Scale: 0 - no visible change, 1 – some cracking, 2 - visible expansion and cracking, 3 - severe expansion and cracking, 4 - partial disintegration, 5 - total disintegration, x – test aborted.

Solution	Time in Days											
	w/c = 0/40				w/c = 0/50				w/c = 0/60			
	8	28	56	84	8	28	56	84	8	28	56	84
Limewater	-	0	0	0	-	0	0	0	-	0	0	0
MgCl_2	-	0-1	1-2	2-3	-	0-1	1-2	1-3	-	0-1	0-1	1-3
CaCl_2	-	0-1	2-3	3	-	0	2-3	3	-	0-1	1-3	2-3
NaCl	-	0	0	0	-	0	0	0	-	0	0	0
CMA	-	0	0	0	-	0	0	0	-	0	0	0

Petrographic Analysis

Thin sections were prepared from the 0.50 w/c mortar cylinders subjected to 56 days of immersion in the five solutions. One cylinder was selected from each of the five solutions: magnesium chloride, calcium chloride, sodium chloride, calcium magnesium acetate, and limewater. The thin sections represent a cross-sectional plane oriented parallel to the finished surface at a depth of about 3/4 of an inch, [19 mm] from the finished surface. Figure illustrate the extensive crack networks of the magnesium chloride and calcium chloride immersed cylinders as compared to the cylinders immersed in the other three solutions. Near the exteriors of the magnesium chloride and calcium chloride cylinders, the cracks are empty. However, cracks further towards the interior of the cylinders are filled with a crystalline material bearing calcium and chlorine, likely calcium oxychloride or the altered remnants of calcium oxychloride. Figure 5.7 shows cross-polarized light images to emphasize the crystalline nature of the remnant calcium oxychloride filling the cracks. Figures 5.8 and 5.9 show close-up views of regions of the cement paste disrupted by cracks filled with calcium oxychloride for both the magnesium chloride and calcium chloride immersed samples. Figure 5.10 shows calcium oxychloride crystals that have formed at the expense of secondary calcium hydroxide crystals in an air void, yet retained the shape of the original calcium hydroxide crystals. The deterioration of the magnesium chloride and calcium chloride immersed samples appears very similar. Both samples exhibit a region of calcium oxychloride filled cracks and voids associated with calcium hydroxide depleted cement paste. Figure 5.11 shows elemental maps for magnesium for all of the thin sections. Magnesium is sequestered at the exterior of the magnesium chloride immersed cylinders, likely resulting in a calcium chloride solution in the interior that is similar to the solution in the interior of the calcium chloride immersed cylinders. Figures 5.12 and 5.13 show brucite and magnesium chloride hydrate crystals filling cracks and voids at the exterior of the magnesium chloride immersed cylinder. Figure 5.14 shows elemental maps for chlorine for all of the thin sections. A chlorine gradient is clearly visible for all three of the chloride-based deicers. It should be noted that the epoxy used to stabilize the billets prior to thin sectioning also contains chlorine.

A complete set of the elemental maps and petrographic images collected from each of the thin sections is included in the Figures A3.34 through A3.58. Additionally, split-tensile testing results for samples exposed in this test are also provided in the Appendix, Section 3. Included in this summary are selected images from the complete data set. Figures 5.15, 5.17, 5.19, 5.21, and 5.23 show Figures 5.16, 5.18, 5.22, and 5.24 show elemental maps for calcium, magnesium, and chlorine Figure 5.20 shows elemental maps for calcium, sodium, and chlorine In all of these sets, back-scattered electron images are provided to illustrate the extensive crack networks. Cross-polarized light images emphasize the crystalline nature of any infilling material and epifluorescent images emphasize areas of different density with darker areas being less dense than lighter areas. Micro-cracks can also be readily seen in the epifluorescent images. Elemental maps show relative elemental distributions or concentration.

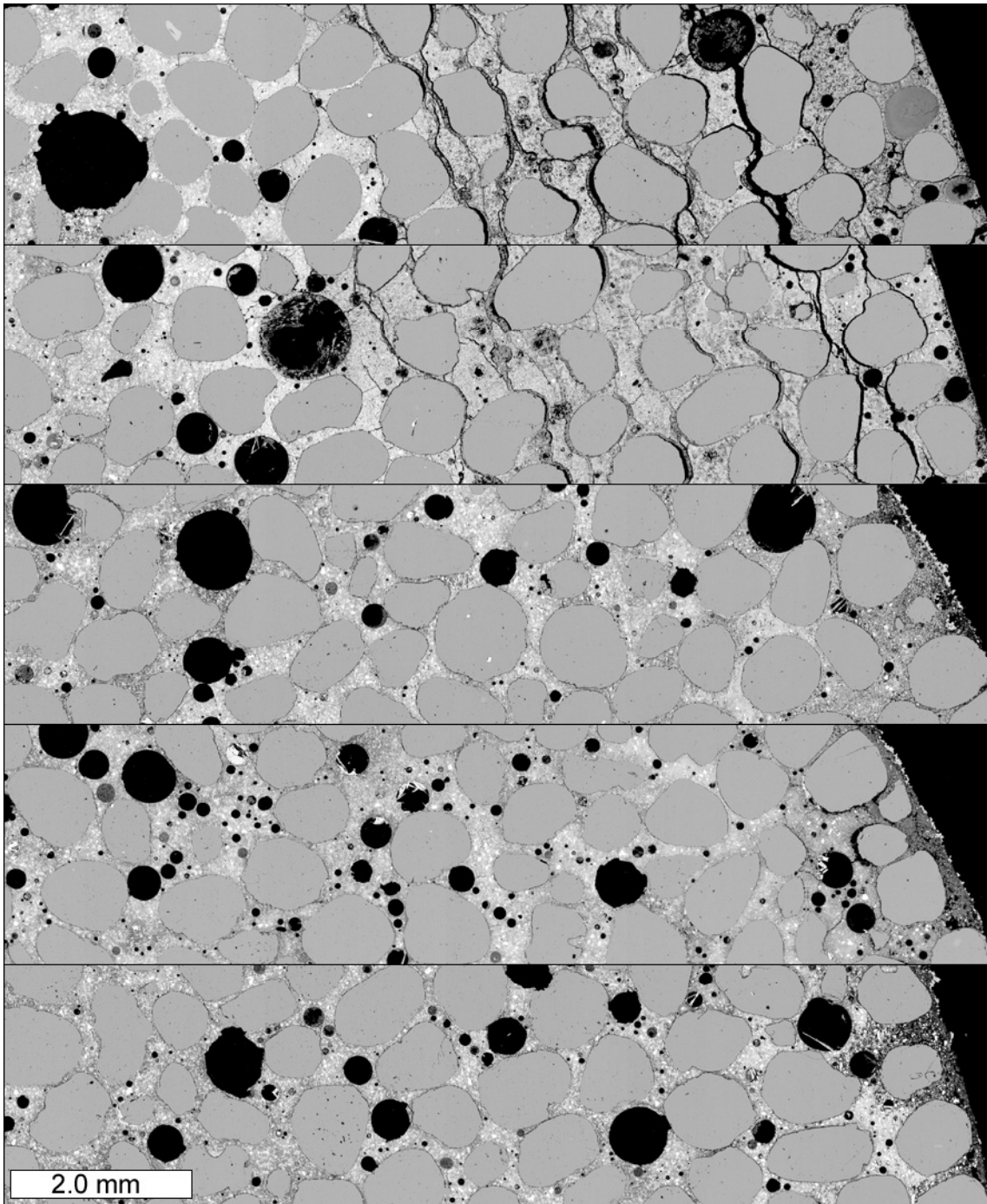


**Figure 5.6. Back-scattered electron images of thin sections prepared from mortar cylinders immersed in chemical solutions.
From top to bottom: magnesium chloride, calcium chloride, sodium chloride, calcium magnesium acetate, and limewater.**

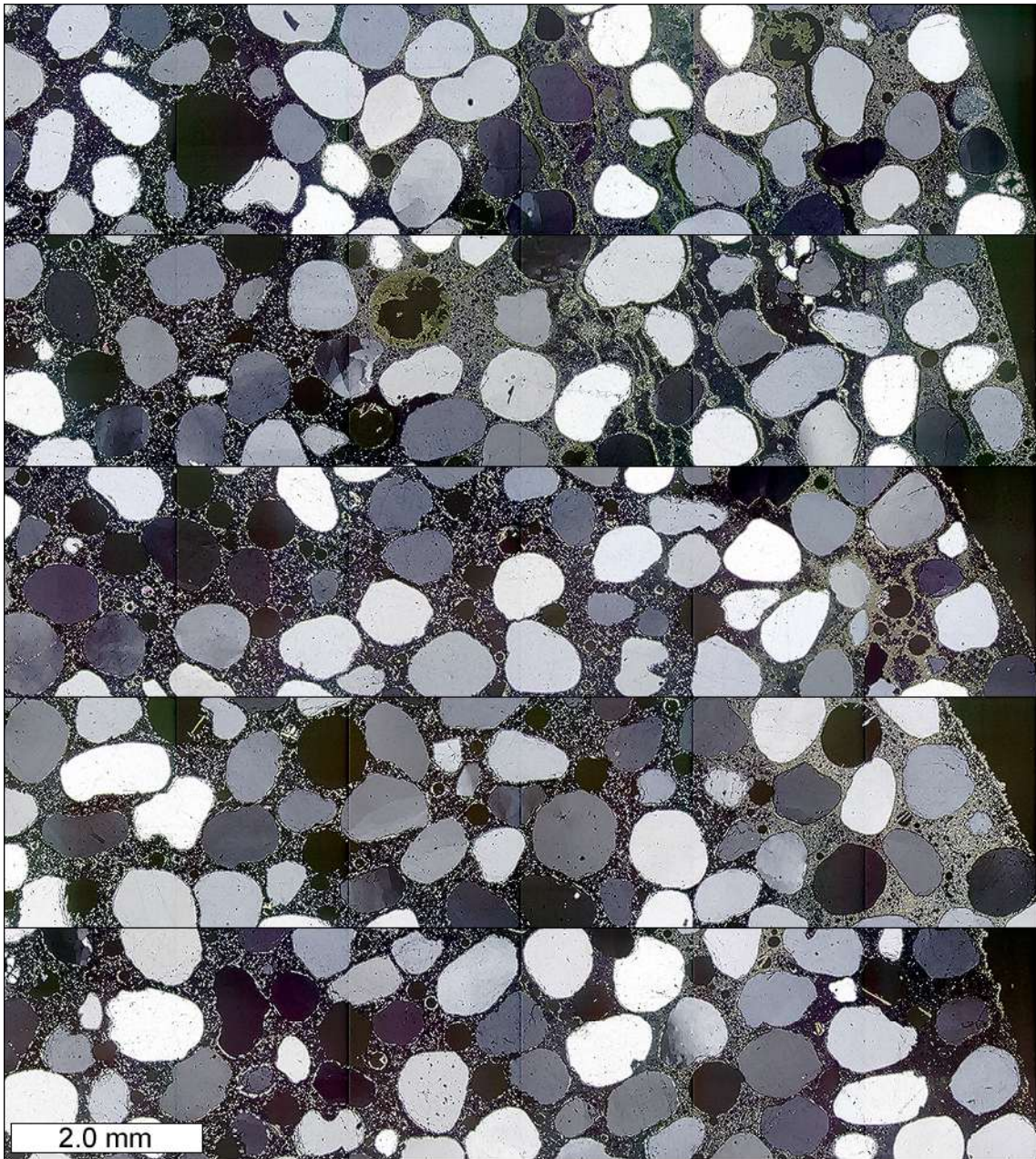


Figure 5.7. Cross-polarized light images of thin sections prepared from mortar cylinders immersed in chemical solutions.

From top to bottom: magnesium chloride, calcium chloride, sodium chloride, calcium magnesium acetate, and limewater.

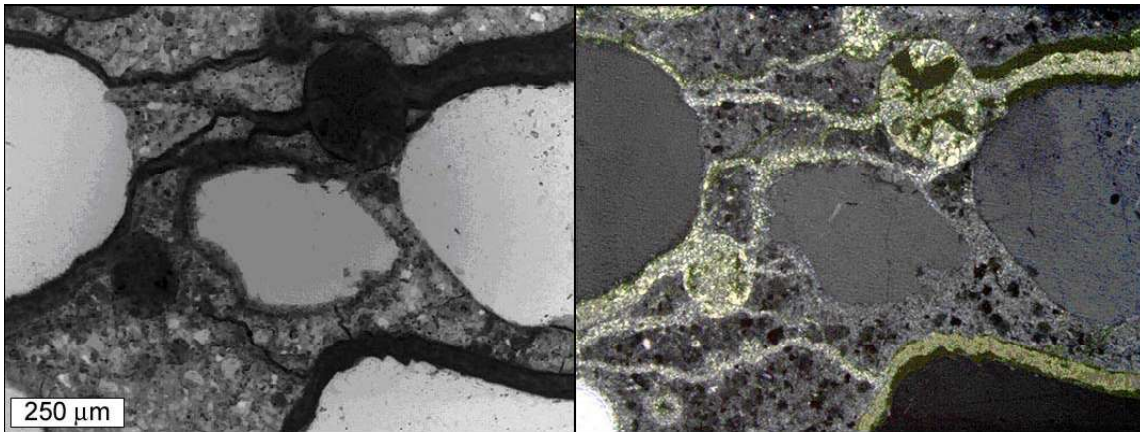


Figure 5.8. Cracks and air voids filled with remnant calcium oxychloride crystals in $MgCl_2$ solution immersed sample. From left to right, epifluorescent and crossed polars.

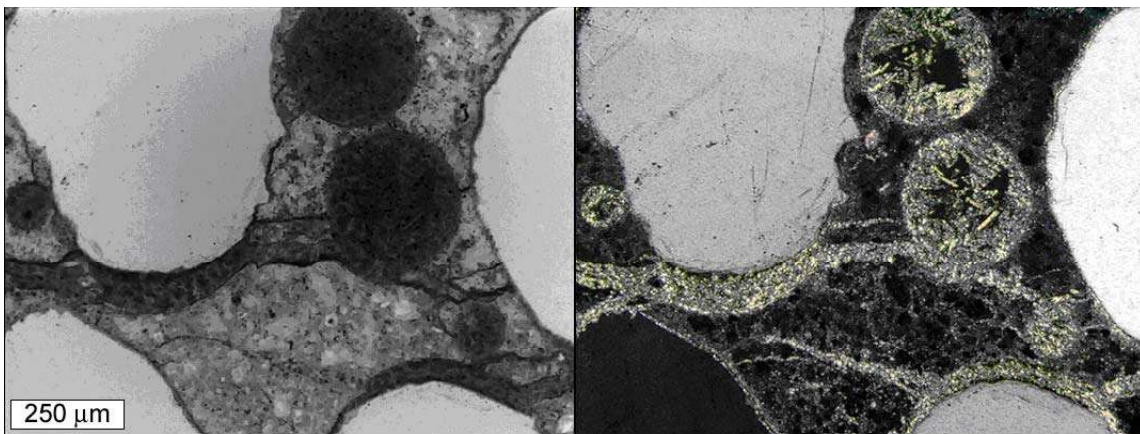


Figure 5.9. Cracks and air voids filled with remnant calcium oxychloride crystals in $CaCl_2$ solution immersed sample. From left to right, epifluorescent and crossed polars.

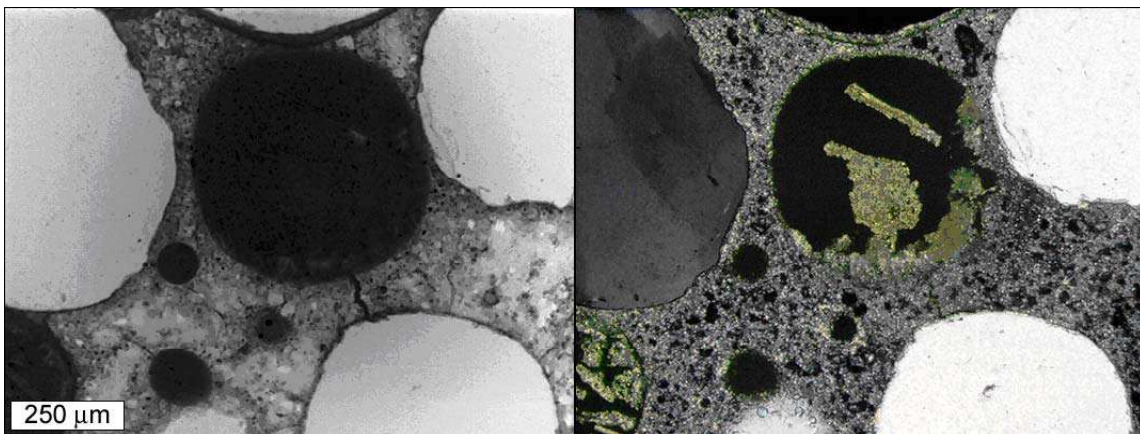
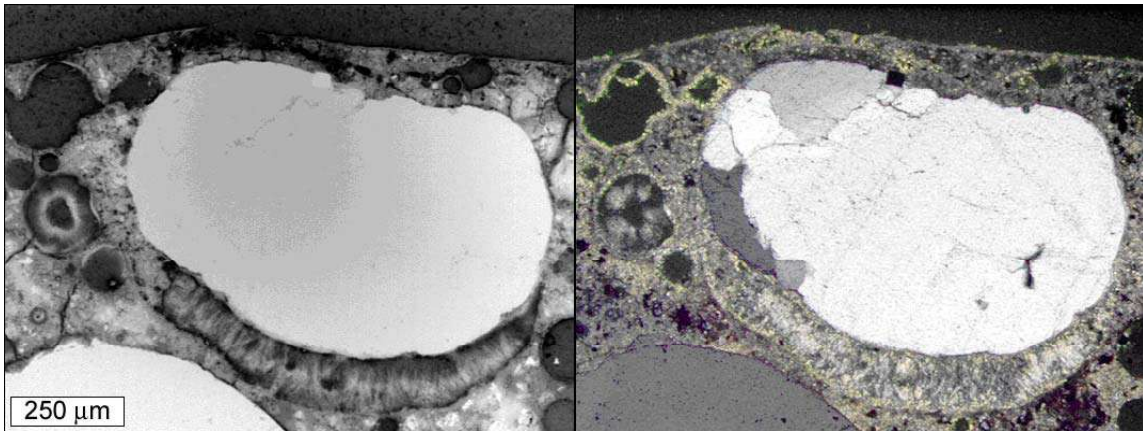


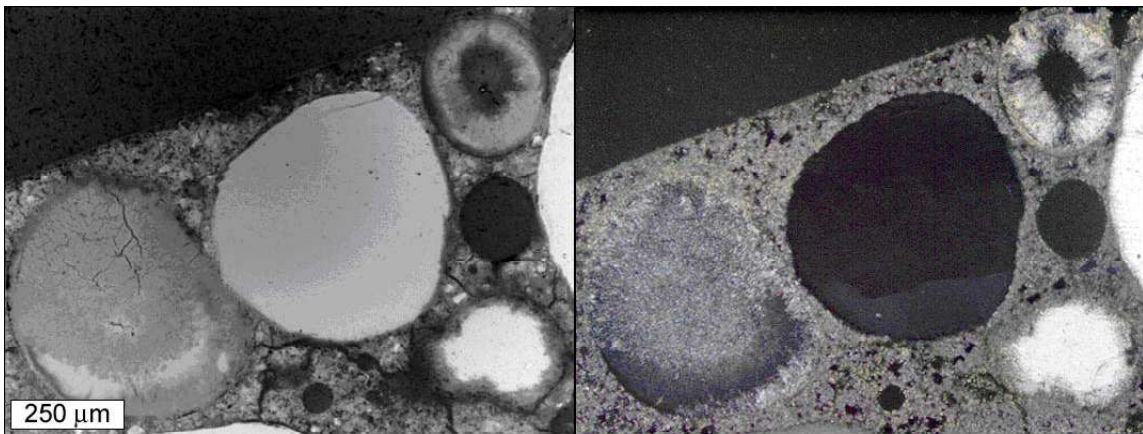
Figure 5.10. Remnant calcium oxychloride crystals that are pseudomorphs of secondary calcium hydroxide crystals formed in an air void from $MgCl_2$ solution immersed sample. From left to right, epifluorescent and crossed polars.



Figure 5.11. Elemental map for magnesium collected from thin sections prepared from mortar cylinders immersed in chemical solutions. From top to bottom: magnesium chloride, calcium chloride, sodium chloride, calcium magnesium acetate, and limewater. Darker areas indicate a higher concentration.



**Figure 5.12. Brucite, (magnesium hydroxide) crystals in air void and seam beneath sand grain near exterior in cylinder immersed in $MgCl_2$ solution.
From left to right, epifluorescent and crossed polars.**



**Figure 5.13. Magnesium chloride hydrate crystals in air voids near exterior in thin section prepared from cylinder immersed in $MgCl_2$ solution.
From left to right, epifluorescent and crossed polars.**

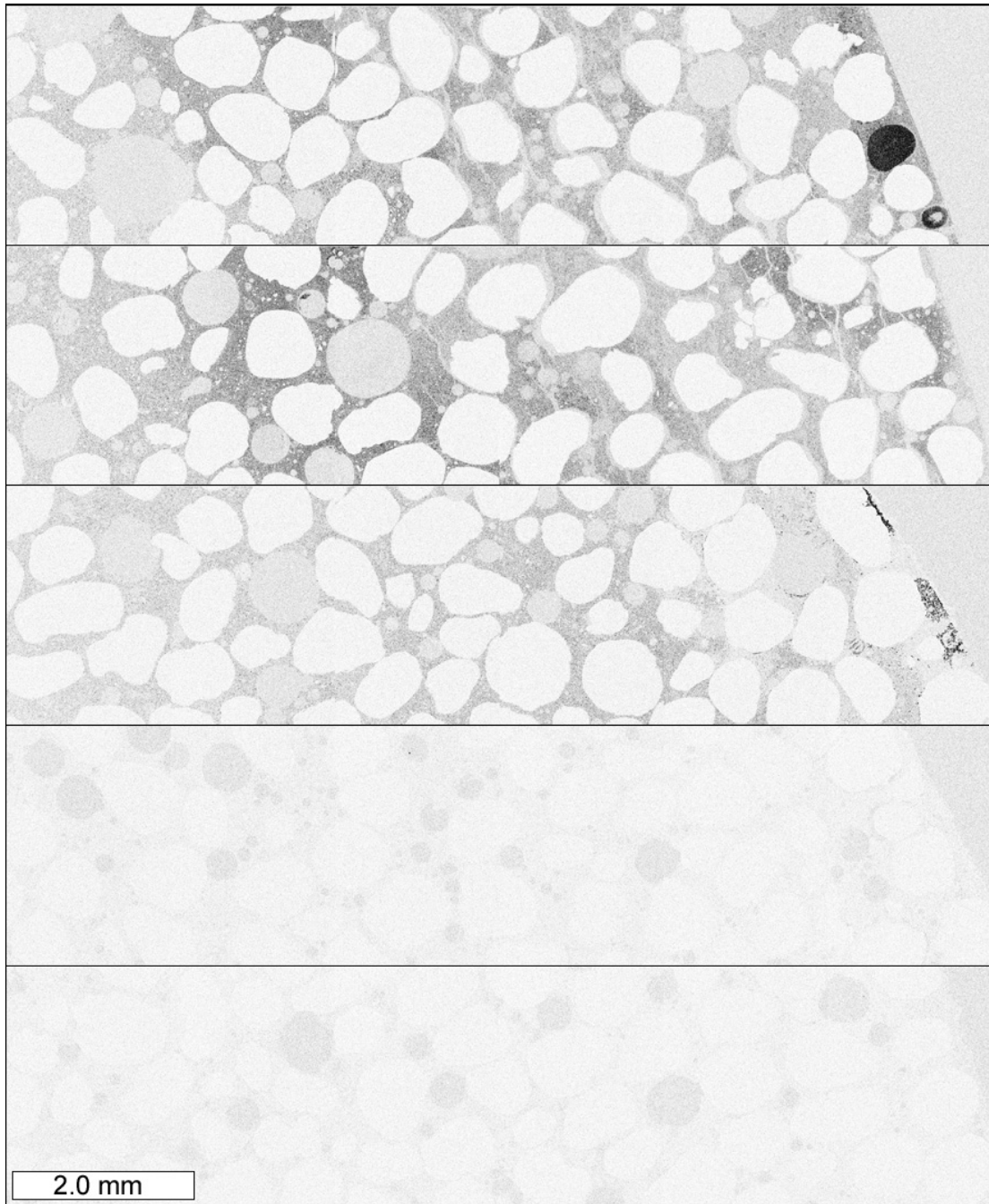


Figure 5.14. Elemental map for chlorine collected from thin sections prepared from mortar cylinders immersed in chemical solutions. From top to bottom: magnesium chloride, calcium chloride, sodium chloride, calcium magnesium acetate, and limewater. Darker areas indicate a higher concentration.

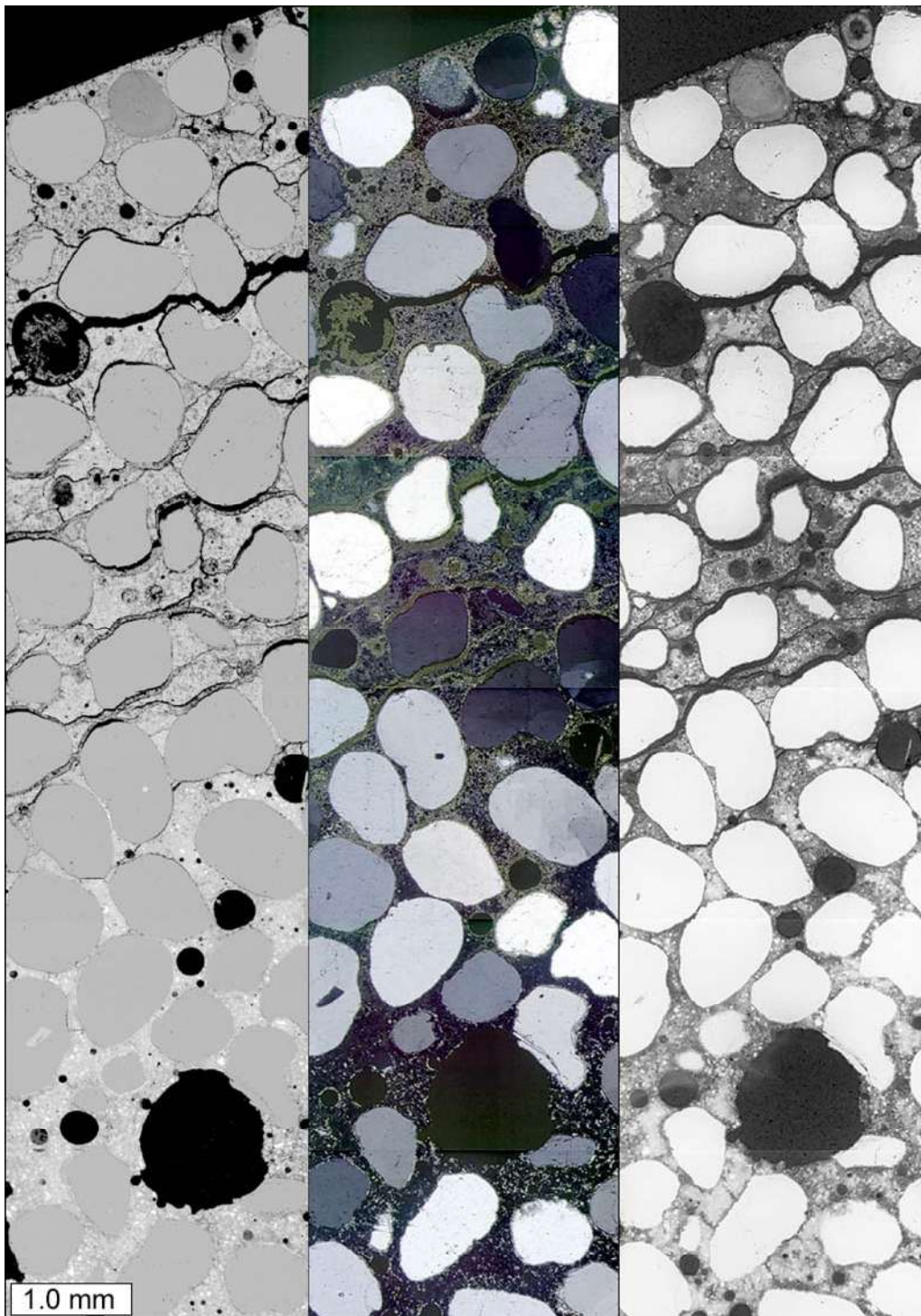


Figure 5.15. From left to right: back scattered electron image, cross polarized light, and epifluorescent mode images of a thin section prepared from a cylinder immersed in magnesium chloride solution.

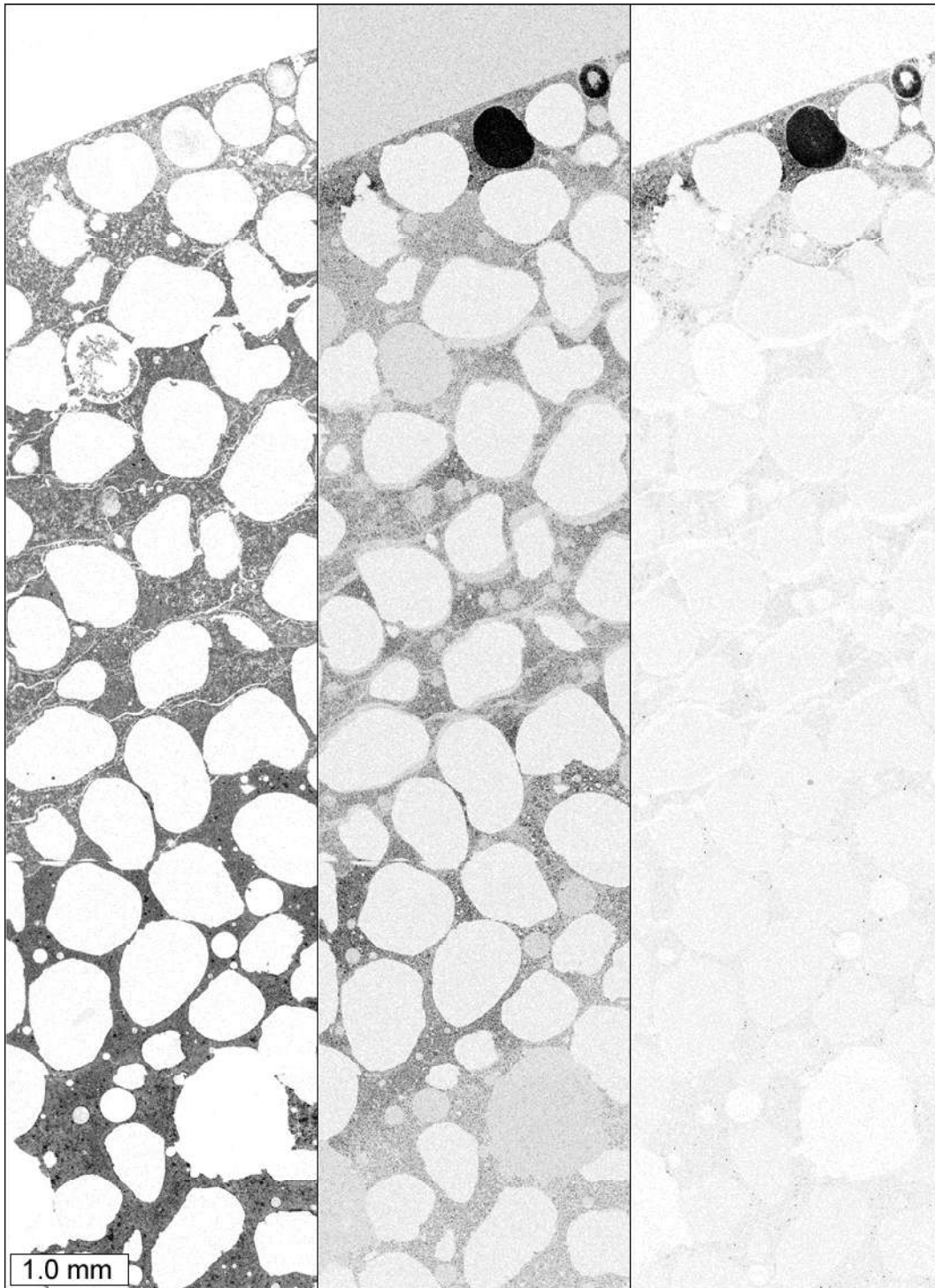


Figure 5.16. Elemental maps, from left to right: calcium, chlorine, and magnesium. The elemental maps were collected from a thin section prepared from a cylinder immersed in magnesium chloride solution. Darker areas indicate a higher concentration.

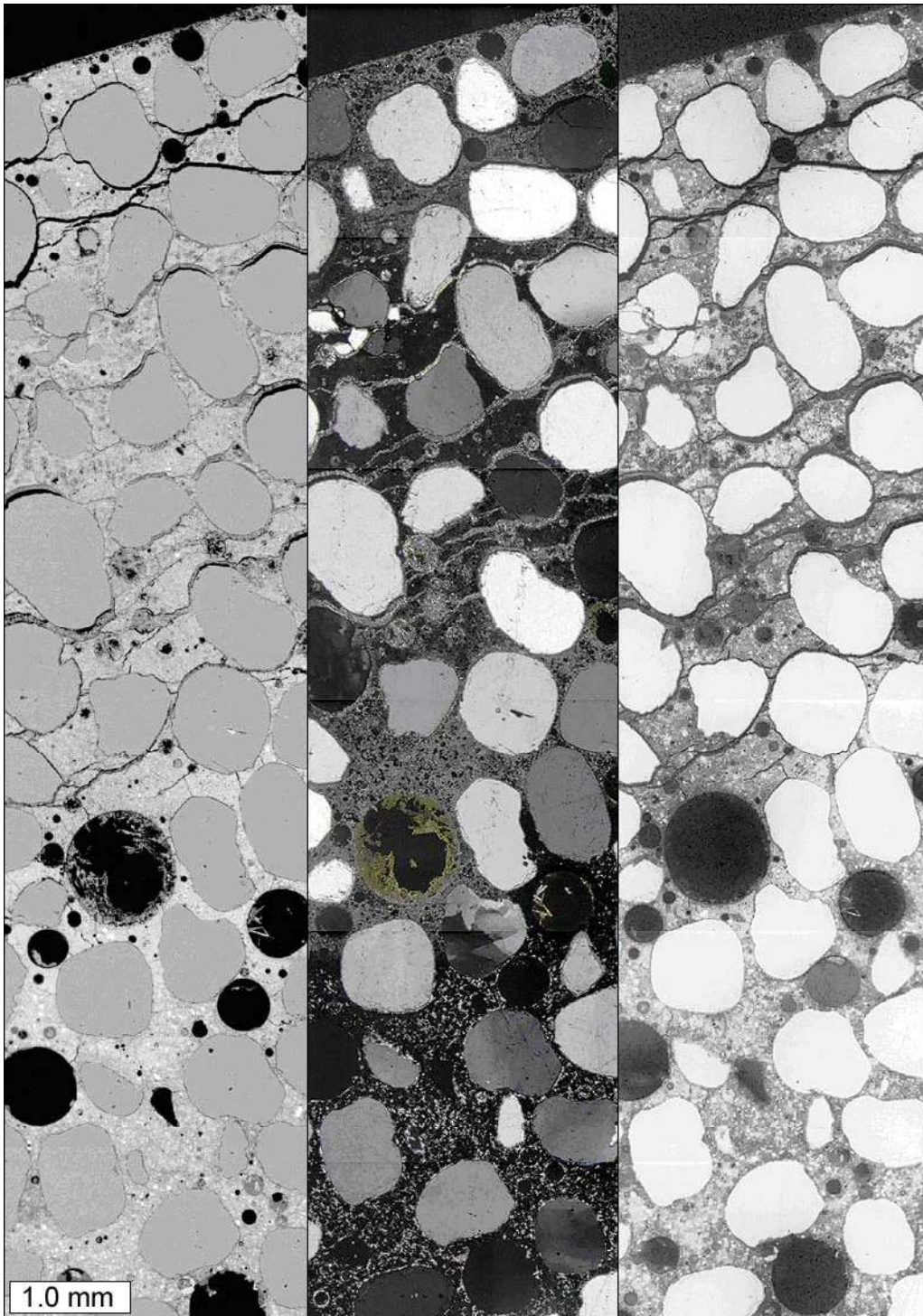


Figure 5.17. From left to right: back scattered electron image, cross polarized light, and epifluorescent mode images of a thin section prepared from a cylinder immersed in calcium chloride solution.

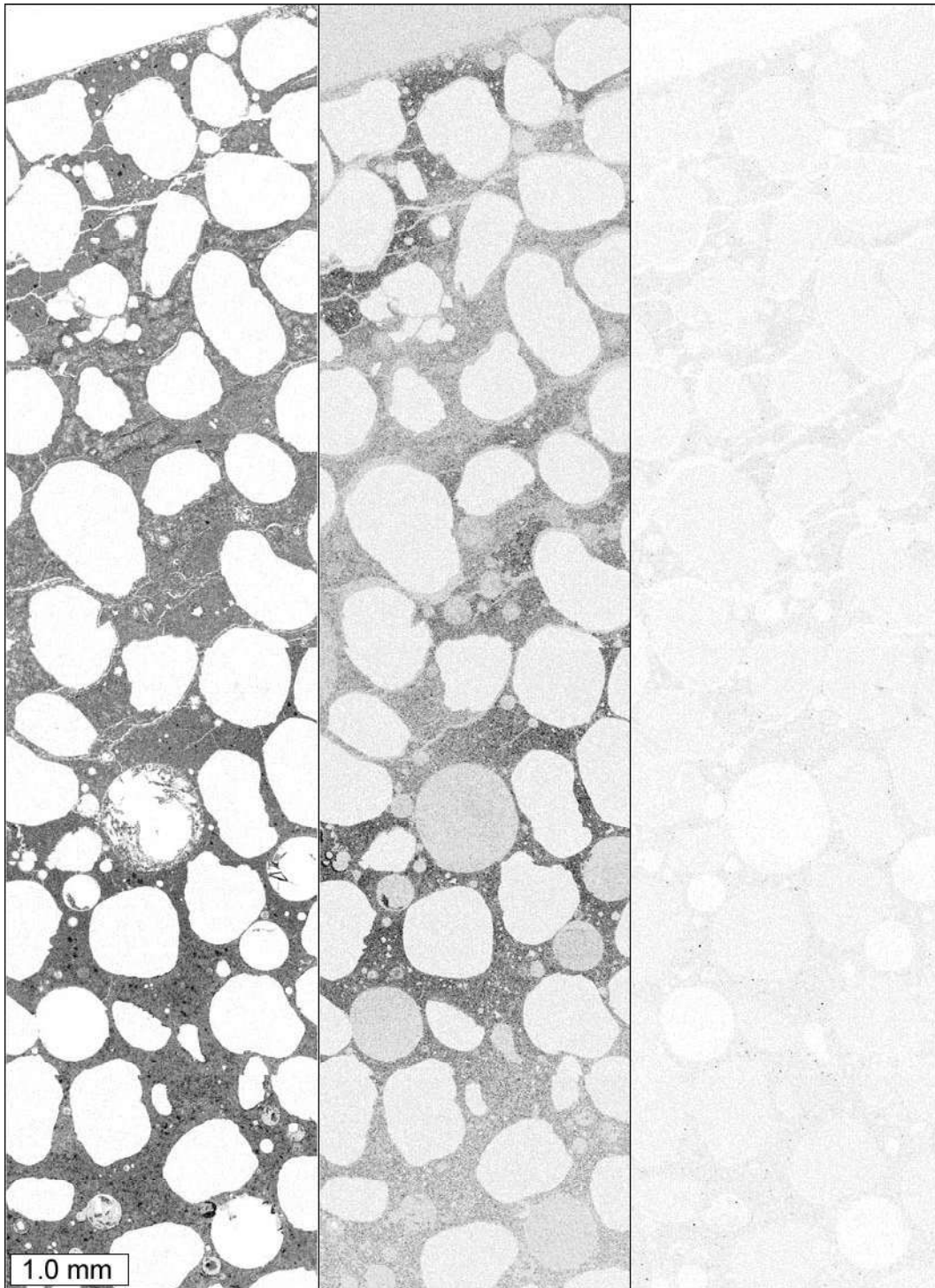


Figure 5.18. Elemental maps, from left to right: calcium, chloride, and magnesium. The elemental maps were collected from a thin section prepared from a cylinder immersed in calcium chloride solution. Darker areas indicate a higher concentration.

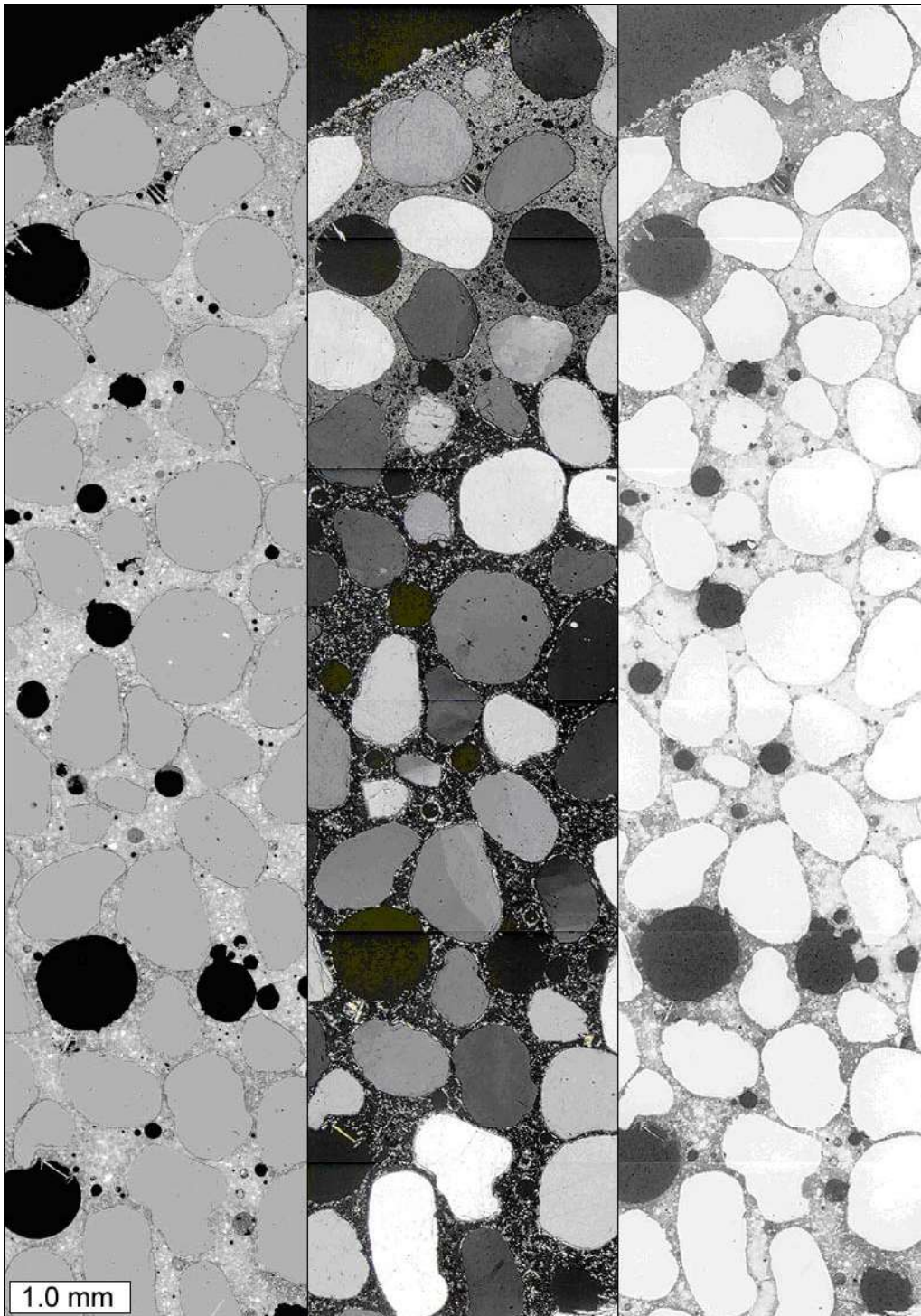


Figure 5.19. From left to right: back scattered electron image, cross polarized light, and epifluorescent mode images of a thin section prepared from a cylinder immersed in sodium chloride solution.

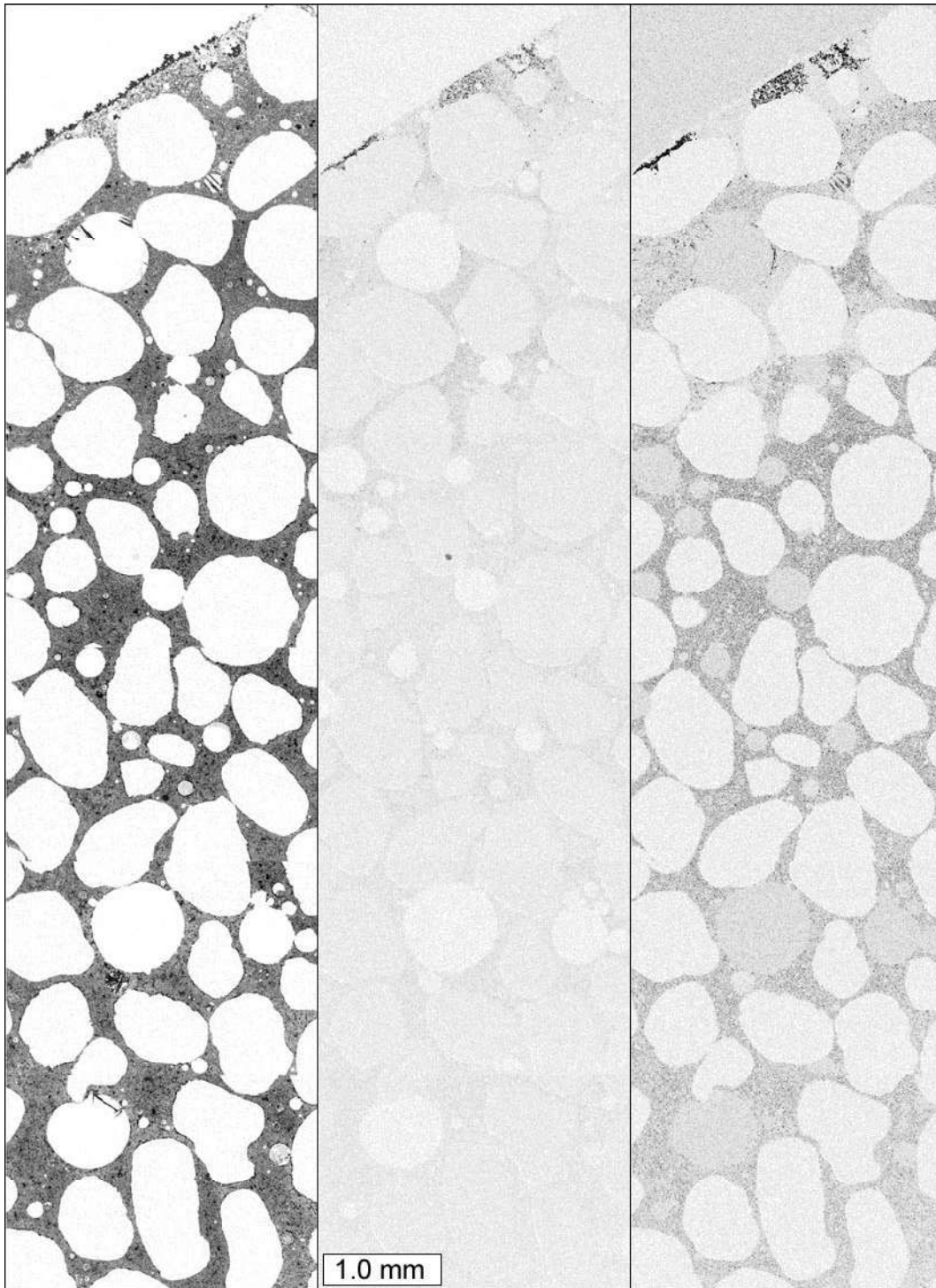


Figure 5.20. Elemental maps, from left to right: calcium, sodium, and chlorine. The elemental maps were collected from a thin section prepared from a cylinder immersed in sodium chloride solution. Darker areas indicate a higher concentration.

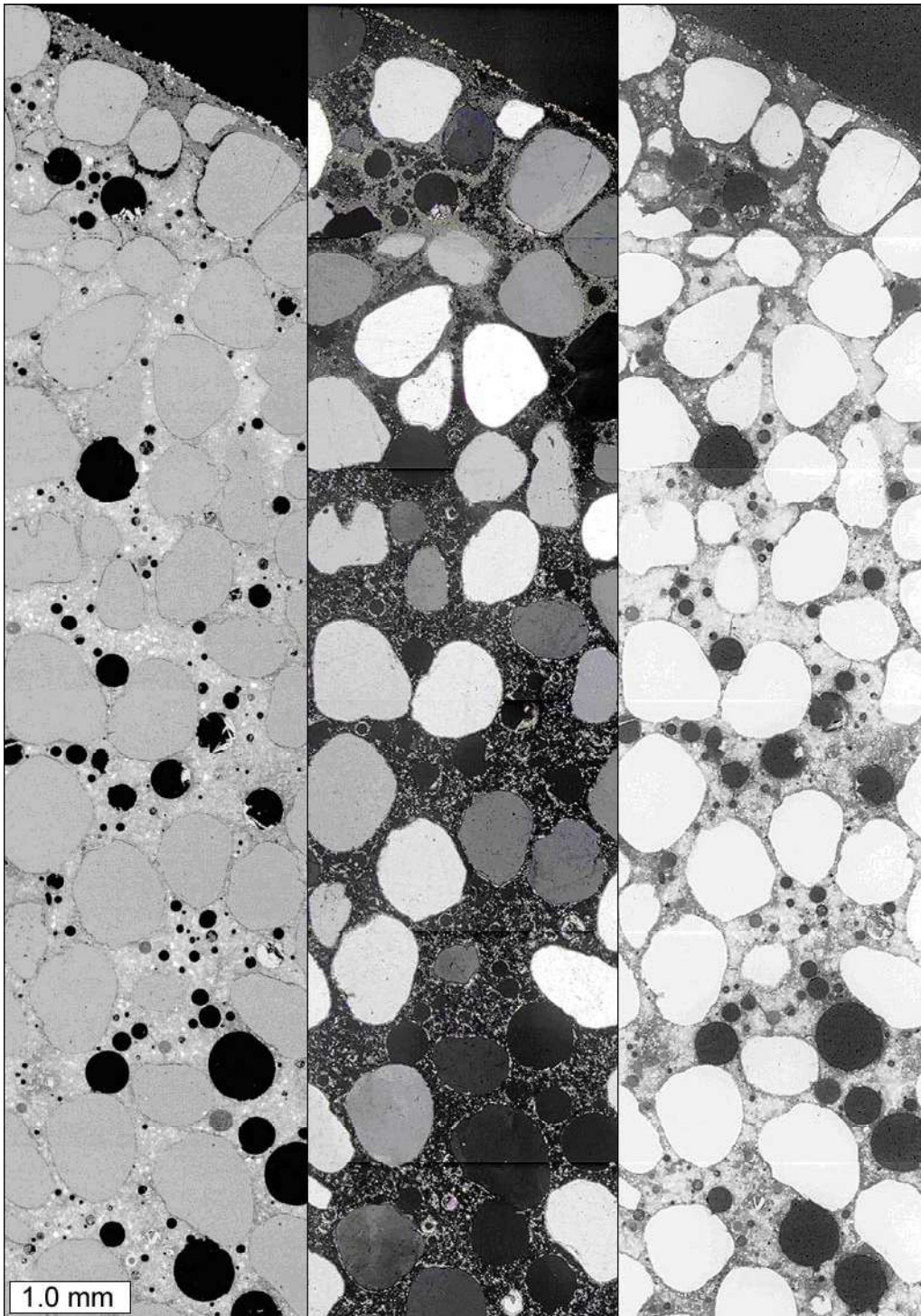


Figure 5.21. From left to right: back scattered electron image, cross polarized light, and epifluorescent mode images of a thin section prepared from a cylinder immersed in calcium magnesium acetate solution.

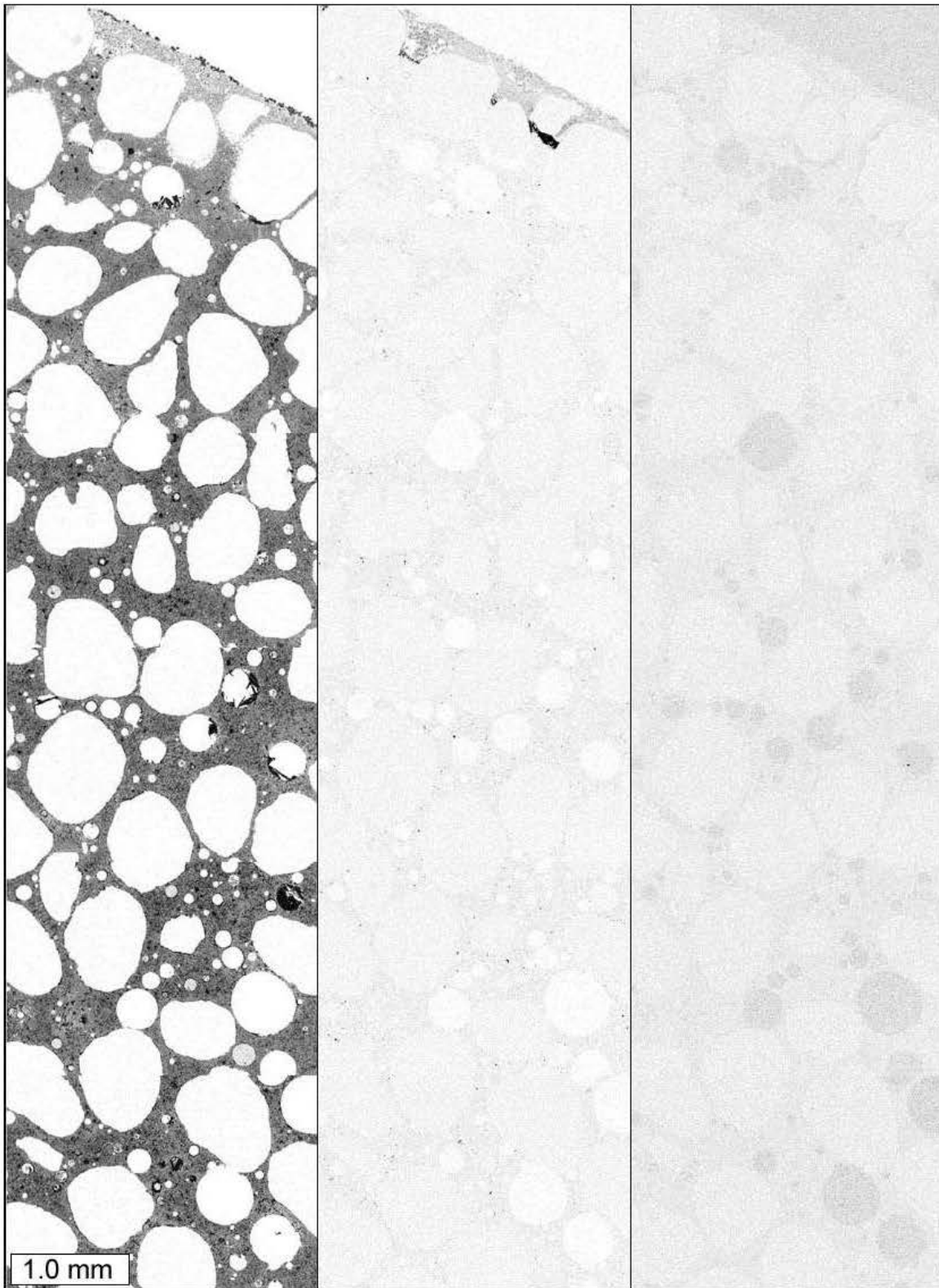


Figure 5.22. Elemental maps, from left to right: calcium, magnesium, and chlorine. The elemental maps were collected from a thin section prepared from a cylinder immersed in calcium magnesium acetate solution. Darker areas indicate a higher concentration.

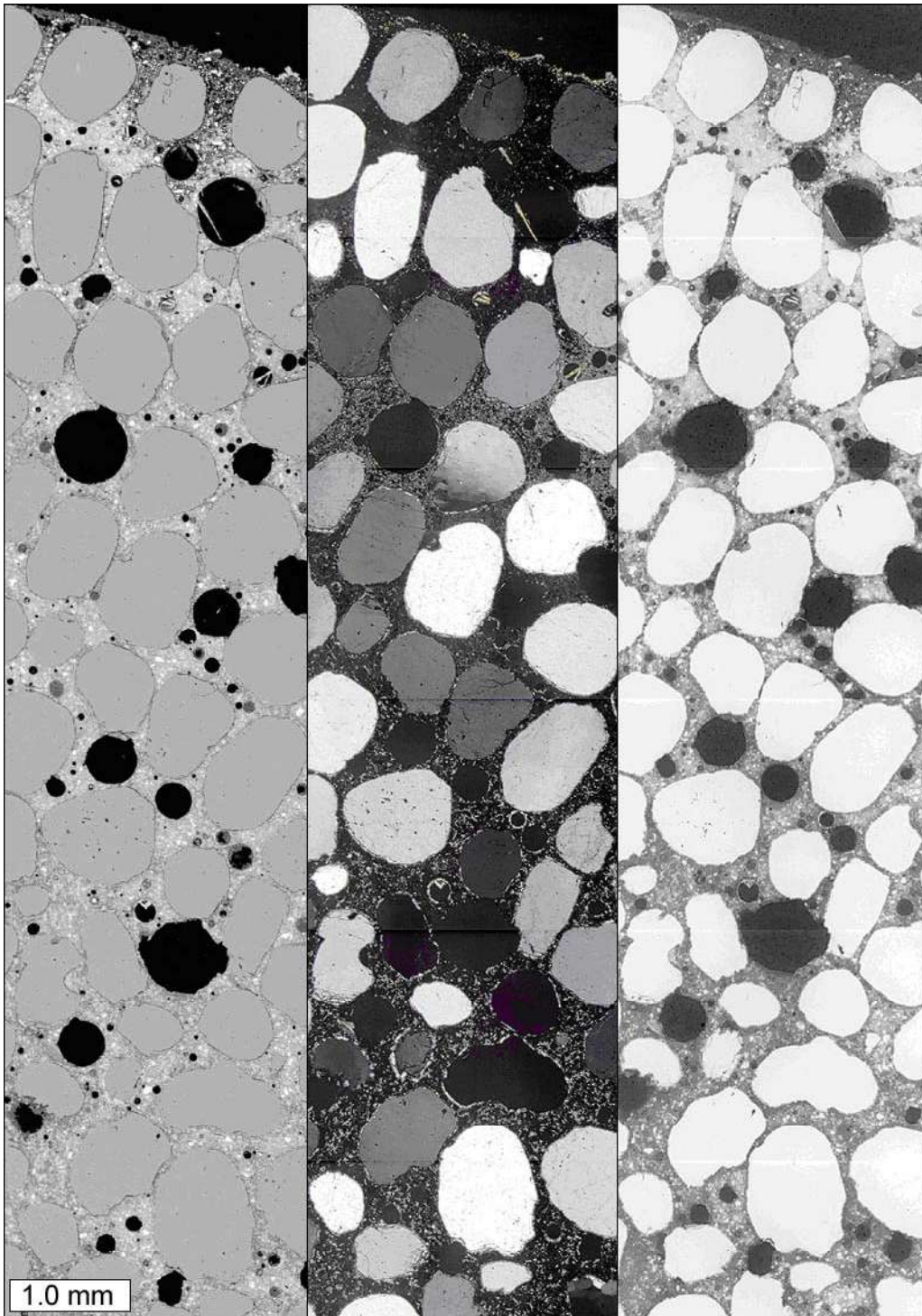


Figure 5.23. From left to right: back scattered electron image, cross polarized light, and epifluorescent mode images of a thin section prepared from a cylinder immersed in limewater.

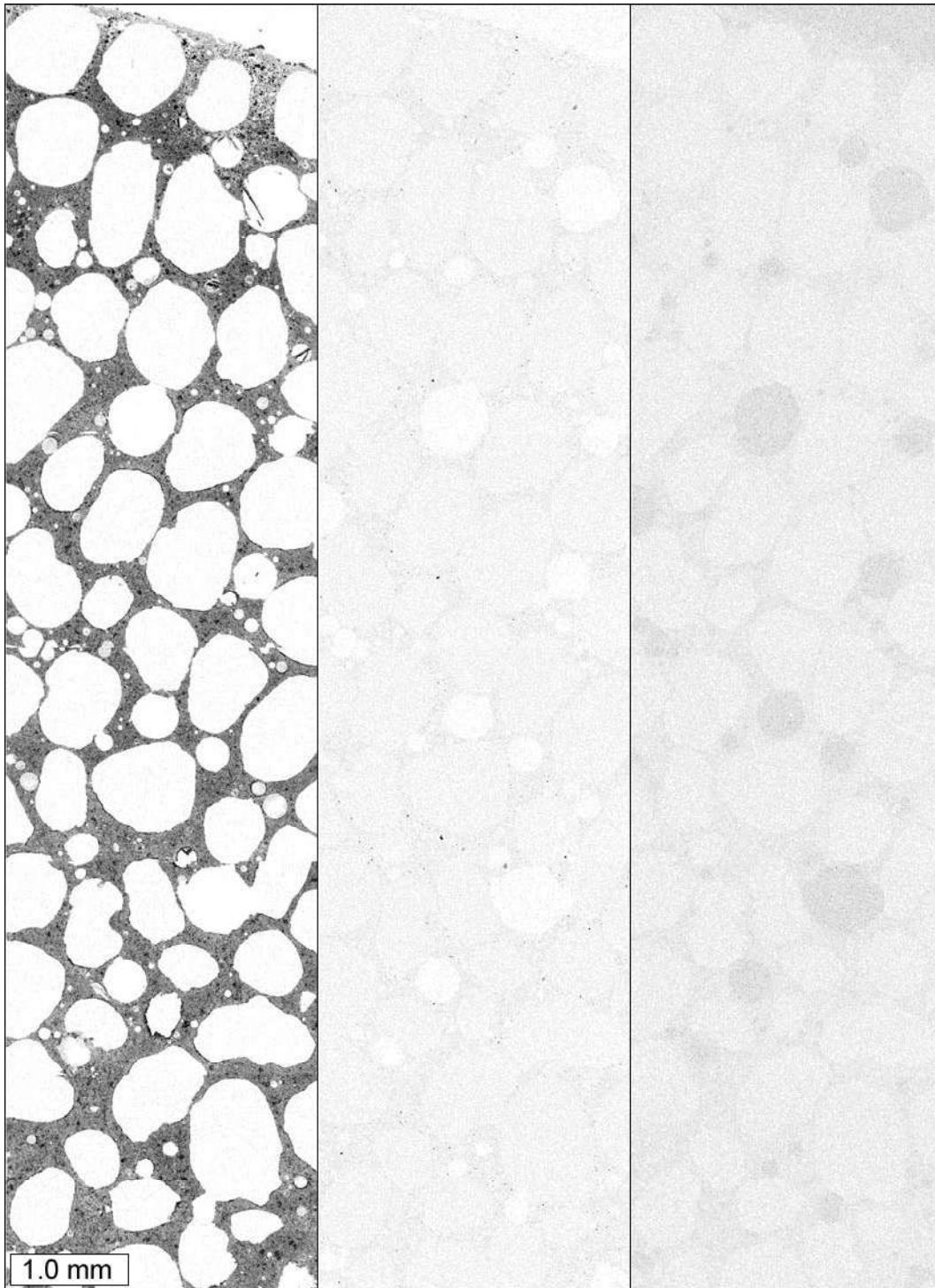


Figure 5.24. Elemental maps, from left to right: calcium, magnesium, and chlorine. The elemental maps were collected from a thin section prepared from a cylinder immersed in limewater. Darker areas in elemental maps indicate a higher concentration.

5.2.1.2 Additional Phase I Experiment

It was determined that the cold temperature experiment showed the clearest damage and therefore this test was used to determine the effect of solution concentration on the observed distress. New mortar samples were exposed to CaCl_2 solutions at varying concentrations. For this experiment, solution concentrations were chosen at 3, 7, 10, and 14 weight percent salt. The specimens were left in solution for 54 days with random samples being removed every 7 days for inspection and analysis.

As can be seen clearly in Figures 5.25 through 5.29, concentration clearly has an affect on the observed damage at a given time for mortars exposed to the low temperature test.



Figure 5.25. Cylinders exposed to 3% CaCl_2 solution after 56 days of constant low temperature test.
From left to right: 0.40, 0.50, and 0.60 w/c.



Figure 5.26. Cylinders exposed to 7% CaCl_2 solution after 56 days of constant low temperature test.
From left to right: 0.40, 0.50, and 0.60 w/c.



Figure 5.27. Cylinders exposed to 10% CaCl_2 solution after 56 days of constant low temperature test.
From left to right: 0.40, 0.50, and 0.60 w/c.



Figure 5.28. Cylinders exposed to 14% CaCl_2 solution after 56 days of constant low temperature test.
From left to right: 0.40, 0.50, and 0.60 w/c.



Figure 5.29. Cylinders exposed to 17% CaCl₂ solution after 56 days of constant low temperature test. From left to right: 0.40, 0.50, and 0.60 w/c.

5.2.2 RESULTS OF PHASE I EXPERIMENTS CONDUCTED AT THE UNIVERSITY OF TORONTO

5.2.2.1 Compressive Strength

Mortar cubes prepared for these tests were tested at 28 days of age and the average compressive strength of the mortar cubes was 6238 psi [43 MPa]. After exposure to the different deicers, the compressive strength decreased for those samples exposed to MBAP, MgCl₂ and CaCl₂. The compressive strength results are shown in Figure 5.30. The compressive strength decreased in the order MgCl₂, MBAP and CaCl₂ by 63, 62 and 23% respectively, when compared with the compressive strength of mortar cubes exposed to saturated calcium hydroxide solution. The mortar cubes exposed to NaCl did not show a decrease in compressive strength and to the contrary, their behavior was similar to those samples exposed to the calcium hydroxide solution. That is, the compressive strength increased with time as is expected with continuous hydration. The samples exposed to MBAP and MgCl₂ showed similar trends in their compressive strength evolution with time.

5.2.2.2 Expansion

Exposure of mortar bars to MBAP, MgCl₂ and CaCl₂ resulted in considerable expansion while those subjected to NaCl showed negligible expansion even after 500 days of exposure, as illustrated in Figure 5.31. MBAP caused the highest expansion of all, 0.75% at 568 days followed by MgCl₂ and CaCl₂ with 0.37 and 0.29% respectively. Although MBAP and MgCl₂ caused the compressive strength to decrease to a similar degree, a similar correlation was not observed with the rate of expansion. The MBAP samples expanded almost twice as much as samples exposed to MgCl₂, with the same exposure period.

5.2.2.3 Mass Change

For those specimens exposed to MBAP, MgCl₂ and CaCl₂, expansion of mortar bars was accompanied by considerable mass gain as shown in Figure 5.32. The greatest mass gain was 5.9% observed for those samples exposed to MBAP, followed by MgCl₂ with 3.6% and CaCl₂ with 2.4% mass gain. The specimens exposed to NaCl and saturated calcium hydroxide solution did not show considerable mass gain with 1.4 and 1.1% recorded, respectively.

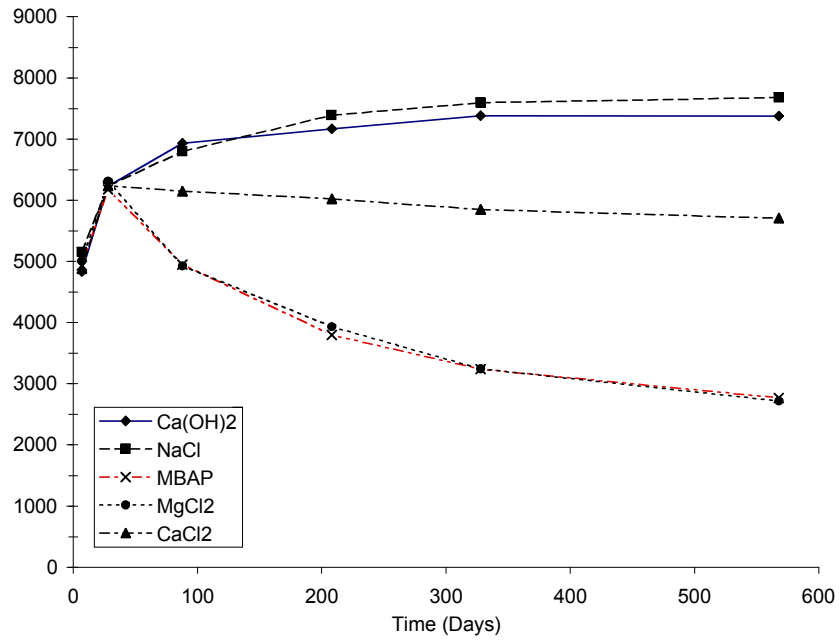


Figure 5.30. Compressive strength evolution with time of mortar cubes exposed to different deicers.

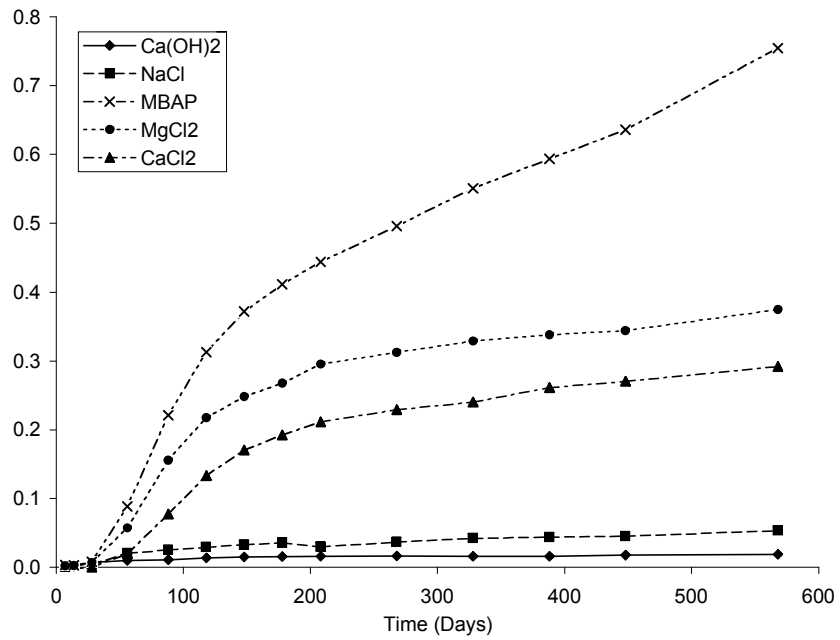


Figure 5.31. Length change of mortar bars with time for mortar bars exposed to different deicers.

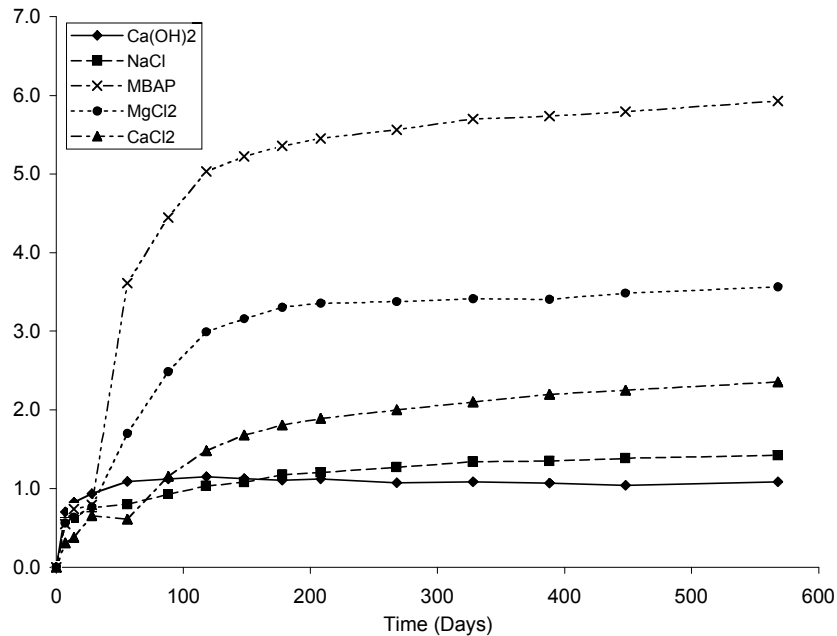


Figure 5.32. Mass change of mortar bars with time of mortar bars exposed to different deicers.

5.2.2.4 Visual Observations

Visual observations of the specimens exposed to MBAP and MgCl₂ that experienced loss of strength, expansion and mass gain revealed a clear feature. Defined zones of chemical interaction of 0 to 0.2 inches [0 to 5 mm] through the cross sectional area of the mortar bars were visible. These zones are easily identified by the changes in color from a light gray in the core of the specimen to a yellowish color at the surface. The presence of micro-cracks was confirmed using the stereo optical microscope.

At early ages (less than 118 days) a white layer developed on the surface of specimens exposed to MBAP and MgCl₂, and it was subsequently identified by X-ray diffraction as brucite. The deterioration front seemed to move deeper into the specimen with exposure time. Softening of the surface and debonding of sand grains were identified. None of these features were identified in samples exposed to either CaCl₂ or NaCl.

5.2.2.5 Mercury Intrusion Porosimetry (MIP)

The observed chemical interaction appeared to proceed inwards from the surface to the core of the specimens, so surface slices of 0.2 inch [5 mm] thickness were analyzed using MIP to determine the effect of the deicers on the porosity of the mortar bars, which in turn effects the diffusion and penetration of the deicers into the specimens for further chemical interaction. Table A3.9 in the Appendix, Section 3, presents the results for MIP at 248 days of exposure time. Those deicers such as MBAP and MgCl₂ that caused considerable expansion, mass gain and loss of compressive strength, showed an increase in the total volume of pores of up 20% when compared with the reference samples exposed to calcium hydroxide. On the other hand, those specimens exposed to NaCl and CaCl₂ did not show the same effect. However, the total pore surface area increased for those samples exposed to CaCl₂.

5.2.2.6 Solution pH

Figure 5.33 shows the change in pH of the various exposure solutions during the exposure period. For the first 28 days, the samples were cured in calcium hydroxide saturated solution with a pH of approximately 12.7. Once the samples were immersed in the deicers, the pH of the exposure solution initially decreased, then increased. This is represented by the pronounced spike towards low pH seen at 28 days in Figure 5.33. For example, the pH of the MBAP and $MgCl_2$ solutions were 7.8 and 8.3, respectively, at the beginning of the salt solution exposure period and increased to up to approximately 8.6 after continued exposure of the mortar specimens to these same solutions. The $CaCl_2$ solution, initially acidic (e.g. pH of 5.6) after immersion of the specimens, increased to approximately 11.4 after exposure. The $NaCl$ solution, with an initial pH of 7.6, increased to a pH of 12.4. This is much higher than that of the MBAP and closer to the pH of the calcium hydroxide solution at 12.7. It is expected that a solution pH less basic than a saturated solution calcium hydroxide solution (e.g. less than pH 10) will leach calcium hydroxide from the mortar samples until either reaching equilibrium with the pH of the pore solution or depleting the calcium hydroxide available for buffering the exposure solution.

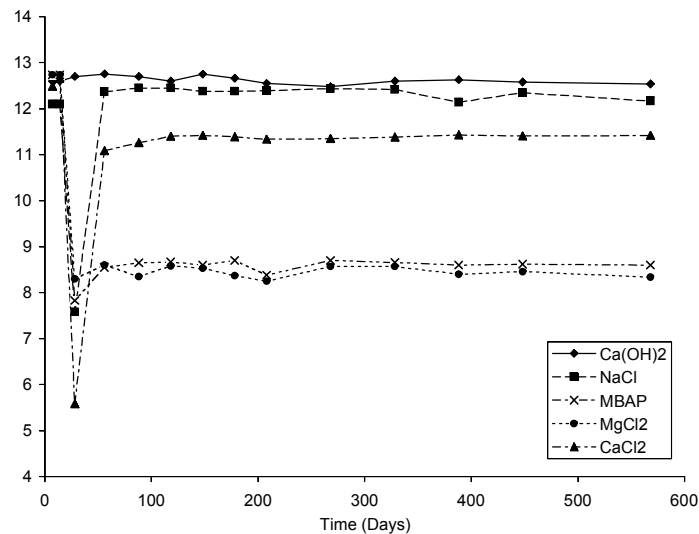


Figure 5.33. Measured pH change during deicer exposure period.

$MgCl_2$ solutions, the equilibrium pH is a function of the solution concentration. This relationship is shown in Figure A3.94 of the Appendix, Section 3. As an example, when mortar specimens were exposed to a solution of 20% $MgCl_2$, the solution pH stabilized at 8.5. However, when mortar specimens were exposed to a solution of 30% $MgCl_2$, the solution pH stabilized at 6.5. This would indicate that the amount of calcium hydroxide dissolved into solution is a function of the solution strength. In the presence of higher $MgCl_2$ concentrations, increasing amounts of less soluble oxychloride phases form, consuming the hydroxide and reducing that available to go into solution.

5.2.2.7 X-ray Diffraction

X-ray diffraction analysis of powder samples taken from the surface of the mortar bars up to a depth of 0.2 inches [5 mm] showed the formation of new phases and the depletion of others. In the case of the samples exposed to the saturated calcium hydroxide solution, no sign of chemical attack was apparent with the main calcium hydroxide peaks as well as peaks for ettringite, silica (i.e. from the Ottawa

sand), and other minor phases clearly defined in the diffractogram shown in the Appendix, Section 3, Figure A3.80.

Those samples exposed to NaCl solutions had phases similar to those exposed to calcium hydroxide solutions, the only difference being the presence of Friedel's salt. A typical X-ray diffraction pattern for a mortar specimen exposed to NaCl solution is shown in the Appendix, Section 3, Figure A3.81. In the case of MBAP, besides Friedel's salt, some peaks of a phase resembling magnesium oxychloride (PDF 00-007-042 $Mg_3(OH)_5Cl \cdot 4H_2O$), was identified as seen in the Appendix, Section 3, Figure A3.82. This phase was not detected in the samples exposed to $MgCl_2$ but instead defined peaks of brucite were found as shown in the Appendix, Section 3, Figure A3.83. For both MBAP and $MgCl_2$ the intensity of the main peaks of calcium hydroxide diminished suggesting depletion of this phase due to chemical attack, leaching or both.

The sample exposed to $CaCl_2$ did not show any new phases and although some depletion of calcium hydroxide was observed, calcium hydroxide was still present. It was expected that the expansion, gain in mass and the slow loss of compressive strength observed would be related to the formation of new phases yet this was not the case. Either the minor depletion of calcium hydroxide was due to leaching, or the amount of a newly formed phase by reaction of calcium chloride with calcium hydroxide was below the detection limit of the X-ray diffraction technique, or both. In the Appendix, Section 3, Figure A3.84 shows the X-ray diffraction pattern of the mortar sample exposed to $CaCl_2$ with Friedel's salt as the only new phase detected. Other phases are normal hydration reaction products.

Samples exposed to CMA at room temperature disintegrated approximately 30 days after immersion. As a result, measurements of length, mass, and compressive strength change were impossible. Figure 5.34 below presents a photograph taken before complete disintegration of the mortar cubes exposed to CMA, illustrating how the mortar lost cohesiveness causing crumbling particles to pile up next to the specimen until nothing was left but debris. Within this time samples were taken for X-ray diffraction analysis and a compound identified as calcium acetate hydrate was present. X-ray diffraction results for this phase are shown in the Appendix, Section 3, Figure A3.86.



Figure 5.34. Disintegration of mortar cubes during exposure to CMA at 73.4 °F [23 °C].

5.2.2.7 Determination of Pessimum Concentration for $MgCl_2$ and $CaCl_2$

Mortar cubes were exposed to different concentrations of $MgCl_2$ and $CaCl_2$ at 41 °F [5 °C] to determine the effect of the exposure solution concentration on 30 day compressive strength of the mortar. The effect of concentration on compressive strength is shown in Figure 5.35. For those samples subjected to $MgCl_2$, the compressive strength increased for concentrations between 25 and 30% by mass of salt. There was no identifiable reason for this increase but additional tests gave similar results. At 20% $MgCl_2$, the compressive strength suffered a dramatic loss of up to 57%. For $CaCl_2$ solutions between 5 and 11% by mass of $CaCl_2$ the compressive strength was not effected at 30 days. Above 11% and up to 28%, the loss of compressive strength was considerable with 58% strength loss at 22% $CaCl_2$.

X-ray diffraction analysis of samples exposed to the pessimum concentration of $MgCl_2$ (i.e. 20%) and $CaCl_2$ (i.e. 22%) showed that the phase formed during the deterioration process of the mortar was a type of magnesium for $MgCl_2$ exposure and calcium oxychloride for $CaCl_2$ exposure. Diffraction results are shown in the Appendix, Section 3, Figure A3.88 and Figure A3.89, respectively. Phase identification of calcium oxychloride is based on the main diffraction peaks at 8.215, 4.139 and 2.768 Å, similar to those reported by other researchers (Colleparidi et al. 1994) of 8.34, 4.17 and 2.78 Å. Appendix, Section 3, Figures A3.90 and A3.91 show photographs illustrating the visual damage of specimens exposed to 20% $MgCl_2$ and 28% $CaCl_2$ respectively after 150 days of exposure.

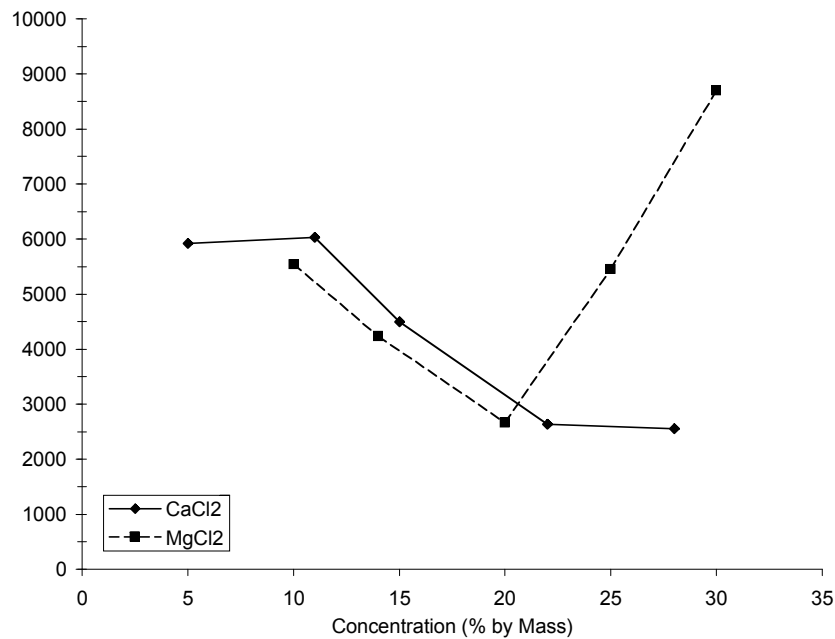


Figure 5.35. Effect of $MgCl_2$ and $CaCl_2$ on compressive strength after 30 days of exposure.

5.3 PHASE II LABORATORY EXPERIMENT RESULTS

5.3.1 RESULTS OF PHASE II EXPERIMENTS JOINTLY CONDUCTED AT MICHIGAN TECH AND THE UNIVERSITY OF TORONTO

5.3.1.1 Physical Characterization of Mortar and Concrete Mixtures

Mortar and concrete mixtures prepared by Michigan Tech for use in Phase II were analyzed at the University of Toronto to determine their sorptivity and bulk diffusion properties. The mortar mixtures were prepared and analyzed to provide baseline information regarding the characteristics of the mixtures used in Phase II. They are not the same mixture designs used in Phase I with the principal difference being the *w/c* used. The *w/c* of the mortars tested were the same as for the concrete mixtures (i.e. 0.45 and 0.55).

The specimens were discs saw cut from 4 x 2 inch [200 by 100 mm] cylinders without the finished surface. A total of 162 samples were provided to be used on three different tests: the rapid chloride permeability test as per ASTM C1202 “*Electrical Indication of Concrete’s Ability to Resist Chloride Ion Penetration*”, bulk diffusion tests as per ASTM C 1556, “*Determining the Apparent Chloride Coefficient of Cementitious Mixtures by Bulk Diffusion*”, and sorptivity as per ASTM C 1585, “*Measurement of Rate of Absorption of Water by Hydraulic Cement Concretes*” Tables 5.10 and 5.11 list the number and type of mixtures tested and the number of samples.

Table 5.2. Mortar samples tested for rapid chloride permeability, bulk diffusion, and sorptivity.

Number of Samples	Mixture	<i>w/cm</i>
12	GGBFS + OPC	0.55
12	GGBFS + OPC	0.45
12	OPC	0.55
12	OPC	0.45
12	15% fly ash + OPC	0.55
12	15% fly ash + OPC	0.45

Table 5.3. Concrete samples tested for rapid chloride permeability, bulk diffusion, and sorptivity.

Number of Samples	Mixture	<i>w/cm</i>
18	GGBFS + OPC	0.55
12	GGBFS + OPC	0.45
18	OPC	0.55
12	OPC	0.45
18	15% fly ash + OPC	0.55
12	15 % fly ash + OPC	0.45

5.3.1.2. Rapid Chloride Permeability Test

This test gives a relative indication of the chloride penetrability and conductivity of the sample so all the mortar and concrete mixtures can be ranked relative to each other based on the charge passed during the test. To avoid misleading results due to heating of the specimen during the test, the total charge reported will be based on the 30 minutes charge (the 30 minute coulomb value was multiplied by 12 to obtain an equivalent 6 hour value). Two specimens per mixture were tested for a total of 24 specimens. Table A3.21 in the Appendix summarizes the results showing the charged passed and the chloride ion penetrability.

5.3.1.3. Bulk Diffusion

This test has two components; first, the determination of the apparent chloride diffusion coefficient on exposed sawn surfaces, and second, the determination of the apparent chloride diffusion coefficient on sealed, sawn surfaces. The type of salt, exposure solution concentration, and exposure temperature have been modified, relative to the standard procedure, to replicate the conditions used under Phase I of this project. That is, 15% magnesium chloride, 17% calcium chloride and 18% NaCl were the exposure solutions used at a constant 41 °F [5 °C] exposure temperature. For the first part five specimens were tested per mix for a total of 60 specimens.

For the second component only concrete mixtures with *w/cm* of 0.55 were tested. The same exposure conditions as mentioned above were used. Two type of sealers were evaluated, a siloxane based product (12% oligomeric organosiloxane solids in water) and a silane based product (40% alkylalkoxysilane solids in 2-propanol). For this part six specimens were tested for a total of 18 specimens.

Concrete samples coated with siloxane did not allow the penetration of chloride ions; therefore, the experimental data cannot be fitted with Fick's 2nd law equation. Instead, 97 - 99 are added for comparison purposes. Concrete samples coated with silane exhibited minor penetration of chloride ions.

5.3.1.4. Sorptivity

For this test, five specimens were tested per mix for a total of 60 specimens. Besides the rate of absorption of water, three deicing salts were included for analysis: magnesium chloride, calcium chloride and sodium chloride. In general, the higher the rate of absorption, the more susceptible the sample is to penetration of the exposure solution. Appendix Section 3, Table A3.19 summarizes the results of sorptivity testing for the mortar mixtures tested. Appendix Section 3, Figure A3.100 – A3.113 present the plots of sorptivity trends for each mortar mixture, and for each solution tested. Shown below, Table 5.4 summarizes the results of sorptivity testing for the concrete mixtures tested. Figures 5.36 – 5.49 present the plots of sorptivity trends for each concrete mixture, and for each solution tested.

Table 5.4. Sorptivity results for concrete samples

Exposure solution / Code*	w/cm = 0.45		w/cm = 0.55	
	Initial Absorption Si (mm/s ^{1/2}) / [r ²]	Secondary Absorption S _s (mm/s ^{1/2}) / [r ²]	Initial Absorption Si (mm/s ^{1/2}) / [r ²]	Secondary Absorption S _s (mm/s ^{1/2}) / [r ²]
Water				
PCW	3.0 x 10 ⁻³ [0.99]	1.9 x 10 ⁻³ [0.96]	6.2 x 10 ⁻³ [0.99]	2.7 x 10 ⁻³ [0.92]
FCW	2.7 x 10 ⁻³ [0.99]	1.8 x 10 ⁻³ [0.99]	6.6 x 10 ⁻³ [0.99]	2.1 x 10 ⁻³ [0.82]
SGW	1.8 x 10 ⁻³ [0.99]	1.1 x 10 ⁻³ [0.99]	2.8 x 10 ⁻³ [0.99]	1.8 x 10 ⁻³ [0.99]
CaCl₂				
PCC	1.2 x 10 ⁻³ [0.99]	4.9 x 10 ⁻⁴ [0.94]	3.0 x 10 ⁻³ [0.99]	1.7 x 10 ⁻³ [0.99]
FCC	2.4 x 10 ⁻³ [0.98]	8.1 x 10 ⁻⁴ [0.99]	4.3 x 10 ⁻³ [0.99]	2.4 x 10 ⁻³ [0.99]
SGC	1.1 x 10 ⁻³ [0.98]	2.2 x 10 ⁻⁴ [0.99]	1.5 x 10 ⁻³ [0.98]	6.1 x 10 ⁻⁴ [0.97]
MgCl₂				
PCM	6.6 x 10 ⁻⁴ [0.99]	7.4 x 10 ⁻⁴ [0.99]	1.3 x 10 ⁻³ [0.97]	1.2 x 10 ⁻³ [0.99]
FCM	4.6 x 10 ⁻⁴ [0.98]	3.3 x 10 ⁻⁴ [0.99]	1.4 x 10 ⁻³ [0.99]	1.3 x 10 ⁻³ [0.99]
SGM	4.2 x 10 ⁻⁴ [0.96]	1.9 x 10 ⁻⁴ [0.99]	6.7 x 10 ⁻⁴ [0.99]	2.5 x 10 ⁻⁴ [0.99]
NaCl				
PCN	1.8 x 10 ⁻³ [0.99]	1.4 x 10 ⁻³ [0.97]	4.0 x 10 ⁻³ [0.99]	2.6 x 10 ⁻³ [0.98]
FCN	2.9 x 10 ⁻³ [0.99]	1.5 x 10 ⁻³ [0.99]	4.4 x 10 ⁻³ [0.99]	2.7 x 10 ⁻³ [0.99]
SGN	1.5 x 10 ⁻³ [0.98]	5.7 x 10 ⁻⁴ [0.99]	2.2 x 10 ⁻³ [0.98]	9.3 x 10 ⁻⁴ [0.99]

PCW: portland cement concrete - tap water
 PCM: portland cement concrete - MgCl₂
 FCW: 15% fly ash concrete - tap water
 FCM: 15% fly ash concrete - MgCl₂
 SGW: GGBFS cement concrete - tap water
 SGM: GGBFS cement concrete - MgCl₂

PCC: portland cement concrete - CaCl₂
 PCN: portland cement concrete - NaCl
 FCC: 15% fly ash concrete - CaCl₂
 FCN: 15% fly ash concrete - NaCl
 SGC: GGBFS cement concrete - CaCl₂
 SGN: GGBFS cement concrete - NaCl

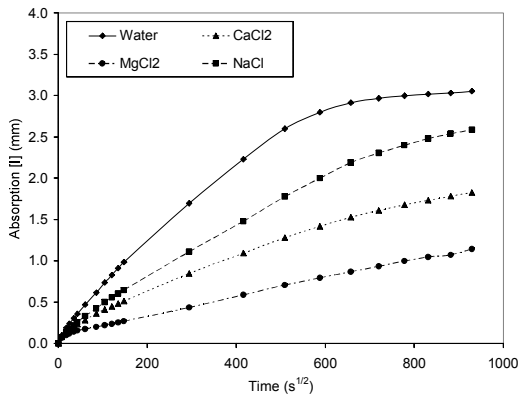


Figure 5.36. Sorptivity of portland cement concrete - w/c - 0.55

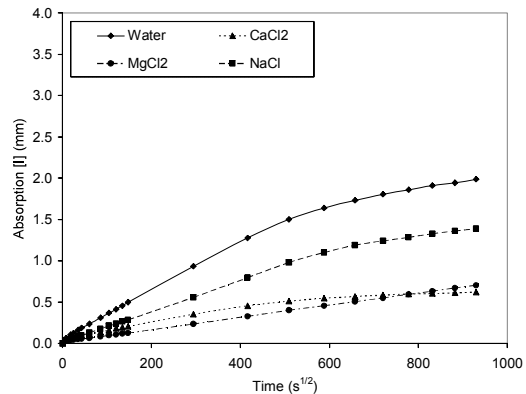


Figure 5.37. Sorptivity of portland cement concrete - w/c - 0.45

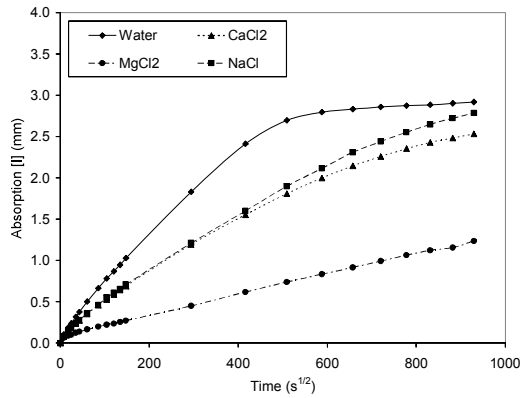


Figure 5.38. Sorptivity - fly ash concrete - w/cm - 0.55

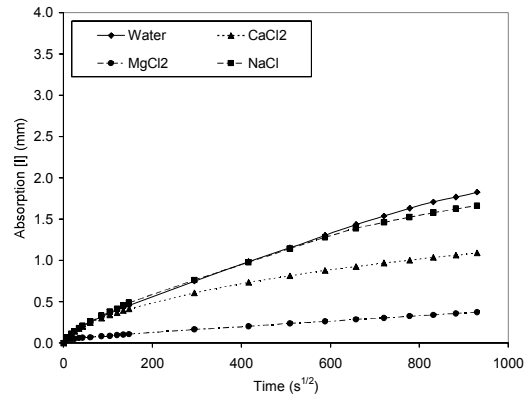


Figure 5.39. Sorptivity - fly ash concrete - w/cm - 0.45

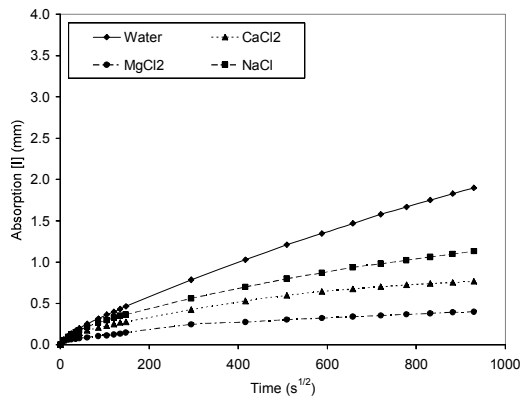


Figure 5.40. Sorptivity - GGBFS concrete - w/cm - 0.55

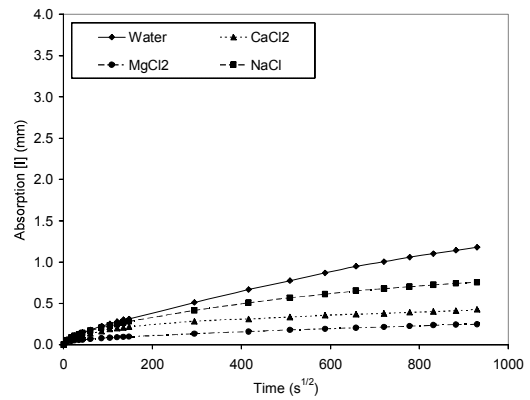


Figure 5.41. Sorptivity - GGBFS concrete - w/cm - 0.45

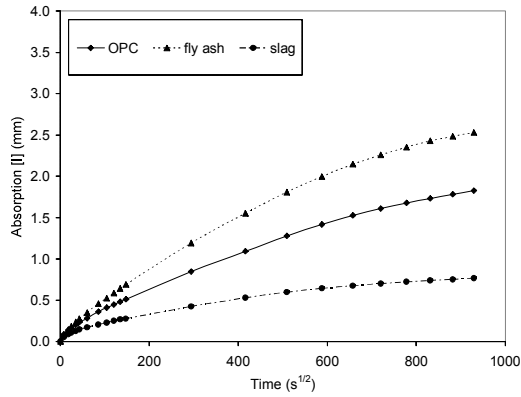


Figure 5.42. Sorptivity - concrete w/cm - 0.55 - $CaCl_2$

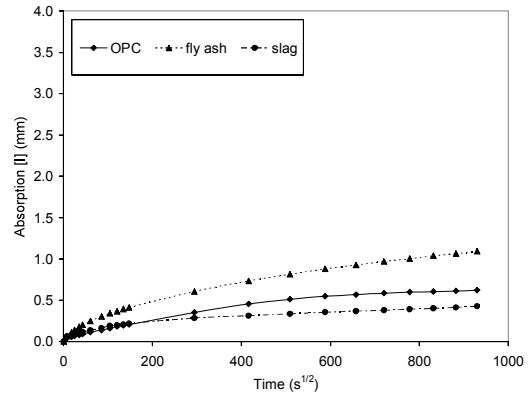


Figure 5.43. Sorptivity - concrete w/cm - 0.45 - $CaCl_2$

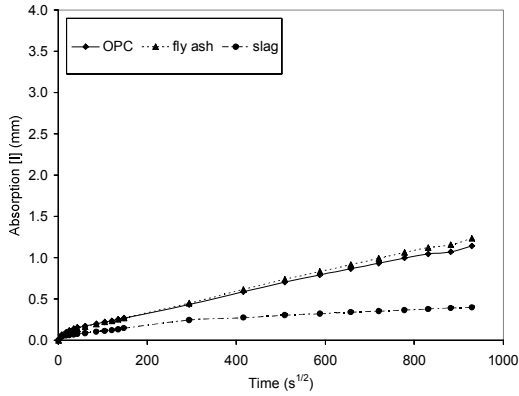


Figure 5.44. Sorptivity - concrete w/cm - 0.55 - $MgCl_2$

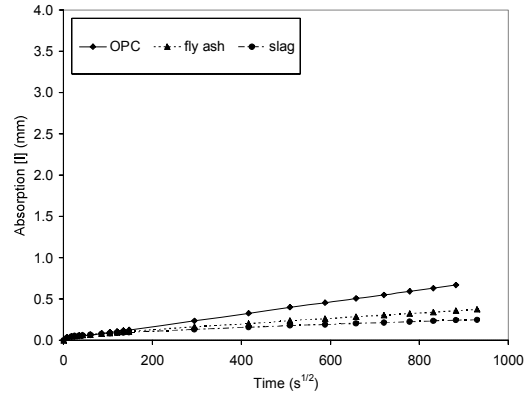


Figure 5.45. Sorptivity - concrete w/cm - 0.45 - $MgCl_2$

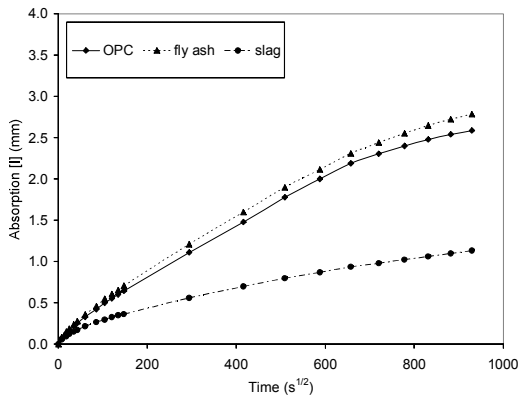


Figure 5.46. Sorptivity - concrete w/cm - 0.55 - $NaCl$

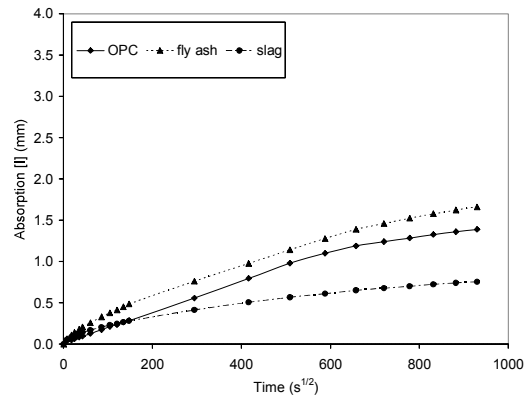


Figure 5.47. Sorptivity - concrete w/cm - 0.45 - $NaCl$

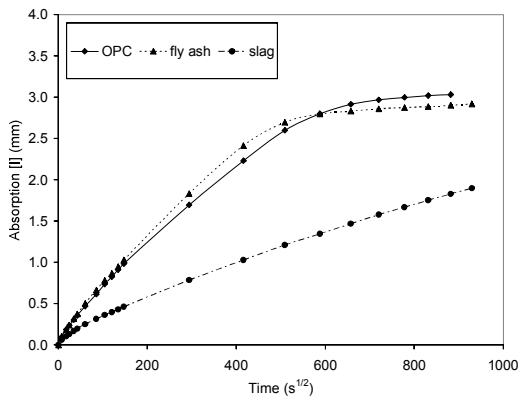


Figure 5.48. Sorptivity - concrete w/cm - 0.55 - water

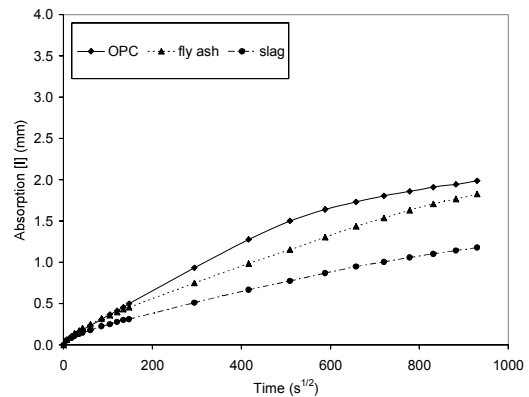


Figure 5.49. Sorptivity - concrete w/cm - 0.45 - water

5.3.2 RESULTS OF PHASE II EXPERIMENTS CONDUCTED AT THE MICHIGAN TECH

5.3.2.1 Macroscopic Observations

Random concrete and mortar specimens were removed from the various brine solutions after 60 days of exposure, with the remainder being removed after 500 days exposure. After

removal from the brines, the specimens were blown dry with an air hose and cut with a kerosene cooled diamond saw. Specimens showing obvious external deterioration or other interesting features were photographed prior to drying. None of the specimens showed any obvious external signs of deterioration at 60 days. At 500 days, many of the specimens from the high-concentration CaCl_2 , MgCl_2 , and MBAP brines exhibited external cracking, examples of which are shown in Figure 5.50.

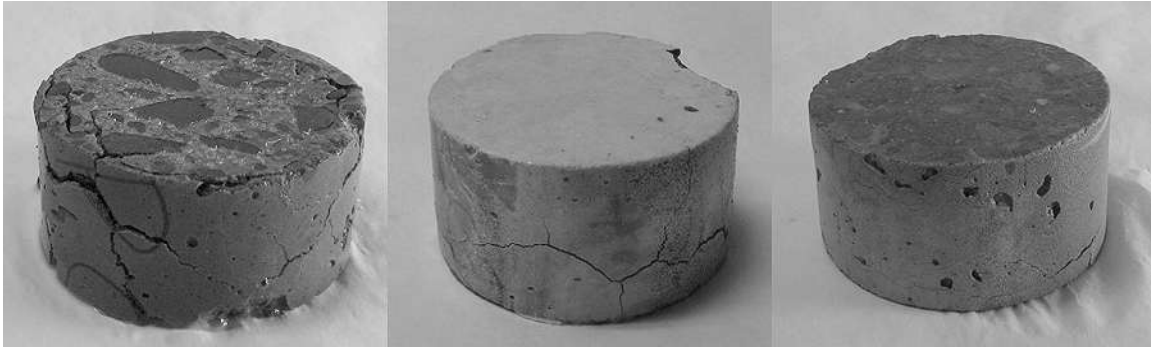


Figure 5.50. Photographs of 4 inch [100 mm] diameter 0.45 w/c ordinary portland cement (OPC) concrete specimens after 500 days in high concentration brines. From left to right: CaCl_2 , MgCl_2 , and MBAP brines.

A coating of mineral precipitates can be seen on the specimens in Figure 5.50. Mineral coatings were typically observed on specimens from the CaCl_2 , MgCl_2 , and MBAP brines. The mineral precipitates on the specimens from the MgCl_2 brine were white and very fine grained. Similar white precipitates were present on the specimens from the MBAP brine, but to a lesser degree. The mineral precipitates on the specimens from the CaCl_2 brine consisted of slender translucent crystals, examples of which are shown in Figure 5.51. External precipitates were not observed on specimens from the other brines, with the exception of specimens immersed in the low-concentration CMA brine. Figure 5.52 illustrates the white very fine-grained precipitate present on the surface of a specimen from the low-concentration CMA brine. Several circular deposits of black mold can also be observed along the sides of the specimen in Figure 5.52.

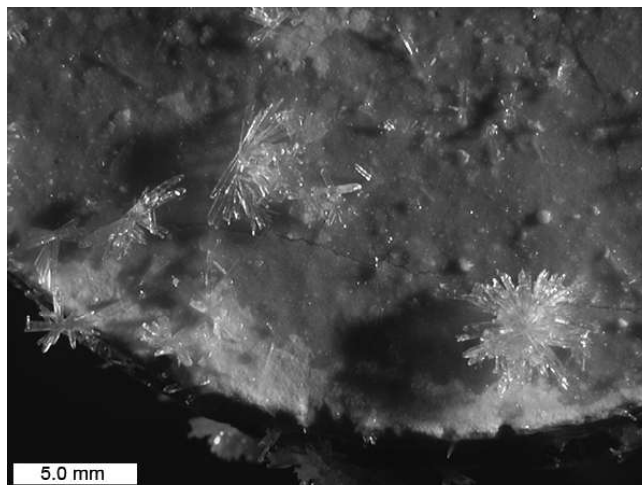


Figure 5.51. Crystals on exterior of concrete specimen after 500 days immersion in high-concentration CaCl_2 solution.



Figure 5.52. White precipitate on exterior of 4 inch [100 mm] diameter concrete specimen after 500 days immersion in low-concentration CMA solution.

During the sawing procedure a slab was removed from the middle of those specimens intended for chloride profiling and/or thin sectioning. These slabs were all oriented in a plane perpendicular to the flat-ends of the specimens. Specimens that were not to be used for chloride profiling were simply cut in half in the same orientation as the slabs. However, the three specimens shown in Figure 5.50 were treated differently than the rest. These specimens, all 0.45 *w/c* ordinary portland cement (OPC) concrete at 500 days, were immediately transferred, still damp with brine, to a 122 °F [50 °C] convection oven and dried overnight. After drying, the three specimens were vacuum impregnated with epoxy resin. After the epoxy had hardened, a slab was cut from each specimen in the same manner as previously described. The epoxy impregnation step was necessary to maintain the integrity of the slabs, which were intended for thin sectioning.

After cutting, the end-pieces were rinsed with kerosene and dried in the 122 °F [50 °C] convection oven. After drying, the cut-faces of the end pieces were scanned with a flatbed scanner in 24 bit RGB color at a resolution of 425 dpi [16.7 dpm]. The digital images were used to make visual estimates of the degree of alteration as exposed in the saw-cut cross-sections of the specimens. The perimeters of each specimen cross-section were outlined and any zones of visible alteration were outlined using Scion Image, (free software based on NIH Image for MacIntosh by Wayne Rasband of National Institutes of Health, USA). The number of pixels within any delineated zone of visible alteration was divided by the number of pixels within the entire specimen cross-section to yield an area percent for the visible alteration.

Figure 5.53 below shows example images from the 0.45 *w/c* mortar specimens from the five high-concentration brine solutions. Tables A3.22 through A3.26 summarize the visible alteration area percent values from all of the specimens measured. Shown below, Figures 5.54 and 5.55 plot the visible alteration area values versus time for the high-concentration brines and the low concentration brines, for all samples measured (i.e. mortars and concrete combined for all values of *w/c*). Figure 5.54 demonstrates that at the high-concentration, the CaCl₂, MgCl₂, and MBAP solutions were more aggressive than the NaCl and CMA solutions. At the low-concentration, all of the brines were less aggressive.

Additional plots are presented in the Appendix to illustrate the observed effected area for different specimens and exposure conditions. For specimens exposed to the five high-concentration brines, Figures A3.134 and A3.135 plot the visible alteration area values versus time for all concrete specimens and mortar, respectively. A general trend of increased alteration was evident for the concrete specimens as compared to the mortar specimens. Figures A3.136 and A3.137 compare the visible alteration area values from 0.45 *w/c* specimens to values from 0.55 *w/c* specimens exposed in the same brines. A general trend of increased alteration was evident for the 0.45 *w/c* specimens as compared to the 0.55 *w/c* specimens. Figures A3.138 through A3.140 illustrate the effect of supplementary cementitious materials for specimens in the high-concentration CaCl₂, MgCl₂, and MBAP brines. A general trend of decreased alteration was evident when fly ash or GGBFS were used.

Figures A3.141 through A3.143 illustrate the effect of silane and siloxane sealants for specimens in the high-concentration CaCl₂, MgCl₂, and MBAP brines. A general trend of decreased alteration was evident when the sealants were used. Figures A3.144 and A3.145 illustrate the effect of pre-soaking 0.55 *w/c* mortar specimens in high-concentration NaCl brine prior to immersion in high-concentration CaCl₂ and MgCl₂ brines.



Figure 5.53. Visible alteration on saw-cut plane through 0.45 w/c mortar specimens. From top to bottom: CaCl₂, MgCl₂, MBAP, NaCl & CMA high concentration brines at 500 days.

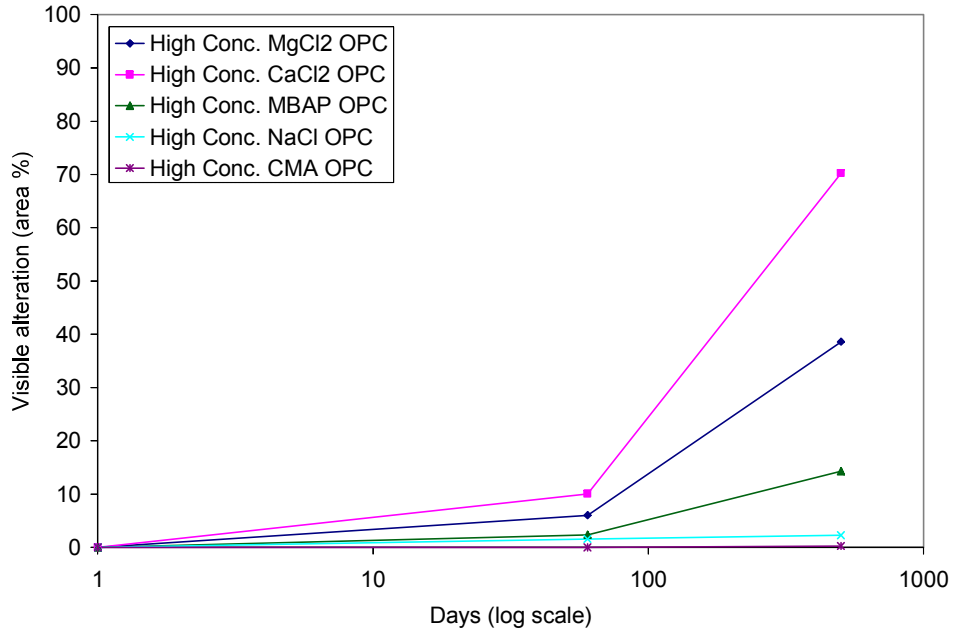


Figure 5.54. Average visible alteration versus time for high concentration brines with 0.45 and 0.55 w/c portland cement concrete specimens and mortar specimens

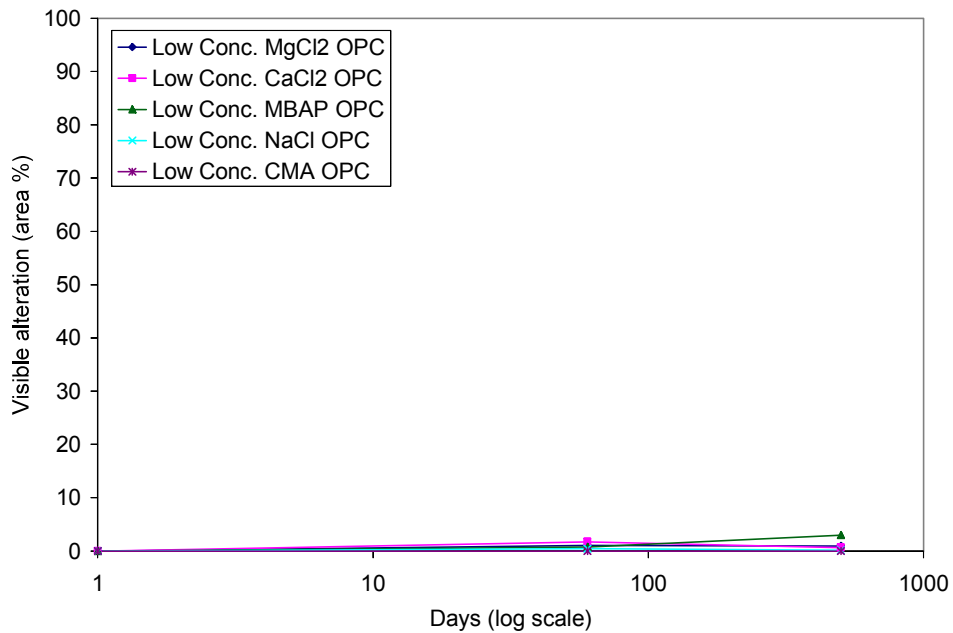


Figure 5.55. Average visible alteration versus time for low concentration brines with 0.45 and 0.55 w/c portland cement concrete specimens and mortar specimens.

The slabs cut from the epoxy stabilized 0.45 w/c concrete specimens from the high-concentration CaCl₂, MgCl₂, and MBAP brines at 500 days were rinsed with kerosene, cut into billets with a smaller kerosene-cooled diamond saw, and dried for a period of one hour in the 122 °F [50 °C] convection oven. Next, the billets were mounted on glass work-slides and one surface ground flat and smooth with a mineral-oil cooled diamond cup wheel. The prepared surfaces were cleaned with kerosene, and

the billets placed again in the oven for a period of one hour. After drying, most of the billets were brought to the vacuum epoxy impregnation unit and the prepared surfaces embedded in epoxy. However, one of the billets representing a cross-section through a corner of a specimen from the MgCl_2 brine was placed in a sealed Pyrex™ container while still warm. A time-lapse movie was recorded over a period of 17 hours to illustrate the phenomenon of the build-up of beads of moisture on the surface of the deteriorated portion of the specimen. 146 shows the before and after images from the time-lapse movie. This phenomenon was also observed during the sample preparation of deteriorated mortar cylinders from high-concentration CaCl_2 , and MgCl_2 brines in Phase I, and was attributed to the hygroscopic nature of salts present in the samples absorbing ambient humidity. The described experiment, which utilized a warm dried billet in a sealed container precludes the interpretation of hygroscopic salts absorbing moisture from the air, and suggests that the moisture may instead be the by-product of the instability of hydrated salt phases present in the samples.

5.3.2.2 Chloride Profiling

Chloride profiling was performed using the X-ray microscope on smooth diamond-ground billets cut to represent a cross-section through the near-surface of the specimens immersed in the brine solutions. The billets came from the center of the specimens to avoid the effects of diffusion of chloride ions from the sides of the specimens. Two billets were used for the collection of profile data for each specimen in most cases. All of the specimens analyzed were removed from their respective brine solutions at 60 days, with two additional 0.45 *w/c* portland cement concrete specimens removed from the high-concentration NaCl brine and from the limewater control at 500 days. Another set of 0.55 *w/c* silane-sealed portland cement concrete specimens were also removed from the high-concentration MgCl_2 and CaCl_2 brines at 500 days. 27 through A3.30 list the parameters derived by fitting the profile data collected from the specimens removed at 60 days to Fick's 2nd Law, as shown in Equation 2.1 of the background chapter (Final Report Chapter 2).

Shown below, Figures 5.56 through 5.58 show profiles for 0.45 *w/cm* concrete specimens immersed in the four different high-concentration brine solutions. Figure 5.56 shows profiles from the straight portland cement concrete specimens. Figure 5.57 shows profiles from the concrete specimens with fly ash, and Figure 5.58 shows profiles from the concrete specimens with GGBFS. The addition of GGBFS resulted in a marked decrease in the chloride concentration near the surfaces of the specimens. Chloride concentration profiles for concrete specimens with fly ash were similar to the profiles from specimens with straight portland cement.

Figure 5.59 shows profiles for the 0.45 *w/c* concrete specimens from the five low-concentration brine solutions. As might be expected, initial chloride concentrations were lower for concrete specimens from the low-concentration brines when compared to the same specimens from the high-concentration brines, (Figure 5.56) with the exception of the specimens immersed in the MBAP brines. Although the initial chloride concentrations were generally lower for concrete specimens in the low-concentration brines, the chloride concentrations at a depth of about ½ inch, [10 to 15 mm] were slightly elevated in the concrete specimens that had been exposed to the CaCl_2 and MgCl_2 low-concentration brines as compared to the same concrete specimens exposed to the CaCl_2 and MgCl_2 high-concentration brines. This trend was also observed in the mortar specimens.

Figure 5.60 shows the profiles for the 0.55 *w/c* portland cement concrete specimens exposed to the high-concentration brines. Compared to 0.45 *w/c* concrete specimens exposed to the same conditions, (Figure 5.56) the 0.55 *w/c* concrete specimens showed similar initial chloride concentrations but generally greater chloride penetration at depth. Figure 5.61 shows the profiles for the 0.55 *w/c* portland

cement mortar specimens exposed to the high-concentration brines. The 0.55 *w/c* mortar specimens from the CaCl_2 and MgCl_2 brines showed much lower initial chloride concentrations than their counterparts from the 0.45 *w/c* mortar specimen experiment, (Figure A3.150). Overall, the 0.55 *w/c* mortar specimens showed greater penetration of chloride at depth when compared to 0.45 *w/c* mortar specimens exposed to the same conditions.

Figures 5.62 and 5.63 show profiles for 0.55 *w/c* concrete specimens treated with silane and siloxane after exposure to the five high-concentration brines. The sealants were very effective at impeding the ingress of chlorides at 60 days. However, at 500 days, chloride ingress was evident from the bases of the specimens.

Although some general trends were observed in the chloride profile data, there were often outliers or exceptions. Some of these inconsistencies, especially in the case of the concrete specimens, can in some cases be attributed to heterogeneities inherent to the material. For example, Figure 5.161 provides an example of the influence a large porous coarse aggregate particle can have on the ingress of chlorides. The scanned image and elemental map shown in Figure 5.64 were taken from a billet cut from a 0.45 *w/cm* fly ash concrete specimen exposed to high-concentration MgCl_2 brine. The scanning and elemental mapping were part of the procedure performed on all of the samples to assist in the location of suitable points in the cement paste for wt% chlorine analyses. For comparison, Figure 5.65 shows a scanned image of a billet and the corresponding elemental map from a 0.45 *w/cm* fly ash mortar specimen immersed in high-concentration MgCl_2 brine. During the selection of points for chloride profiling, areas such as the chloride-enriched zone adjacent to the large porous sandstone coarse aggregate particle of Figure 5.64 were avoided. Furthermore, bright spots in the chloride map due to diffraction events in the aggregate fraction were also avoided.

As part of the profiling procedure, the measured wt% values for chloride in the hardened cement paste were converted to wt% chloride in the bulk concrete or mortar specimen based on mix design information prior to fitting with Fick's 2nd Law. Figures A3.165 and A3.166 show corrected profiles after fitting. The raw-data diffusion profiles shown in Figures A3.163 and A3.164 were similar since both originated from points in a 0.45 *w/cm* fly ash blend cement paste exposed to the same MgCl_2 brine. However, since the profile in Figure A3.165 came from the concrete specimen, and the profile in Figure A3.166 came from the mortar specimen, the weight-corrected chloride profile from the concrete specimen appears dramatically lower in concentration than the chloride profile from the mortar specimen. Chloride ions diffuse just as far in concrete as in mortar, if not farther in the case of concrete with porous coarse aggregate particles, but this fact is not always evident when the results are plotted in terms of wt% chloride in the bulk material. The complete set of chloride profile data is presented in the Appendix Section 3.

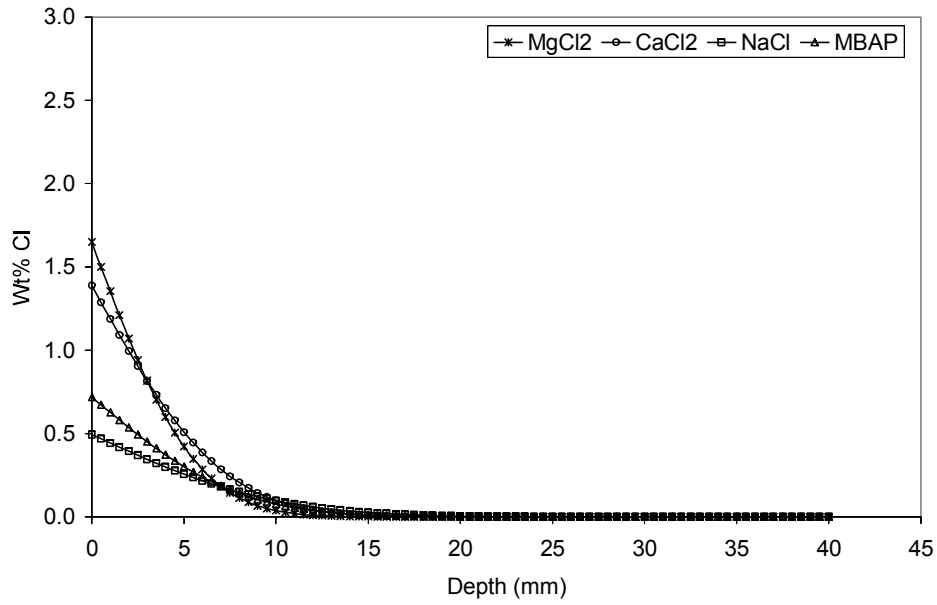


Figure 5.56. Fitted chloride profiles for 0.45 w/c straight portland cement concrete specimens immersed in high-concentration brines at 60 days.

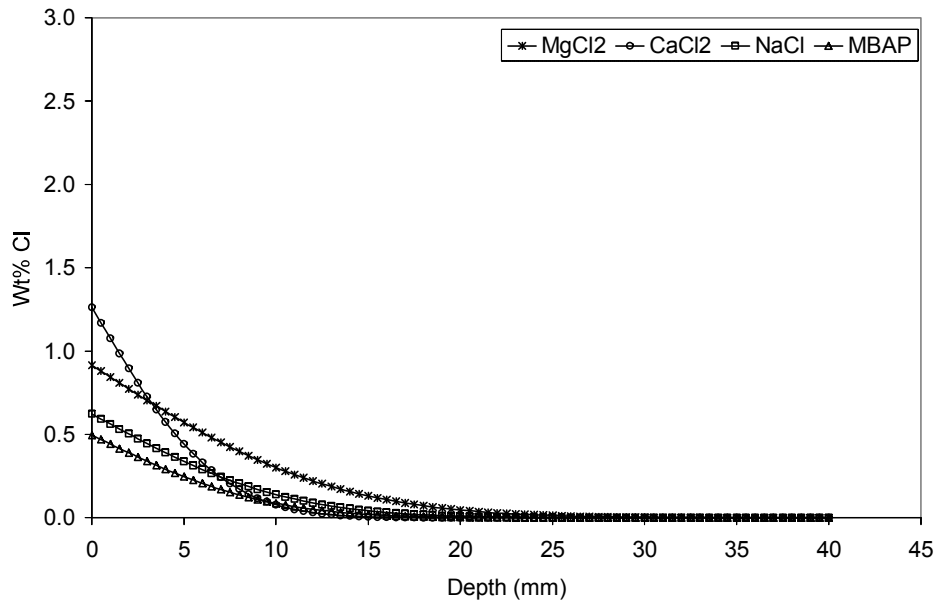


Figure 5.57. Fitted chloride profiles for 0.45 w/cm fly ash concrete specimens immersed in high-concentration brines at 60 days.

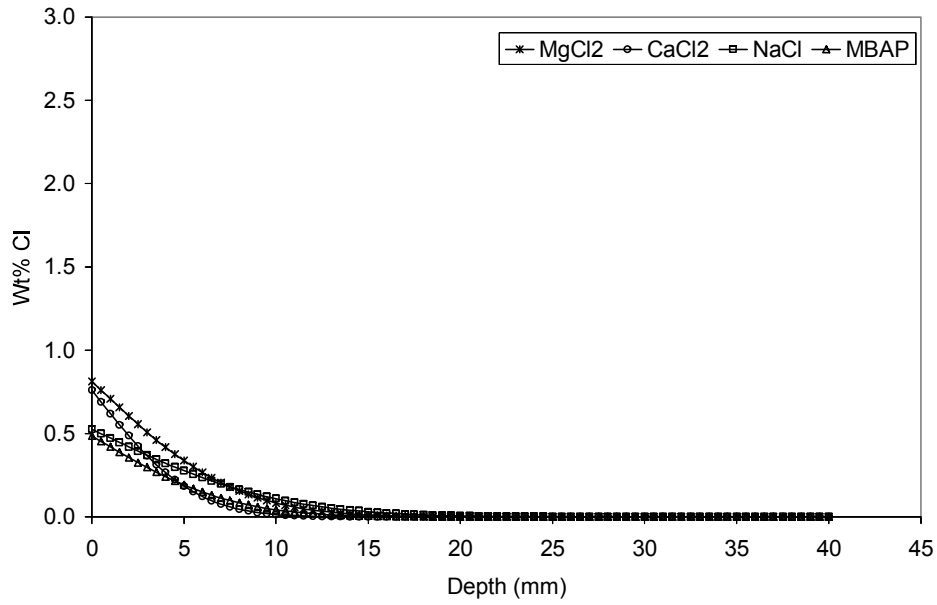


Figure 5.58. Fitted chloride profiles for 0.45 w/cm GGBFS concrete specimens immersed in high-concentration brines at 60 days.

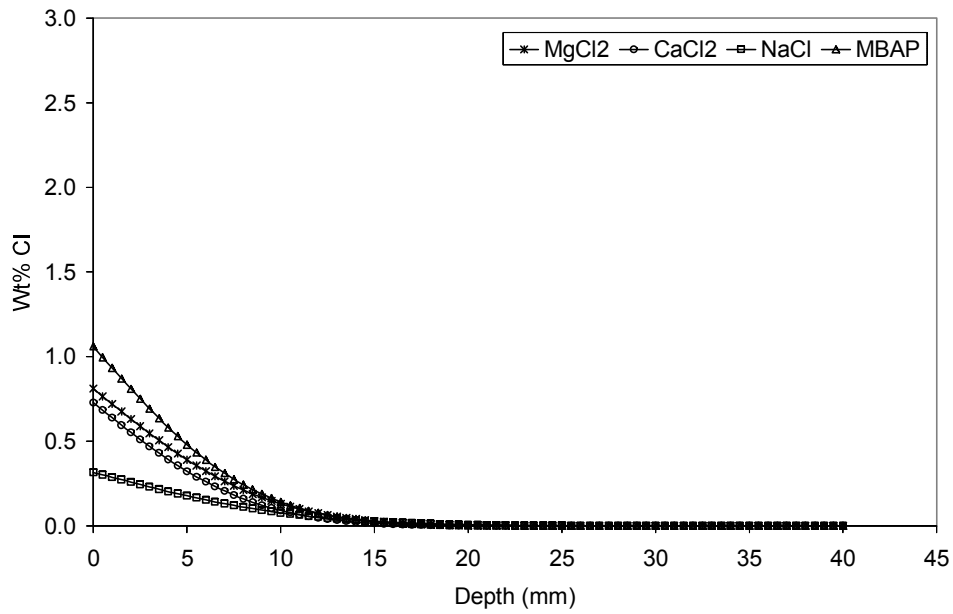


Figure 5.59. Fitted chloride profiles for 0.45 w/c straight portland cement concrete specimens immersed in low-concentration brines at 60 days.

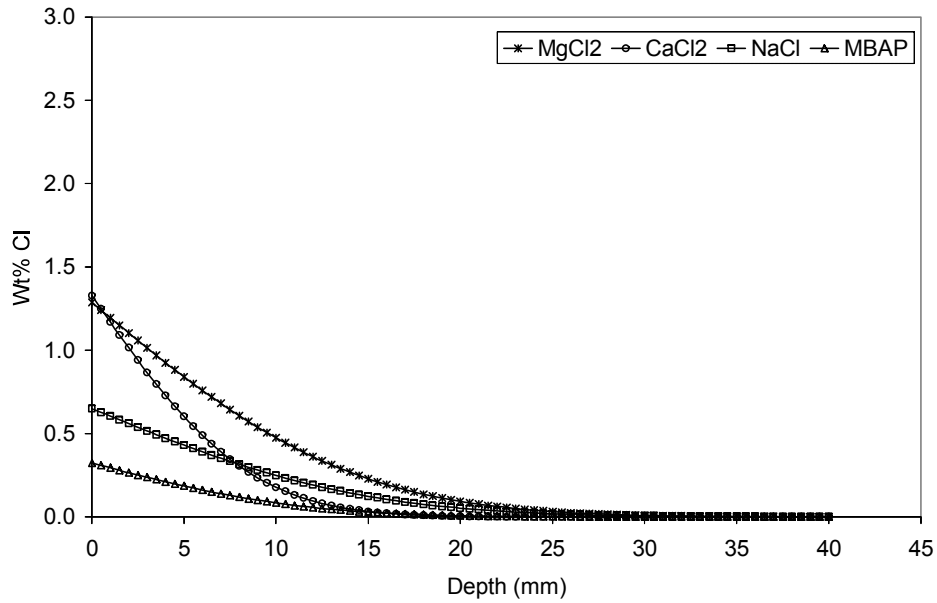


Figure 5.60. Fitted chloride profiles for 0.55 w/c straight portland cement concrete specimens immersed in high-concentration brines at 60 days.

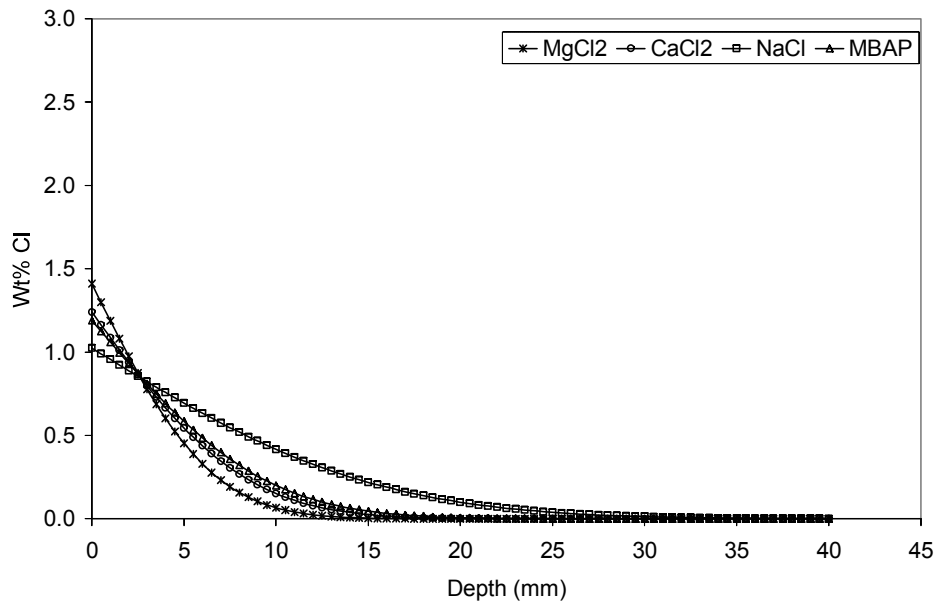


Figure 5.61. Fitted chloride profiles for 0.55 w/c straight portland cement mortar specimens immersed in high-concentration brines at 60 days.

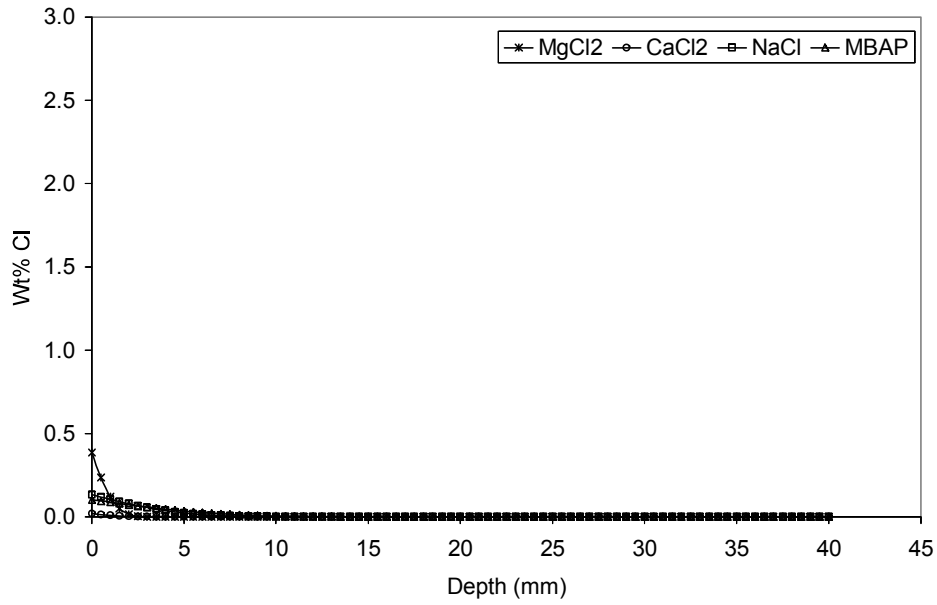


Figure 5.62. Fitted chloride profiles for 0.55 w/c straight portland cement concrete specimens sealed with silane and immersed in high-concentration brines at 60 days.

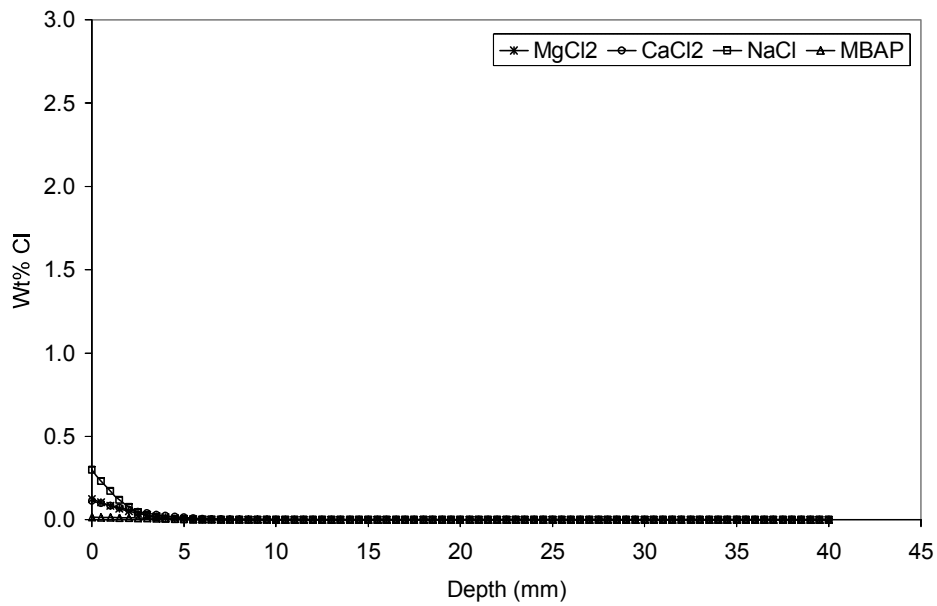


Figure 5.63. Fitted chloride profiles for 0.55 w/c straight portland cement concrete specimens sealed with siloxane and immersed in high-concentration brines at 60 days.

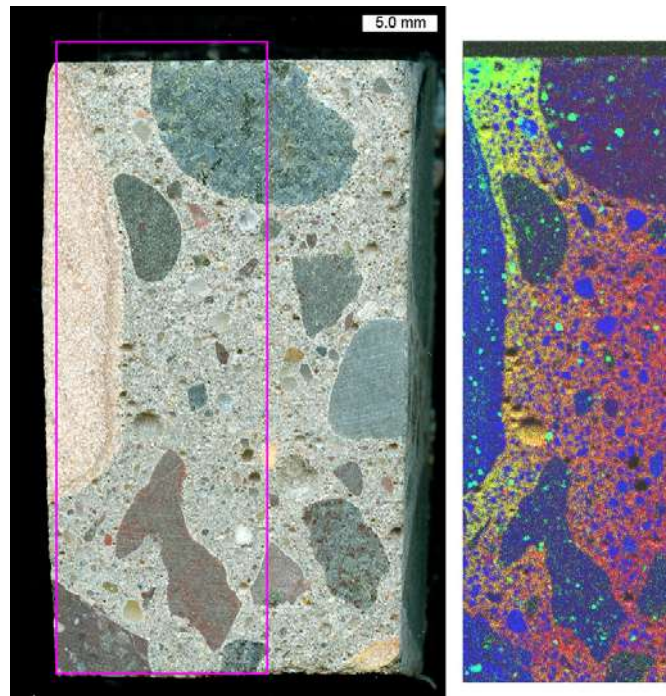


Figure 5.64. Scanned image, (left) and elemental map, (right) from billet cross-section through the near-surface of a 0.45 *w/cm* fly ash concrete specimen immersed 60 days in 15% MgCl_2 .
 In the elemental map, the R-band = Ca, G-band = Cl, and B-band = Si.

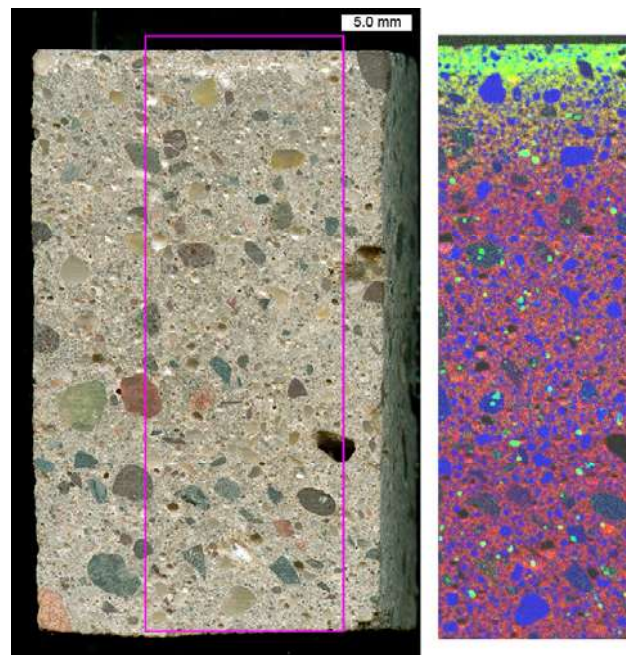


Figure 5.65. Scanned image, (left) and elemental map, (right) from billet cross-section through the near-surface of a 0.45 *w/cm* fly ash mortar specimen immersed 60 days in 15% MgCl_2 .
 In the elemental map, the R-band = Ca, G-band = Cl, and B-band = Si.

5.3.2.2. X-ray Diffraction

Cement paste was extracted from the deteriorated concrete samples exposed for 500 days to the high concentration MgCl_2 and CaCl_2 brines. The paste was extracted by working portions of the deteriorated concrete through 50 mesh and 200 mesh sieves. The collected material was ground with a mortar and pestle, and examined by XRD. Mineral precipitates that formed on the external surfaces of the concrete samples exposed to the MgCl_2 , CaCl_2 , MBAP and CMA brines were also collected, ground and analyzed. XRD patterns in most cases were collected from the samples in both the wet and dry condition.

An XRD pattern from the wet paste extracted from the concrete exposed to the CaCl_2 brine is shown in Figure 5.66, along with an XRD pattern from the wet mineral precipitate collected from the exterior of the concrete exposed to the CaCl_2 brine. The patterns are very similar, and show that the primary phase is the 8.34, 4.13, 2.76 angstrom calcium oxychloride phase first described by Monosi and Collepari (1990). They described the phase as $3\text{CaO}\cdot\text{CaCl}_2\cdot 15\text{H}_2\text{O}$, but the XRD pattern listed for $3\text{CaO}\cdot\text{CaCl}_2\cdot 15\text{H}_2\text{O}$, Joint Committee on Powder Diffraction Standards (JCPDS) Card No. 02-0280, does not match the XRD pattern they reported. The difference is shown in Figure 5.67. The calcium oxychloride crystals collected from the exterior of the concrete were subsequently oven dried at 122 °F [50 °C] overnight and re-analyzed. At high-temperature, the calcium oxychloride reverted to $\text{CaO}\cdot\text{CaCl}_2\cdot 2\text{H}_2\text{O}$, (JCPDS Card No. 02-1099) as shown in Figure 5.68. A time-lapse movie was recorded to observe the phase change from calcium oxychloride to $\text{CaO}\cdot\text{CaCl}_2\cdot 2\text{H}_2\text{O}$. Figure 5.69 shows the before and after images from the time-lapse movie. Another time-lapse movie was recorded to observe the same $\text{CaO}\cdot\text{CaCl}_2\cdot 2\text{H}_2\text{O}$ crystals after immersion in distilled water in equilibrium with atmospheric CO_2 at room temperature overnight. Figure 5.70 shows the before and after images from the time-lapse movie. The XRD pattern, (Figure 5.71) of the resultant material from the $\text{CaO}\cdot\text{CaCl}_2\cdot 2\text{H}_2\text{O}$ immersion experiment showed that the $\text{CaO}\cdot\text{CaCl}_2\cdot 2\text{H}_2\text{O}$ was converted to calcium carbonate (CaCO_3) (JCPDS Card No. 05-0586) (Note: calcium carbonate is cataloged by its mineral name, calcite, in the JCPDS diffraction database). A second sample of calcium oxychloride was subjected to a brine-cure treatment where it was heated to 122 °F [50 °C] overnight in a sealed container filled with CaCl_2 brine. Figure 5.72 shows before and after images of a time-lapse movie recorded of the hot brine-cure experiment. After treatment, the XRD pattern (Figure 5.73) showed that some calcium oxychloride remained, but there were also new peaks present for calcium hydroxide, JCPDS Card No. 04-0733 (Note: calcium hydroxide is cataloged by its mineral name, portlandite, in the JCPDS diffraction database). In another experiment, the extracted cement paste sample was allowed to air dry for one week and re-analyzed. Peaks for calcite (CaCO_3 , JCPDS Card No. 05-0586) and quartz (SiO_2 , JCPDS Card No. 46-1045) were observed in the dried paste, and no peaks were observed for calcium oxychloride or $\text{CaO}\cdot\text{CaCl}_2\cdot 2\text{H}_2\text{O}$, as shown in Figure 5.74.

The XRD pattern from the wet paste extracted from the concrete exposed to the MgCl_2 brine, and the XRD pattern from the wet mineral precipitate collected from the exterior concrete exposed to the MgCl_2 brine showed very little similarity. Peaks for $\text{Mg}_3(\text{OH})_5\text{Cl}\cdot 4\text{H}_2\text{O}$, (JCPDS Card no. 07-0420) were observed in the exterior mineral precipitate, but not in the wet paste. The calcium oxychloride phase was not observed in either of the XRD patterns. The patterns are shown in Figure 5.75. The $\text{Mg}_3(\text{OH})_5\text{Cl}\cdot 4\text{H}_2\text{O}$ crystals collected from the exterior of the concrete were subsequently oven dried at 122 °F [50 °C] overnight and re-analyzed. After the high-temperature experiment, some $\text{Mg}_3(\text{OH})_5\text{Cl}\cdot 4\text{H}_2\text{O}$ remained, but new peaks for $\text{MgCl}_2\cdot 6\text{H}_2\text{O}$ (JCPDS Card No. 25-0515) were also observed, as shown in Figure 5.76. The extracted paste was allowed to air dry and was re-analyzed.

The patterns from the wet extracted paste and the air-dried extracted paste were very similar, as shown in Figure 5.77. The wet paste sample dried very quickly in the diffractometer and displayed cracking after the first X-ray analysis was completed.

Wet mineral precipitates collected from the exterior of concrete that was exposed to the MBAP solution consisted primarily of $Mg_3(OH)_5Cl \cdot 4H_2O$, as shown in Figure 5.78.

Mineral precipitates collected from the exterior of concrete that was soaked in the low-concentration calcium magnesium acetate (CMA) solution consisted primarily of calcite, as shown in Figure 5.79.

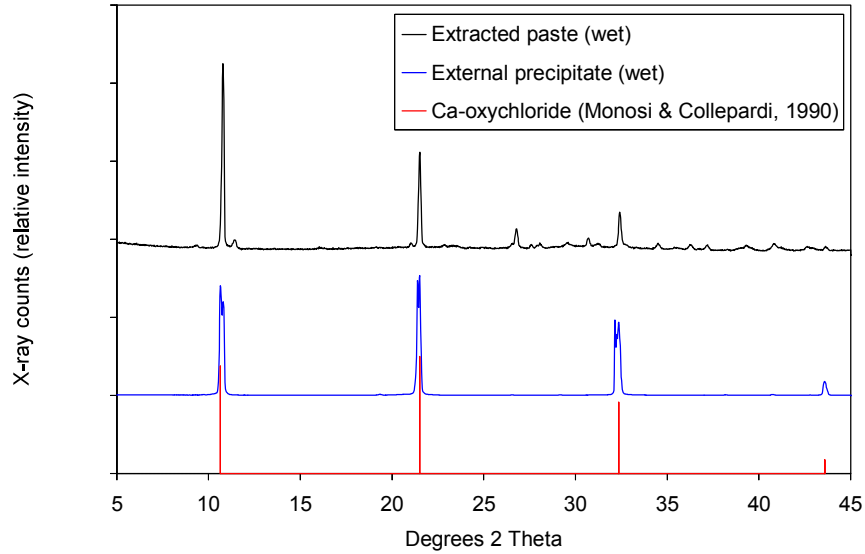


Figure 5.66. XRD patterns from the wet extracted paste and the wet exterior precipitate collected from concrete exposed to $CaCl_2$ brine for 500 days compared to the reference 8.34, 4.13, 2.76 angstrom peaks for Monosi and Collepari's calcium oxychloride phase.

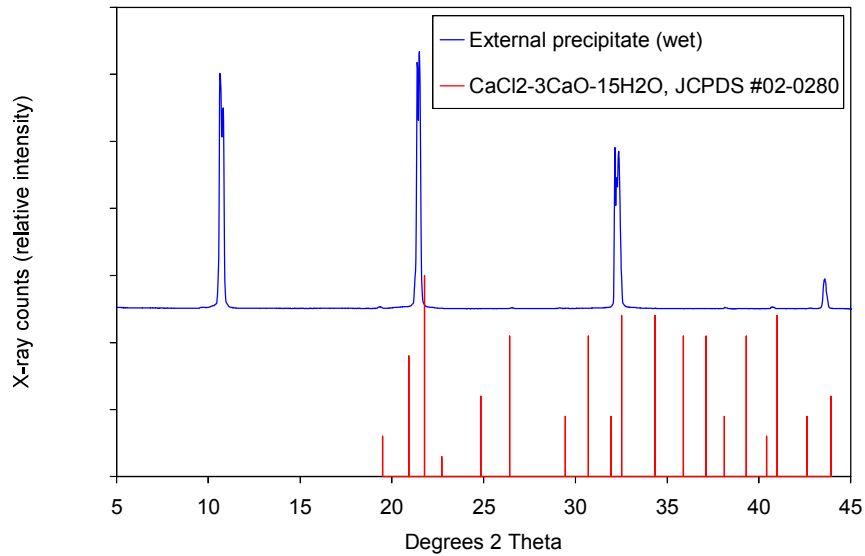


Figure 5.67. XRD pattern from the wet precipitate collected from the exterior of concrete exposed to CaCl₂ brine for 500 days compared to 3CaO·CaCl₂·15H₂O reference peaks.

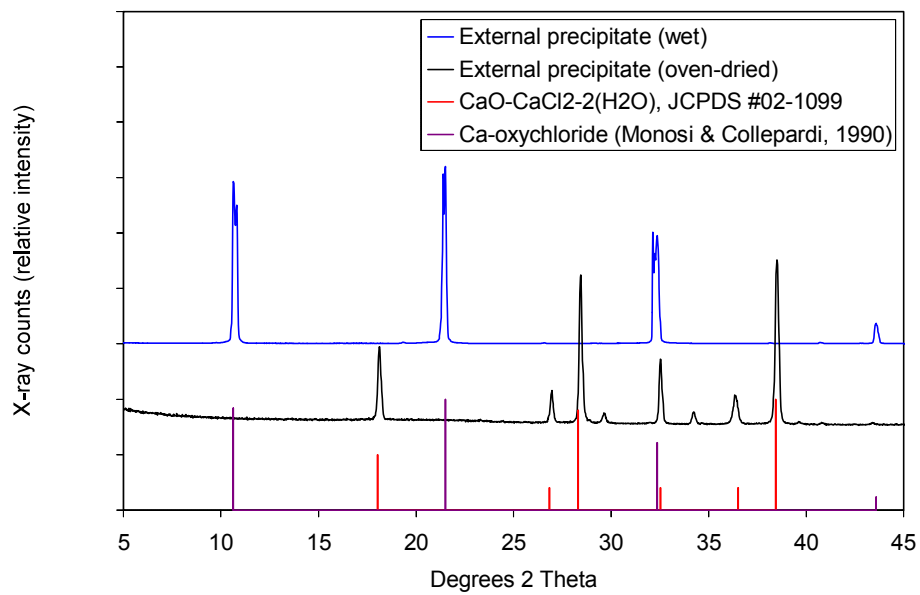


Figure 5.68. XRD patterns from the wet and oven-dried external precipitate collected from concrete exposed to CaCl₂ brine for 500 days compared to reference patterns for calcium oxychloride and CaCl₂·Ca(OH)₂·2H₂O.

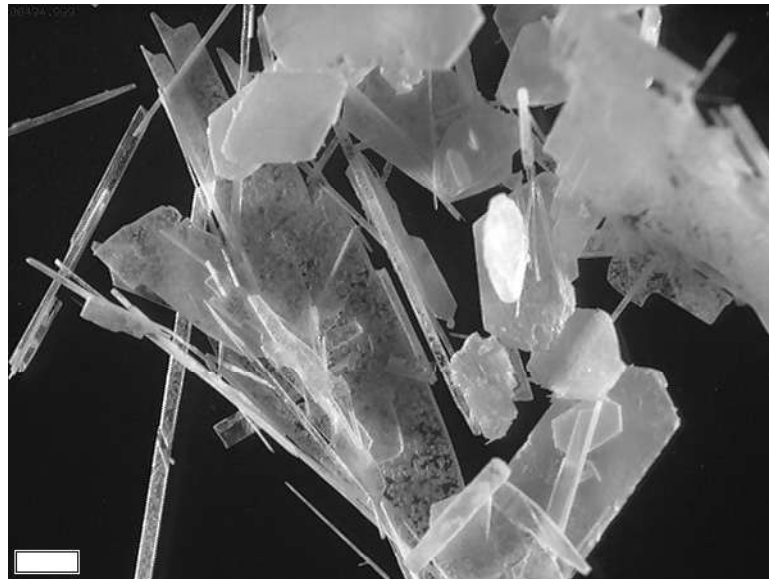
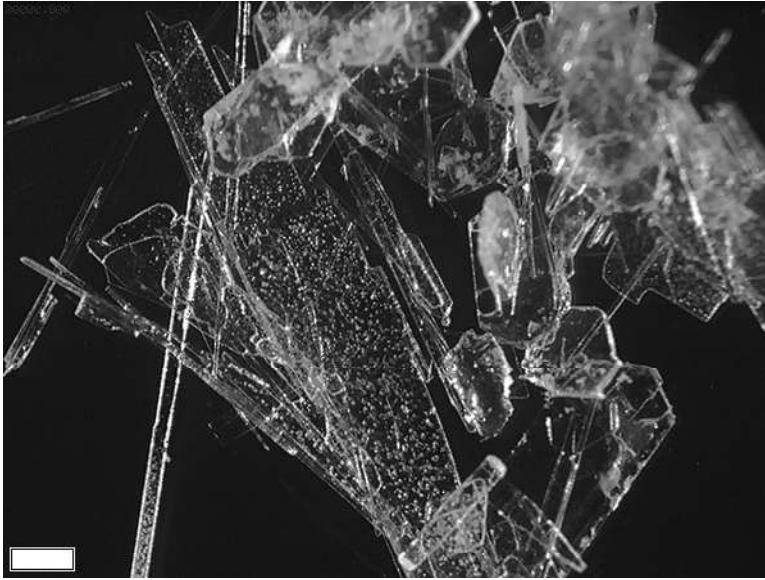
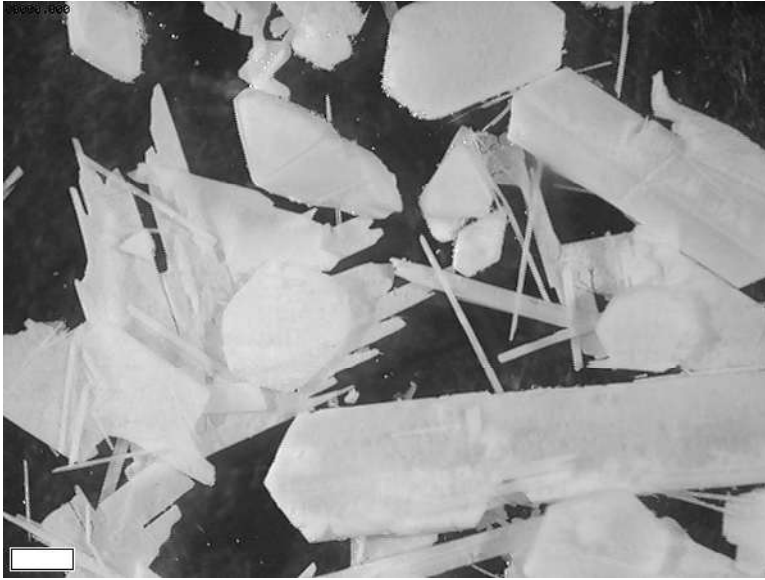


Figure 5.69. Fresh calcium oxochloride crystals before, (top) and after oven drying and conversion to $\text{CaCl}_2 \cdot \text{Ca}(\text{OH})_2 \cdot 2\text{H}_2\text{O}$. (Bottom) scale bar = 1 mm.



**Figure 5.70. $\text{CaCl}_2 \cdot \text{Ca}(\text{OH})_2 \cdot 2\text{H}_2\text{O}$ crystals before, (top) and after immersion in distilled water in atmospheric equilibrium with CO_2 at room temperature and subsequent alteration.
(Bottom) scale bar = 1 mm.**

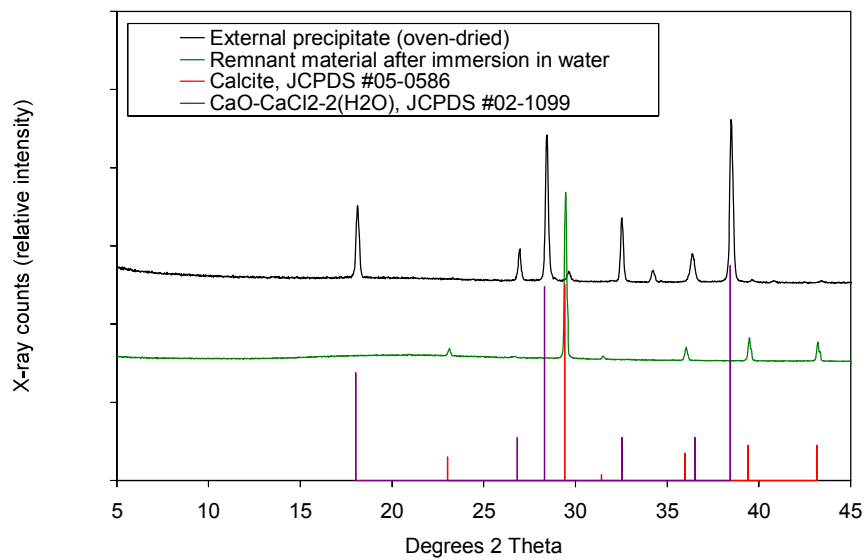


Figure 5.71. XRD patterns from oven-dried external precipitate crystals, and the resultant remnant material after immersion in room temperature water, as compared to a reference patterns for calcite and $\text{CaCl}_2 \cdot \text{Ca}(\text{OH})_2 \cdot 2\text{H}_2\text{O}$.

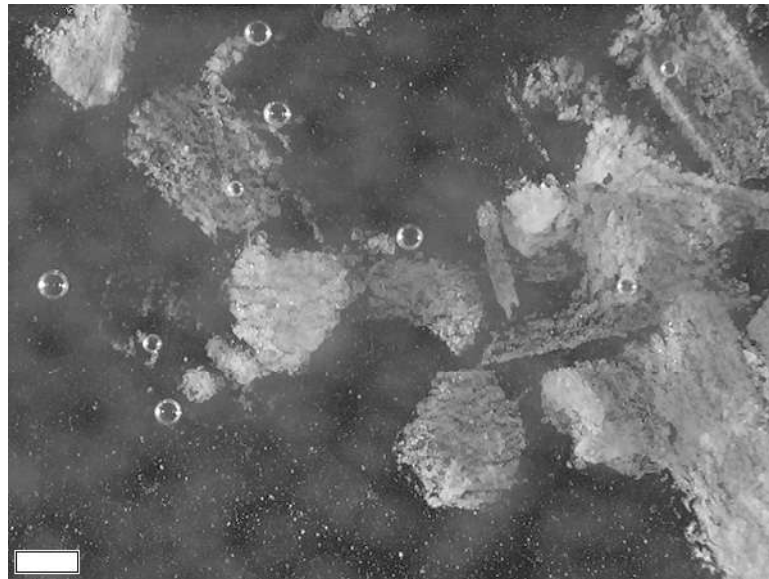
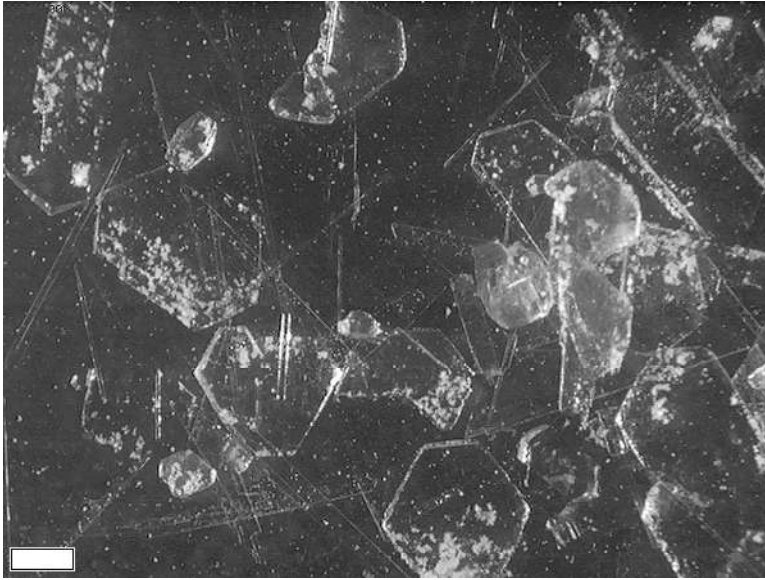


Figure 5.72. Fresh calcium oxochloride crystals before, (top) and after immersion in a sealed container of hot CaCl_2 brine. (Bottom) scale bar = 1 mm.

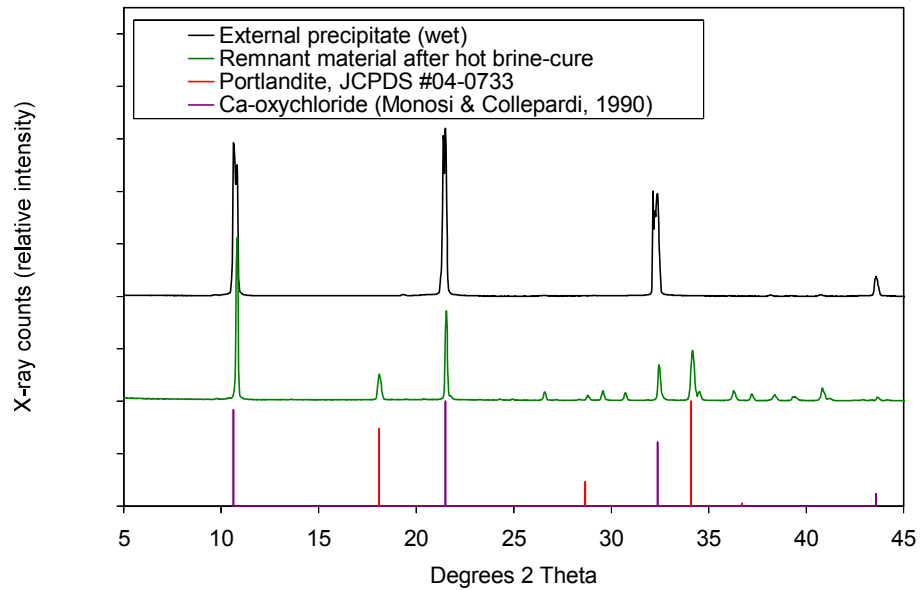


Figure 5.73. XRD patterns from wet external precipitate, and the resultant remnant material after curing in hot CaCl_2 brine, with reference patterns for calcium oxychloride and portlandite.

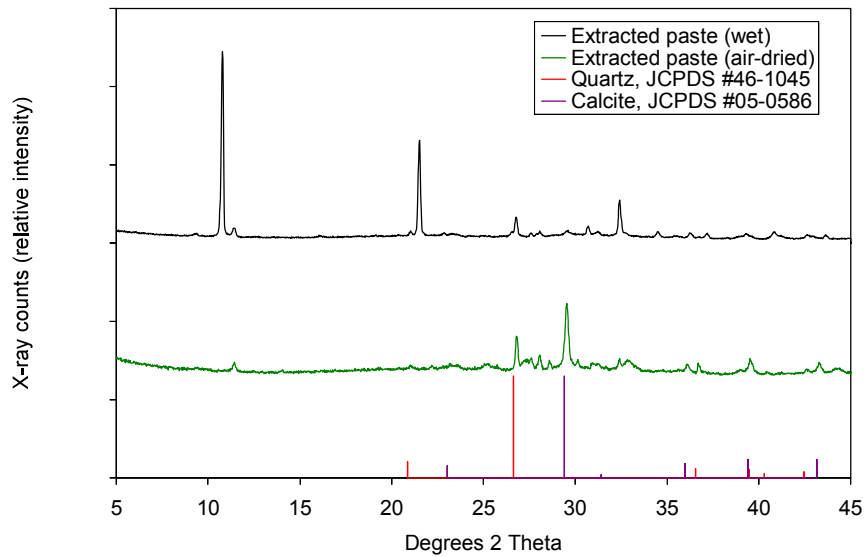


Figure 5.74. XRD patterns from the wet and air-dried extracted paste collected from concrete specimens exposed to CaCl_2 brine for 500 days, with reference patterns for calcite and quartz.

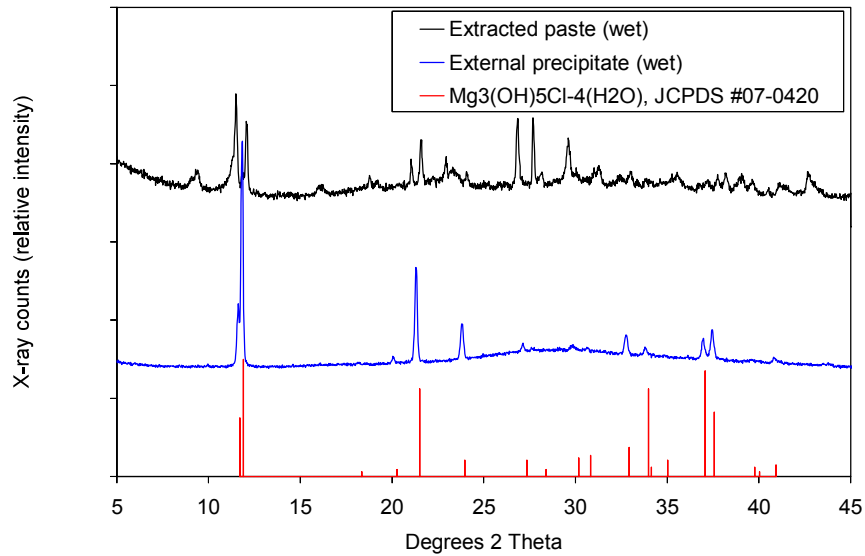


Figure 5.75. XRD patterns from the wet extracted paste and wet external precipitate collected from concrete exposed to MgCl₂ brine for 500 days, with reference pattern for Mg₃(OH)₅Cl·4H₂O.

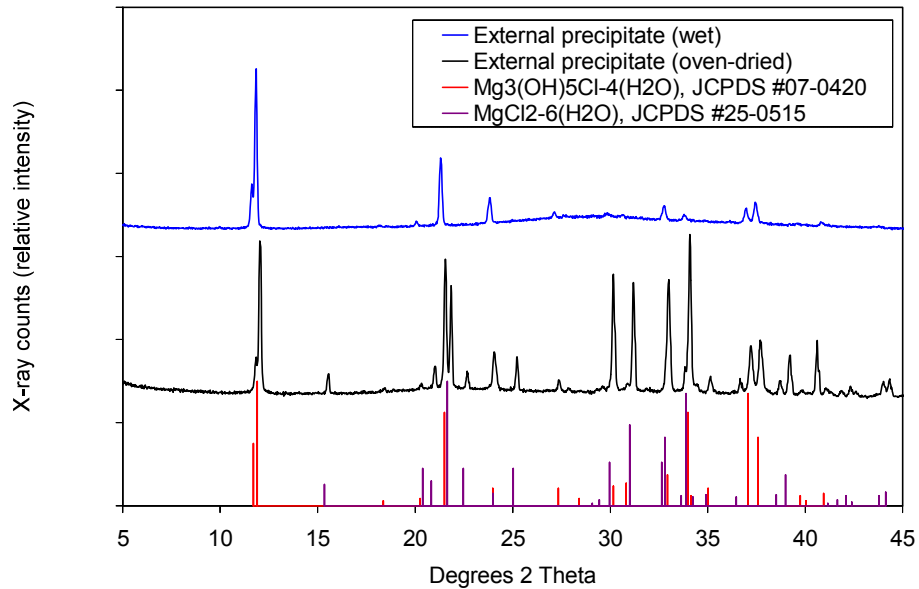


Figure 5.76. XRD patterns from the wet and oven dried external precipitate collected from concrete exposed to MgCl₂ brine for 500 days, with reference patterns for Mg₃(OH)₅Cl·4H₂O and MgCl₂·6H₂O.

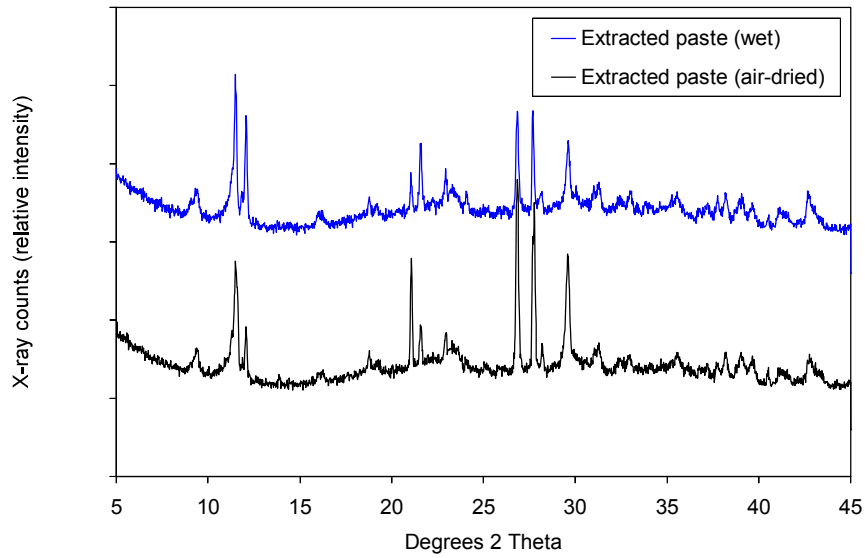


Figure 5.77. XRD patterns from the wet and air-dried extracted paste collected from concrete exposed to MgCl_2 brine for 500 days.

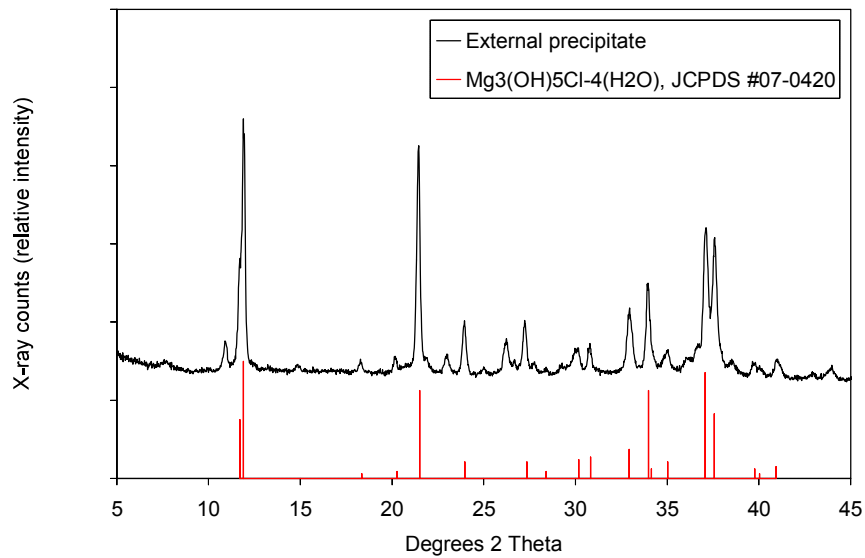


Figure 5.78. XRD pattern from the external precipitate collected from concrete exposed to MBAP solution for 500 days, with reference pattern for $\text{Mg}_3(\text{OH})_5\text{Cl}\cdot 4\text{H}_2\text{O}$.

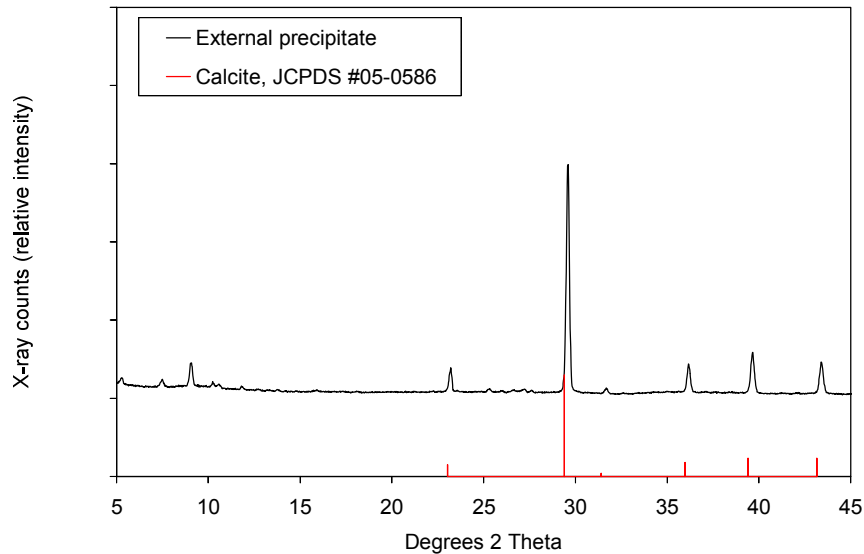


Figure 5.79. XRD pattern from the external precipitate collected from concrete exposed to CMA solution for 500 days, with reference pattern for calcite.

5.3.2.3 Optical Microscopy

Sample Preparation

Thin sections were prepared from 0.45 *w/c* portland cement concrete specimens to represent all of the high-concentration brines and the limewater control after 500 days of immersion. Thin sections were also prepared from 0.45 *w/cm* concrete specimens with supplementary fly ash and GGBFS, but only those exposed to the CaCl_2 , MgCl_2 , and MBAP brine solutions for 500 days. An additional thin section was also prepared from a 0.55 *w/c* concrete specimen that had been sealed with silane and immersed in high-concentration MgCl_2 brine for 500 days. Specimens that were in an advanced state of deterioration, namely the 0.45 *w/c* specimens from the CaCl_2 , MgCl_2 , and MBAP brines, were dried in a 122 °F [50 °C] convection oven overnight, and then vacuum impregnated with epoxy. After stabilization, these specimens, along with the others, were cut into slabs with a kerosene cooled diamond saw. The slabs were further cut into billets, and the billets prepared in thin section using water-free methods.

Comparison of the 0.45 *w/c* Portland Cement Concrete Specimens from the Six Solutions

Figure 5.80 shows epifluorescent mode images from all of the 0.45 *w/c* straight portland cement concrete specimens. The images depict the specimens in cross-section, with the top surfaces of each specimen facing towards the right hand-side. Cracking planes sub-parallel to the surface are evident in the specimens exposed to the CaCl_2 , MgCl_2 , and MBAP brines, while the specimens exposed to the CMA and NaCl brines, and the specimen exposed to the limewater, do not show any cracking. Figure 5.81 shows further close-up epifluorescent mode images from the same areas outlined in pink from Figure 5.80. Figures 5.82 through 5.84 show close-up images of the cracks in the specimens exposed to CaCl_2 , MgCl_2 , and MBAP brines. In all of these specimens, a similar pattern of blocky birefringent crystals is observed in the cracks and air voids in the deteriorated regions. The crystals have the same birefringence colors as calcium hydroxide, but their blocky appearance departs from the usual calcium

hydroxide morphology, which generally occurs as stacks of thin hexagonal plates, or as isolated thin hexagonal plates. The cement paste in the deteriorated portions is generally devoid of calcium hydroxide. The lack of calcium hydroxide in the paste is most noticeable when viewed under crossed polars. The cement paste, usually speckled with bright patches of birefringent calcium hydroxide appears dark when calcium hydroxide is not present. Figures 5.85 through 5.87 show images of cement paste with abundant calcium hydroxide. These images were taken from areas just below the surfaces of the 0.45 *w/c* straight portland concrete specimens exposed to the NaCl, CMA, and limewater solutions. Secondary calcium hydroxide deposits are present in the air voids of the specimen immersed in limewater, as shown in Figure 5.87. The shape of these calcium hydroxide crystals, long and thin in cross-section, is a typical morphology for secondary calcium hydroxide, and in contrast to the blocky morphology demonstrated in the air voids and cracks of the deteriorated specimens (Figures 5.82 through 5.84).

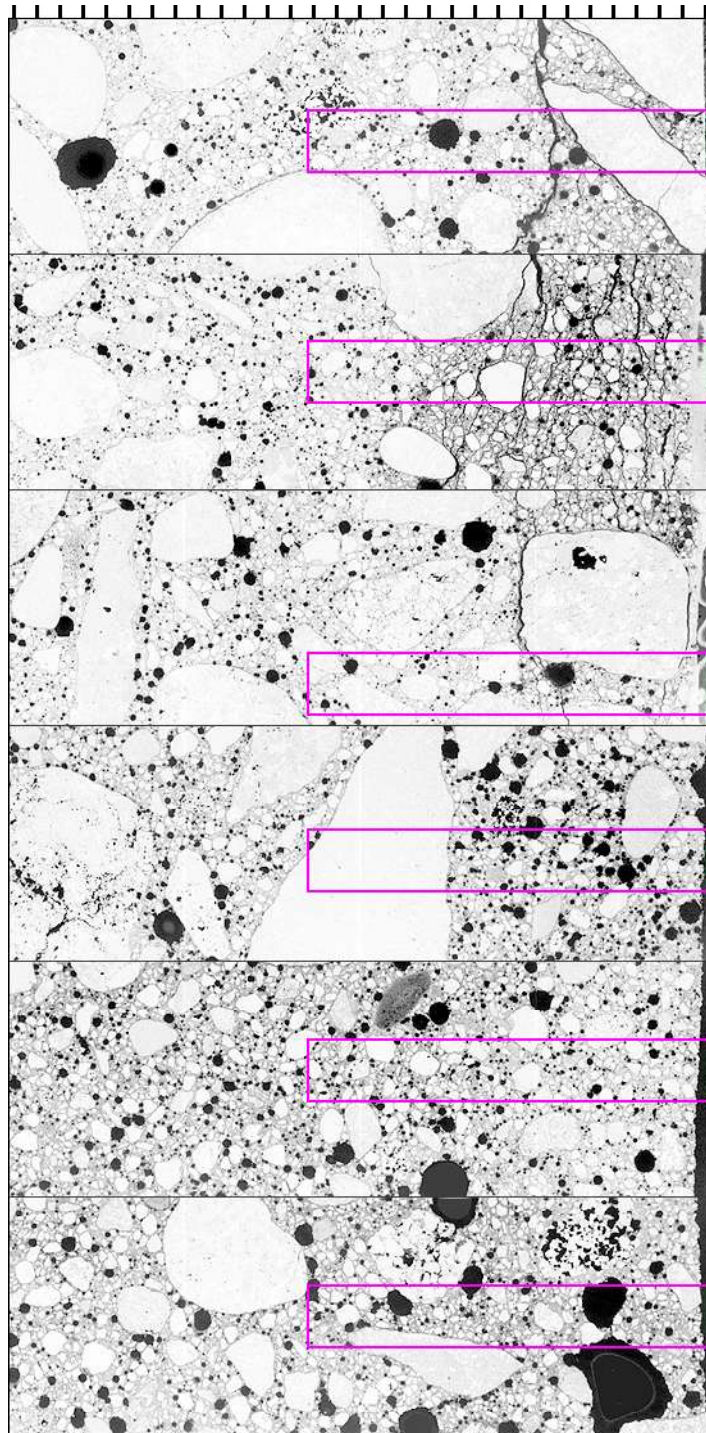


Figure 5.80. Epifluorescent thin section views of the 0.45 w/c concrete specimens immersed in solution for 500 days, exterior surfaces to the right. From top to bottom: CaCl₂, MgCl₂, MBAP, NaCl, CMA, and limewater, tic marks every mm. Pink boxes highlight close-up regions shown in Figure 5.81.

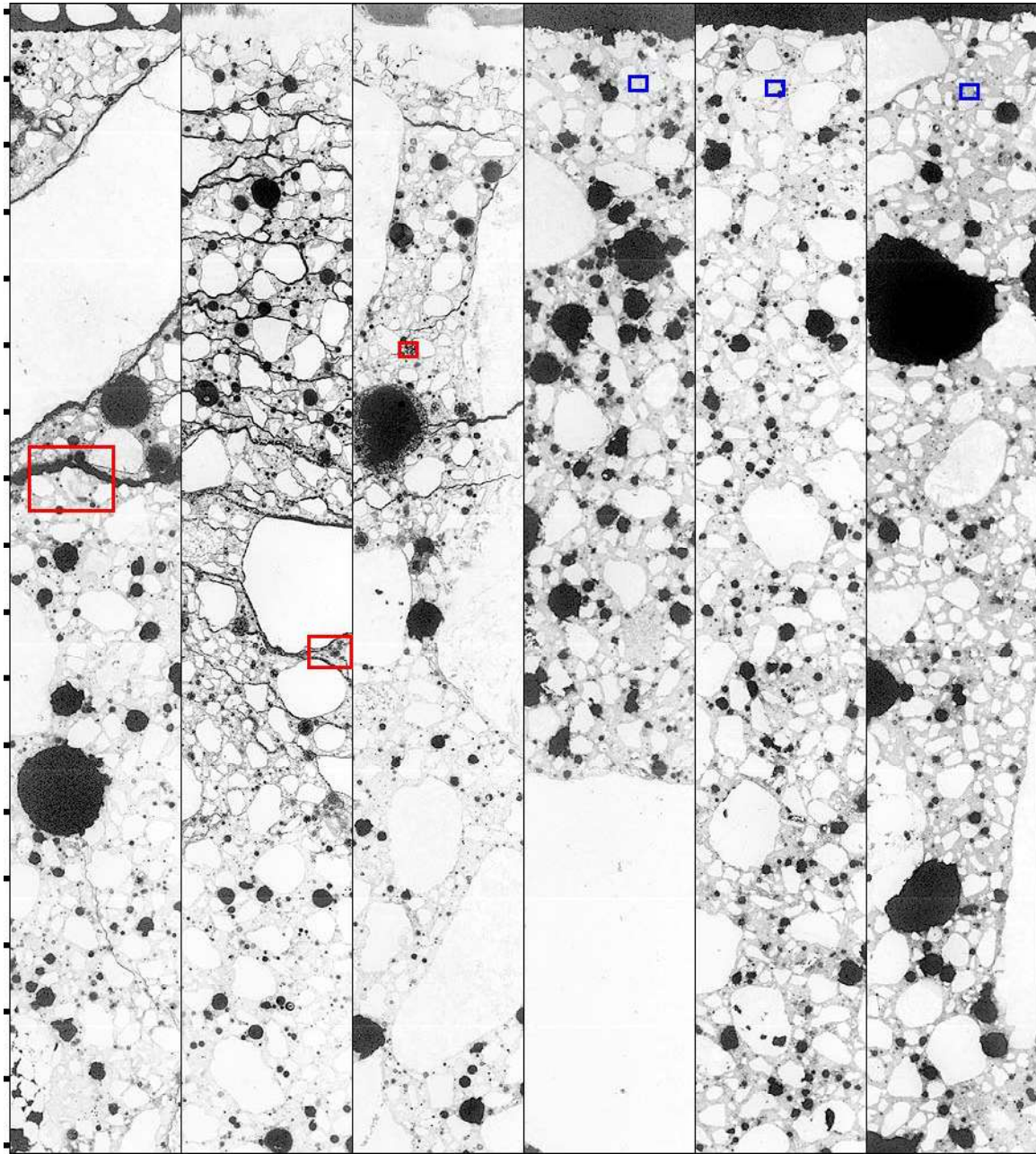


Figure 5.81. Close-up views of regions outlined in pink in Figure 5.183, but with exterior surfaces oriented towards the top. Cross-sectional epifluorescent mode images of the 0.45 *w/c* concrete specimens after 500 days of immersion in solution.

From left to right: CaCl_2 , MgCl_2 , MBAP, NaCl, CMA, and limewater, tic marks every mm. Red boxes highlight locations of close-up images of deterioration in Figures 5.82 through 5.84. Blue boxes show locations of close-up images of calcium hydroxide in the cement paste in Figures 5.85 through 5.87.

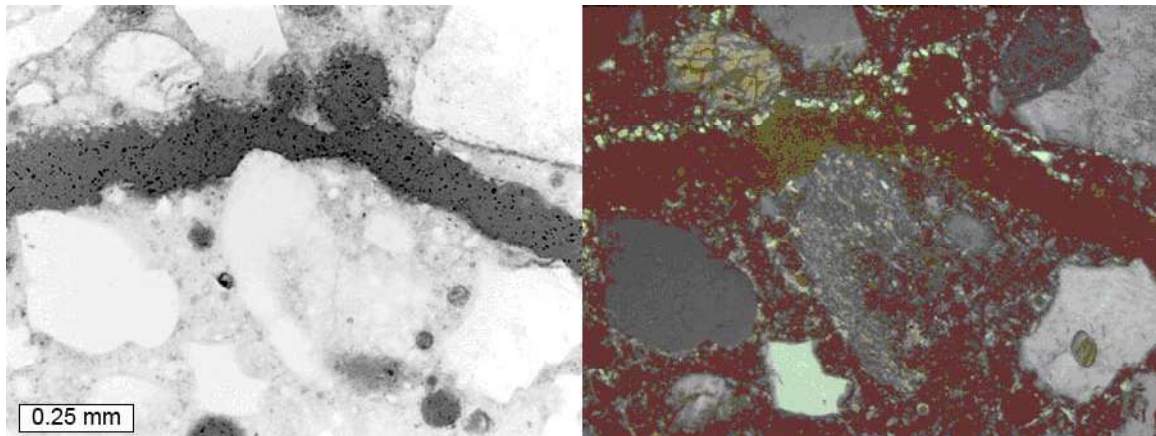


Figure 5.82. Close-up view of deteriorated portion from 0.45 w/c straight portland concrete exposed to CaCl_2 brine. From left to right: epifluorescent and crossed polars.

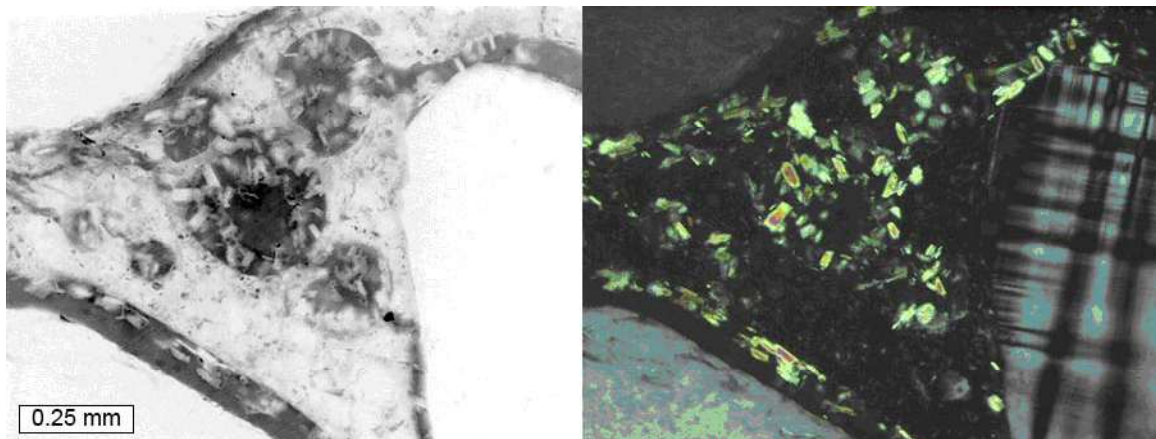


Figure 5.83. Close-up view of deteriorated portion from 0.45 w/c straight portland concrete exposed to MgCl_2 brine. From left to right: epifluorescent and crossed polars.

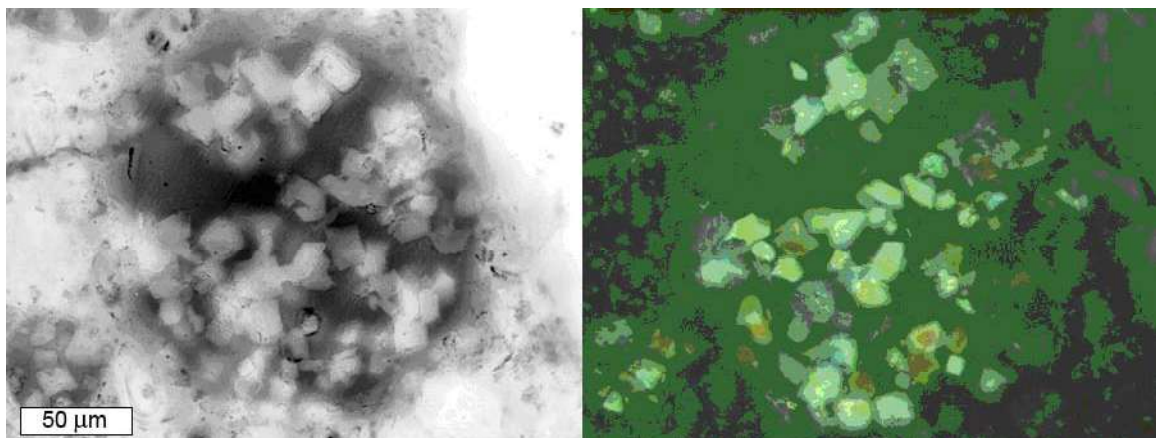


Figure 5.84. Close-up view of deteriorated portion from 0.45 w/c straight portland concrete exposed to MBAP brine. From left to right: epifluorescent and crossed polars.

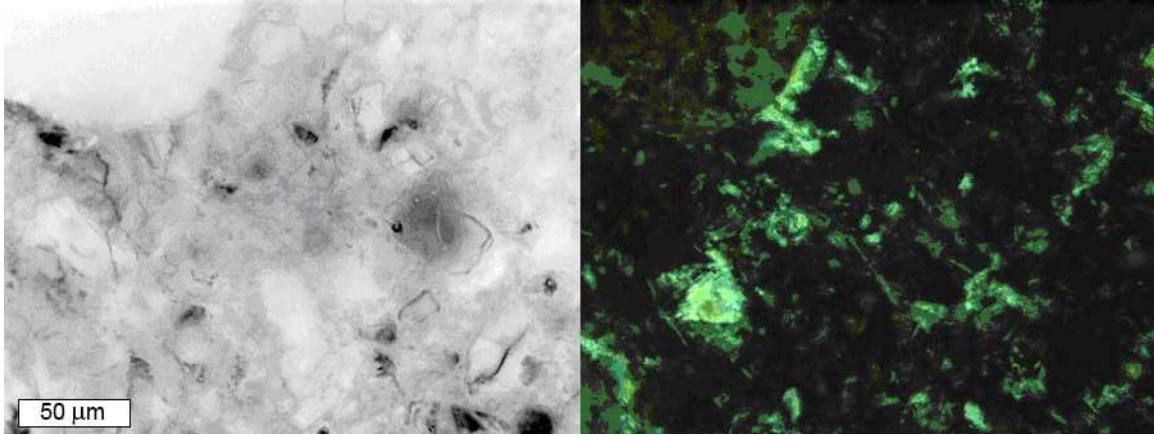


Figure 5.85. Cement paste just below the surface from 0.45 w/c straight portland cement concrete exposed to NaCl brine. From left to right: epifluorescent and crossed polars.

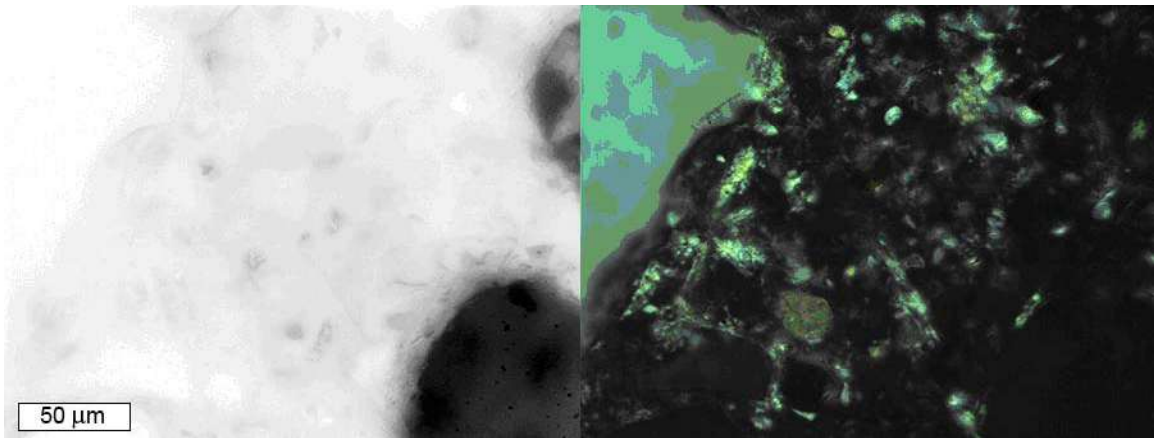


Figure 5.86. Cement paste just below the surface from 0.45 w/c straight portland cement concrete exposed to CMA brine. From left to right: epifluorescent and crossed polars.

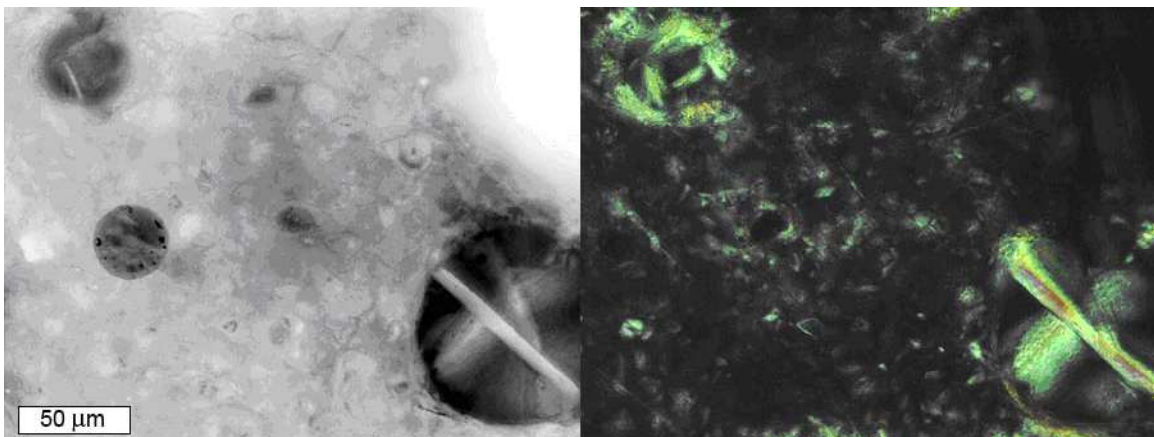


Figure 5.87. Cement paste just below the surface from 0.45 w/c straight portland cement concrete exposed to limewater. $\text{Ca}(\text{OH})_2$ deposits in air voids. From left to right: epifluorescent and crossed polars.

Comparison of the 0.45 w/cm Concrete Specimens Immersed in CaCl₂ Brine

Figure 5.88 shows epifluorescent mode images from the 0.45 w/cm straight portland cement, fly ash, and GGBFS concrete specimens after 500 days immersion the high-concentration CaCl₂ brine. The images depict the specimens in cross-section, with the top surfaces of each specimen facing towards the right hand-side. Figure 5.89 shows further close-up epifluorescent mode images from the areas outlined in pink from Figure 5.88. In Figure 5.89, the straight portland cement concrete specimen shows the most severe cracking. Cracks are also present in the fly ash concrete specimen, but to a lesser degree. At the scale of the image in Figure 5.89, cracks are not observed in the GGBFS concrete specimen. The green-dashed lines in Figure 5.89 approximately mark the extent of calcium hydroxide depletion in the cement paste, which occurred in all three of the specimens. Above the green lines, calcium hydroxide is depleted from the cement paste, below the green lines, calcium hydroxide is present in the cement paste. Example images of depleted and non-depleted paste from the three specimens are included in Figures 5.90 through 5.92. The red lines show the horizons where images were taken of calcium hydroxide depleted-paste. The blue lines show the horizons where images were taken with calcium hydroxide still present in the paste. In the non-depleted regions of cement paste, calcium hydroxide appears most abundant and well-distributed in the straight portland cement concrete. Calcium hydroxide in the cement paste of the fly ash concrete appeared slightly less abundant overall than in the straight portland cement concrete, but tended to be more dispersed and occurred in larger patches. Calcium hydroxide was least abundant in the cement paste of the GGBFS concrete. All of the specimens exhibited blocky secondary calcium hydroxide crystals in air voids within the zone of calcium hydroxide-depleted cement paste, as shown in Figures 5.93 through 5.95. Blocky calcium hydroxide crystals were present in the large cracks of the straight portland cement concrete specimen, as previously shown, (Figure 5.82) but were not present in the tighter cracks of the fly ash and GGBFS concrete specimens, (Figures 5.94 and 5.95).

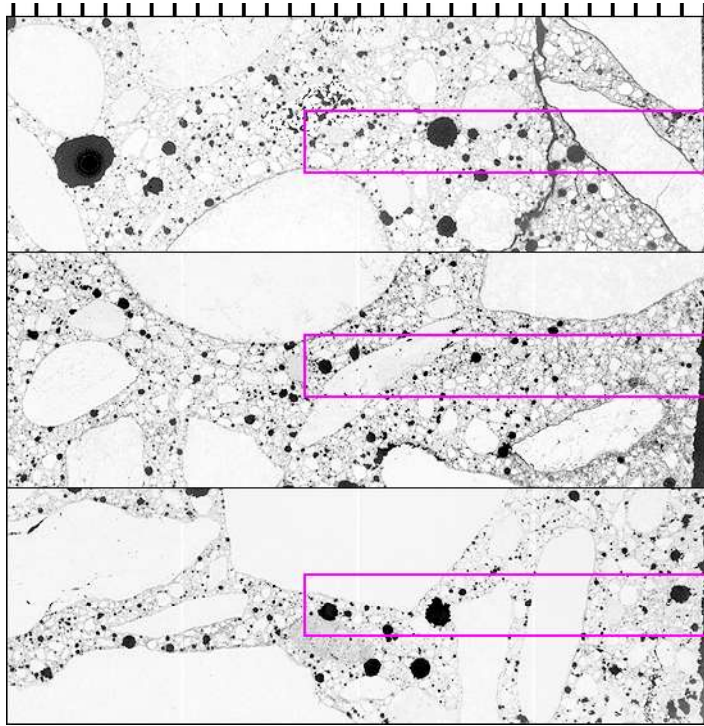


Figure 5.88. Epifluorescent thin section views of the 0.45 *w/cm* concrete specimens immersed in CaCl_2 solution for 500 days, exterior surfaces to the right. From top to bottom: straight portland cement concrete, supplementary fly ash concrete, and supplementary GGBFS concrete, tic marks every mm. Pink boxes highlight close-up regions shown in Figure 5.89.

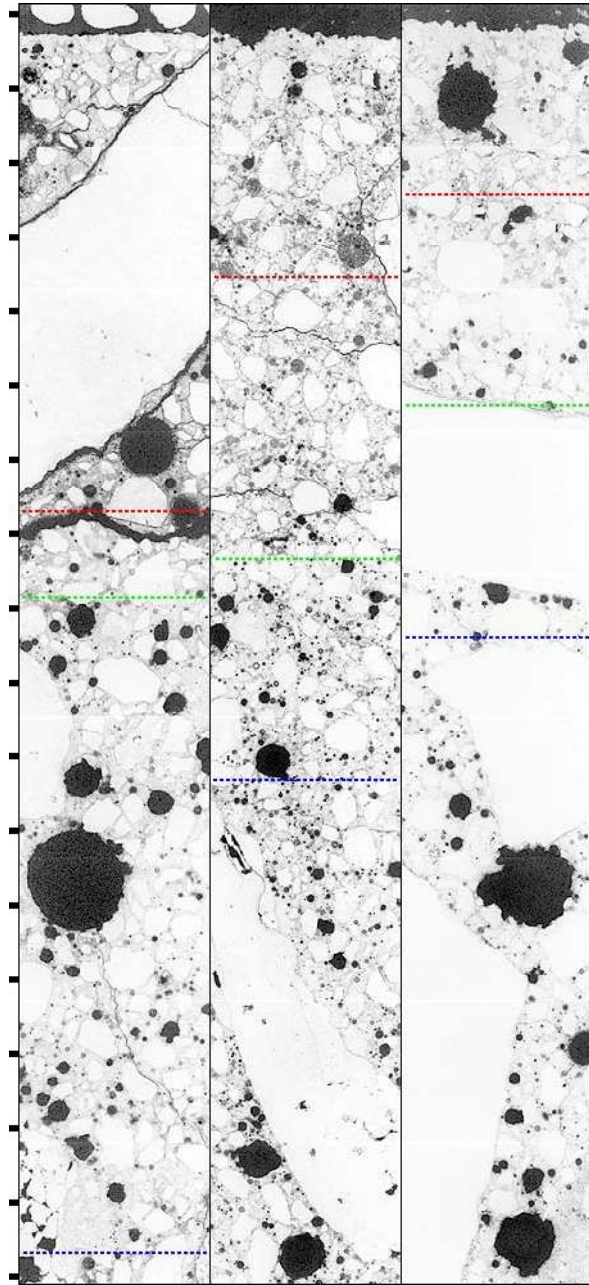


Figure 5.89. Close-up views of regions outlined in pink in Figure 5.88, but with exterior surfaces oriented towards the top. Cross-sectional epifluorescent mode images of the 0.45 *w/cm* concrete specimens after 500 days of immersion in CaCl_2 solution. From left to right: straight portland cement concrete, supplementary fly ash concrete, and supplementary GGBFS concrete, tic marks every mm. Green lines show extent of Ca(OH)_2 depleted cement paste. Red lines show horizons where photos of depleted paste were taken. Blue lines show horizons where photos were taken of paste with Ca(OH)_2 still present.

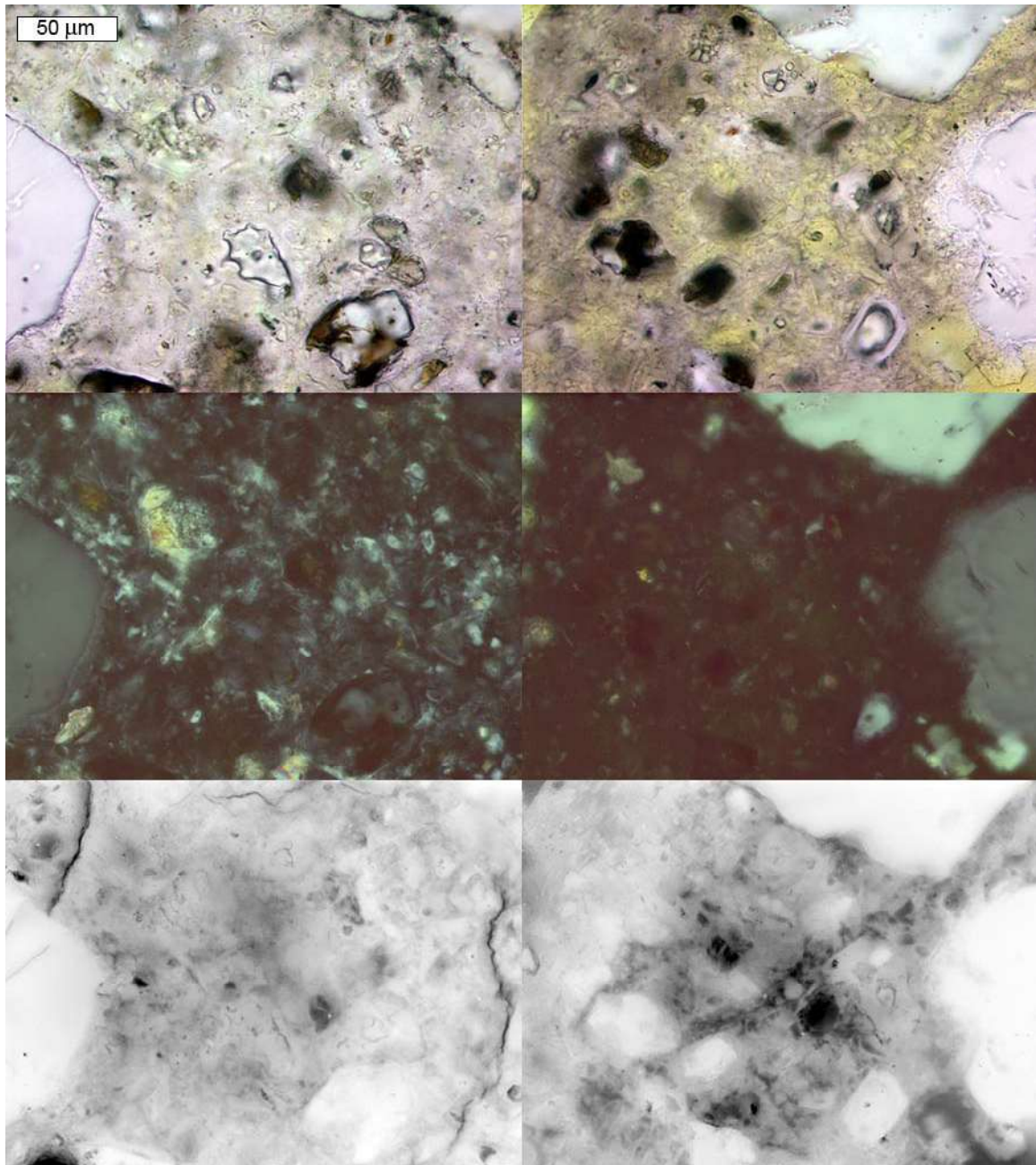
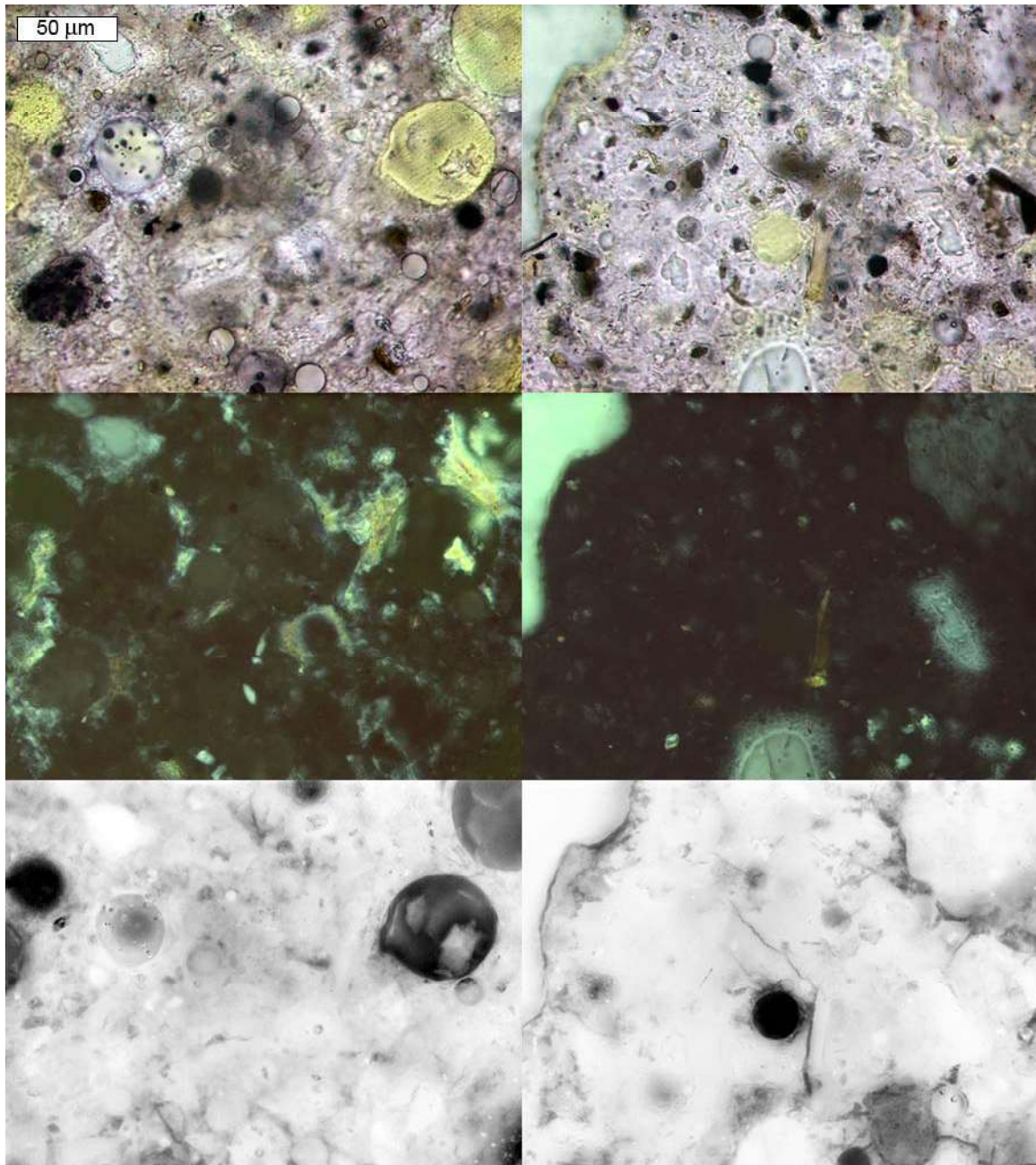


Figure 5.90. Regions of cement paste in 0.45 w/c straight portland cement concrete exposed to CaCl_2 brine where Ca(OH)_2 is depleted, (right) and still present, (left). From top to bottom: transmitted light, crossed polars, and epifluorescent mode images.



**Figure 5.91. Regions of cement paste in 0.45 *w/cm* fly ash concrete exposed to CaCl₂ brine where Ca(OH)₂ is depleted, (right) and still present, (left).
From top to bottom: transmitted light, crossed polars, and epifluorescent mode images.**

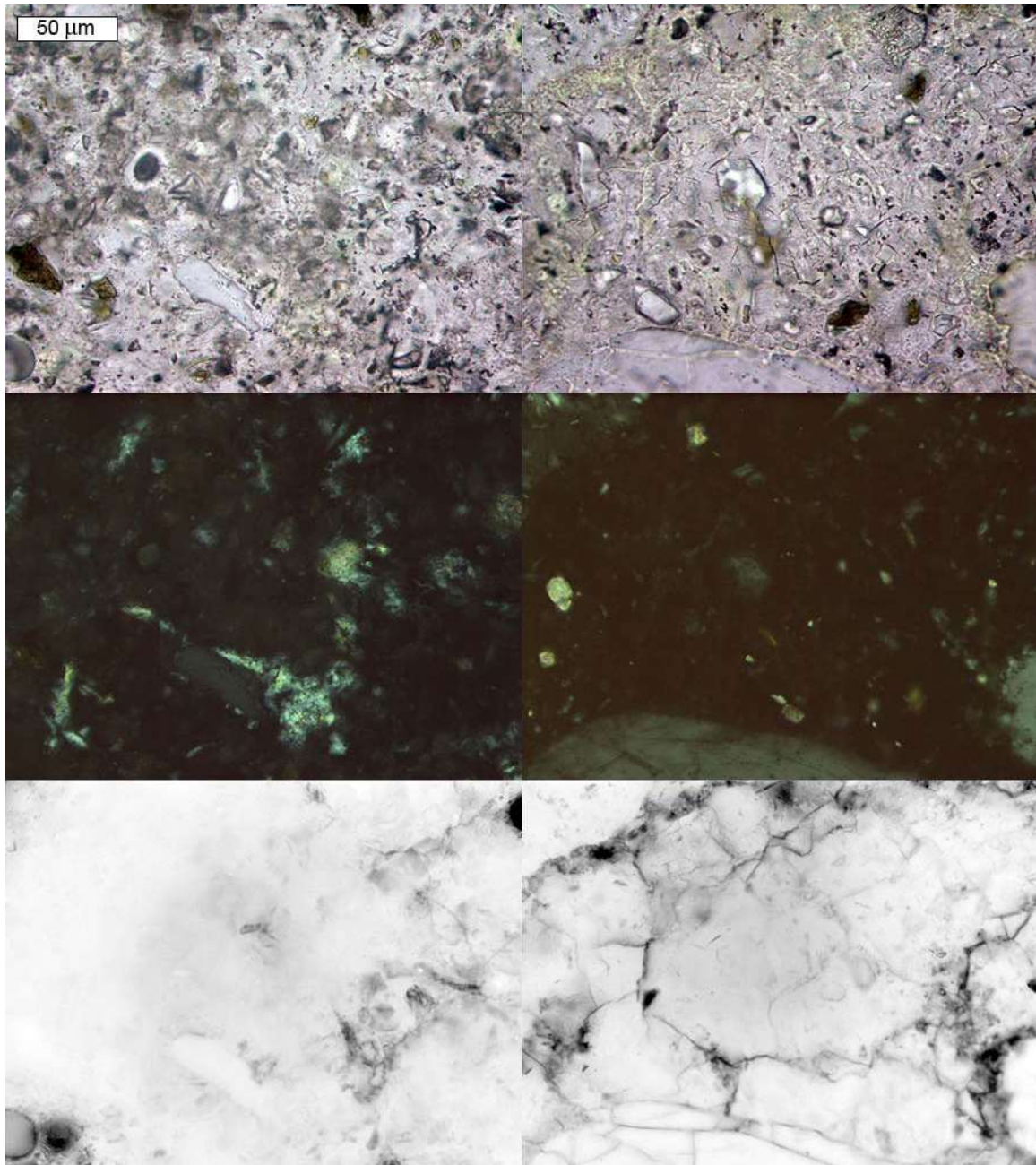
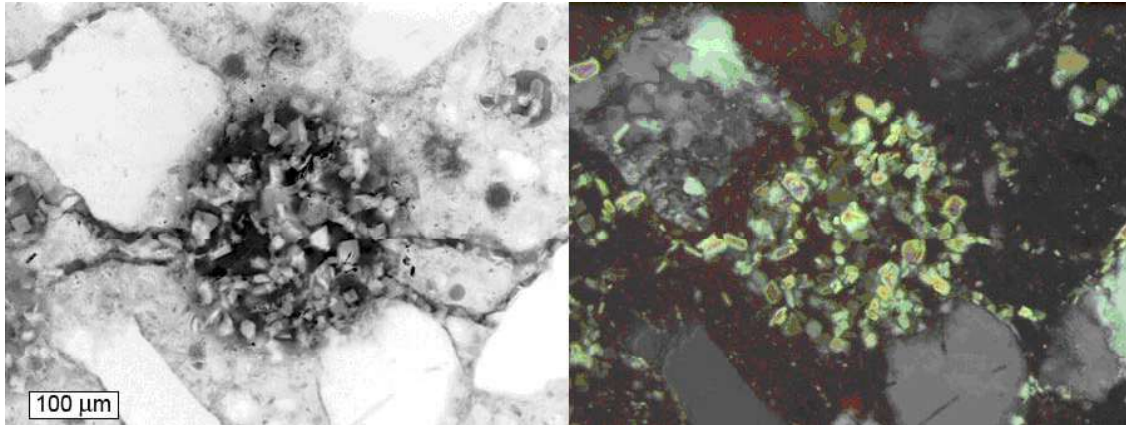
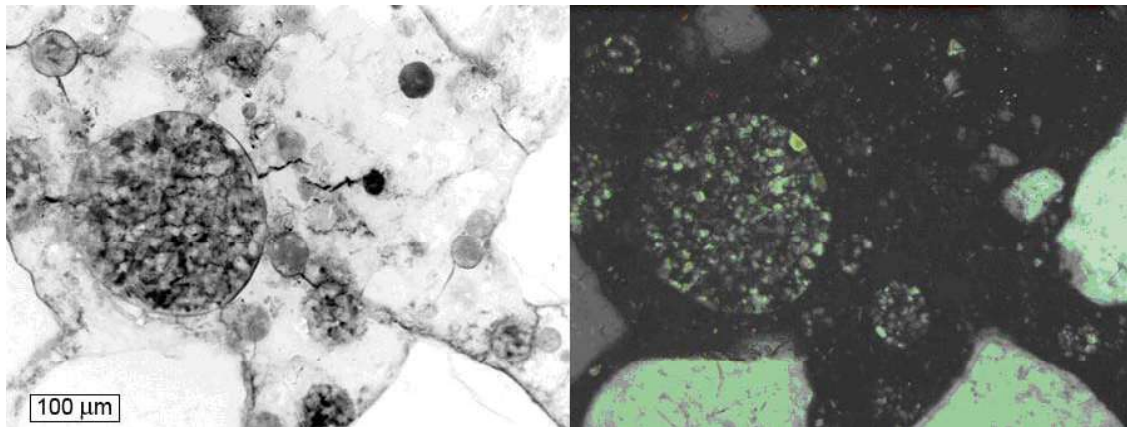


Figure 5.92. Regions of cement paste in 0.45 *w/cm* GGBFS concrete exposed to CaCl_2 brine where Ca(OH)_2 is depleted, (right) and still present, (left). From top to bottom: transmitted light, crossed polars, and epifluorescent mode images.



**Figure 5.93. Deteriorated portion from 0.45 w/c straight portland cement concrete exposed to CaCl_2 brine with blocky Ca(OH)_2 crystals.
From left to right: epifluorescent and crossed polars.**



**Figure 5.94. Deteriorated portion from 0.45 w/cm fly ash concrete exposed to CaCl_2 brine with blocky Ca(OH)_2 crystals.
From left to right: epifluorescent and crossed polars.**

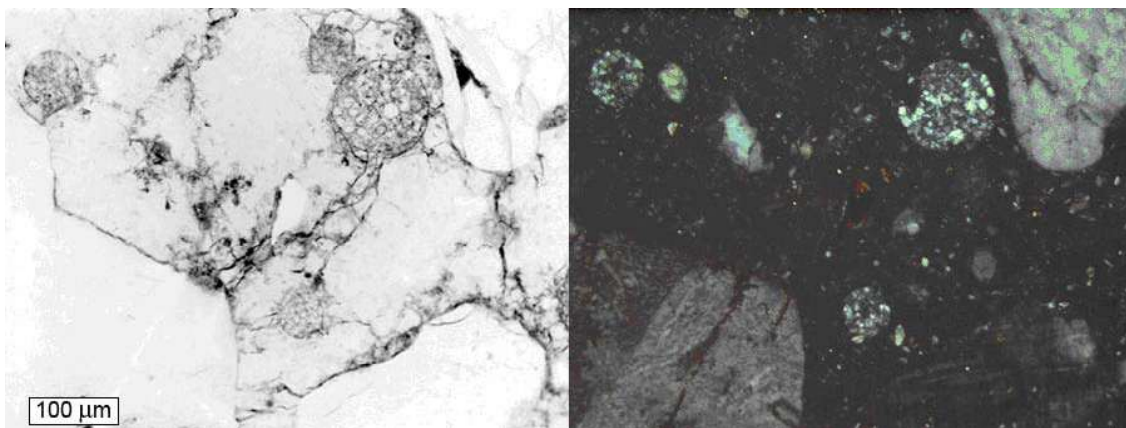


**Figure 5.95. Secondary blocky calcium hydroxide crystals in air voids of 0.45 w/cm GGBFS concrete exposed to CaCl_2 .
From left to right: epifluorescent and crossed polars.**

Comparison of the 0.45 w/cm Concrete Specimens Immersed in MgCl₂ Brine

Figure 5.96 shows epifluorescent mode images from 0.45 w/cm straight portland cement, fly ash, GGBFS concrete specimens, and a 0.55 w/c straight portland cement concrete specimen treated with silane after 500 days immersion the high-concentration MgCl₂ brine. The images depict the specimens in cross-section with the top surfaces of each specimen facing towards the right hand-side. Figure 5.97 shows further close-up epifluorescent mode images from the areas outlined in pink from Figure 5.96. As with the straight portland cement specimens exposed to CaCl₂ brine, the straight portland cement concrete specimens exposed to MgCl₂ brine showed the most severe cracking, as can be seen in Figure 5.97. Cracks are also visible in the GGBFS concrete specimen, but to a lesser degree. At the scale of the image in Figure 5.97, cracks are not observed in the fly ash concrete specimen. The same trend noted from the CaCl₂ brine of calcium hydroxide depletion, (Figures 5.98 through 5.100) coupled with blocky secondary deposits of calcium hydroxide in air voids and large cracks in the depleted zone, (Figures 5.101 through 5.103) was observed in the straight portland cement, fly ash, and GGBFS specimens exposed to MgCl₂ brine. However, in contrast to the same specimens exposed to the CaCl₂, the specimens exposed to the MgCl₂ brine all exhibited fibrous mineral precipitates on the surface and in the air voids and cracks near the surface, examples of which are shown in Figures 5.104 and 5.105. Figure 5.106 shows calcium hydroxide in the cement paste from a horizon just below the surface from the concrete specimen treated with silane. Neither calcium hydroxide depleted paste nor blocky secondary calcium hydroxide crystals were observed in the silane-sealed specimen. The silane-sealed specimen in Figure 5.106 appears to be in good condition.

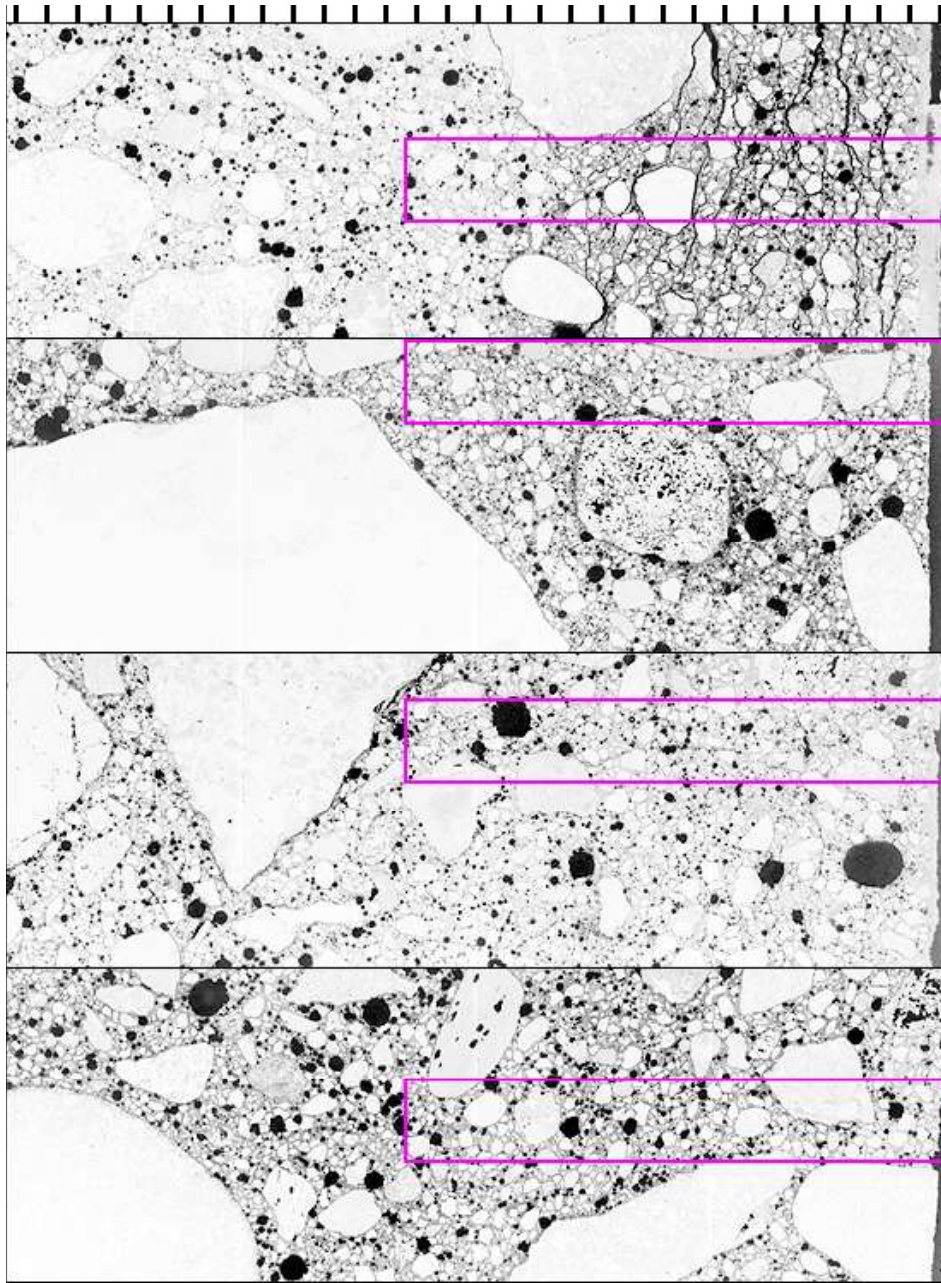


Figure 5.96. Epifluorescent thin section views of 0.45 *w/cm* concrete specimens, and a 0.55 *w/c* concrete silane-sealed specimen, all immersed in $MgCl_2$ solution for 500 days, exterior surfaces to the right.

From top to bottom: straight portland cement concrete, supplementary fly ash concrete, supplementary GGBFS concrete, and the 0.55 *w/c* silane-sealed concrete, tic marks every mm. Pink boxes highlight close-up regions shown in Figure 5.97.

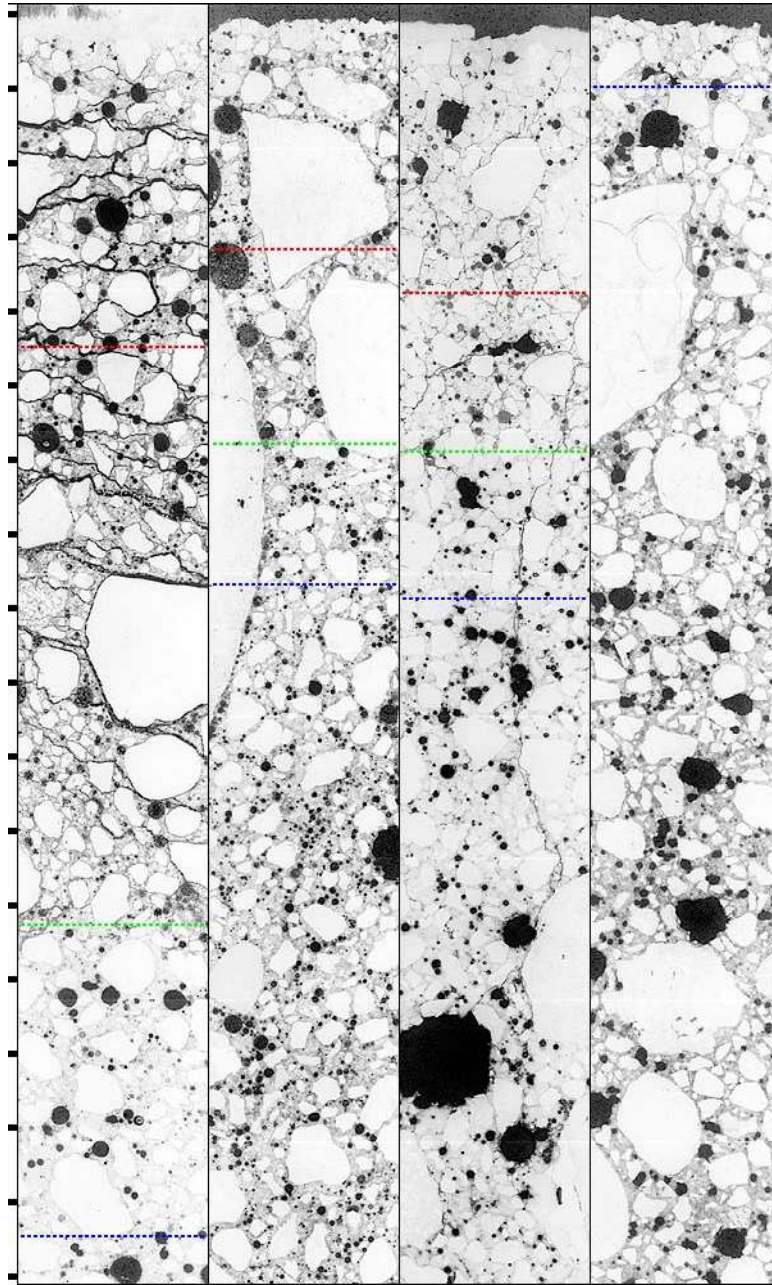
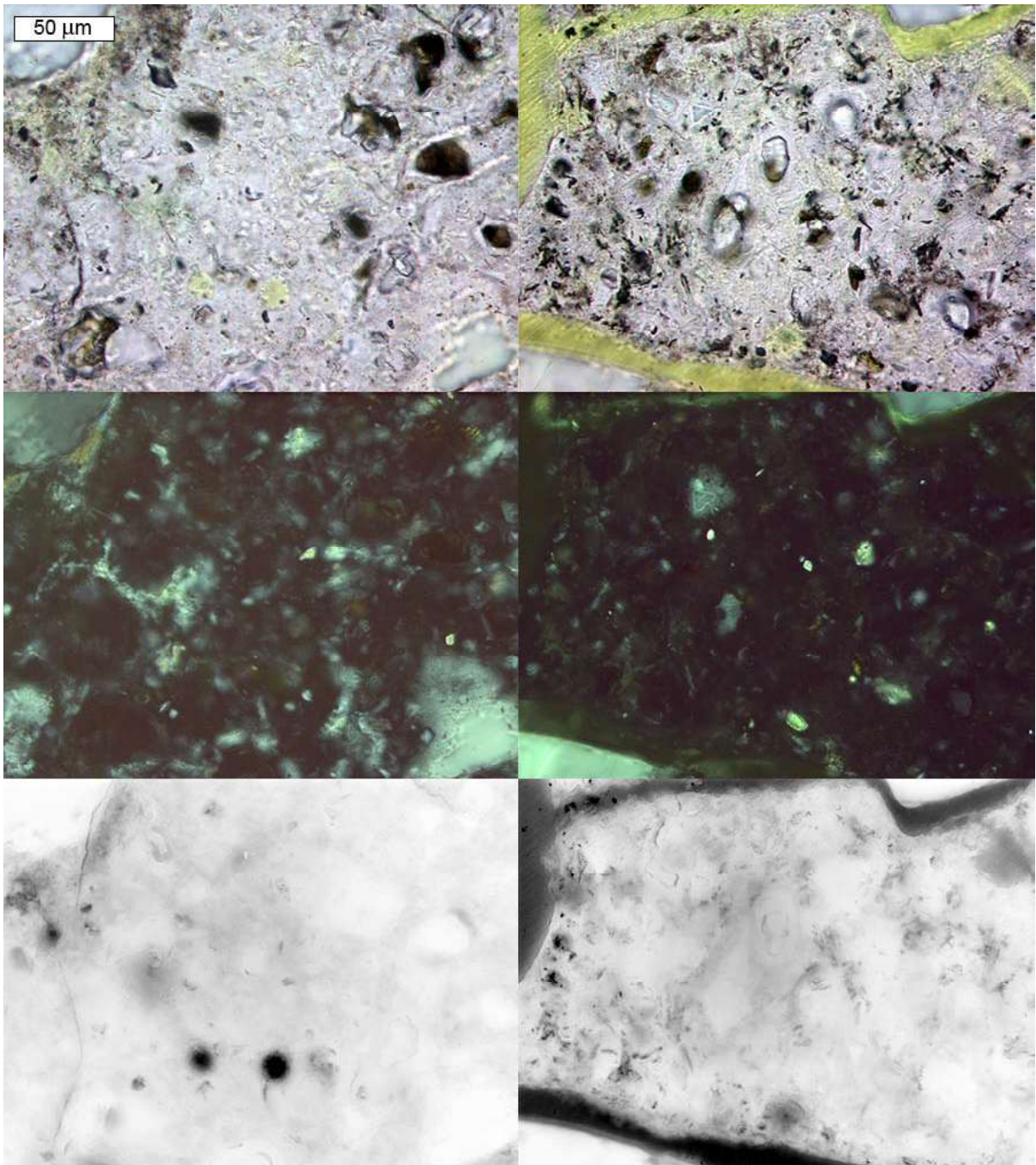


Figure 5.97. Close-up views of regions outlined in pink in Figure 5.96, but with exterior surfaces oriented towards the top. Cross-sectional epifluorescent mode images of 0.45 w/cm concrete specimens, and a 0.55 w/c concrete specimen after 500 days of immersion in $MgCl_2$ solution.

From left to right: straight portland cement concrete, supplementary fly ash concrete, supplementary GGBFS concrete, and the 0.55 w/c silane-sealed concrete, tic marks every mm. Green lines show extent of $Ca(OH)_2$ depleted cement paste. Red lines show horizons where photos of depleted paste were taken. Blue lines show horizons where photos were taken of paste with $Ca(OH)_2$ still present.



**Figure 5.98. Regions of cement paste in 0.45 w/c straight portland cement concrete exposed to $MgCl_2$ brine where $Ca(OH)_2$ is depleted, (right) and still present, (left).
From top to bottom: transmitted light, crossed polars, and epifluorescent mode images.**

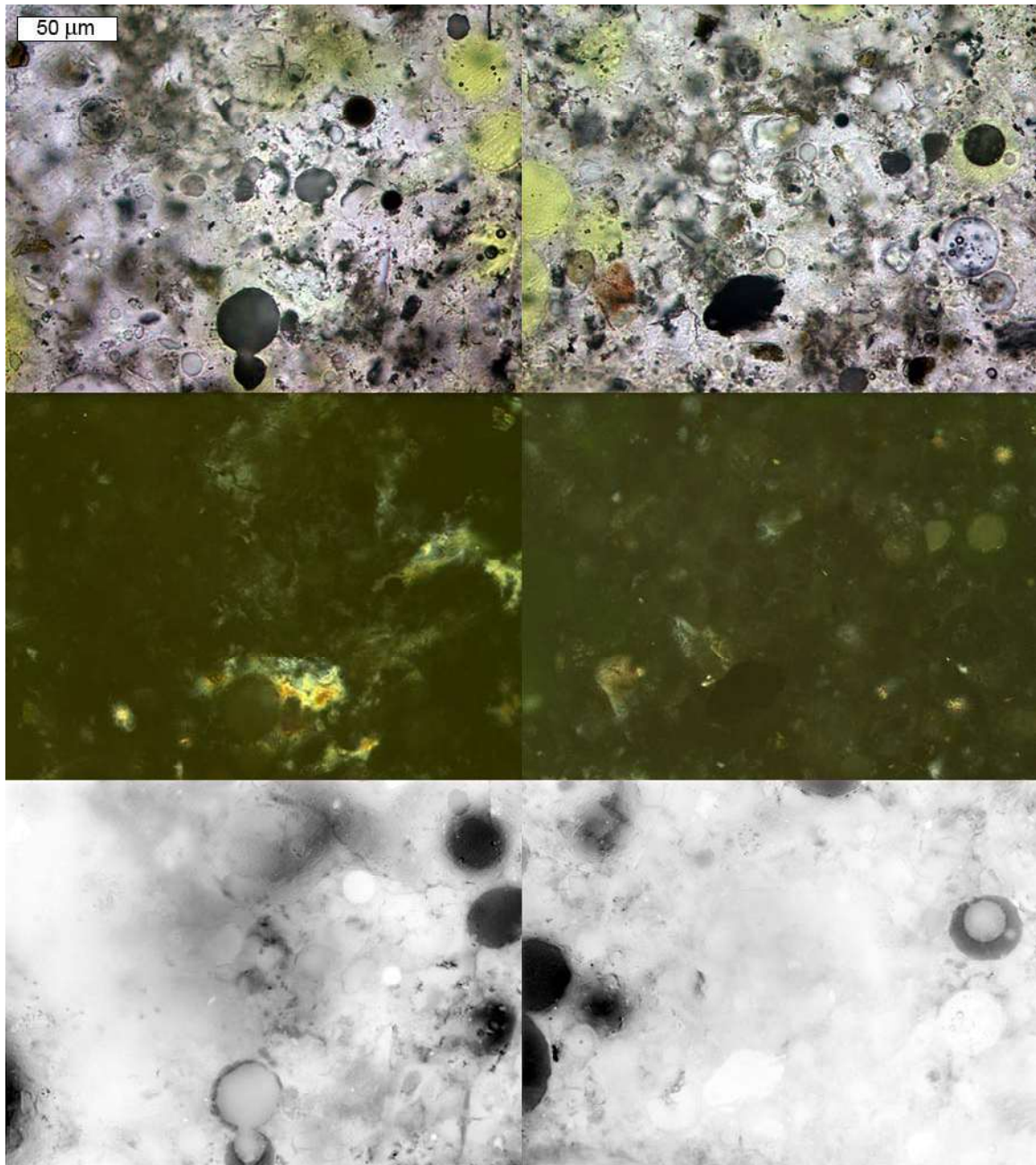


Figure 5.99. Regions of cement paste in 0.45 *w/cm* fly ash concrete exposed to MgCl_2 brine where Ca(OH)_2 is depleted, (right) and still present, (left).
 From top to bottom: transmitted light, crossed polars, and epifluorescent mode images.

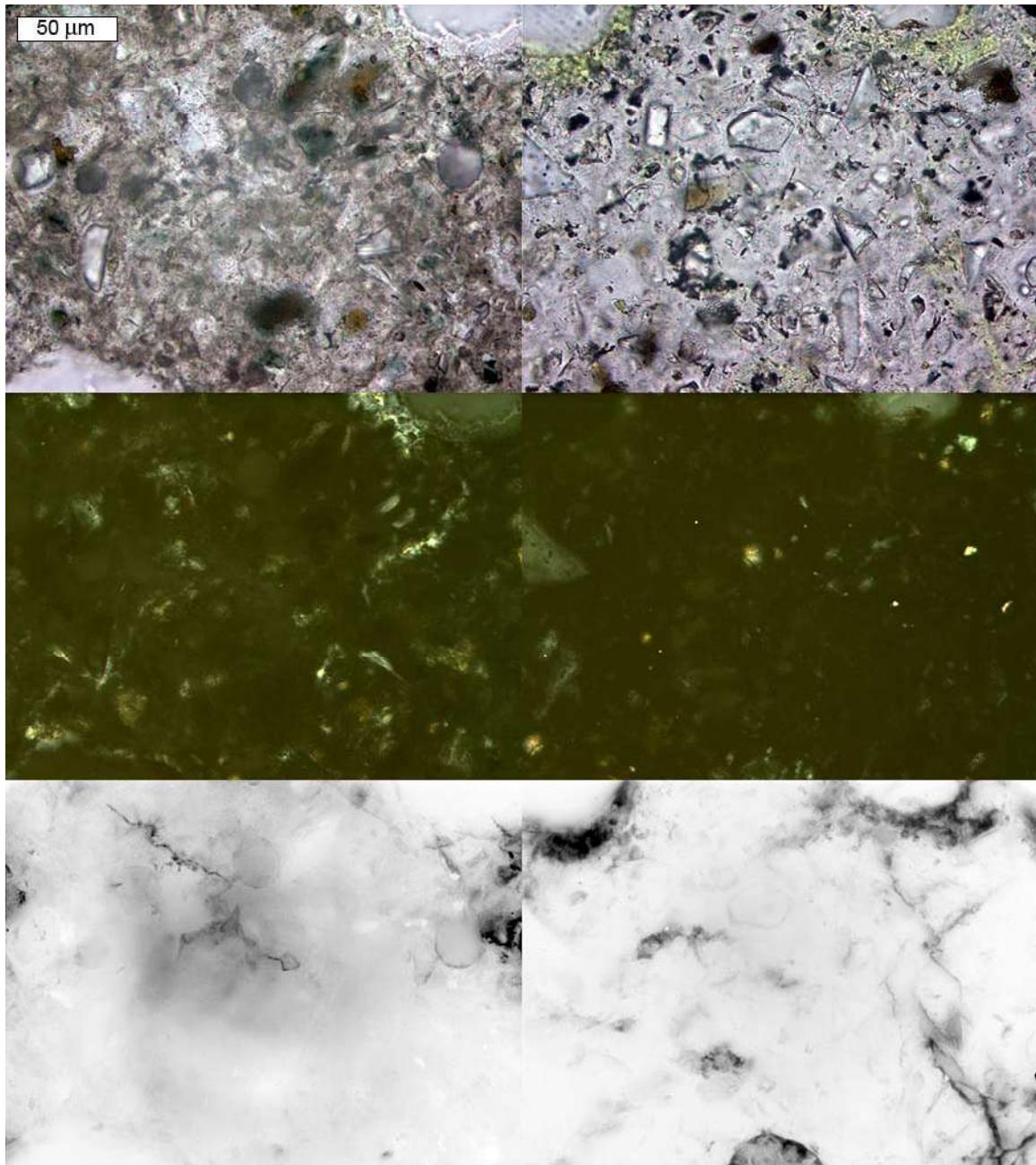
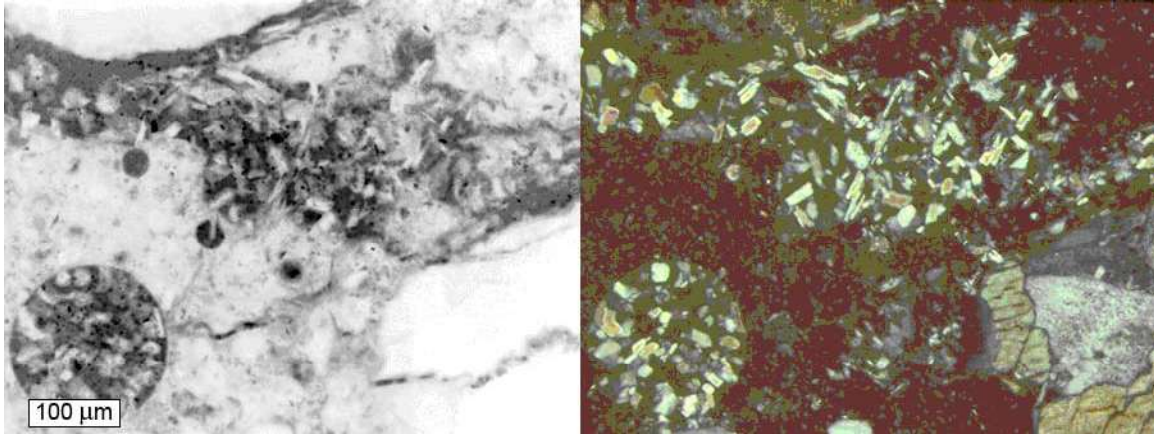
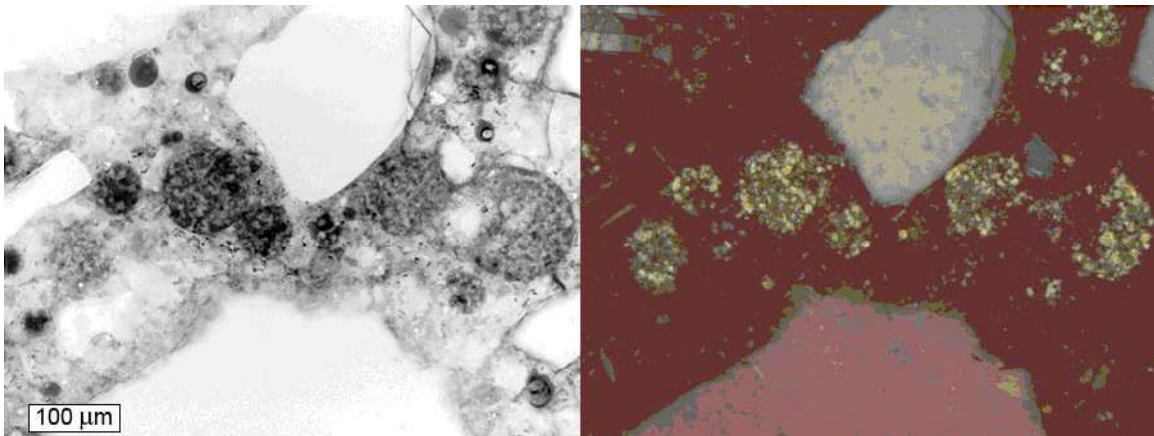


Figure 5.100. Regions of cement paste in 0.45 w/cm GGBFS concrete exposed to MgCl₂ brine where Ca(OH)₂ is depleted, (right) and still present, (left). From top to bottom: transmitted light, crossed polars, and epifluorescent mode images.



**Figure 5.101. Deteriorated 0.45 w/c straight portland cement concrete exposed to $MgCl_2$ brine with blocky $Ca(OH)_2$ crystals.
From left to right: epifluorescent and crossed polars.**



**Figure 5.102. Secondary blocky $Ca(OH)_2$ crystals in air voids of 0.45 w/cm fly ash concrete exposed to $MgCl_2$.
From left to right: epifluorescent and crossed polars.**

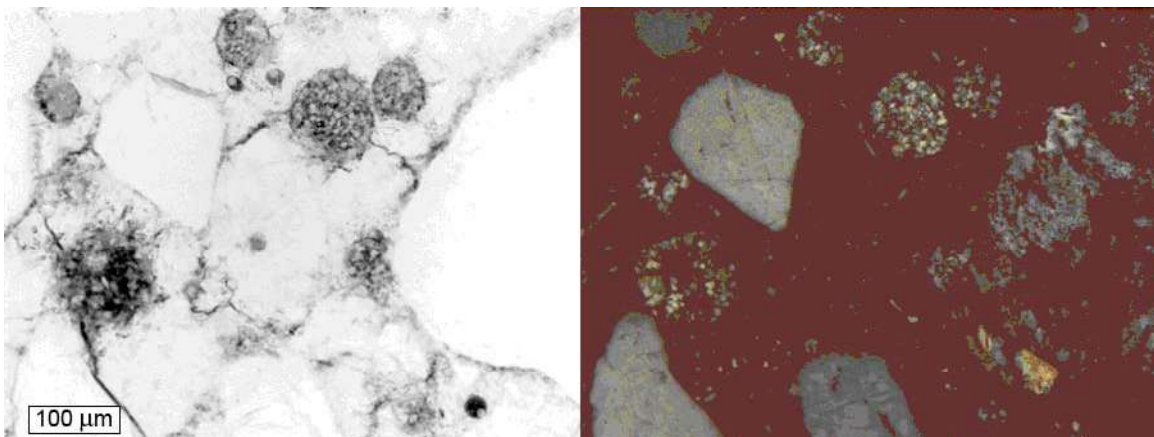


Figure 5.103. Deteriorated 0.45 w/cm GGBFS concrete exposed to $MgCl_2$ brine with blocky $Ca(OH)_2$ crystals in air voids. From left to right: epifluorescent and crossed polars.

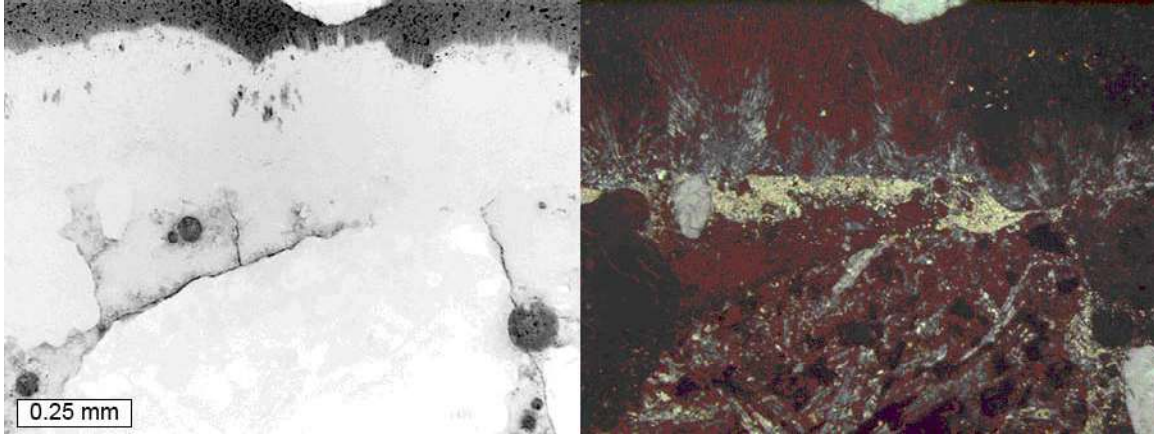


Figure 5.104. Fibrous crystals at surface of 0.45 w/c straight portland cement concrete exposed to $MgCl_2$ brine.
From left to right: epifluorescent and crossed polars.

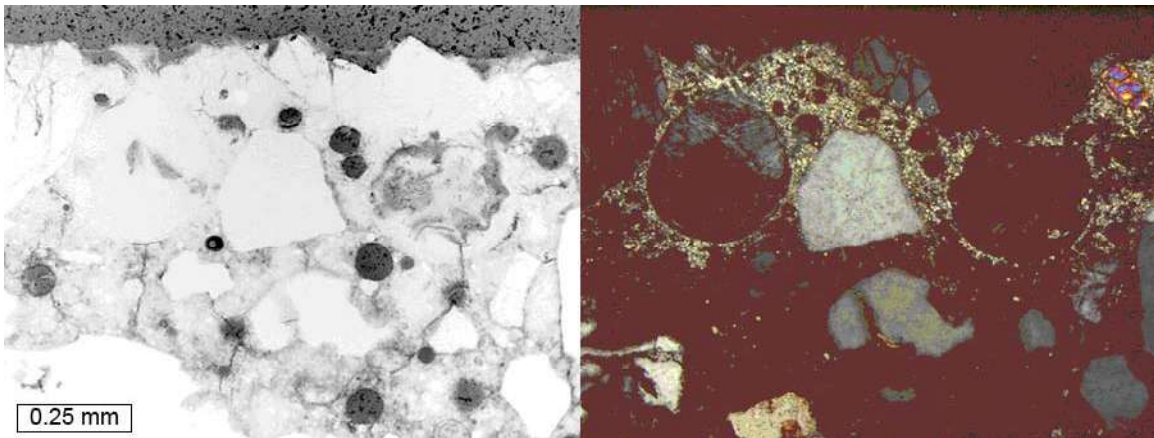


Figure 5.105. Fibrous crystals in voids near surface of 0.45 w/c straight portland cement concrete exposed to $MgCl_2$ brine.
From left to right: epifluorescent and crossed polars.

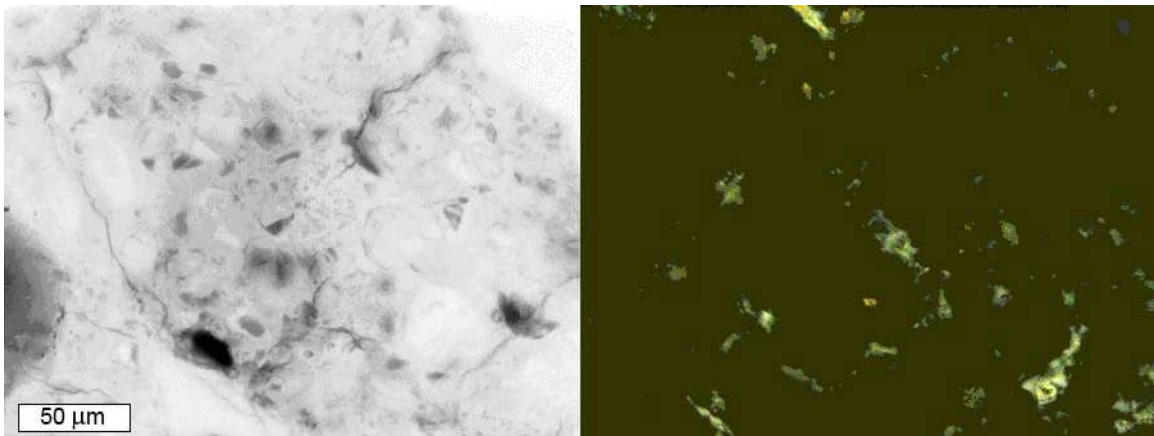


Figure 5.106. Cement paste just below surface, 0.45 w/c straight portland cement concrete, silane-sealed, exposed to $MgCl_2$ brine.
Left to right: epifluorescent and crossed polars.

Comparison of the 0.45 w/cm Concrete Specimens Immersed in MBAP Brine

Complete results and micrographs are presented in the Appendix to the Report, Section 3. The only specimen to show signs of severe cracking was the straight portland cement concrete specimen, as shown in Figure 5.50 of this section of this report. The same trend noted from the CaCl_2 and MgCl_2 brines of calcium hydroxide depletion, (Appendix Section 3, Figures A3.5.212 through A3.214) coupled with blocky secondary deposits of calcium hydroxide in air voids and large cracks in the depleted zone, (Figures A3.215 through A3.217) was observed in the straight portland cement, fly ash, and GGBFS specimens exposed to MBAP brine. As with the specimens exposed to the MgCl_2 brine, all of the specimens from the MBAP brine exhibited fibrous mineral precipitates on the surface and in the air voids and cracks near the surface.

5.3.2.4. Scanning Electron Microscopy

The same thin sections prepared from the 0.45 w/c straight portland cement concrete specimens exposed to the high concentration brines and the limewater control for 500 days were examined with a scanning electron microscope (SEM). Figure 5.107 shows back-scattered electron (BSE) images from the same areas examined optically in Figure 5.81. Elemental maps were also collected, but only for the samples exposed to the CaCl_2 , MgCl_2 , and MBAP brines, and are shown in Figures 5.108 through 5.110.

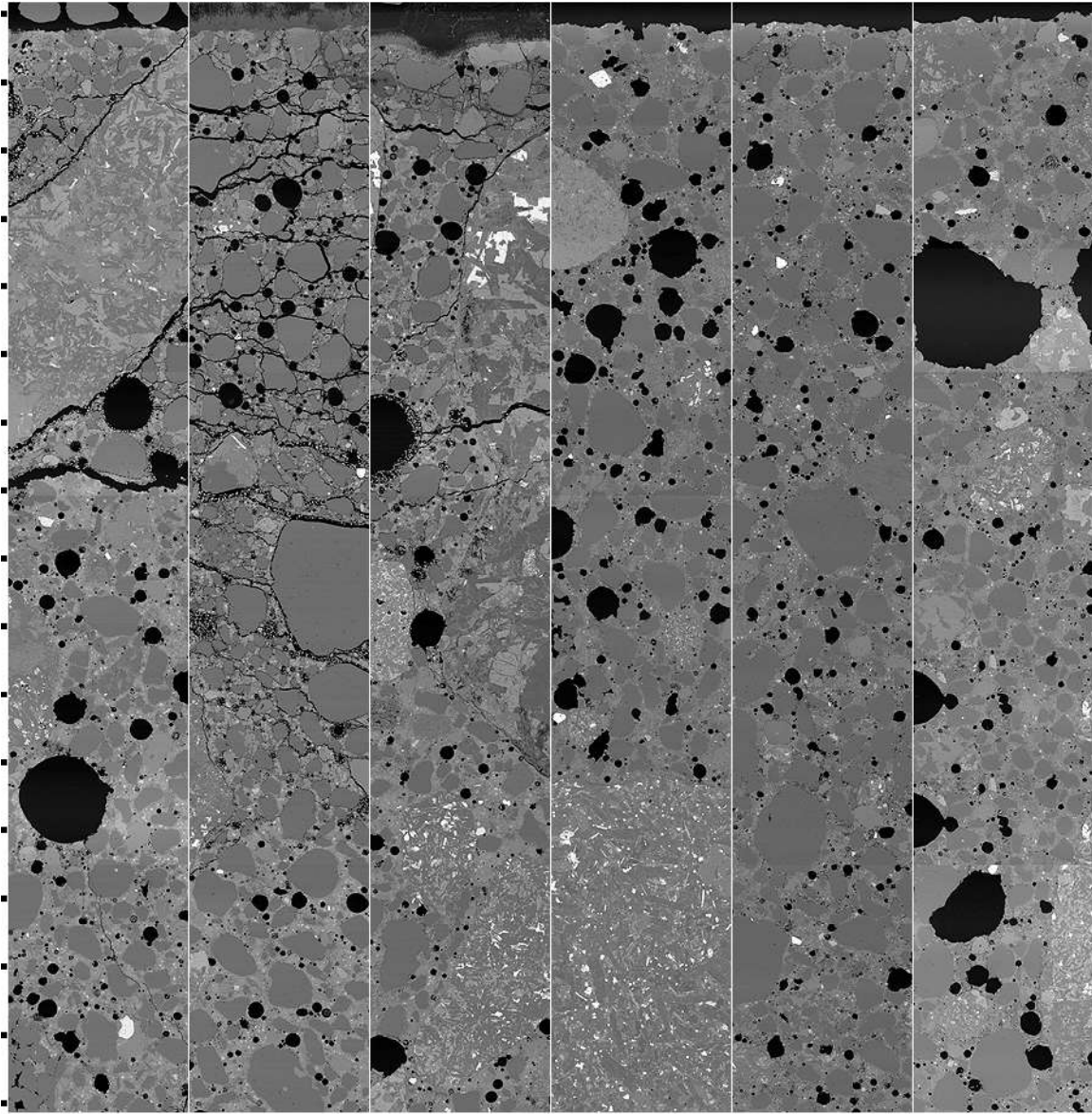


Figure 5.107. BSE images from 0.45 w/c concrete specimens exposed to high concentration brines and the limewater control after 500 days. From left to right, CaCl₂, MgCl₂, MBAP, NaCl, CMA, and limewater.

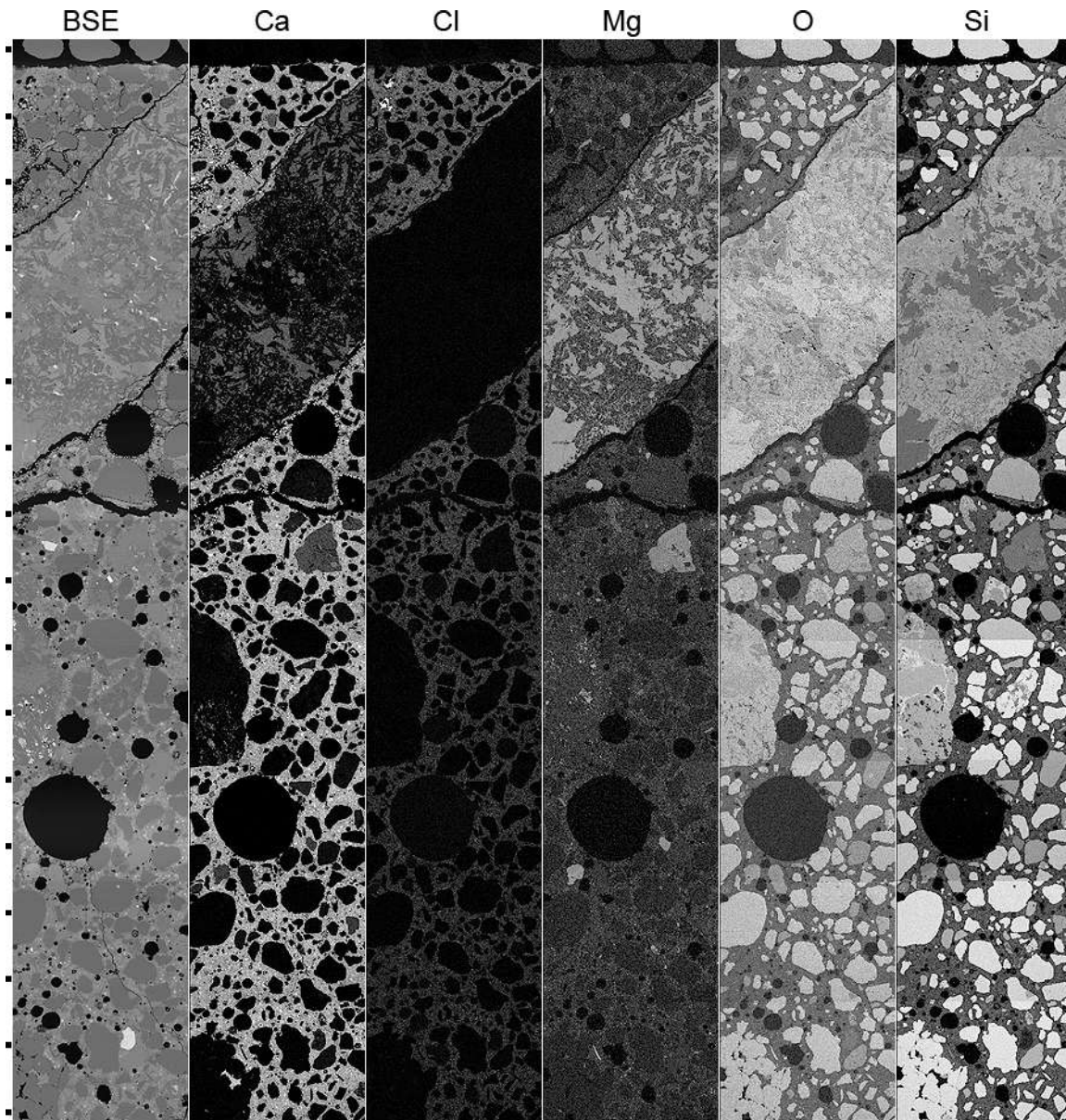


Figure 5.108. Elemental maps collected from 0.45 w/c concrete specimen immersed in CaCl_2 brine at 500 days. Brighter regions correspond to higher counts for characteristic elemental X-rays.

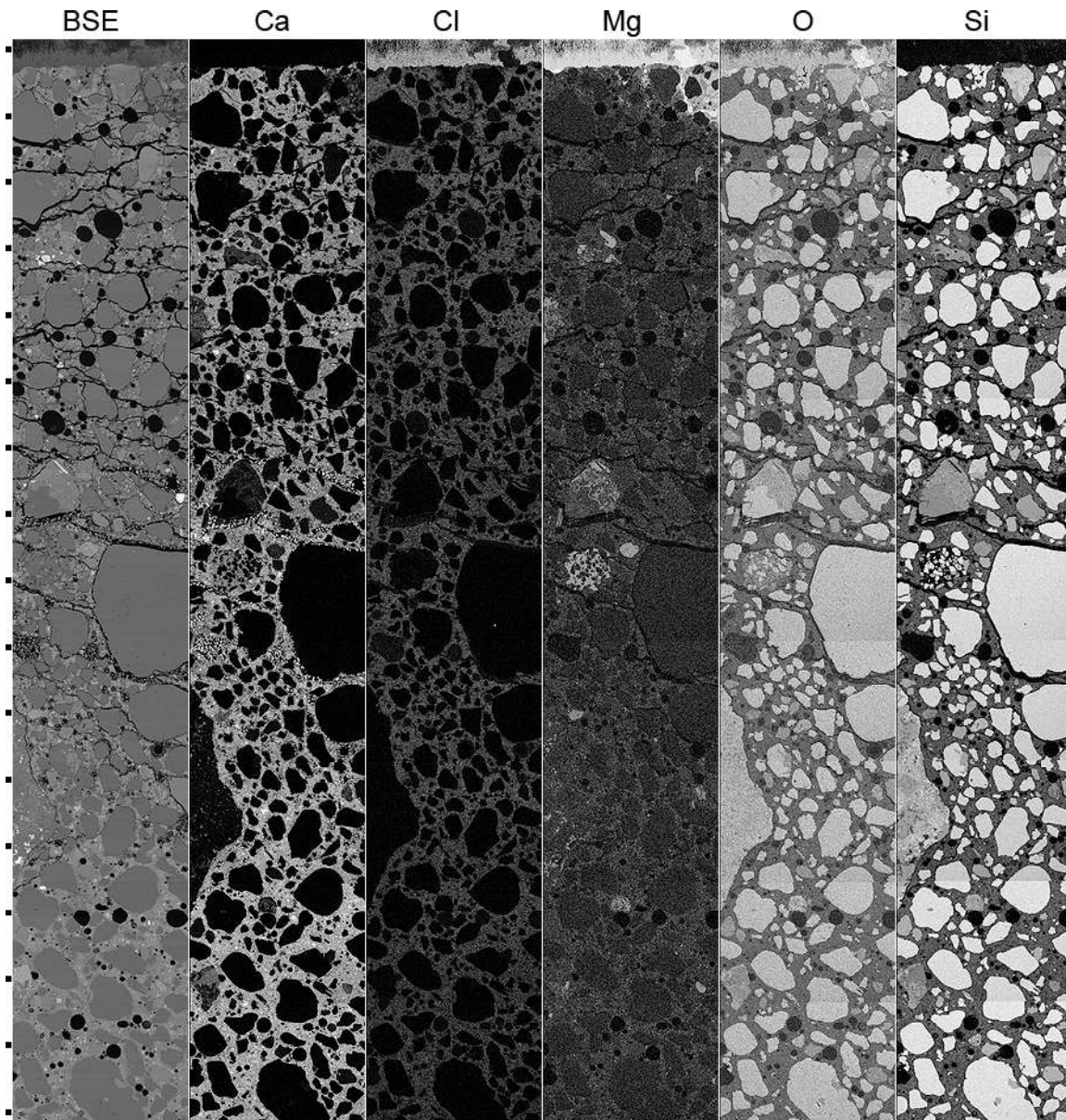


Figure 5.109. Elemental maps collected from 0.45 w/c concrete specimen immersed in MgCl_2 brine at 500 days. Brighter regions correspond to higher counts for characteristic elemental X-rays.

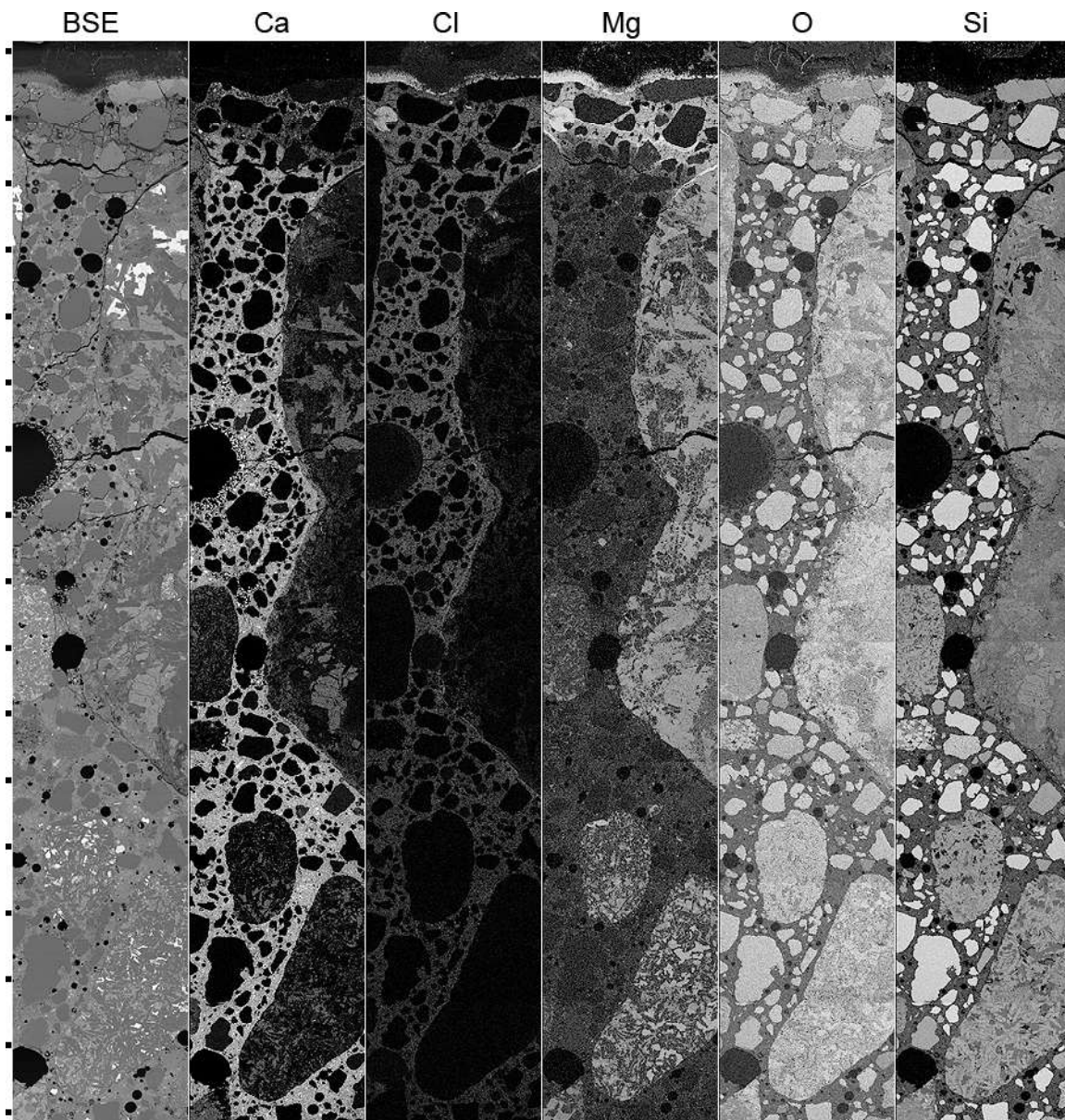


Figure 5.110. Elemental maps collected from 0.45 w/c concrete specimen immersed in MBAP brine at 500 days.

Brighter regions correspond to higher counts for characteristic elemental X-rays.

All of the areas mapped show a chloride gradient with higher concentrations near the surface. All of the maps also show a slight calcium gradient, with higher concentrations in the cement paste at depth. Only the maps from MgCl₂ and MBAP immersed specimens show magnesium enrichment near the surface. Magnesium and chlorine concentrations are particularly high in the mineral precipitate crust at the surface. Energy dispersive spectroscopy (EDS) analyses were performed on the fibrous minerals near or at the surface of the specimens exposed to MgCl₂ and MBAP, and the results are summarized in Table 5.5. Figure 5.111 shows a BSE image of the multi-phase fibrous mineral crust, with compositions similar to magnesium chloride hydroxide hydrate and brucite, with possible Ca²⁺ substitution for Mg²⁺ and Cl⁻ substitution for OH⁻.

Table 5.5. Typical EDS measurements from crystals in magnesium-enriched near-surface zone of specimens immersed in high concentration MBAP or MgCl₂ brines, compared to ideal mineral compositions for brucite and magnesium chloride hydroxide hydrate.

Element (Wt%)	Interior Fibrous Crystals	Exterior Fibrous Crystals	Mg(OH) ₂	Mg ₃ (OH) ₅ Cl•4H ₂ O
H*	-	-	3.5	4.6
O*	-	-	54.9	54.5
C*	-	-	0.0	0.0
Na	0.2	0.2	0.0	0.0
Mg	38.5	28.8	41.7	27.5
Al	0.0	0.0	0.0	0.0
Si	0.2	0.1	0.0	0.0
P	0.1	0.0	0.0	0.0
S	0.0	0.1	0.0	0.0
Cl	1.6	13.4	0.0	13.4
K	0.0	0.0	0.0	0.0
Ca	0.9	0.0	0.0	0.0
Mn	0.0	0.0	0.0	0.0
Fe	0.1	0.0	0.0	0.0
Sum	41.6	42.6	100.0	100.0

* Not included in EDS analysis.

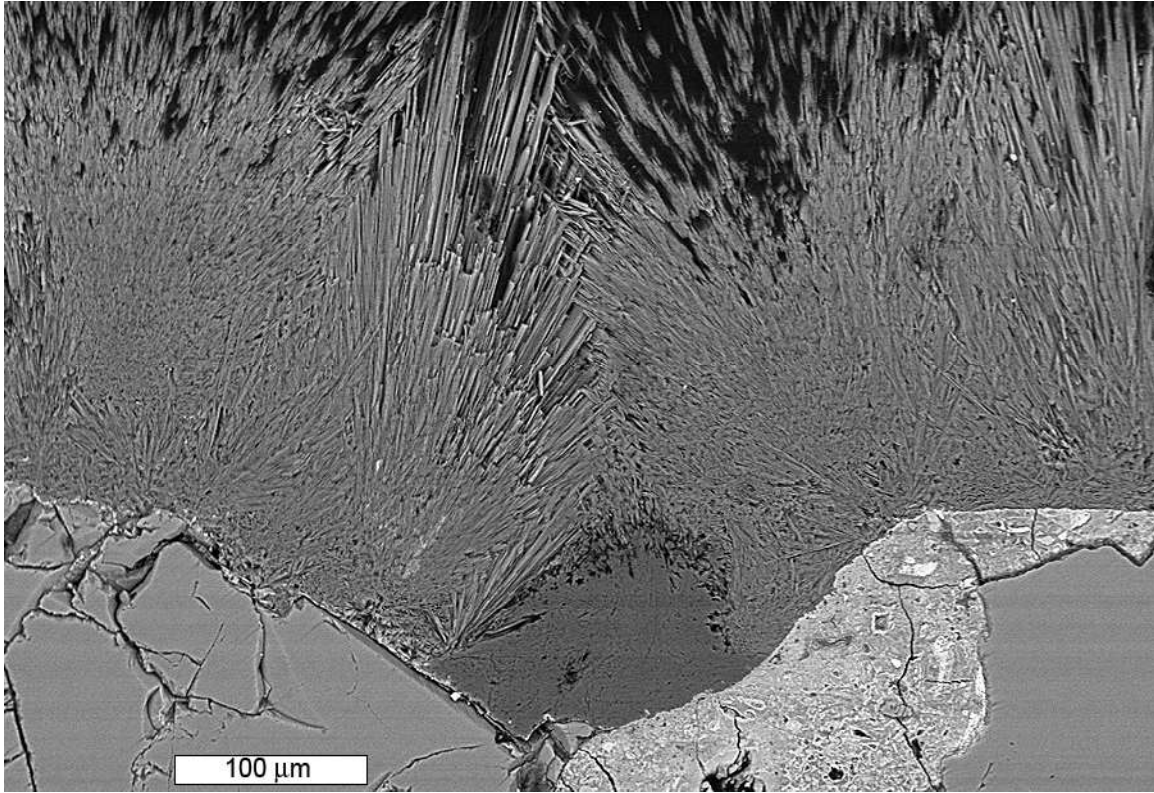


Figure 5.111. BSE image of magnesium chloride hydroxide hydrate (lighter) and brucite (darker) crystals at surface of 0.45 w/c concrete specimen exposed to MgCl_2 brine.

EDS analyses were also performed on the blocky secondary calcium hydroxide crystals observed by optical microscopy in all of the deteriorated specimens immersed in CaCl_2 , MgCl_2 , and MBAP brines. The results are summarized in Table 5.6. The small percentage of chlorine in the analyses may be due to minor Cl^- substitution for OH^- in the calcium hydroxide. A close examination of secondary deposits in the specimen immersed in CaCl_2 brine also revealed another bladed crystalline phase that had apparently replaced the blocky secondary crystals, but only near the surface. Figure 5.112 compares the blocky secondary calcium hydroxide crystals observed at depth to the bladed crystals near the surface. Table 5.7 shows the results of EDS analyses from the bladed crystals, which have a composition similar to calcium chloride hydroxide hydrate.

Table 5.6. Typical EDS measurements from blocky crystals in cracks and voids at depth in specimens immersed in high concentration CaCl₂, MgCl₂ and MBAP brines, compared to ideal mineral compositions for calcium hydroxide and calcite.

Element (Wt%)	Blocky Crystals	Ca(OH) ₂	CaCO ₃
H*	-	2.7	0.0
O*	-	43.2	48.0
C*	-	0.0	12.0
Na	0.0	0.0	0.0
Mg	0.0	0.0	0.0
Al	0.0	0.0	0.0
Si	0.0	0.0	0.0
P	0.1	0.0	0.0
S	0.0	0.0	0.0
Cl	3.4	0.0	0.0
K	0.1	0.0	0.0
Ca	50.9	54.1	40.0
Mn	0.0	0.0	0.0
Fe	0.0	0.0	0.0
Sum	54.5	100.0	100.0

Table 5.7. Typical EDS measurements from bladed crystals observed in cracks and voids in near-surface zone of specimen immersed in high concentration CaCl₂ brine, compared to ideal mineral composition for calcium chloride hydroxide hydrate.

Element (Wt%)	Bladed Crystals	CaO•CaCl ₂ •2H ₂ O
H*	-	1.8
O*	-	23.8
C*	-	0.0
Na	0.0	0.0
Mg	0.0	0.0
Al	0.0	0.0
Si	0.0	0.0
P	0.0	0.0
S	0.2	0.0
Cl	30.7	34.9
K	0.1	0.0
Ca	42.4	39.5
Mn	0.1	0.0
Fe	0.3	0.0
Sum	73.8	100.0

* Not included in EDS analysis

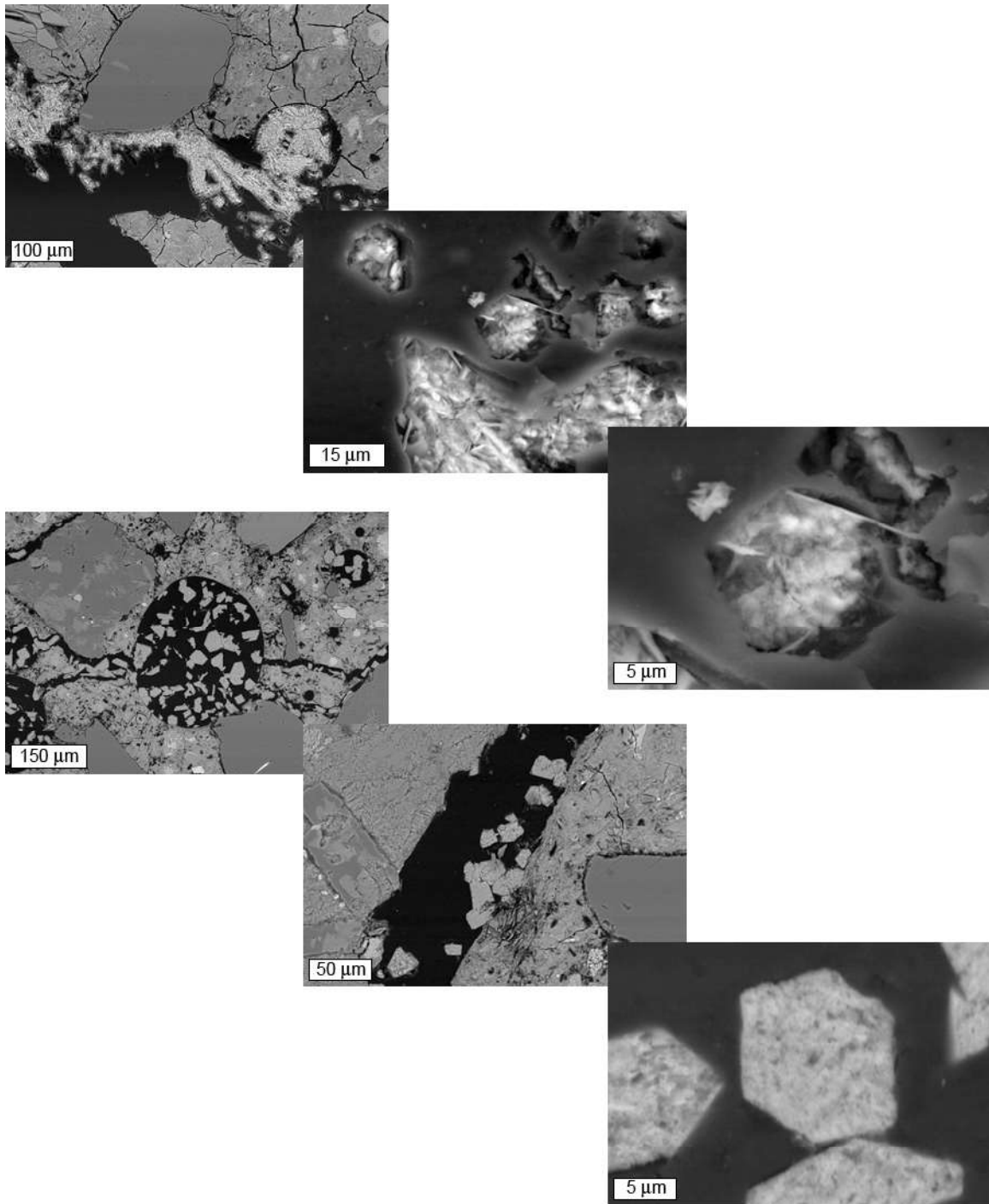


Figure 5.112. BSE images comparing bladed crystals observed near the top of the specimen exposed to CaCl_2 brine, (upper images) to secondary blocky calcium hydroxide crystals observed at depth (lower images).

5.3.3 RESULTS OF PHASE II EXPERIMENTS CONDUCTED AT THE UNIVERSITY OF TORONTO

5.3.3.1 ASTM C 666 Freeze Thaw Testing

The concrete prisms subjected to freeze-thaw testing showed behavior similar to the mortar samples tested in Phase I. That is, concrete prisms exposed to $MgCl_2$ and $CaCl_2$ expanded above 0.1%, which is considered by ASTM C 666 to represent failure. Figure 5.113 shows the length change of the specimens. While prisms exposed to $NaCl$ did not expand more than 0.04% for 300 cycles, prisms exposed to $MgCl_2$ and $CaCl_2$ expanded considerably with 0.17 and 0.18% length change respectively. It was observed that the prisms subjected to $MgCl_2$ started to expand only after 150 cycles while those exposed to $CaCl_2$ expanded gradually from the start of the test. One deviation from the normal ASTM C 666 procedure was that specimens expanding more than 0.1% were not removed from the freeze-thaw chamber until all specimens were subjected to 300 cycles. This approach provided deteriorated material for X-ray diffraction analysis to investigate the formation of new phases associated with this expansion. Note that the concentration of the exposure solution did not allow freezing during the test, eliminating physical attack as the sole mechanism of deterioration.

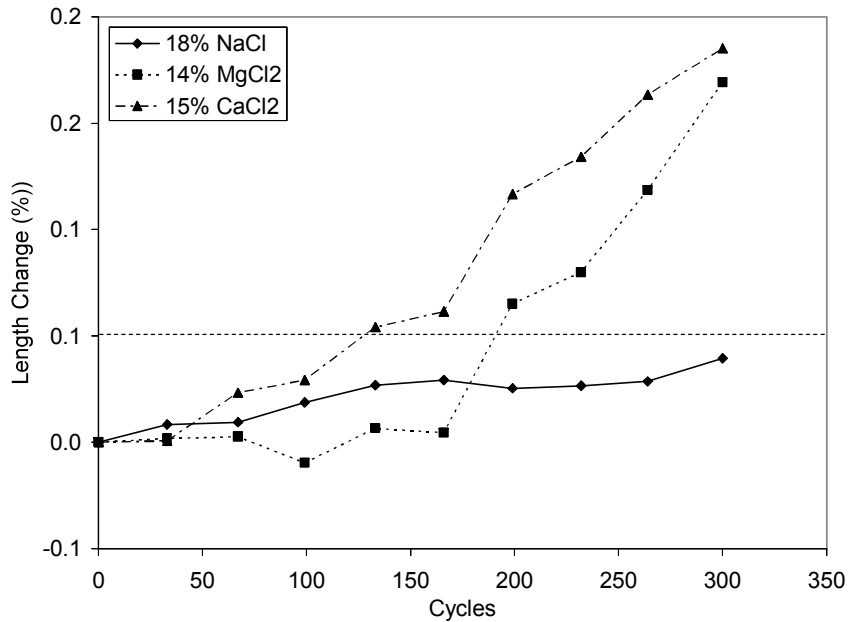


Figure 5.113. Length change of concrete prisms exposed to deicers under freezing and thawing cycles.

The determination of mass change during the ASTM C 666 test is not a requirement. However, Phase I results suggested that any formation of new phases seems to be accompanied with considerable changes in mass and therefore it was monitored. As seen in Figure 5.114, the specimens exposed to $MgCl_2$ gained considerable mass during the test. Those exposed to $CaCl_2$ had the opposite behavior with a recorded loss of mass. These two opposite reactions were evident after 100 cycles. The specimens exposed to $NaCl$ showed negligible expansion even after 300 cycles. Although the observed length and mass change for the $MgCl_2$ and $CaCl_2$ specimens suggested that the minimum relative dynamic modulus of elasticity (i.e. 60% of the initial value) should have been reached after 100 cycles, this was not the case. Only after 250 cycles did the modulus drop below the minimum value for continuing the test. Figure 5.115 illustrates the gradual loss of the dynamic modulus of

elasticity for those samples exposed to $MgCl_2$ and $CaCl_2$. For $NaCl$, no detrimental effect on the modulus was found even after 300 cycles of freezing and thawing.

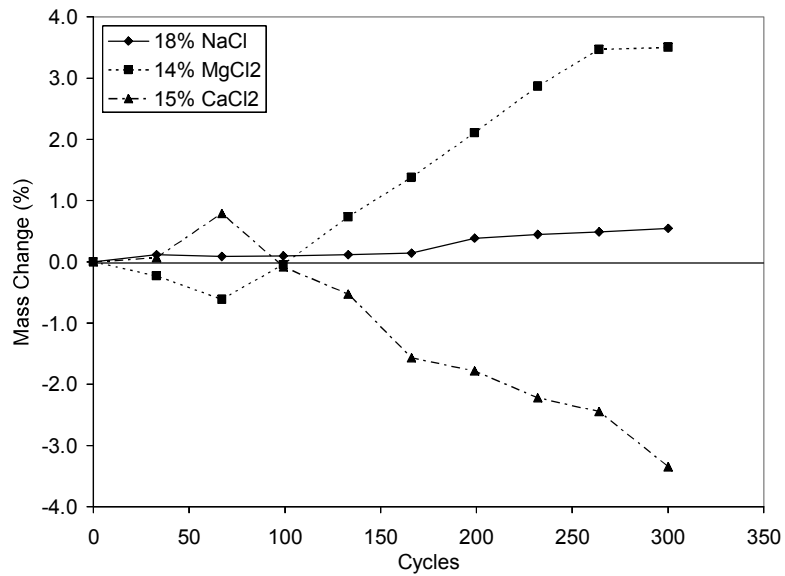


Figure 5.114. Mass change of concrete prisms exposed to deicers under freezing and thawing cycles.

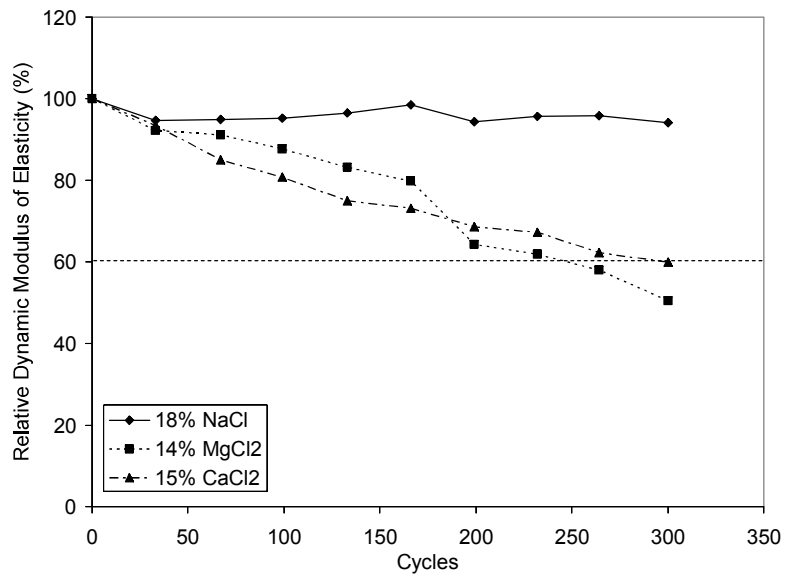


Figure 5.115. Relative dynamic modulus of elasticity of concrete prisms exposed to deicers under freezing and thawing cycles.

After determining the durability factor, it is clear that MgCl_2 and CaCl_2 solutions reduce the concrete's resistance to freezing and thawing when compared with NaCl as observed in Figure 5.116. The durability factors of 60 for CaCl_2 and 51 for MgCl_2 show the negative impact of these deicers on the resistance of concrete to freezing and thawing. Note that although there is no universally accepted limit for the durability factor, 80 is typically accepted as the threshold between durable and non-durable concrete.

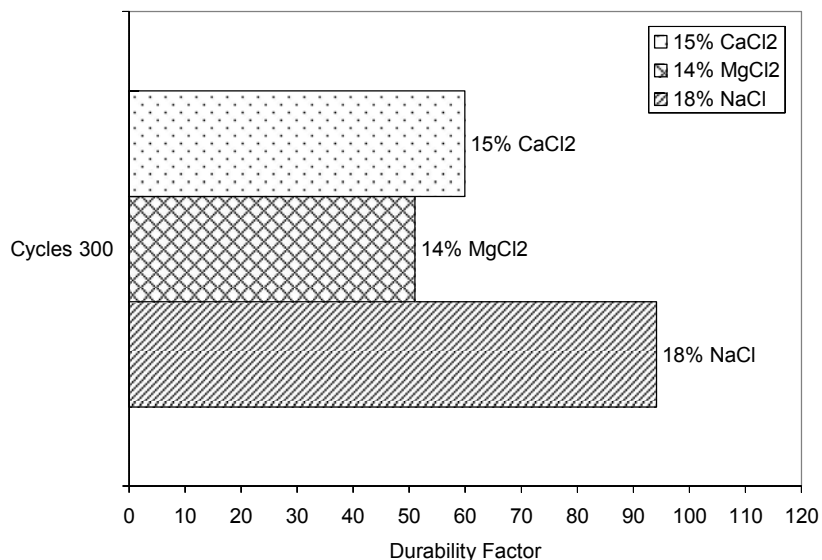


Figure 5.116. Durability factor of concrete prisms exposed to deicers under freezing and thawing cycles.

5.3.3.2 Scaling Resistance

It was observed that after exposing concrete slabs to CaCl_2 solutions, the chemical interaction of this deicer with the concrete surface diminished the concrete's ability to properly withstand environmental conditions involving application of deicers during winter. After a year of ponding the surface of the slabs with 22% CaCl_2 , the appearance of the surface did not suggest any problems and no signs of deterioration were observed. Once the slabs were subjected to freezing and thawing cycles in the presence of 4% CaCl_2 , the surface started to scale gradually up to 50 cycles of exposure. At 50 cycles it was decided to continue the test as an unusual scaling pattern was developing on the surface with areas scaling deeper below the surface exposing the aggregate in localized areas of the slab. After 50 cycles, the amount of scaled material increased dramatically causing the surface to expose all the coarse aggregate and paste-aggregate debonding was evident. The test was discontinued once the scaling progressed so deep into the concrete that the solution could not be kept in place due to leakage down below the Styrofoam dike.

Parallel tests were run on slabs that were exposed to highly concentrated solutions of NaCl (23% by mass) and then tested with 3% NaCl solution. Those slabs did not show any sign of scaling (e.g. their visual rating was only 1 compared to 5 for specimens exposed to 22% CaCl_2 before the start of the salt scaling test.) Figure 5.117 compares the salt scaling resistance of slabs that were preconditioned by exposing them to 22% CaCl_2 before the start of the test, and those preconditioned in 23% NaCl until the start of the salt scaling test.

Figures 5.118, 5.119 and 5.120 show photographs of the concrete surface of slabs tested under the above conditions at different cycles, illustrating the unusual scaling of those preconditioned with 22% CaCl_2 and the excellent state of the slabs that were pretreated with 23% NaCl before starting the salt scaling test.

X-ray diffraction analysis was performed on concrete slabs subjected to the same pretreatment conditions, but kept for analysis instead of being tested for salt scaling resistance. The surface of the slab pretreated with 23% NaCl did not show any formation of new phases besides some Friedel's salt but those slabs exposed to 22% CaCl_2 showed the distinctive peaks of calcium oxychloride in addition to Friedel's salt.

Those slabs pretreated with MgCl_2 and tested for salt scaling resistance did not scale and their visual rating and behavior was similar to those exposed to NaCl . No new phases were formed that were detectable by X-ray diffraction.

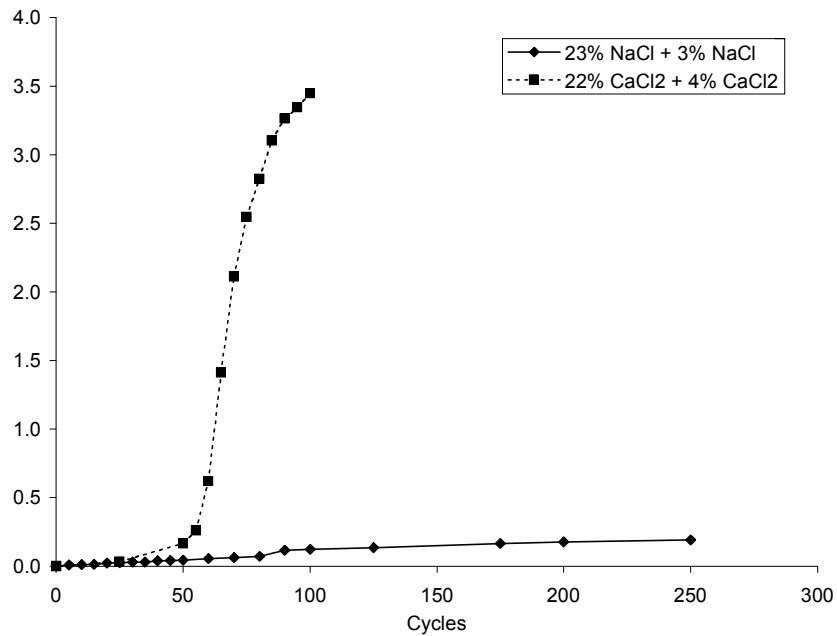
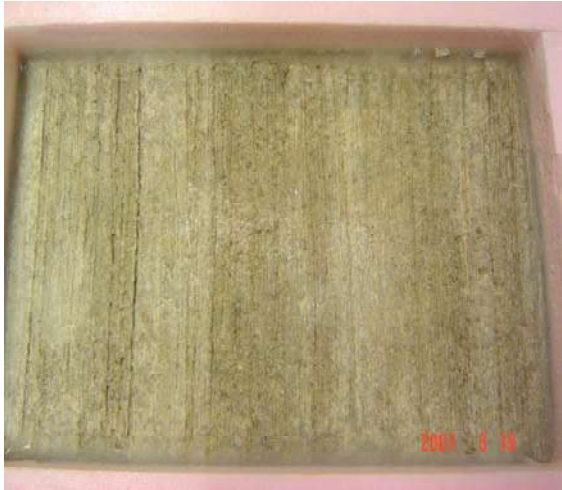


Figure 5.117. Scaled material of concrete slabs exposed to 22% CaCl_2 in comparison with those exposed to 23% NaCl before the start of the salt scaling test.



(a)



(b)

Figure 5.118. Photographs of concrete surfaces at cycle 0 (a) pretreated with 23% NaCl and tested with 3% NaCl and (b) pretreated with 22% CaCl₂ and tested with 4% CaCl₂.



(a)



(b)

Figure 5.119. Photographs of concrete surfaces at cycle 50 (a) pretreated with 23% NaCl and tested with 3% NaCl and (b) pretreated with 22% CaCl₂ and tested with 4% CaCl₂.



(a)



(b)

Figure 5.120. Photographs of concrete surfaces at cycle 100 (a) pretreated with 23% NaCl and tested with 3% NaCl and (b) pretreated with 22% CaCl₂ and tested with 4% CaCl₂.

SECTION 6. DISCUSSION

6.1. OVERVIEW

This section will provide an analysis and discussion of the data presented in Sections 4 and 5 of this report. The discussion will be organized based upon project Tasks 7, 8, and 9, which were to be addressed based upon the results of Tasks 5 and 6.

6.2. EFFECTS OF VARIOUS DEICING/ANTI-ICING CHEMICALS

Through the work conducted in this research project, a clearer picture has been developed of the detrimental effects that various deicing chemicals may have on concrete pavements and bridge decks. Four key deicing brines were evaluated: sodium chloride (NaCl), magnesium chloride (MgCl₂), calcium chloride (CaCl₂), and calcium magnesium acetate (CMA). Additionally, a magnesium chloride based agricultural product (MBAP) was also tested. Each brine will be discussed separately.

Certain tests performed proved to be ineffective at identifying the effects of deicers on mortar and concrete. Specifically, the cyclic temperature test and the high temperature test conducted as part of Phase I were ineffective and were not continued in Phase II. Results from these tests will not be used in identifying detrimental effects of deicers, but results of these tests will be discussed as appropriate to help illustrate the shortcomings of each.

After reviewing the literature and conducting the battery of experiments used in this research, the metrics used to assess the effects of these chemicals are:

1. Visible deterioration after exposure to deicers
2. Petrographic evidence of chemical interaction resulting in distress
3. Physical evidence of distress after exposure such as:
 - a. Expansion after exposure
 - b. Loss of compressive strength after exposure
 - c. Mass change after exposure
 - d. Freeze-thaw performance (ASTM C666 and ASTM C672)

The data to address these metrics result from the various laboratory experiments conducted. The effects of these various deicing chemicals will be discussed with respect to these metrics.

6.2.1. EFFECTS OF SODIUM CHLORIDE (NaCl) ON CONCRETE PAVEMENTS AND BRIDGE DECKS

6.2.1.1. Visible Deterioration After Exposure to Deicers

A variety of tests were performed where distress would be visible, if it were occurring. In almost all of these tests, no visible distress was detected when specimens were exposed to concentrated NaCl solutions. The Phase I mortar tests conducted at Michigan Tech initially had significant failures reported for NaCl exposure. All of these failures were associated with the cyclical temperature test. After much investigation, no sign of chemical interaction could be associated with these failures. All evidence, both obtained independently in the laboratory and obtained through review of the literature, indicates that the observed distress was physical and it was an artifact of the experimental approach. It is postulated that the distress was a combination of factors. First, the specimens in the NaCl brine achieved a higher level of saturation as compared to the control specimens in limewater. Once saturated, the specimens in the NaCl brine froze completely, as did those in limewater. However, upon

temperature cycling, the specimens in NaCl brine were subjected to high internal stresses from 1) salt crystallization, 2) the high coefficient of thermal expansion of salt relative to water, and 3) the restrained thermal expansion of ice, and subsequently of water, as the specimens progressed from -15 °F to 135 °F [-26 °C to 57 °C] (Grimm 1985). In the latter case, the restraint occurred as the salt filled pores did not allow water to easily migrate from the specimens as the ice in the pore structure melted. For all other tests including the cold temperature test (Phase I), immersion tests to assess strength loss, etc. (Phase I), Phase II immersion tests, scaling test (ASTM C672), and freeze-thaw testing (ASTM C666), little to no visible distress was detected for specimens exposed to concentrated NaCl solutions.

6.2.1.2. Petrographic Evidence of Chemical Interaction Resulting in Distress

In this research, the predominate characteristics identified with chemical attack by deicers are the dissolution of calcium hydroxide from the hardened cement paste and the formation of secondary phases, most importantly calcium or magnesium oxochloride. Freidel's salt and brucite were also identified in many cases but were not associated with distress in mortar or concrete for any of the deicers studied, including NaCl.

For the laboratory specimens exposed to NaCl, and examined by petrographic methods, no evidence of chemical interaction was observed. Calcium hydroxide depletion was seen near the surface of some mortar specimens, but not at depth in the sample as seen in the case of exposure to other deicers. No evidence of oxochloride formation was observed. From a practical perspective, the chemical interaction between NaCl and hardened cement paste was minimal to none existent.

6.2.1.3. Expansion After Exposure

In the mortar tests conducted in Phase 1, expansion as a result of exposure to NaCl was negligible. Expansion in the NaCl exposed samples was 0.05% after 568 days as compared to 0.02% for specimens exposed to limewater.

6.2.1.4. Loss of Compressive Strength After Exposure

For samples exposed to NaCl solutions, there was no loss in strength; in fact the specimens gained strength in a manner similar to samples exposed to limewater for the same time period. The final strength recorded for the samples exposed to NaCl solutions for 568 days was 7676 psi [52.9 MPa], as compared to the specimens exposed to limewater 7372 psi [50.8 MPa] after the same time period.

6.2.1.5. Mass Change after Exposure

For mortar samples exposed to NaCl solutions, there was negligible mass gain as compared to specimens exposed to limewater. The former had a mass gain of 1.42% and the latter had a mass gain of 1.08% after 568 days.

6.2.1.6. Freeze-Thaw Performance (ASTM C666 and ASTM C672)

The concrete specimens exposed to NaCl were the only specimens that did not exceed the 0.1% expansion limit after 300 cycles. Likewise, samples tested for freeze-thaw performance in a NaCl environment had the only acceptable durability factor at 94.1%. There appeared to be no demonstrable freeze-thaw durability problem with concrete exposed to NaCl as a result of this testing.

Regarding scaling performance, the test performed involved pre-treating the slabs for one year in 23% NaCl, and then testing in accordance with ASTM C672. After 50 cycles, the observed damage rating was 1. There was no significant scaling problem associated with NaCl exposure.

6.2.1.7. Assessment of the Effects of NaCl

In general, NaCl was the most chemically benign of the three principal deicers (i.e. NaCl, MgCl₂, and CaCl₂) in terms of attacking the concrete. There were minimal negative effects identified with exposure of mortar and concrete to concentrated solutions of NaCl. It should be noted however that there is ample evidence in the literature regarding the detrimental effects of NaCl deicers with respect to corrosion of embedded steel in concrete and corrosion of vehicles. Work performed in this study showed that NaCl had the highest sorptivity rate of all the deicers and this is a major concern regarding corrosion in concrete. Therefore, NaCl should not be viewed as a completely benign alternative and mitigation strategies should be employed when using this chemical including a reduction in chemical use and achieving decreased concrete permeability through the use of SCMs in the concrete mixture and sealants on in-place concrete.

6.2.2. EFFECTS OF MAGNESIUM CHLORIDE (MgCl₂) ON CONCRETE PAVEMENTS AND BRIDGE DECKS

6.2.2.1. Visible Deterioration After Exposure to Deicers

For all tests conducted, visible distress was commonly associated with exposure of mortar and concrete to concentrated solutions of MgCl₂. In Phase I experiments, mortar cylinders significantly expanded and cracked. In Phase II experiments similar behavior was observed. One area where only negligible physical damage was observed was in the scaling tests. Those slabs pretreated with MgCl₂ and tested for salt scaling resistance did not scale and their visual rating and behavior was similar to those exposed to NaCl.

6.2.2.2. Petrographic Evidence of Chemical Interaction Resulting in Distress

There was strong petrographic evidence of detrimental chemical interactions between MgCl₂ and hardened cement paste. At depth in mortar specimens, calcium hydroxide depletion was common as were deposits of calcium and magnesium oxychloride. X-ray diffraction confirmed the presence of the oxychloride phases as did petrographic microscopy and scanning electron microscopy. Strong evidence was found linking the dissolution of calcium hydroxide and re-deposition of calcium and magnesium oxychloride. Specifically, pseudo-morphs of calcium oxychloride after calcium hydroxide were observed. Oxychloride phases re-deposited in cracks formed in the specimens and the oxychloride phases appeared to be the source of expansion leading to distress. The proposed reaction path is shown below in equation 6.1.



The CaCl₂ can come directly from the deicer or, in the case of MgCl₂ deicers, through a two step process where the MgCl₂ first reacts to form brucite producing CaCl₂ as a reaction product as shown in equation 6-2 or with calcium silicate hydrate (CSH) (i.e. hardened cement paste) as shown in equation 6-3 where magnesium silicate hydrate (MSH) is a reaction product.



The magnesium oxychloride can form in a reaction similar to 6-1. Many researchers have reported the presence of brucite (Mg(OH)₂) in concrete or mortar exposed to MgCl₂ and also MSH. The oxychloride phases are easily overlooked as they are not stable under normal laboratory conditions,

Special care must be exercised and special sample preparation techniques must be utilized to identify these phases by petrography or x-ray diffraction. As the oxychloride phase loses its water of hydration (i.e. the number of waters can vary from 2-15), the phase becomes amorphous and to some extent, the ability to detect it by optical petrography or x-ray diffraction diminishes.

Further evidence was presented in this research that the transition from calcium hydroxide to calcium oxychloride is reversible and therefore calcium hydroxide deposits seen in field concrete could possibly be meta-stable phases that will revert to oxychloride once exposed to deicer solutions. Additionally, it was shown that the oxychloride phase easily converts to calcium carbonate (calcite) and therefore calcite deposits commonly seen under bridge decks may be oxychloride that has converted to calcite. In all cases of distress identified in laboratory specimens analyzed in this study, calcium or magnesium oxychloride phases were identified as being present in the specimen. Collepari et al. (1990) reported that the formation of oxychloride proceeds fastest at temperatures just above freezing (i.e. 39-50°F [4–10 °C]).

Calcium hydroxide dissolution was widespread and evidence of this was seen through petrography. The fact that calcium hydroxide is being converted to calcium oxychloride was supported by monitoring the pH of the exposure solutions during Phase I testing. As seen in Section 5, Figure 5.94, exposure solution pH dropped to ~8.4 when specimens were first introduced to the MgCl₂ solution at 28 days, and remained stable at that pH for the duration of the exposure. This measured pH is much lower than the equilibrium pH for a saturated calcium hydroxide solution (i.e. ~12.5) indicating that hydroxide is not going into solution, although petrographically it is documented that it is dissolving from the hydrated cement paste. The hydroxide is being consumed to form less soluble phases such as the oxychloride phases and brucite. This is consistent with petrographic evidence indicating oxychloride and brucite are forming. Additionally, the brucite layer that forms near the surface of the specimens would impede hydroxide entering the solution and serve to keep the solution and specimen from reaching equilibrium. This brucite layer may have some protective ability by hindering ingress of the chloride solution into the concrete or mortar. However, it also would hinder hydroxide from reaching the solution, maintaining “excess” hydroxide in the porewater solution of the specimen. The hydroxide in the porewater solution would be available to form oxychloride, brucite, or calcium hydroxide. This would tend to favor formation of new phases and would account for the mass increase seen in the Phase I testing.

6.2.2.3. Expansion After Exposure

In the mortar tests conducted in Phase 1, expansion as a result of exposure to MgCl₂ was significant. Expansion in the MgCl₂ exposed samples was 0.38% after 568 days as compared to 0.02% for specimens exposed to limewater. The samples exposed to MgCl₂ expanded the most of the three principal deicers. Only samples exposed to the MBAP deicer expanded more but that deicer is also MgCl₂ based.

6.2.2.4. Loss of Compressive Strength After Exposure

For samples exposed to MgCl₂ solutions, there was a very significant strength loss. Mortar specimens went from an initial strength of 6311 psi [43.5 MPa] to 2718 psi [18.7 MPa], a reduction of 57% over 568 days. This is compared to the specimens exposed to limewater that increased from 6234 psi [48 MPa] to 7372 psi [50.8 MPa] over the same time period, an increase of 24%.

6.2.2.5. Mass Change after Exposure

For mortar samples exposed to $MgCl_2$ solutions, there was considerable mass gain as compared to specimens exposed to limewater. The former had a mass gain of 3.6% and the latter had a mass gain of 1.08% after 568 days. The mass gain is attributed to the oxychloride phases formed.

6.2.2.6. Freeze-Thaw Performance (ASTM C666 and ASTM 672)

The concrete specimens exposed to $MgCl_2$ also performed poorly in the freeze-thaw testing. The specimens well exceeded the 0.1% expansion limit in only 200 cycles. The measured durability factor at 300 cycles was 51% and it dropped below the generally accepted limit of 89% after 166 cycles.

With respect to scaling, the $MgCl_2$ specimens performed satisfactorily, which was surprising as the most common field complaint associated with $MgCl_2$ is scaling. Those slabs pretreated with $MgCl_2$ and tested for salt scaling resistance did not scale and their visual rating and behavior was similar to those exposed to NaCl.

6.2.2.7. Assessment of the Effects of $MgCl_2$

It is clear from the results of these laboratory experiments that $MgCl_2$ based deicers chemically attack mortar and concrete causing expansion, volume change, loss of compressive strength, and microcracks. The chemical attack appears to be temperature and concentration dependent with 20% $MgCl_2$ being the pessimum concentration at temperatures below 73 °F [23 °C].^B

The phases associated with the damage of mortar and concrete samples observed are the highly hydrated basic salts calcium oxychloride and magnesium oxychloride. These phases are formed by the chemical reaction of the deicer with calcium hydroxide in the hardened cement paste. Only under careful sample preparation are these two phases identified. Both are very unstable under ambient laboratory conditions.

The formation of brucite at the surface of a specimen may slow down the deterioration process however it is expected that this layer will not indefinitely protect the mortar and concrete against chemical attack.

6.2.3. EFFECTS OF CALCIUM CHLORIDE ($CaCl_2$) ON CONCRETE PAVEMENTS AND BRIDGE DECKS

6.2.3.1. Visible Deterioration After Exposure to Deicers

As was the case with $MgCl_2$, visible distress was commonly associated with exposure of mortar and concrete to concentrated solutions of $CaCl_2$. In all cases, the visible distress was more pronounced and occurred more quickly with exposure of mortar and concrete to concentrated solutions of $CaCl_2$ than was seen with any other deicer. For example, in the Phase I tests, visible distress was apparent at 56 days with $CaCl_2$ exposure where it was only beginning to manifest in specimens exposed to $MgCl_2$ at the same point in time. In Phase II experiments similar behavior was observed. Based upon visual assessment alone, $CaCl_2$ exposure created the most distress.

6.2.3.2. Petrographic Evidence of Chemical Interaction Resulting in Distress

Specimens exposed to $CaCl_2$ also exhibited conclusive evidence of calcium oxychloride formation in all occurrences of distress. These observations were confirmed by multiple techniques including petrography, x-ray diffraction, and scanning electron microscopy. Calcium hydroxide dissolution was identified and the effects of this could be seen not only through petrography, but also by monitoring the pH of the exposure solutions during Phase I testing. As seen in Section 5, Figure 5.94, exposure solution pH dropped to 5.6 when specimens were first introduced at 28 days, but increased to 11.1 at 56 days and stabilized at 11.4 for the duration of the exposure. This measured pH is near to, but less

than the equilibrium pH for a saturated calcium hydroxide solution (i.e. ~12.5) indicating that not all dissolved hydroxide is going into solution. It is most likely that the hydroxide is being consumed in forming less soluble phases such as the oxychloride phase. The fact that the pH comes closer to equilibrium, as compared to the $MgCl_2$ solutions, indicates that most of the hydroxide is free to exit the specimen (i.e. no brucite layer to impede diffusion). This would tend to support the mass loss seen in the freeze-thaw testing. As the mass loss increases, the pore structure opens, verified by MIP in mortars, and the calcium silicate hydrate (CSH) becomes a main source of calcium to form oxychloride. This consumption of CSH would be consistent with the lower but steady strength loss seen in the Phase I tests. That is, rather than having strength loss through microcracking caused by expansive phases, the strength loss occurs through the slower process of CSH dissolution.

6.2.3.3. Expansion After Exposure

In the mortar tests conducted in Phase 1, expansion as a result of exposure to $CaCl_2$ was significant but not as severe as was seen with the $MgCl_2$ exposed samples. Measured expansion was 0.29% after 568 days as compared to 0.02% for specimens exposed to limewater.

6.2.3.4. Loss of Compressive Strength After Exposure

For samples exposed to $CaCl_2$ solutions, there was strength loss but not as severe as was seen with $MgCl_2$. Mortar specimens went from an initial strength of 6236 psi [43 MPa] to 5703 psi [39 MPa], a reduction of 11% over 568 days. This is compared to the specimens exposed to limewater that increased from 6234 psi [48 MPa] to 7372 psi [50.8 MPa] over the same time period, an increase of 24%.

6.2.3.5. Mass Change after Exposure

For mortar samples exposed to $CaCl_2$ solutions, there was a significant mass gain as compared to specimens exposed to limewater. The samples exposed to $CaCl_2$ solutions had a mass gain of 2.4% after 568 days and the specimens exposed to limewater had a mass gain of 1.08% after 568 days.

6.2.3.6. Freeze-Thaw Performance (ASTM C666 and ASTM 672)

The concrete specimens exposed to $CaCl_2$ also performed poorly in the freeze-thaw testing. The specimens exceeded the 0.1% expansion limit in 133 cycles. The measured durability factor at 300 cycles was 60% and it dropped below the generally accepted limit of 80% after 95 cycles.

With respect to scaling, the $CaCl_2$ specimens scaled severely. After a year of ponding the surface of the slabs with 22% $CaCl_2$, the slabs were subjected to freezing and thawing cycles in the presence of 4% $CaCl_2$. The surface started to scale gradually up to 50 cycles of exposure. After 50 cycles, the amount of scaled material increased dramatically causing the surface to expose all the coarse aggregate and paste-aggregate debonding was evident.

Parallel tests were run on slabs that were exposed to highly concentrated solutions of NaCl (23% by mass) and then tested with 3% NaCl solution. Those slabs did not show any sign of scaling .

X-ray diffraction analysis was performed on concrete slabs subjected to the same pretreatment conditions, but kept for analysis instead of being tested for salt scaling resistance. Slabs exposed to 22% $CaCl_2$ showed the distinctive peaks of calcium oxychloride in addition to Friedel's salt.

6.2.3.7. Assessment of the Effects of $CaCl_2$

Results of these laboratory experiments indicate that $CaCl_2$ based deicers chemically attack mortar and concrete causing expansion, volume change, loss of compressive strength, and cracking. The phase

associated with the damage of mortar and concrete samples observed was calcium oxychloride. This phase is formed by the chemical reaction of the deicer with phases in the hardened cement paste, certainly calcium hydroxide and possibly CSH. Only under careful sample preparation is the oxychloride phase identified. Evidence of the formation of this phase was also reported in the literature (Collepari et. al., 1990).

The formation of calcium oxychloride in the concrete matrix decreases dramatically the salt scaling and freeze-thaw resistance of concrete mixtures that are otherwise immune to the effect of freezing and thawing cycles in the presence of low concentrated CaCl_2 solutions. The fact that the concrete slabs tested deteriorated in the last stage of the test, and more cycles were needed to completely expose this otherwise silent chemical attack, indicates that standardized test methods do not effectively evaluate the potential for chemical attack of concrete by the deicers tested. This stems from the fact that calcium chloride is not exacerbating a physical attack, it is creating a chemical attack that slowly weakens the hardened cement paste by attacking the CSH in addition to the calcium hydroxide.

6.2.4. EFFECTS OF CALCIUM MAGNESIUM ACETATE (CMA) ON CONCRETE PAVEMENTS AND BRIDGE DECKS

6.2.4.1. Visible Deterioration After Exposure to Deicers

Samples exposed to CMA showed mixed results, but did show some visible signs of deterioration. For Phase I work conducted at Michigan Tech, cylinders in the CMA solution showed little to no distress after 84 days, although there was some staining evident in the 0.60 *w/c* cylinders. However, as part of Phase I work conducted at the University of Toronto, samples exposed to CMA disintegrated approximately 30 days after immersion. As a result, measurements of length, mass, and compressive strength change could not be conducted. In the University of Toronto experiments, mortar samples lost cohesiveness and disintegrated completely. There is no explanation available for why the two tests had such different results. The CMA concentrations used were comparable (i.e. 25% CMA used at Michigan Tech, 28% CMA used at the University of Toronto). The only significant difference was that specimens exposed to CMA at Michigan Tech were done so at 40 °F [4.4 °C]. At the University of Toronto, the specimens were exposed to CMA at room temperature.

Notably, the high temperature experiment conducted at Michigan Tech did result in visible damage and in the deposition of calcium acetate hydrate crystals as was seen at the University of Toronto. However, the distress seen was similar to an acid attack in appearance and it is postulated that the CMA decomposed to a weak acetic acid at the higher temperatures.

6.2.4.2. Petrographic Evidence of Chemical Interaction Resulting in Distress

As indicated, the only petrographic evidence of chemical interaction was the formation of calcium acetate hydrate phases in the separate Phase I experiments. The University of Toronto work demonstrated these occurring in room temperature solutions while the Michigan Tech work only identified this phase in the high temperature experiment (i.e. 135 °F [57.2 °C]).

6.2.4.3. Expansion After Exposure

Given the disintegration of the specimens exposed to CMA, limited testing was performed. Prior to disintegration, a few expansion measurements were made. The final measured expansion was 0.026% at 88 days.

6.2.4.4. Loss of Compressive Strength After Exposure

Given the disintegration of the specimens exposed to CMA, this testing was not performed.

6.2.4.5. Mass Change after Exposure

Given the disintegration of the specimens exposed to CMA, limited testing was performed. Prior to disintegration, a few measurements of mass change were made. The final measured mass loss was 29.7% at 88 days.

6.2.4.6. Freeze-Thaw Performance (ASTM C666 and ASTM 672)

This testing was not performed.

6.2.4.7. Assessment of the Effects of CMA

Evidence of detrimental effects of CMA is mixed. Based upon this work it is not possible to draw hard conclusions regarding how this deicer affects concrete. There is evidence to indicate that there may be a concern but additional testing would be required to establish any conclusive relationship between CMA and chemical attack to hardened concrete.

6.2.5. EFFECTS OF MAGNESIUM CHLORIDE BASED AGRICULTURAL PRODUCT (MBAP) ON CONCRETE PAVEMENTS AND BRIDGE DECKS

6.2.5.1. Visible Deterioration After Exposure to Deicers

Mortar specimens were not tested in MBAP as part of Phase I at Michigan Tech so comparisons with other samples under the conditions described for Phase I is not possible. As part of Phase I at the University of Toronto, some observations were made of sectioned specimens, after exposure to MBAP that experienced loss of strength, expansion and mass gain. Defined zones of chemical interaction of 0 to 0.2 in. [0 to 5 mm] through the cross sectional area of the mortar bar were visible. These zones were easily identified by the changes in color from a light gray in the core of the specimen to a yellowish color at the surface. The presence of microcracks was confirmed using the stereo optical microscope. Softening of the surface and debonding of sand grains were identified.

6.2.5.2. Petrographic Evidence of Chemical Interaction Resulting in Distress

At early ages (less than 118 days) a white layer developed on the surface and it was subsequently identified by x-ray diffraction as brucite. The deterioration front seemed to move deeper into the specimen with exposure time. Softening of the surface and debonding of sand grains were identified. Concrete specimens prepared with only plain portland cement and exposed to MBAP did show the same type of distress as was seen with specimens exposed to $MgCl_2$ and $CaCl_2$. Microcracking, calcium hydroxide depletion, redeposition of blocky calcium hydroxide, and the presence of calcium oxychloride were all observed. For specimens prepared with fly ash and GGBFS, the distress was not as pronounced.

6.2.5.3. Expansion After Exposure

In the mortar tests conducted in Phase 1, expansion as a result of exposure to MBAP was massive. Expansion in the MBAP exposed samples was 0.75% after 568 days as compared to 0.02% for specimens exposed to limewater. Samples exposed to MBAP expanded more than specimens in any other exposure condition.

6.2.5.4. Loss of Compressive Strength After Exposure

For samples exposed to MBAP solutions, there was a strength loss almost identical to specimens exposed to $MgCl_2$. Mortar specimens went from an initial strength of 6176 psi [43 MPa] to 2769 psi [19 MPa], a reduction of 55% over 568 days. This is compared to the specimens exposed to limewater that increased from 6234 psi [48 MPa] to 7372 psi [50.8 MPa] over the same time period, an increase of 24%.

6.2.5.5. Mass Change after Exposure

For mortar samples exposed to MBAP solutions, there was significant mass gain. The MBAP specimens had a mass gain of 5.93%. This was the highest mass gain of any specimens tested. This seemed to be a combination of mass gain as was seen with $MgCl_2$, but also there was possibly the formation of organic salts that contributed.

6.2.5.6. Freeze-Thaw Performance (ASTM C666 and ASTM 672)

This testing was not performed.

6.2.5.7. Assessment of the Effects of MBAP

In general, MBAP performed in a manner very similar to $MgCl_2$. Although it was not taken through every test performed using $MgCl_2$, enough testing was performed including, volume change, loss of compressive strength, and petrography, to establish that MBAP will most likely cause distress in a manner similar to concentrated $MgCl_2$.

6.3. ASSESSING AND MINIMIZING THE IMPACT OF DEICING/ANTI-ICING CHEMICALS

A clear mechanism for chemical attack by at least two deicers – $CaCl_2$ and $MgCl_2$ - seems clear. Therefore, it is necessary that SHAs examine mitigation strategies. Of course one simple strategy is to use less of these chemicals for anti-icing and deicing. This will be discussed in the next chapter. The other strategy is to construct concrete pavements and bridge decks that are less susceptible to attack. This research examined different approaches to modifying the concrete itself, in particular decreasing the permeability of the concrete. To this end mixtures were tested at different values of w/c and also with the addition of fly ash or ground GGBFS. Also, the use of sealants was examined as an approach to reducing permeability. Various tests were performed and the efficacy of these tests for assessing permeability was examined.

In general, a reduction in concrete or mortar permeability resulted in less damage in the same amount of exposure time for similar mixtures and exposure solutions. The only inconsistency, which cannot be fully explained at this time, is that for Phase II testing on concrete, and to some extent for Phase I on mortars, a reduction in w/c did not improve performance. If anything, the lower w/c mixtures exhibited more damage in less time than did the higher w/c mixtures. As stated, it is not clear why this occurred. Looking at Figures 5.161 and 5.162, the visible alteration of the 0.45 w/c samples exposed to $CaCl_2$ was significantly higher as compared to the 0.55 samples exposed to the same solution. For samples exposed to $MgCl_2$, the performance was about equal. If the $CaCl_2$ attacks the CSH ($CaCl_2$ damage model) rather than causing microcracking that becomes increasingly progressive ($MgCl_2$ damage model), then possibly the lower w/c mixture with more abundant CSH relative to calcium hydroxide, and a more impermeable matrix, serves to hold chemically altered porewater within the sample allowing for chemical interaction to occur. Although it is not clear why the lower w/c mixtures did not perform better than the higher w/c mixtures, it is clear that lowering w/c by itself is not a reasonable strategy for mitigating deicer attack.

However, the use of SCMs did significantly improve the concrete performance. It is thought that this is the result of SCMs consuming calcium hydroxide in the hydration reaction thereby providing less calcium hydroxide in the cement paste to chemically react, and also results from a decrease in permeability.

The calculated bulk diffusion values (D_a) for the exposed surfaces (no sealer) are shown in Tables 5.13 – 5.15 for concretes and Tables 5.16 – 5.18 for mortars (In these tables, D_a is the bulk diffusion value, C_s is the calculate chloride concentration at the surface, r^2 is the correlation coefficient, and $P(0.1\%)$ is the depth that chlorides penetrated to a concentration of 0.1% by mass of sample—an alternate way of determining chloride penetration resistance). Chloride penetration profiles are shown in section 5.3.2.2.

As expected, bulk diffusion values for the 0.45 *w/c* concrete were lower than for the 0.55 *w/c* concretes, contributing to the mystery of why the mixtures did not perform better. It was also found that the chloride bulk diffusion values were approximately 3 to 6 times higher when NaCl was used and that calcium and magnesium chloride solutions gave similar, but much lower values. This is possibly explained by the chlorides becoming tied up in oxychlorides when calcium and magnesium chlorides were used. However it does also support the fact that NaCl penetrates concrete more readily and therefore is easily able to reach embedded steel and cause corrosion.

In general, regardless of the type of salt solution used, GGBFS cement concretes gave lower bulk diffusion coefficients than the portland cement concretes, while the 15% fly ash concretes had the highest values. However, visually it was noted that the fly ash concretes had more entrapped air voids, and this might have contributed to their unexpected poor performance. This explanation is borne out by the mortar tests, where the portland cement mortars had the highest bulk diffusion values, followed by the fly ash mortars, with GGBFS cement mortars being the lowest. Additionally, the fly ash concrete specimens were cured for only 28 days before testing, as were the other concretes. A longer curing time would have improved the performance of the fly ash concrete mixtures.

Petrographic evidence also supports the fact that the use of SCMs greatly improved performance. In section 5.3.2.4 evidence is presented that reduced cracking was seen for mixtures containing, in order of effectiveness, ground GGBFS and fly ash.

Likewise, sealants proved to be very effective at reducing the impact of deicing chemicals. As can be observed from Figures 5.123 – 5.125, concrete samples coated with the siloxane sealer did not allow the penetration of chloride ions. In Figures 5.123 – 5.125, the chloride levels measured are very low and likely represent the chlorides contained in the limestone coarse aggregate.

Clearly, SHAs that continue to use these deicing chemicals should begin developing concrete mixtures that utilize ground GGBFS and fly ash as a mitigation strategy. As a maintenance strategy, sealants should be employed to help slow the ingress of the deicing chemicals, thereby minimizing the impact these chemicals will have on concrete pavement and structures.

6.4. LIFE CYCLE COST ANALYSIS

As part of the original proposal, it was stated that a life cycle cost analysis would be performed to describe the potential impacts of the various deicers relative to the service life of the pavement. This proposal was predicated on having the necessary data to accomplish the analysis, which includes in general two types of information. The first is laboratory data describing the behavior of the laboratory prepared mixtures when exposed to the various deicers. This would include information such as the rate of ingress and the rate at which observed distresses progressed. To a large extent, the research was successful in obtaining this information. The second type of information required is field examples of distressed pavements, coupled with adequate maintenance records to establish the amount and type of deicer used, and preferably examples of distressed pavements that had been exposed to one type of deicer exclusively. Additionally, these distressed pavements would need to be failing as a result of the

same mechanisms identified in the laboratory experiment. The purpose of the field examples is to calibrate the laboratory observations making the prediction of the rate of progressivity possible. Clearly, exposing concrete to a deicer in the laboratory twenty-four hours a day, seven days a week, for hundreds of days, does not give a definitive measure of damage rate that translates directly to the field. Real pavements do not see continual exposure to high concentration brines. Rather, they see intermittent exposure to brines of widely varying concentration. However, if field examples can be identified as described, the distress seen in that concrete can be identified along the timeline of the laboratory experiments and predictions of failure could be provided and a life cycle analysis performed.

This research was unable to identify pavements that provided this second type of information. None of the pavements examined as part of the field examination could be absolutely identified as ones exhibiting distress solely as a result of deicer application. In addition, most of the pavements sampled and examined have been exposed to different deicers over their service life making the association of distress with any one deicer impossible. Last, because of the instability of the oxychloride phase, which was linked to most of the observed laboratory distress, it is practically impossible to capture in field samples. Although distress seen in some field sites bared very strong resemblance to that seen in the laboratory, it can never be absolutely stated that the same deterioration seen in the laboratory correlate with that seen in the field. As a result, the research team is only left with laboratory results on which to base a life cycle model. In the opinion of the research team, any predictions made solely on the basis of laboratory tests would be flawed and it would be counter-productive to present an analysis that was based on inadequate data.

It can be said that clearly, chemical attack of concrete from the use of CaCl_2 and MgCl_2 based deicers occurs. Conversely, NaCl appears to have little to no potential for chemical interaction with the cement paste and therefore appears to be safe for use on concrete pavements and bridge decks from the stand point of chemical attack of the concrete. However, NaCl is well documented as a cause of corrosion so in the end, pavement design changes and maintenance strategies required for protecting concrete from CaCl_2 and MgCl_2 should also be adopted to protect concrete from corrosion of embedded steel in the presence of NaCl deicers. Also, the mechanisms identified in the laboratory are real, they have been confirmed through multiple experiments at different institutions, and are most certainly active in field concrete.

What is also clear from review of the literature and from the survey performed early in this project, CaCl_2 and MgCl_2 are effective deicers and are a tool any maintenance engineer wants to have available to keep roads safe and passable. Therefore, as will be described in Section 7, it is recommended that state SHAs adopt mitigation strategies to minimize the impacts of these chemicals and maximize the service life of pavements and bridge decks. Even with these strategies, a reduction in service life should be expected when CaCl_2 and MgCl_2 based chemicals are used for deicing and anti-icing.

SECTION 7. MITIGATION STRATEGIES

7.1. MITIGATION STRATEGIES – MAINTENANCE

Mitigation strategies that can be implemented from a maintenance perspective are three-fold. They are 1) use less deicing chemicals, 2) use NaCl brines whenever possible, and 3) use concrete sealants and concrete mixtures including SCMs to slow deicer ingress.

1) *Use Less Chemicals* – The research conducted here shows that regardless of the distress mechanism, reducing deicer solution concentrations reduces the distress and distress rate. Therefore, any effort to reduce deicer application concentrations or rates will result in less damage to concrete structures. At a minimum, applying deicing chemicals with an initial concentration less than the pessimum amount (i.e. 20% for MgCl₂ and 22% for CaCl₂) would help significantly as the deicer would be diluted from that concentration with the effect of reducing its chemical impact. Currently, with application concentrations above the pessimum, as the chemical dilutes on the road surface, the negative impact is increasing until the pessimum concentration is reached.

2) *Use NaCl Brines* – All evidence from this study indicates that NaCl brines have a minimal impact on concrete. However, they are known to be highly corrosive to steel. Maintenance strategies should consider using NaCl brines as much as possible, and investigating methods of depressing the freezing point of these brines to extend their useful temperature range. Mixing with small amounts of MgCl₂ or CaCl₂ may be a good approach as long as the required amount of these additive salts is kept low, certainly below the pessimum values. Suppliers should investigate organic additives that can be used to depress the freezing point of NaCl brines without adding MgCl₂ or CaCl₂ if at all possible. Mitigation strategies such as sealants and the inclusion of SCMs in the concrete mixture still need to be adopted when using NaCl brines to prevent corrosion.

3) *Use Sealants* – The siloxane sealant studied in this research was effective at significantly slowing the ingress of deicing chemicals into concrete or mortar. To a lesser extent the silane sealant was also effective. The effectiveness of either sealant is lost after some time (e.g. 3-5 years) and as result, maintenance strategies should include periodic reapplication of sealants to pavements and bridge decks.

7.2. MITIGATION STRATEGIES – ENGINEERING

The only certain engineering solution is to utilize SCMs in pavement concrete. For this study, 30% ground GGBFS substitution for portland cement greatly improved the durability of the mixtures tested. Fly ash as a concrete admixture also improved durability. State DOT's need to develop concrete mixture designs with a higher percentage substitution of SCMs for portland cement. Reducing the *w/c*, by itself, did not improve the durability of concrete and mortar tested in this research.

SECTION 8. CONCLUSIONS

Based on the review of the the literature, the following conclusions are presented:

- Both physical and chemical interactions occur within concrete when it is exposed to freeze-thaw conditions and deicing chemicals.
- Physical interaction is initiated when the saturated concrete freezes, subjecting the concrete to volume change and the development of internal stresses that are amplified by the presence of deicer ions in the pore solution and the thermal shock that occurs as ice is melted.
- Damage from physical mechanisms of attack are most commonly scaling, map cracking, or paste disintegration. Internal microcracking caused by freeze-thaw damage will eventually progress to scaling on the surface of the pavement. Once cracking begins, the damage gradually worsens, increasing the permeability of the concrete and thus its susceptibility to further moisture ingress.
- Chemical interaction results from the application of deicing chemicals, leading to possible degradation of the concrete structure. Chemical interactions result in map cracking, paste disintegration, internal microcracking, strength loss, mass gain, and expansion.
- One interaction resulting from the long-term application of chloride deicers is the dissolution of calcium hydroxide ($\text{Ca}(\text{OH})_2$).
- Some interactions of Mg^{2+} and Cl^- ions with the cement hydration products in cement paste are known to cause damaging alterations to the cement paste structure, reducing concrete strength while increasing porosity. These changes result from the ability of Mg^{2+} and Cl^- ions to deplete $\text{Ca}(\text{OH})_2$ to form brucite ($\text{Mg}(\text{OH})_2$) and CaCl_2 . These ions also cause decalcification of the hydration product calcium-silicate-hydrate (CSH), making the paste very porous and converting it to the secondary product, magnesium-silicate-hydrate (MSH).
- A number of studies have concluded that CaCl_2 , another common deicer and a product of the reaction between MgCl_2 and $\text{Ca}(\text{OH})_2$, is associated with a deleterious chemical reaction with concrete. The chemical attack is accompanied by the formation of a hydrated calcium oxychloride.
- There are also direct chemical effects of CaCl_2 on the cement paste. For example, when exposed to CaCl_2 deicer, chloride concentrations tend to increase within the paste causing discoloration. This may be due to the formation of CaCl_2 hydrate or to adsorption of Cl^- by CSH.
- All chloride solutions will cause a transformation of ettringite to chloroaluminate. Therefore, in the presence of CaCl_2 solutions, pre-existing ettringite will be transformed to calcium chloroaluminate or trichloroaluminate, which has an appearance similar to ettringite.

Based on the characterization of field specimens, the following conclusions are presented:

- Colorado, State Highway 83, South of Denver near Milepost 57
 - This pavement, constructed in 1996, exhibited visible signs of distress.
 - The pavement has been exposed primarily to NaCl deicer.
 - Laboratory investigation of field specimens did not reveal any macro-cracking.
 - Samples examined showed adequate entrained air.
 - Some alkali silica reactivity (ASR) was observed with minor gel production and cracking.
 - No definitive correlation could be made between the observed distress and the use of deicers.
- Iowa, eastbound US Highway 34, western end of the Burlington Bridge.
 - This bridge deck was reportedly exposed exclusively to CMA deicer.
 - Laboratory investigation of field specimens did not reveal any macro-cracking in either of the cores, other than the obvious surface crack of core IA-6, which extended both through the overlay and into the original concrete below.
 - The overlay from both slabs exhibited borderline entrained air parameters, with spacing factors of 0.276 mm and 0.217 mm for cores IA-5 and IA-6 respectively.
 - Some alkali silica reactivity was observed with minor gel production but no cracking was observed associated with the ASR.
 - All of the profiles show an increase in chloride concentration near the pavement surface. Although CMA may have been used exclusively on the bridge deck, it is possible that contamination from the preceding roadway contributed to the observed chloride gradient..
 - A comparison of the profiles from cores IA-3 and IA-11 shows an increased chloride penetration in core IA-3, which was taken directly over a surface crack in the pavement.
 - Secondary calcium hydroxide deposits in air voids were commonly observed in the concrete overlay.
 - The petrographic analysis of these cores did not reveal any specific degradation related to chemical attack from deicers. The only significant observation was the marginal air-void system, which may have contributed to the observed distress.
- Idaho, westbound Interstate Highway 184 west of Boise, near milepost 3
 - This pavement was constructed in 1992 and was reported to have been exposed to $MgCl_2$ for anti-icing, and NaCl for deicing.
 - Laboratory investigation of field specimens did not reveal any macro-cracking in either of the cores, except for one crack at depth in core IDL-7.
 - Air-void system parameters varied considerably, from a low spacing factor value of 0.118 mm for core IDR-3, to a high spacing factor value of 0.267 mm for core IDL-6.
 - The chloride profile from core IDL-1 (at joint) showed increased chloride penetration as compared to the profile from core IDL-5 (mid-panel).

- Montana, westbound Interstate Highway 90 bridge deck near milepost 117
 - Partial depth cores 5 to 6 inches in depth were received from this bridge deck.
 - The top 2 inches of the cores consisted of a latex modified concrete overlay.
 - The deck was reported to have been exposed to $MgCl_2$ for anti-icing, and NaCl for deicing.
 - A variation in surface wear was observed on some of the cores.
 - Laboratory investigation of field specimens did not reveal any macro-cracking in any of the cores
 - The overlay from both slabs exhibited inadequate entrained air parameters, with spacing factors of 0.432 mm and 0.687 mm for cores MT-2 and MT-8 respectively. However, air entrainment is not likely as a critical requirement for a latex-modified overlay.
 - The transition from overlay to original concrete is apparent in the profiles, and it appears that there is some diffusion of chlorine from the original concrete up into the base of the overlay.
- South Dakota, eastbound 26th Street left turn lane
 - This pavement was placed on November 1, 1996 and exposed to $MgCl_2$ brine shortly thereafter on November 15, 1996.
 - The pavement surface was described to be in good condition, but field reports indicated cores taken near the joint looked like they had been deteriorated. What had been interpreted as deterioration was just the normal appearance of a concrete joint as exposed in cross section.
 - Laboratory investigation of field specimens did not reveal any macro-cracking in any of the cores.
 - Both sets of slabs showed adequate entrained air.
 - For thin sections prepared and observed using epifluorescence, the samples prepared from near the joint consistently fluoresced brighter than the samples prepared from mid-panel, indicating a higher permeability resulting from either differences in the as-placed concrete mixtures or alteration of the concrete as a result of exposure.
- Montana, eastbound Interstate Highway 90 bridge deck, near milepost 61.8, Tarkio interchange
 - Maintenance personnel indicated both $MgCl_2$ brine and a combination of NaCl and sand have been used on this bridge deck.
 - The bridge deck exhibited spalling.
 - The underside of the bridge deck showed pronounced efflorescence, especially in areas directly below regions covered with cold patch material.
 - Core T-1 exhibited a crack plane at a depth of about 45 mm.
 - Laboratory investigation of field specimens did not reveal any macro-cracking in any of the cores.

- Overall, the slab showed inadequate entrained air, with a spacing factor of 0.296 mm.
- Elemental mapping showed magnesium enrichment at the surface of the bridge deck, similar to that seen on laboratory specimens exposed to $MgCl_2$ brine.
- Montana, westbound Interstate Highway 90 bridge deck, near milepost 37.2, Sloway interchange
 - Maintenance personnel indicated both $MgCl_2$ brine and a combination of NaCl and sand have been used on this bridge deck.
 - The bridge deck exhibited spalling.
 - Core S-1 exhibited a crack plane at a depth of about 30 mm coinciding with reinforcement steel.
 - The black and white treatment did not reveal any macro-cracking, with the exception of a small crack perpendicular to the pavement surface.
 - The slab showed adequate entrained air, with a spacing factor of 0.173 mm.
 - Elemental mapping shows chlorine enrichment along the top surface of the crack at depth indicating enhanced penetration of deicing chemicals along cracks.
- General Observations from Field Specimens
 - In general, the sites initially identified lacked unambiguous evidence of distress associated with deicers.
 - Additional sites added for examination showed distress but this could not be definitively associated with the deicing chemicals used. Further, the exact treatment of these bridges, in terms of the deicing chemicals used, was not clear.

Based on the Phase I laboratory tests, the following conclusions are presented:

- The cyclic temperature and high temperature experiments performed at Michigan Tech were ineffective at identifying distress mechanisms associated with exposure of mortar specimens to deicing solutions.
- The low temperature test performed at Michigan Tech was effective at identifying distress mechanisms associated with exposure of mortar specimens to deicing solutions.
- Mortar cylinders exposed to 17.8 wt% NaCl solution showed no deterioration after 84 days.
- For the low temperature test, at 28 days, the mortar cylinders in the 15 wt. % $MgCl_2$ and 17 wt. % $CaCl_2$ solutions began to show some signs of cracking and expansion.
- By 56 days, the cylinders in the $MgCl_2$ and $CaCl_2$ solutions exhibited advanced deterioration.
- By 84 days the cylinders exposed to $MgCl_2$ and $CaCl_2$ solutions were severely deteriorated.
- The control cylinders exposed to limewater were in good condition at 84 days.
- The cylinders exposed to the 25 wt. % CMA solution showed little to no distress after 84 days, although there was some staining evident in the 0.60 w/c cylinders.

- Near the exteriors of the MgCl_2 and CaCl_2 exposed cylinders, the cracks are empty. However, cracks further towards the interior of the cylinders are filled with calcium oxychloride or the altered remnants of calcium oxychloride.
- The deterioration of the MgCl_2 and CaCl_2 immersed samples appears very similar. Both samples exhibit a region of calcium oxychloride filled cracks and voids associated with calcium hydroxide depleted cement paste.
- A magnesium crust formed at the exterior of the magnesium chloride immersed sample as well as the calcium magnesium acetate immersed sample.
- Control specimens exposed to limewater showed no deterioration or alteration.
- Work performed at the University of Toronto examined the effects of various deicing solutions on the compressive strength, expansion, and mass change of specimens exposed to those solutions, with the following results
 - After exposure to the different deicers, the compressive strength decreased for those samples exposed to MBAP, MgCl_2 and CaCl_2
 - The compressive strength decreased in the order MgCl_2 , MBAP and CaCl_2 by 63, 62 and 23% respectively, when compared with the compressive strength of mortar cubes exposed to saturated calcium hydroxide solution.
 - The mortar cubes exposed to NaCl exhibited an increase in compressive strength similar to those samples exposed to calcium hydroxide solution.
 - The samples exposed to MBAP and MgCl_2 presented similar trends in their compressive strength evolution with time.
 - Exposure of mortar bars to MBAP, MgCl_2 and CaCl_2 resulted in considerable expansion while those subjected to NaCl showed negligible expansion even after 500 days of exposure.
 - MBAP caused the highest expansion of all, 0.75% at 568d, followed by MgCl_2 and CaCl_2 with 0.37 and 0.29% respectively.
 - The MBAP samples expanded almost twice as much as samples exposed to MgCl_2 , with the same exposure period.
 - For those specimens exposed to MBAP, MgCl_2 and CaCl_2 , expansion of mortar bars was accompanied by considerable mass gain. The greatest mass gain was 5.9% observed for those samples exposed to MBAP, followed by MgCl_2 with 3.6% and CaCl_2 with 2.4% mass gain.
 - The specimens exposed to NaCl and $\text{Ca}(\text{OH})_2$ did not show considerable mass gain with 1.4 and 1.1% recorded, respectively.
 - Visual observations of the specimens exposed to MBAP and MgCl_2 that experienced loss of strength, expansion and mass gain revealed defined zones of chemical interaction between 0 and 0.2 in. [0 and 5 mm] through the cross sectional area of the mortar bar were visible
- When samples were immersed in the deicers, the pH of the exposure solution initially decreased, then increased. The pH of the MBAP and MgCl_2 solutions were 7.8 and 8.3,

respectively, at the beginning of the salt solution exposure period and increased to up to approximately 8.6 after continued exposure of the mortar specimens to these same solutions. The CaCl_2 -based deicer, initially acidic, (e.g. pH of 5.6) increased to approximately 11.4 after exposure. The NaCl solution, with an initial pH of 7.6, increased to a pH of 12.4.

- The significant difference between the MBAP and MgCl_2 solution pH, and that of the saturated calcium hydroxide solution (i.e. pH 12.5), coupled with the significant mass gain, indicates hydroxide dissolving out of the MBAP and MgCl_2 specimens is being tied up forming brucite, oxychloride, or secondary calcium hydroxide.
- Those deicers such as MBAP and MgCl_2 that caused considerable expansion, mass gain and loss of compressive strength, showed an increase in the total volume of pores of up to 20% when compared with the reference samples exposed to $\text{Ca}(\text{OH})_2$.
- The total pore surface area increased for those samples exposed to CaCl_2 .
- Those samples exposed to NaCl solutions had phases similar to those exposed to calcium hydroxide solutions, the only difference being the presence of Friedel's salt.
- In the case of MBAP, besides Friedel's salt, a phase resembling magnesium oxychloride was identified. This phase was not detected in the samples exposed to MgCl_2 but instead defined peaks of brucite were found.
- In XRD analysis of both MBAP and MgCl_2 exposed specimens, the intensity of the main peaks of calcium hydroxide diminished suggesting depletion of this phase due to chemical attack, leaching or both.
- For testing performed at the University of Toronto, in contrast to experiments at Michigan Tech, samples exposed to CMA disintegrated approximately 30 days after immersion.
- For those samples exposed to MgCl_2 , at 20% MgCl_2 the compressive strength suffered a maximum loss of 57%. For CaCl_2 solutions the loss of compressive strength was a maximum at 22% CaCl_2 with 58% strength loss.
- X-ray diffraction analysis of specimens exposed to 20% MgCl_2 confirmed the formation of magnesium oxychloride in these samples.

Based on the Phase II laboratory tests, the following conclusions are presented:

- Bulk diffusion tests indicated that concrete mixtures with a w/c of 0.45 had a lower diffusion coefficient as compared to mixtures prepared with a w/c of 0.55.
- Bulk diffusion tests indicated that diffusion coefficients for NaCl solutions are significantly higher than those for the other solutions.
- Concrete samples coated with tri-silane did not perform as well as with tri-siloxane. Although tri-silane slowed down the chloride penetration, it did allow the penetration of chloride ions in considerable quantities.
- Sorptivity tests showed a general trend of decreased sorptivity with decreasing w/c .
- Sorptivity was lowest for mixtures prepared with GGBFS, next lowest for those prepared with fly ash, and highest for plain portland cement mixtures.

- For mortars, sorptivity decreased from highest to lowest in the order NaCl, water, CaCl₂, and MgCl₂.
- In general for concrete, sorptivity decreased from highest to lowest in the order water, NaCl, CaCl₂, and MgCl₂.
- The low temperature experiment conducted for Phase I was repeated with concrete specimens. None of the specimens showed any obvious external signs of deterioration at 60 days. At 500 days, many of the specimens from the high-concentration CaCl₂, MgCl₂, and MBAP brines exhibited external cracking.
- Based upon visual alteration, the high-concentration CaCl₂, MgCl₂, and MBAP solutions were more aggressive than the NaCl and CMA solutions. At the low-concentration, all of the brines were less aggressive.
- Based upon visual alteration, a general trend of increased alteration was evident for the concrete specimens as compared to the mortar specimens.
- Based upon visual alteration, a general trend of increased alteration was evident for the 0.45 *w/c* specimens as compared to the 0.55 *w/c* specimens.
- Based upon visual alteration, a general trend of decreased alteration was evident when fly ash or GGBFS was used.
- Based upon visual alteration, a general trend of decreased alteration was evident when the sealants were used.
- Based upon visual alteration, a trend of increased alteration was evident when a NaCl pre-soak was employed.
- For 0.45 *w/c* concrete specimens immersed in the five different high-concentration brine solutions, chloride profiles were obtained using the x-ray microscope. The addition of GGBFS resulted in a marked decrease in the chloride concentration near the surfaces of the specimens. Chloride concentration profiles for concrete specimens with fly ash were similar to the profiles from specimens with straight portland cement.
- For 0.45 *w/c* mortar specimens immersed in the five high-concentration brine solutions, chloride profiles were obtained using the x-ray microscope. The chloride concentrations reported for the mortar specimens are approximately double the values from the concrete specimens. A well-defined trend of higher chloride concentration near the surface was observed for mortar specimens immersed in the MgCl₂ and CaCl₂ brines relative to the other brines. At depth, chloride concentrations were consistently higher for the mortar specimens immersed in the NaCl brine relative to the other brines. Chloride concentrations were lowest overall for specimens immersed in the MBAP brine.
- For 0.45 *w/c* concrete specimens immersed in the five different low-concentration brine solutions, initial chloride concentrations were lower when compared to the same specimens from the high-concentration brines, with the exception of the specimens immersed in the MBAP brines.
- Although the initial chloride concentrations were generally lower for concrete specimens in the low-concentration brines, the chloride concentrations at a depth of about ½ inch, (10 to 15 mm) were slightly elevated in the concrete specimens that had been exposed to the CaCl₂ and

MgCl₂ low-concentration brines as compared to the same concrete specimens exposed to the CaCl₂ and MgCl₂ high-concentration brines. This trend was also observed in the mortar specimens.

- Compared to 0.45 *w/c* concrete specimens exposed to the same conditions, the 0.55 *w/c* concrete specimens showed similar initial chloride concentrations but generally greater chloride penetration at depth.
- The 0.55 *w/c* mortar specimens from the CaCl₂ and MgCl₂ brines showed much lower initial chloride concentrations than their counterparts from the 0.45 *w/c* mortar specimen experiment. Overall, the 0.55 *w/c* mortar specimens showed greater penetration of chloride at depth when compared to 0.45 *w/c* mortar specimens exposed to the same conditions.
- Chloride profiles for 0.55 *w/c* concrete specimens treated with silane and siloxane, after exposure to the five high-concentration brines, showed that the sealants were very effective at impeding the ingress of chlorides at 60 days. However, at 500 days, chloride ingress was evident from the bases of the specimens.
- Although some general trends were observed in the chloride profile data, there were often outliers or exceptions. Most of these inconsistencies, especially in the case of the concrete specimens, can in some cases be attributed to heterogeneities inherent to the material.
- The XRD traces from the wet extracted paste and wet precipitates collected from CaCl₂-exposed specimens show that the main secondary phase is the same 8.34, 4.13, 2.76 angstrom calcium oxychloride described by Monosi and Collepari.
- Evidence that calcium oxychloride reverts to CaOH₂ was established. This reversibility is important in understanding why the oxychloride phase is not seen in field concrete samples. Further evidence was identified that the calcium oxychloride can convert to calcite. This is a possible source of calcite deposits commonly found under bridge decks.
- The wet extracted paste and wet precipitate collected from the MgCl₂ exposed specimens showed very little similarity. The precipitate showed peaks for a Mg₃(OH)₅Cl•4H₂O phase, but these peaks were not observed in the wet paste. The calcium oxychloride phase is also not present.
- Samples of external precipitate were also collected from a specimen that was exposed to the MBAP solution for 500 days. Diffraction analysis revealed that the main phase in this material was the Mg₃(OH)₅Cl•4H₂O phase.
- An external precipitate was also collected from a specimen that was soaked in the low-concentration calcium magnesium acetate (CMA) solution for 500 days. From the XRD analysis, it is shown that this precipitate consists of calcite.
- By optical petrography, cracking planes sub-parallel to the surface are evident in the concrete specimens exposed to the CaCl₂, MgCl₂, and MBAP brines, while the specimens exposed to the CMA and NaCl brines, and the specimen exposed to the limewater, do not show any cracking.
- In the CaCl₂, MgCl₂, and MBAP specimens, a similar pattern of blocky birefringent crystals is observed in the cracks and air voids in the deteriorated regions. The crystals have the same

birefringence colors as calcium hydroxide, $\text{Ca}(\text{OH})_2$, but their blocky appearance departs from the usual calcium hydroxide morphology.

- The cement paste in the deteriorated CaCl_2 , MgCl_2 , and MBAP specimens is generally devoid of calcium hydroxide.
- Portland concrete specimens exposed to the NaCl , CMA, and limewater solutions show abundant calcium hydroxide. Secondary calcium hydroxide deposits are present in the air voids of the specimen immersed in limewater, but the shape of these calcium hydroxide crystals, long and thin in cross-section, is the typical morphology for secondary calcium hydroxide.
- For straight portland cement specimens immersed in CaCl_2 and MgCl_2 , cracking was the worst. Cracks are also present in the fly ash concrete specimens, but to a lesser degree. Cracks were even less perceptible cracks in the GGBFS concrete specimens.
- Concrete prepared with GGBFS showed the lowest amount of calcium hydroxide in the non-depleted regions, fly ash concrete next, and straight portland cement showed the highest amount of calcium hydroxide.
- Specimens exposed to the MgCl_2 brine all exhibited fibrous mineral precipitates on the surface and in the air voids and cracks near the surface.
- Neither calcium hydroxide depleted paste nor blocky secondary calcium hydroxide crystals were observed in the silane-sealed specimen.
- For MBAP exposed samples, the only specimen to show signs of severe cracking was the straight portland cement concrete specimen. The same trend noted from the CaCl_2 and MgCl_2 brines of calcium hydroxide depletion, coupled with blocky secondary deposits of calcium hydroxide in air voids and large cracks in the depleted zone, was observed in the straight portland cement, fly ash, and GGBFS specimens exposed to MBAP brine.
- As with the specimens exposed to the MgCl_2 brine, all of the specimens from the MBAP brine exhibited fibrous mineral precipitates on the surface and in the air voids and cracks near the surface.
- Energy dispersive spectroscopy (EDS) analyses were performed on the fibrous minerals near or at the surface of the specimens exposed to MgCl_2 and MBAP. The results show mineral compositions similar to magnesium chloride hydroxide hydrate and brucite, with possible Ca^{2+} substitution for Mg^{2+} and Cl^- substitution for OH^- .
- EDS analyses were also performed on the blocky secondary calcium hydroxide crystals observed by optical microscopy in all of the deteriorated specimens immersed in CaCl_2 , MgCl_2 , and MBAP brines. The results show $\text{Ca}(\text{OH})_2$ with Cl^- substitution for OH^- in the calcium hydroxide. It is suspected that these blocky $\text{Ca}(\text{OH})_2$ deposits are calcium oxychloride phases that have reverted to $\text{Ca}(\text{OH})_2$.
- A close examination of secondary deposits in the specimen immersed in CaCl_2 brine also revealed another bladed crystalline phase that had apparently replaced the blocky secondary crystals, but only near the surface. The results of EDS analyses from the bladed crystals show a composition similar to calcium chloride hydroxide hydrate.

- In freeze-thaw testing, the concrete prisms exposed to $MgCl_2$ and $CaCl_2$ expanded above 0.1%, which is considered by ASTM C666 to represent failure.
- Prisms exposed to NaCl did not expand more than 0.04% for 300 cycles, prisms exposed to $MgCl_2$ and $CaCl_2$ expanded considerably with 0.17 and 0.18% length change respectively.
- Specimens exposed to $MgCl_2$ gained mass during ASTM C666 testing. Those exposed to $CaCl_2$ had the opposite behavior with a recorded loss of mass. The specimens exposed to NaCl showed negligible expansion and mass gain even after 300 cycles.
- For the $MgCl_2$ and $CaCl_2$ specimens, the minimum relative dynamic modulus of elasticity (i.e. 60% of the initial value) was reached after 250 cycles. For NaCl, no detrimental effect on the modulus was found even after 300 cycles of freezing and thawing.
- After determining the durability factor, it is clear that $MgCl_2$ and $CaCl_2$ solutions reduce the concrete's resistance to freezing and thawing when compared with NaCl. The durability factors of 60 for $CaCl_2$ and 51 for $MgCl_2$ show the negative impact of these deicers on the resistance of concrete to freezing and thawing.
- After a year of ponding the surface of the slabs with 22% $CaCl_2$, then subjecting the specimens to freezing and thawing cycles in the presence of 4% $CaCl_2$, the specimen surfaces started to scale gradually up to 50 cycles of exposure. After 50 cycles, the amount of scaled material increased dramatically causing the surface to expose all the coarse aggregate and paste-aggregate debonding was evident.
- Similar scaling tests performed on slabs that were exposed to highly concentrated solutions of NaCl (23% by mass) and then tested with 3% NaCl solution, showed minor evidence of scaling.
- Specimens pretreated with $MgCl_2$ and tested for salt scaling resistance did not scale and their visual rating and behavior was similar to those exposed to NaCl.

Based on the overall project results, the following conclusions are presented:

- Exposure of concrete and mortar to NaCl results in little to no chemical interaction or related distress. NaCl appears to be safe for use as a deicing and anti-icing chemical with respect to possible chemical interaction with concrete. NaCl should still be considered harmful to concrete in terms of its potential to induce corrosion in embedded steel given its demonstrated ability to easily diffuse into concrete more readily than the other deicers tested.
- Exposure of concrete and mortar to $MgCl_2$ and $MgCl_2$ based deicing chemicals results in significant chemical interaction and related distress. $MgCl_2$ appears not to be safe for use as a deicing and anti-icing chemical with respect to possible chemical damage to concrete.
- Exposure of concrete and mortar to $CaCl_2$ and $CaCl_2$ based deicing chemicals results in significant chemical interaction and related distress. $CaCl_2$ appears not to be safe for use as a deicing and anti-icing chemical with respect to possible damage to concrete.
- In all cases, the observed distress is less as the concentration of deicer is reduced. Therefore, if $MgCl_2$ and $CaCl_2$ based deicing chemicals are to be used, they should be used at the lowest possible concentration.
- The pessimum concentration for $MgCl_2$ and $CaCl_2$ based deicing chemicals are 20% and 22% by weight $MgCl_2$ and $CaCl_2$, respectively.

- It is not conclusive if CMA is detrimental to concrete or mortar.
- Results were mixed regarding the effect of w/c on performance of concrete and mortars exposed to deicing chemicals. Although the general parameters (i.e. sorptivity, bulk diffusion, rapid chloride permeability) improved with decreasing w/c as expected, the performance in low temperature immersion was the opposite as expected. That is, the low w/c mixtures performed worse.
- In general, concrete mixtures containing GGBFS showed the lowest susceptibility to deicing chemicals, concrete mixtures containing fly ash were next best, and straight portland cement mixtures were the worst performing. One exception is that with the tests performed, concrete mixtures containing fly ash had a diffusion coefficient higher than that measured for straight portland cement mixtures. However, in other experiments such as the low temperature immersion concrete mixtures containing fly ash performed better.
- In general sealants were very effective at reducing chloride ingress at 60 days. The siloxane appeared to perform better than the silane. At 500 days, both sealants lost effectiveness.

SECTION 9. RECOMMENDATIONS

SHA's should plan that the use of any deicing chemical will negatively impact the durability of concrete pavements and bridges. The mechanisms of attack differ; NaCl being known to readily induce corrosion of steel embedded in concrete, MgCl₂ and CaCl₂ have been shown to attack the hardened cement paste, and CMA appears to potentially be harmful to concrete through dissolution of the hardened cement paste.

SHAs should adopt a strategy of preparing durable concrete mixtures that resist penetration of deicing chemicals. To accomplish this the following recommendations are made:

- Include supplementary cementitious materials (SCMs) to decrease permeability, particularly include the use of GGBFS whenever possible. Fly ash is also useful for reducing permeability. SCMs also consume calcium hydroxide through the pozzolanic reaction thereby limiting the formation of oxychloride.
- Use durable aggregates that are not reactive or susceptible to freeze-thaw.
- Establish an air-void system targeted to the severity of the environmental exposure.

Likewise, SHAs should construct well-consolidated concrete free of plastic shrinkage cracks (and other early-age cracking) and without surficial defects. To accomplish this the following recommendations are made:

- Avoid construction under extreme weather conditions.
- Perform adequate consolidation to remove entrapped air.
- Use corrosion-resistant dowel bars or tie bars at joints and cracks.
- Ensure reinforcing steel has adequate concrete cover (2.5 inches [63.5 mm] minimum suggested).
- Ensure bleed water has disappeared before finishing, and avoid overworking surface.
- Provide adequate curing using an effective curing compound. Make sure that the proper amount is uniformly applied to the surface.
- Employ a 30-day "drying period" before applying deicing chemicals to new concrete.

SHAs should adopt maintenance strategies that minimize the deleterious effects of deicing chemicals on in-service concrete structures. Steps to accomplish this goal include:

- Reduce application of deicing chemicals and maximize effectiveness of each deicing application.
- Use deicing chemicals at the lowest possible concentration levels and preferably less than the pessimum amount reported in this research (i.e. 20% for MgCl₂ and 22% for CaCl₂).
- Consider increased use of sodium chloride brines wherever possible.
- Consider surface sealers (particularly the use of siloxanes or possibly silanes) at areas of heavy deicing applications to reduce ingress of chemicals.

SHAs should consider future research regarding the effects of deicing chemicals on concrete. Focus areas for future research include the following:

- To better understand the life cycle cost impact of deicing strategies, a controlled test environment is needed, which could be a dedicated test pavement or a portion of an in-service pavement. Multiple sections should be adopted so that different deicers could be tested. The sections should be newly placed concrete, not existing sections that have already been exposed to deicers, and whose construction history is well documented. The amount and type of deicer used on each section, along with detailed records of weather events, including ice/snow accumulation, should be recorded. Periodically, the concrete sections should be sampled and examined petrographically to determine the effects of the deicers on the concrete over time. Having the above information obtained in a controlled environment would allow for accurate determination of the effects of the maintenance strategies used. Additionally, sealants could be tested on the same sections and their effectiveness monitored to help establish the necessary cycle of replacing those sealants.
- In-service pavements should be examined by coring in the wintertime to facilitate identification of the oxychloride phases in field concrete. This information would be useful to unequivocally confirm the applicability of the laboratory observations reported here.
- Additional testing of CMA is required to determine long term impacts of this deicing chemical given that results from this research were mixed.
- Further testing should be performed to determine the effect of different replacement levels of SCMs on the resistance of concrete to deicers.
- The results of this study indicate that reducing the w/c of a concrete mixture does not improve resistance to deicer attack and in fact reducing the w/c appeared to make concrete mixtures more susceptible to deicer attack. This aspect needs further study as this observation is contrary to accepted practice.
- New approaches to freezing point depression of NaCl brines, or altogether new deicing chemicals, should be investigated to allow for use of these brines at lower temperatures.

SECTION 10. BIBLIOGRAPHY

- ACI (1989). *Corrosion of Metals in Concrete*. ACI Manual Practice ACI 222R-89. American Concrete Institute. Farmington Hills, Michigan.
- ACI (1992a). *Guide to Making a Condition Survey of Concrete in Service*. ACI Manual of Concrete Practice. Part 1. ACI 201.1R-92. ISSN 0065-7875. American Concrete Institute. Farmington Hills, Michigan.
- ACI (1992b). *Guide to Durable Concrete*. ACI Manual of Concrete Practice. Part 1. ACI 201.2R-92. ISSN 0065-7875. American Concrete Institute. Farmington Hills, Michigan.
- ACPA (1992). *Scale-Resistance Concrete Pavements*. Concrete. IS117.02P. American Concrete Pavement Association. Skokie, IL.
- Altmaier, M., Metz, V., Neck, V., Muller, R., & Ganghanel, T.H. (2003). *Solid-Liquid Equilibria of $Mg(OH)_2(cr)$ and $Mg(OH)_3Cl \cdot 4H_2O(cr)$ in the System $Mg-Na-H-OH-Cl-H_2O$ at 25°C*. Geochimica et Cosmochimica Acta, Vol. 64(19), pp. 3595-3601.
- Andrade, C. (1993). *Calculation of Chloride Diffusion Coefficients in Concrete from Ionic Migration Measurements*. Cement and Concrete Research, Vol. 23, pp. 724-742.
- Arya, C., Burnfeld, M.R., & Newman, J.B. (1990). *Factors Influencing Chloride-Binding in Concrete*. Cement and Concrete Research, Vol. 20, pp. 291-300.
- Barnes, P., Fentiman, C.H., & Jeffery, J.W. (1980). *Structurally Related Dicalcium Silicate Phases*. Acta Crystallographica, Section A, **36**, pp. 353-356.
- Basheer, P. A. M., Long, A. E., & Montgomery, F.R. (1994). *An Interaction Model for Causes of Deterioration and Permeability of Concrete*. Concrete Technology Past, Present, and Future. V. M. Mohan Malhotra Symposium. ACI. SP-144. American Concrete Institute, Farmington Hills, MI. pp. 213-231.
- Beaudoin, J.J., Catinaud, S., & Marchand, J., (2001). *Volume Stability of Calcium Hydroxide in Aggressive Solutions*. Cement and Concrete Research, Vol. 31, pp. 149-151.
- Beaudoin, J.J., Ramachandran, V.S., & Feldman, R.F. (1990). *Interaction of Chloride and C-S-H*. Cement and Concrete Research, Vol. 20, pp. 875-883.
- Bentz, D.P. (2000) *Influence of Silica Fume on Diffusivity in Cement-Based Materials II: Multi-Scale Modeling of Concrete Diffusivity*. Cement and Concrete Research, Vol. 30, pp.1121-1129.
- Berntsson, L., & Chandra, S. (1982). *Damage by Concrete Sleepers by Calcium Chloride*. Cement and Concrete Research, Vol. 12, pp. 87-92.
- Bilodeau, A., Carette, G. G., Malhotra, V. M., & Langley, W. S. (1991). *Influence of Curing and Drying on Salt Scaling Resistance of Fly Ash Concrete*. Durability of Concrete. Second International Conference, Montreal, Canada. Volume I. ACI. SP-126. pp. 201-228.

- Bilodeau, A., & Malhotra, V. M. (1992). *Concrete Incorporating High Volumes of ASTM Class F Fly Ashes: Mechanical Properties and Resistance to Deicing Salt Scaling and to Chloride-Ion Penetration*. Fly Ash, Silica Fume, and Natural Pozzolans in Concrete. V.M. Malhotra, Ed. Proceedings, Fourth International Conference. ACI SP-132. pp. 319-349.
- Birnin-Yauri, U.A., & Glasser, F.P. (1998). *Friedel's Salt $Ca_2Al(OH)_6(Cl,OH).2H_2O$: Its Solid Solutions and their Role in Chloride Binding*. Cement and Concrete Research, Vol. 28(2), pp. 1713-1723.
- Bleszynski, R.F., Hooton, R.D., Thomas, M.D.A., & Rogers, C.A. (2002). *Investigations into the Durability of Ternary Blend Concrete Laboratory and Outdoor Exposure Site Studies*. TRB 2002 Annual Meeting CD-ROM. Transportation Research Board. Washington, D.C.
- Bonen, D. & Sarkar, S.L. (1994), *Environmental attack on concrete*. Proceedings of the 16th International Conference on Cement Microscopy. Gouda, G.R., Nisperos, A, & Bayles, J., Eds International Cement Microscopy Association, Texas, pp. 11-23.
- Boulfiza, M., Sakai, K., Banthia, N., & Yoshida, H. (2003). *Prediction of Chloride Ions Ingress In Uncracked and Cracked Concrete*. ACI Materials Journal, Vol. 100, No. 1, pp. 38-48.
- Brew, D.R.M., & Glasser, F.P. (2005). *Synthesis and Characterization of Magnesium Silicate Hydrate Gels*. Cement and Concrete Research, Vol. 35, pp. 85-98.
- Brown, P.W., & Doerr, A. (2000). *Chemical Changes in Concrete due to the Ingress of Aggressive Species*. Cement and Concrete Research, Vol. 30, pp. 411-418.
- Brown, P.W., & Clifton, J.R. (1988). *Mechanisms of Deterioration in Cement-Based Materials and in Lime Mortar*. Durability of Building Materials, Vol. 5(3&4), pp. 409-420.
- Buck, A. D. (1985a). *A Discussion of the Paper "The Penetration of Chlorides into Hardened Cement Pastes" by H.D. Midgley and J. M. Illston*. Cement and Concrete Research. Vol. 15, No. 5, pp. 933-934.
- Butler, W. B. (1982). *A Critical Look at ASTM C 618 and C 311*. Cement, Concrete, and Aggregates, Vol. 4, No. 2, ASTM, Winter, pp. 68-72.
- Byfors, K. (1987). *Influence of Silica Fume and Fly Ash on Chloride Diffusion and pH Values in Cement Paste*. Cement and Concrete Research, Vol. 17, No. 1, pp. 115-129.
- Carde, C., & Francois, R. (1997). *Effect of the Leaching of Calcium Hydroxide from Cement Paste on Mechanical and Physical Properties*. Cement and Concrete Research, Vol. 27(4), pp. 539-550.
- Carde, C., Francois, R., & Torrenti, J. M. (1996). *Leaching of both Calcium Hydroxide and C-S-H from Cement Paste: Modeling the Mechanical Behavior*. Cement and Concrete Research, Vol. 26(8), pp. 1257-1268.
- Carde, C., & Francois, R. (1999). *Modelling the Loss of Strength and Porosity Increase due to the Leaching of Cement Pastes*. Cement and Concrete Composite, Vol. 21, pp. 181-188.
- Chatterji, S., & Thaulow, N. (1997). *Unambiguous Demonstration of Destructive Crystal Growth Pressure*. Cement and Concrete Research, Vol. 27(6), pp. 811-816.
- Chatterji, S. (1979). *The Role of $Ca(OH)_2$ in the Breakdown of Portland Cement Concrete Due to Alkali-Silica Reaction*. Cement and Concrete Research, Vol. 9, pp. 185-188.
- Chatterji, S. (1994). *A Discussion of the Paper "The Effectiveness of Supplementary Cementing Materials in Suppressing Expansion Due to ASR. Part I. Concrete Expansion and Portlandite Depletion"*. Cement and Concrete Research, Vol. 24, pp. 1572-1573.

- Chatterji, S. (1994). *Transportation of Ions Through Cement Based Materials. Part 2: Adaptation of the Fundamental Equations and Relevant Comments*. Cement and Concrete Research, Vol. 24, No. 6, pp. 1010-1014.
- Chatterji, S. (1994). *Transportation of Ions Through Cement Based Materials. Part 3: Experimental Evidence for the Basic Equations and Some Important Deductions*. Cement and Concrete Research, Vol. 24, No. 7, pp. 1229-1236.
- Chen, J.J., Thomas, J.J., & Jennings, H.M. (2006). *Decalcification Shrinkage of Cement Paste*. Cement and Concrete Research, Vol. 36, pp. 801-809.
- Cody, R.D., Spry, P.G., Cody, A.M., & Gan, G. (1994). *The Role of Magnesium in Concrete Deterioration*. Final Report for Iowa DOT HR-355. Iowa Highway Research Board. Ames, IA. November. pp. 171.
- Cody, R.D., Cody, A.M., Spry, P.G., & Gan G. (1996). *Experimental Deterioration of Highway Concrete by Chloride Deicing Salts*. Environmental and Engineering Geoscience, Volume II, No. 4, Winter, pp. 575-588.
- Collepari, M., Marcialis, A., & Turriziani, R. (1972). *Penetration of Chloride Ions into Cement Pastes and Concretes*. JACS, Vol. 55(1), pp. 534-535.
- Collepari, M., Coppola, L., & Pistolesi, C. (1994). *Durability of Concrete Structures Exposed to CaCl₂ Based Deicing Salts*. Durability of Concrete, ACI SP-145. V.M. Malhotra, Ed., Third International Conference, Nice, France. pp. 107-120.
- Colville, A.A., & Geller, S. (1971). *The Crystal Structure of Brownmillerite, Ca₂FeAlO₅*. Acta Crystallographica, Section B, **27**, pp. 2311-2315.
- Colville, A.A., & Geller, S. (1972). *Crystal Structures of Ca₂Fe_{1.43}Al_{0.57}O₅ and Ca₂Fe_{1.28}Al_{0.72}O₅*. Acta Crystallographica, Section B, **28**, pp. 3196-3200.
- Costa, A., & Appleton, J. (1999). *Chloride Penetration Into Concrete in Marine Environment. Part II: Prediction of Long Term Chloride Penetration*. Materials and Structures, Vol. 32, pp. 354-359.
- Crumpton, C. F., Smith, B. J., & Jayaprakash, G. P. (1989). *Salt Weathering of Limestone Aggregate and Concrete Without Freeze-Thaw*. Transportation Research Record 1250. Transportation Research Board. pp. 8-16.
- Day, R.L (1992) *The Effects of Secondary Ettringite Formation on Durability of Concrete: A Literature Analysis*. PCA Research and Development Bulletin RD108T, pp. 1-115.
- De Castellar, M.D., Lorente, J.C., Traveria, A., & Tura, J.M. (1996). *Cracks in Sorel's Cement Polishing Bricks as a Result of Magnesium Oxychloride Carbonation*. Cement and Concrete Research, Vol. 26(8), pp. 1199-1202.
- Dehua, D., & Chuanmei, Z. (1996). *The Effect of Aluminate Minerals on the Phases in Magnesium Oxychloride Cement*. Cement and Concrete Research, Vol. 26(8), pp. 1203-1211.
- Dehua, D., & Chuanmei, Z. (1999). *The Formation Mechanism of the Hydrate Phases in Magnesium Oxychloride Cement*. Cement and Concrete Research, Vol. 29, pp. 1365-1371.
- Delagrave, A., Pigeon, M., & Revertegat, E. (1994). *Influence of Chloride Ions and pH Level on the Durability of High Performance Cement Pastes*. Cement and Concrete Research, Vol. 24(8), pp. 1433-1443.
- Delagrave, A., Pigeon, M., Marchand, J., & Revertegat, E. (1996). *Influence of Chloride Ions and pH Level on the Durability of High Performance Cement Pastes (Part II)*. Cement and Concrete Research, Vol. 26(5), pp. 749-760.

- Delagrave, A., Gerard, B., & Marchand, J. (1997). *Modelling the Calcium Leaching Mechanisms in Hydrated Cement Pastes. Mechanism of Chemical Degradation of Cement-Based System*, K.L. Scrivener and J.F. Young Eds., E&FN Spon. London, UK, pp. 38-49.
- Deng, D. (2003). *The Mechanism for Soluble Phosphates to Improve the Water Resistance of Magnesium Oxychloride Cement*. Cement and Concrete Research, Vol. 33, pp. 1311-1317.
- Detwiler, R. J., Fapohunda, C. A., & Natale, J. (1994). *Use of Supplementary Cementing Materials to Increase the Resistance to Chloride Penetration of Concretes Cured at Elevated Temperatures*. ACI Materials Journal, Vol. 91, No. 1, January-February, pp. 63-66.
- Dorsey, N. E. (1940). Properties of Ordinary Water Substance, Reinhold Publishing Corp., New York, N.Y.
- Dow Chemical Company (1999). The Very Short Course, Dow Chemical Company. Midland, MI.
- Dubberke, W., & Marks, V.J. (1985). *The Effects of Deicing Salts on Aggregate Durability*. Transportation Research Record, [1031] (Geotechnical Engineering Research), pp. 27-34.
- Elsen, J., Lens, N. Aarre, T., Quenard, D., & Smolej, V (1995). *Determination of the w/c Ratio of Hardened Cement Paste and Concrete Samples on Thin Sections Using Automated Image Analysis Techniques*. Cement and Concrete Research, Vol. 25, No. 4, pp. 827-834.
- Feldman, R.F., & Ramachandran, V.S. (1980). *New Accelerated Methods for Predicting Durability of Cementitious Materials*. ASTM STP 691 - Durability of Building Materials. pp. 313-325.
- Feldman, R. F., Chan, G. W., Brousseau, R. J., & Tumidajski, P. J. (1994). *Investigation of the Rapid Chloride Permeability Test*. ACI Materials Journal. Vol. 91. No. 2. May-June. pp. 246-255.
- Frigione, G., & Sersale, R. (1989). *The Action of Some Aggressive Solutions on Portland, Pozzolanic and Blast-furnace Slag Cement Mortars*. Cement and Concrete Research, Vol. 19, pp. 885-893.
- Ftikos, C., & Parissakis, G. (1985). *The Combined Action of Mg^{2+} and Cl^- Ions in Cement Pastes*. Cement and Concrete Research, Vol. 15, No. 4, pp. 593-599.
- Gagne, R., Pigeon, M., Revertegat, E., & Aitcin, P.C. (1992). *Chloride Ions in Cement pastes: Influence of the Cement Type and Long Time Effect of the Concentration of Chlorides*. Cement and Concrete Research, Vol. 22, No. 2-3, pp. 451-457.
- Gebler, S. H., & Klieger, P. (1986). *Effect of Fly Ash on the Durability of Air-Entrained Concrete*. Research and Development Bulletin RD090.01T, Portland Cement Association, Skokie, IL.
- Gegout, P., Revertegat, E., & Moine, G. (1992). *Chloride Ion Attack on Low Water-Cement Ratio pastes Containing Silica Fume*. ACI SP-132. V. Malhotra Ed., pp. 1471-1490.
- Gerard, B., & Marchand, J. (2000). *Influence of cracking on the diffusion properties of cement-based materials Part I: Influence of continuous cracks on the steady-state regime*. Cement and Concrete Research, Vol. 30, pp. 37-43.
- Gerold B. T. (2000). Estimation of water-cement ratios using fluorescent petrography and extreme value distributions, (Master of Science Thesis, Michigan Technological University, 1996).
- Ghafoori, N., & Mathis, R. P. (1997). *Scaling Resistance of Concrete Paving Block Surface Exposed to Deicing Chemicals*. ACI Materials Journal, Vol. 94, No. 1, January-February, pp. 32-38.
- Gilfillan, G. (2000). *Road Safety Benefits of Liquid Anti-Icing Strategies and Agents*. Transportation Research Record No. 1700. Transportation Research Board, Washington, D.C.

- Gilfillan, G. (2001). *Environmental Impacts of New Technology in Winter Maintenance*. Presented at the Fifth Annual Roads, Rails and Environment Workshop. March 13-14, 2001. Revelstoke, BC, Canada.
- Gillott, J. E., & Rogers, C. A. (1994). *Alkali-Aggregate Reaction and Internal Release of Alkalis*. Magazine of Concrete Research, Vol. 46, No. 167, pp. 99-112.
- Girard, R.J., Myers, W., Manchester G.D., & Trimm W.L. (1982). *D-cracking: Pavement Design and Construction Variables*. Transportation Research Record, [853] (Concrete Analysis and Deterioration), pp. 1-9.
- Glasser, F.P., Pedersen, J., Goldthorpe, K., & Atkins, M. (2005). *Solubility Reactions of cement Components with NaCl Solutions: I. Ca(OH)₂ and C-S-H*. Advance in Cement Research, Vol. 17(2), pp. 57-64.
- Gowripalan, N., Cabrera, J. G., Cusens, A. R. & Wainwright, P. J. (1993). *Effect of Curing on Durability*. Durable Concrete. ACI Compilation 24. pp. 47-54.
- Gress, D. (1997). *Preventing Early Distress in Concrete Pavements*. Report No. FHWA-SA-97-045. Final Report. Federal Highway Administration. Washington, D.C.
- Grimm, C. T. (1985). *Durability of Brick Masonry: A Review of the Literature*. Masonry: Research, Application, and Problems, ASTM STP 871, J. C. Grogan and J. T. Conway, Eds., American Society for Testing and Materials, Philadelphia, pp. 202-234.
- Guthrie, G. G. Jr., & Carey, J. W. (1997). *A Simple Environmentally Friendly, and Chemically Specific Method for the Identification and Evaluation of the Alkali-Silica Reaction*. Cement and Concrete Research, Vol. 27, No. 9, pp. 1407-1417.
- Haga, K., Shibata, M., Hironaga, M., Tanaka, S., & Nagasaki, S. (2005) *Change in Pore Structure and Composition of Hardened Cement Paste during the Process of Dissolution*. Cement and Concrete Research, Vol. 35, pp. 943-950.
- Haga, K., Shibata, M., Hironaga, M., Tanaka, S., & Nagasaki, S. (2005) *Effect of Porosity on Leaching of Ca from Hardened Ordinary Portland Cement Paste*. Cement and Concrete Research, Vol. 35, pp. 1764-1775.
- Halamickova, P., Detwiler, R.J., Bentz, D.P., & Garboczi, E.J. (1995) *Water Permeability and Chloride Ion Diffusion in Portland Cement Mortars: Relationship to Sand Content and Critical Pore Diameter*. Cement and Concrete Research, Vol. 25, pp. 790-802.
- Hanke, H. (1998). *New Experiences with the Use of Abrasives in Germany*. Proceedings from the Xth PIARC International Winter Road Congress, Vol. 2, March 1998. Lulea, Sweden, pp. 469-475.
- Hansen, W. C. (1963). *Crystal Growth as a Source of Expansion in Portland-Cement Concrete*. Proceedings, American Society for Testing and Materials, Vol. 63, pp. 932-945.
- Hansson, C.M., & Laurent, A. (2000). *Magnesium Chloride De-Icing Salt*. Minutes of Meeting TAC Spring 2002, pp. 13-14.
- Harnik, A. B., Meier, U., & Šli, A. R. (1980). *Combined Influence of Freezing and Deicing Salt on Concrete - Physical Aspects*. ASTM STP 691. American Society for Testing and Materials. pp. 474-484.
- Hauer, J., Berger, G., Feige, J.M., Feige, D., Reimer, C., & Romness, R. (1995). *Snow and Ice Control: A Best Practices Review*. Office of the Legislative Auditor, State of Minnesota, May 1995.

- Helmy, I.M., Amer, A.A., & El-Didamony, H. (1991). *Chemical Attack on Hardened Pastes of Blended Cements Part I: Attack of Chloride Solutions*. ZKG International, Vol. 44, pp. 46-50.
- Hoffman, D.W. (1984). *Changes in Structure and Chemistry of Cement Mortars Stressed by a Sodium Chloride Solution*. Cement and Concrete Research, Vol. 14, No. 1, pp. 49-56.
- Hofmeister, W., & Von Platen, H. (1992). *Crystal Chemistry and Atomic Order in Brucite-Related Double-Layer Structures*. Crystallography Reviews, Vol. 3, pp. 3-29.
- Jakobsen, U. H., Johansen, V., & Thaulow, N. (1995). *Estimating the capillary porosity of cement paste by fluorescence microscopy and image analysis*. Materials Research Society Symposium Proceedings, vol. 370, pp. 227-236.
- Jakobsen, U. H., Johansen, V., & Thaulow, N. (1997). *Optical microscopy - A primary tool in concrete examination*. Proceedings of the 19th International Conference on Cement Microscopy, pp. 275-286, 1997.
- Jang, J., & Iwasaki, I. (1993). *Effect of Salt Additives on Concrete Degradation*. Report No. MN/RD-93/10. Minnesota Department of Transportation, St. Paul, MN.
- Jeffery, J.W. (1952). *The Crystal Structure of Tricalcium Silicate*. Acta Crystallographica, 5, pp. 26-35.
- Kaufmann, J. (2000). *Experimental Identification of Damage Mechanisms in Cementitious Porous Materials on Phase Transition of Pore Solution Under Frost Deicing Salt Attack*. EMPA (Swiss Federal Laboratories for Materials Testing and Research) Publication 248, pp. 7-177.
- Ketcham, S.A., Minsk, L.D., Blackburn, R.R., & Fleege, E.J. (1996). *Manual of Practice for an Effective Anti-icing Program: A Guide for Highway Winter Maintenance Personnel*. Federal Highway Administration, Washington, D.C.
- Klieger, P., & Gebler, S. (1987). *Fly Ash and Concrete Durability*. Concrete Durability. ACI. SP-100-56, pp.1043-1069.
- Kosmatka, S. H., Kerkhoff, B., & Panarese, W.C. (2002). *Design and Control of Concrete Mixtures*. Fourteenth Edition. Engineering Bulletin 001. Portland Cement Association, Skokie, IL. p. 358.
- Kuemmel, D., & Bari, Q. (1996). *Benefit/Cost Comparisons of Salt Only Vs. Salt/Abrasive Mixtures Used in Winter Highway Maintenance in the USA*. 4th International Symposium on Snow Removal and Ice Control Technology, Reno, Nevada, August 1996.
- Kurdowski, W., Trybalska, B., & Duszak, S. (1995). *SEM Studies of Corrosion of Cement Paste in Chloride Solution*. Proceedings of the 16th International Conference on Cement Microscopy, Gouda, G.R., Nisperos, A, & Bayles, J., Eds. International Cement Microscopy Association, Texas. pp. 80-89.
- Lambert, P., Page, C.L., & Short, N.R. (1984). *Diffusion of Chloride Ions in hardened Cement Pastes Containing Pure Cement Minerals*. British Ceramic Proceedings N.35 - The Chemistry and Chemically-Related Properties of Cement, Glasser, F.P. Ed., BCP No.35, pp. 267-276.
- Lambert, P., Page, C.L., & Short, N.R. (1985) *Pore Solution of the Hydrated System Tricalcium Silicate/Sodium Chloride/Water*. Cement and Concrete Research, Vol. 15, pp. 675-680.
- Lamond, J. F. (1983). *Twenty-Five Years' Experience Using Fly Ash Concrete*. Fly Ash, Silica Fume, Slag & Other Mineral By-Products in Concrete, Volume I. ACI, SP-79. pp. 47-69.
- Lee, H., Cody, R.D., Cody, A.M., & Spry, P.G. (1998). *PCC Pavement Deterioration and Expansive Mineral Growth*. Transportation Conference Proceedings, pp. 71-75.

- Lee, H., Cody, R.D., Cody, A.M., & Spry, P.G. (2000). *Effects of Various Deicing Chemicals on Pavement Concrete Deterioration*. Mid-Continent Transportation Symposium Proceedings, pp. 151-155.
- Li, G., Yu, Y., Li, J., Wang, Y., & Liu, H. (2003). *Experimental Study on Urban Refuse / Magnesium Oxychloride Cement Compound Floor Tile*. Cement and Concrete Research, Vol. 33, pp. 1663-1668.
- Litvan, G.G. (1975). *Phase Transitions Of Adsorbates: VI, Effect Of Deicing Agents On The Freezing Of Cement Paste*. Journal of the American Ceramic Society, **58**(1-2), p. 26-30.
- Lu, X. (1997). *Application of the Nernst-Einstein Equation to Concrete*. Cement and Concrete Research, Vol. 27, No. 2, pp. 293-302.
- Malek, R. I. A., & Roy, D. M. (1988). *The Permeability of Chloride Ions in Fly Ash-Cement Pastes, Mortars and Concrete*. Material Research Society Symposium Proceedings: Volume 114. Materials Research Society, pp. 325-335.
- Malhotra, V. M., Carette, G. C., Bilodeau, A., & Sivasundaram, V. (1991). *Some Aspects of Durability of High-Volume ASTM Class F (Low Calcium) Fly Ash Concrete*. Durability of Concrete. Second International Conference, Montreal, Canada. Volume I. ACI. SP-126. pp. 65-82.
- Mangat, P.S., Gurusamy, & Kribanandan (1987). *Chloride Diffusion in Steel Fibre Reinforced Marine Concrete*. Cement and Concrete Research, Vol. 17, pp. 385-396.
- Marchand, J., Sellevold, E. J., & Pigeon, M. (1994). *The Deicer Salt Scaling Deterioration of Concrete - An Overview*. Durability of Concrete, ACI SP-145. V. M. Malhotra, Ed., Third International Conference, Nice, France. pp. 1-46.
- Mayfield, B. (1990). *The quantitative evaluation of the water/cement ratio using fluorescence microscopy*. Magazine of Concrete Research, Vol. 42, No. 150, pp. 227-236.
- Mehta, P.K., & Monteiro, P.J.M. (2006). Concrete: Microstructure, Properties, and Materials, Third Edition. 2006: McGraw-Hill Companies, Inc.
- McCrum, R.L. (1989). *Calcium Magnesium Acetate and Sodium Chloride as Highway Deicing Salts*. Environmental Treatment & Control, MP Dec. 1989, pp. 24-28.
- McDonald, D.B., & Perenchio, W.F. (1997). *Effects of Salt Type on Concrete Scaling*. Concrete International, pp. 23-26.
- Mehta, P. K. (1991). *Durability of Concrete - Fifty Years of Progress?* Durability of Concrete. Second International Conference, Montreal, Canada. Volume I. ACI. SP-126. pp. 1-31.
- Mehta, P. K., & Monteiro, P.J.M. (1993). Concrete: Structure, Properties, and Materials. Second Edition. Prentice Hall. Englewoods Cliffs, NJ.
- Mehta, P. K. (1997). *Durability—Critical Issues for the Future*. Concrete International. Volume 19, No. 7, July, pp. 27-33.
- Meier, U.G., & Harnik, A.B. (1978) *Freezing of Water in Cement Paste with Coatings to Prevent Evaporation*. Cement and Concrete Research, Vol. 8, No. 5, pp. 545-551.
- Midgley, H.G., & Illston, J.M. (1984). *The Penetration of Chlorides into Hardened Cement Pastes*. Cement and Concrete Research, Vol. 14, pp. 546-558.
- Mindess, S., & Young, J.F. (1981). Concrete. Englewood Cliffs, N.J.: Prentice-Hall, Inc.
- Mindess, S., Young, J., & Darwin, D. (2003). Concrete, 2nd ed., Pearson Education, Inc., NY.
- Minsk, L.D. (1998). Snow and Ice Control Manual for Transportation Facilities. McGraw Hill.

- Misra, S., Yamamoto, A., Tsutsumi, T., & Motohashi, K. (1994). *Application of Rapid Chloride Permeability Test to Quality Control of Concrete*. Durability of Concrete, ACI SP-145. V. M. Malhotra, Ed., Third International Conference, Nice, France. pp. 487-502.
- Mobasher, B., & Mitchell, T.M. (1988). *Laboratory Experience with the Rapid Chloride Permeability Test*. Permeability of Concrete, ACI. SP-108. pp. 117-143.
- Mondal, P., & Jeffery, J.W. (1975). *The Crystal Structure of Tricalcium Aluminate, $Ca_3Al_2O_6$* . Acta Crystallographica, Section B, **31**, pp. 689-696.
- Monosi, S., & Collepardi, M. (1993). *Chemical Attack of Magnesium Chloride on the Portland Cement Paste*. IL Cemento, Vol. 90(3), pp. 169-173.
- Monosi, S., & Collepardi, M. (1990). *Research on $3CaO \cdot CaCl_2 \cdot 15H_2O$ Identified in Concrete Damage by $CaCl_2$ Attack*. IL Cemento, Vol. 87, pp. 3-8.
- Moukwa, M. (1990). *The Attack of Cement Paste by $MgSO_4$ and $MgCl_2$ from the Pore Structure Measurements*. Cement and Concrete Research, Vol. 20, pp. 148-158.
- Mu, Ru, Miao, Changwen, Luo, Xin, Sun, & Wei (2002). *Interaction Between Loading, Freeze-Thaw Cycles, and Chloride Salt Attack of Concrete With and Without Steel Fiber Reinforcement*. Cement and Concrete Research, Vol. 32, pp. 1061-1066.
- Muethel, R. W. (1997). *Investigation of Calcium Hydroxide Depletion as a Cause of Concrete Pavement Deterioration*. Research Report R-1353. Michigan Department of Transportation, Materials and Technology Division. November.
- Munoz, S. R., & Chou, E. Y. J. (1994). *Durability of Concrete Materials Under Pavement Joints. Infrastructure: New Materials and Methods of Repair — Proceedings of the Third Materials Engineering Conference*. ASCE, San Diego, CA, Nov 13-16. pp. 1-7.
- Nagesh M., & Bhattacharjee, B. (1998). *Modeling of Chloride Diffusion in Concrete and Determination of Diffusion Coefficients*. ACI Materials Journal, Vol. 95, No. 2, pp. 113-120.
- Neville, A. M. (1996). Properties of Concrete. John Wiley and Sons, Inc., New York, New York.
- Neville, A. M. (1997). *Suggestions of Research Areas Likely to Improve Concrete*. Reprint for Transportation Research Board Forum on January 12, 1997.
- Newton, C.J., & Sykes, J.M. (1987). *The Effect of Salt Additions on the Alkalinity of $Ca(OH)_2$ Solutions*. Cement and Concrete Research, Vol. 17, pp. 765-776.
- Nixon, P., & Page, C. (1987). *Pore Solution Chemistry and Alkali Aggregate Reaction*. Concrete Durability. J.M. Scanlon, Ed. Katherine and Bryant Mather International Conference. ACI SP-100. pp. 1833-1863.
- Nixon, W. A. (2001). *The Use of Abrasives in Winter Maintenance*. Final Report of Project TR 434, Iowa DOT & Iowa Highway Research Board, March 2001.
- Page, C.L., Short, N.R., & El Tarras, A. (1981) *Diffusion of Chloride Ions in Hardened Cement Pastes*. Cement and Concrete Research, Vol. 11, pp. 395-406.
- Papadakis, V.G., Fardis, M.N., & Vayenas, C.G. (1996). *Physicochemical Processes and Mathematical Modeling of Concrete Chlorination*. Chemical Engineering Science, **51**, No. 4, pp. 505-513.
- Pavlik, V. (2000). *Water Extraction of Chloride, Hydroxide and other Ions from Hardened Cement Pastes*. Cement and Concrete Research, Vol. 30, pp. 895-906.

- PCA (1992). Design and Control of Concrete Mixtures. Thirteenth Edition. Portland Cement Association. Skokie, IL.
- Perchanok, M.S., Comfort, G.A., & Dinovitzer, A. (1997). *Winter Sand Application & Stopping Distance on Snow & Ice Covered Highways*. Analysis and Application Paper for 1997 XIIIth IRF World Meeting, Ontario Ministry of Transport, 1997.
- Pereira, C.J., & Hegedus, L.L. (1984). *Diffusion and Reaction of Chloride Ions in Porous Concrete*. Proceedings of the 8th International Symposium of Chemical Reaction Engineering, Edinburgh.
- Perenchio, W. F. (1994). *Corrosion of Reinforcing Steel*. Significance of Tests and Properties of Concrete and Concrete-Making Materials, STP 169C. Publication Code Number 04-169030-07. American Society for Testing and Materials, Philadelphia, PA. pp. 164-172.
- Peterson, O. (1995). *Chemical Effects on Cement Mortar of Calcium Magnesium Acetate as a Deicing Salt*. Cement and Concrete Research, Vol. 25(3), pp. 617-626.
- Pigeon, M. (1994). *Frost Resistance, A Critical Look*. Concrete Technology Past, Present, and Future. V.M. Mohan, Ed. Malhotra Symposium. ACI. SP-144. pp. 141-157.
- Pigeon, M., & R. Plateau (1995). *Durability of Concrete in Cold Climates*. E & FN Spon. ISBN: 0-419-19260-3. p. 244.
- Piltner, R., & Monteiro, P.J.M. (2000) *Stress Analysis of Expansive Reactions in Concrete*. Cement and Concrete Research, Vol. 30, pp. 843-848.
- Powers, T.C., & Helmuth, R.A. (1953). *Theory of Volume Changes in Hardened Portland-Cement Paste during Freezing*. Proceedings of Highway Research Board.
- Powers T.C. (1975). *Freezing Effects in Concrete*. Durability of Concrete. ACI Special Publication SP-47-1. pp. 1-12.
- QCL Group (Australian) (1999). *Sulphate Attack and Chloride Ion Penetration: Their Role in Concrete Durability*. QCL Group Technical Notes, pp. 1-8.
- Ramachandran, V.S. (1976). Calcium Chloride in Concrete. Applied Science Publishers Ltd, London. p. 207.
- Reid Crowther Consulting Inc. (2000). *The Economic Impact of Magnesium Chloride Deicer on Concrete Bridge Decks*. A Study for Montana Department of Transportation, 2000.
- Rezansoff, T., & Scott, D. (1988). *Durability of Concrete Containing Chloride Based Accelerating Admixtures*. Canadian Journal of Civil Engineering, Vol. 17, pp. 102-112.
- Roosevelt, D.S., & Fitch, G.M. (2000). *Evaluation of an Ice Ban Product as a Prewetting Agent for Snow Removal and Ice Control Operations*, VTRC 00-R12, Jan. 2000.
- Rösli, A., & Harnik, A.B. (1980). *Improving the Durability of Concrete to Freezing and Deicing Salts*. Durability of Building Materials and Components, ASTM STP 691, P.J. Serada and G.G. Litvan, Eds., American Society for Testing and Materials, pp. 464-473.
- Roskopf, P.A., Linton, F.J., & Peppler, R.B. (1975). *Effect of Various Accelerating Chemical Admixtures on Setting and Strength Development of Concrete*. Journal of Testing and Evaluation, Vol. 3, No.4, pp. 322-330.
- Roy, D. M., Cady, P. D., Sabol, S. A., & Licastro, P.H. (1993a). *Concrete Microstructure: Recommended Revision to Test Methods*. SHRP-C-339. Strategic Highway Research Program. National Research Council, Washington DC.

- Roy, D. M., & Idorn, G.M. (1993b). *Concrete Microscopy*. SHRP-C-340. Strategic Highway Research Program, Washington, DC.
- Santagata, M.C., & Collepardi, M. (2000). *The Effect of CMA Deicers on Concrete Properties*. Cement and Concrete Research, Vol. 30, pp. 1389-1394.
- Santhanam, M., Cohen, M., & Olek, J. (2003). *Study of Magnesium Ion Attack in Portland Cement Mortars*. Proceedings from the 11th International Congress on The Chemistry of Cement, pp. 1460-1474.
- Scrivener, K.L., & Gartner, E.M. (1988). *Microstructural Gradients in Cement Paste around Aggregate Particles*. Materials Research Society Symposium Proceedings Volume 114- Bonding in Cementitious Composites, S. Mindess and S.P. Shah, Eds., Vol. 114, pp. 77-85.
- Setzer, M.J. (1997). *Action of Frost and Deicing Chemicals-Basic Phenomena and Testing*. Freeze-Thaw Durability of Concrete, J. Marchand, M. Pigeon and M. Zetzer, Eds., E&FN Spon, London, pp. 3-22.
- Shi, C. (2001). *Formation and Stability of $3CaO \cdot CaCl_2 \cdot 12H_2O$* . Cement and Concrete Research, Vol. 31, pp. 1373-1375.
- Snow, Peter G. (2001). *Magnesium Chloride as a Road Deicer: A Critical Review*. Available at <http://www.nrmca.org/engineering/MagChloride/MagchlorideWhitePaper.pdf>. Burns Concrete, Inc., Idaho Falls, Idaho.
- Stanish, K. D., Hooton, R. D., & Thomas, M. D. A. (2000). *Testing the Chloride Penetration Resistance of Concrete: A literature Review*. FHWA Contract DTFH61-97-R-00022, University of Toronto, Toronto, Ontario, Canada.
- Stark, J., & Ludwig, H.M. (1997). *Freeze-Thaw and Freeze-Deicing Salt Resistance of Concrete Containing Cement Rich in Granulated Blast Furnace Slag*. ACI Materials Journal, Vol. 94, No. 1, January-February, pp. 47-55.
- Suryavanshi, A.K., Scantlebury, J.D., & Lyon, S.B. (1996). *Mechanism of Friedel's Salt Formation in Cements Rich in Tri-calcium Aluminate*. Cement and Concrete Research, Vol. 26(5), pp. 717-727.
- Suryavanshi, A.K., & Swamy, R.N. (1996). *Stability of Friedel's Salt in Carbonated Concrete Structural Elements*. Cement and Concrete Research, 1996, Vol. 26(5), pp. 729-741.
- Sutter, L.L., Peterson, K.R., Van Dam, T.J., Smith, K.D., & Wade, M.J. (2001). *Guidelines for Detection, Analysis, and Treatment of Materials-Related Distress in Concrete Pavements, Volume 3: Case Studies Using the Guidelines*. FHWA-RD-01-164, Federal Highway Administration, Turner-Fairbank Highway Research Center, McLean, VA, September, 2001.
- Sutter, L.L., Van Dam, T.J., Peterson, K.R., & Ganguly, A. (2003). *The X-Ray Microscope: A New Tool for Determining Chloride Ion Diffusion in Hardened Concrete*. Proceedings of the Conference on Advances in Cement and Concrete, Copper Mountain, Colorado, August 10-14, 2003.
- Suryavanshi, A.K., Swamy, R.N., & McHugh, S. (1998). *Chloride Penetration Into Reinforced Concrete Slabs*. Canadian Journal of Civil Engineering, Vol. 25, pp. 87-95.
- Taylor, H.F.W., & Gollop, R.S. (1997). *Some Chemical and Microstructural Aspects of Concrete Durability Mechanism of Chemical Degradation of Cement-Based Systems*. Proceedings of the Materials Research Society's Symposium (Boston, 1995), K.L. Scrivener and J.F. Young, Eds., E&FN Spon, London 1997, pp. 177-184.
- Taylor, H.F.W. (1990). Cement Chemistry. Academic Press Ltd., London.

- Theissing, E.M., Hest-Wardenier, P.V., & De Wind, G. (1978). *The Combining of Sodium Chloride and Calcium Chloride by a Number of Different Hardened Cement Pastes*. Cement and Concrete Research, Vol. 8, pp. 683-691.
- Thomas, M.D.A., & Bamforth, P.B. (1999). *Modeling Chloride Diffusion in Concrete, Effect of Fly Ash and Slag*. Cement and Concrete Research, Vol. 29, pp. 487-495.
- Tooper, B., & Cartz, L. (1966). *Structure and Formation of Magnesium Oxychloride Sorel Cements*. Nature, Vol. 211, pp. 64-66.
- Torri, K., & Kawamura, M. (1992). *Pore Structure and Chloride Permeability of Concrete Containing Fly Ash, Blast Furnace Slag and Silica Fume*. Fly Ash, Silica Fume, and Natural Pozzolans in Concrete. V. M. Malhotra, Ed. Proceedings, Fourth International Conference. ACI SP-132. Istanbul, Turkey, May. pp. 135-150.
- Transportation Research Board (TRB) (1999). *Durability of Concrete*. Transportation Research Circular. Transportation Research Board, National Academies of Science, Washington, DC.
- Tritthart, J. (1989). *Chloride Binding in Cement*. Cement and Concrete Research, Vol. 19, pp. 586-594.
- Truc, O., Ollivier, J.P., & Carcasses, M. (2000). *A New Way for Determining the Chloride Diffusion Coefficient in Concrete from Steady State Migration Test*. Cement and Concrete Research, Vol. 30, pp. 217-226.
- Tumidajski, P.J., & Chan, G.W. (1996). *Durability of High Performance Concrete in Magnesium Brine*. Cement and Concrete Research, Vol. 26, No. 4, pp. 557-565.
- Valenza Ii, J.J., & Scherer, G.W. (2005). *Mechanisms of Salt Scaling*. Materials and Structures/Materiaux et Constructions, **38**(278), pp. 479-488.
- Valenza Ii, J.J., & Scherer, G.W. (2006). *Mechanism for salt scaling*. Journal of the American Ceramic Society, **89**(4), pp. 1161-1179.
- Valenza Ii, J.J., & Scherer, G.W. (2007) *A review of salt scaling: I. Phenomenology*. Cement and Concrete Research, Vol. 37, No. 7, pp. 1007-1021.
- Valenza Ii, J.J., & Scherer, G.W. (2007) *A review of salt scaling: II. Mechanisms*. Cement and Concrete Research, Vol. 37, No. 7, pp. 1022-1034.
- Van Dam, T.J., Sutter, L.L., Smith, K.D., Wade, M.J., & Peterson, K.R. (2002a). *Guidelines for Detection, Analysis, and Treatment of Materials-Related Distress in Concrete Pavements, Volume 1: Final Report*. FHWA-RD-01-163. Federal Highway Administration. Turner-Fairbank Highway Research Center, McLean, VA.
- Van Dam, T.J., Sutter, L.L., Smith, K.D., Wade, M.J., & Peterson, K.R. (2002b). *Guidelines For Detection, Analysis, And Treatment Of Materials-Related Distress In Concrete Pavements - Volume 2: Guidelines Description and Use*. FHWA-RD-01-164. Federal Highway Administration. Turner-Fairbank Highway Research Center, McLean, VA. p. 233.
- Walker, H. N., & Marshall, B. F. (1979). *Methods and Equipment Used in Preparing and Examining Fluorescent Ultrathin Sections of Portland Cement Concrete*. Cement, Concrete, and Aggregates, Vol. 1, No. 1, pp. 3-9.
- Walker, H. N. (1980). *Formula for Calculating Spacing Factor for Entrained Air Voids*. Cement, Concrete, and Aggregates, Vol. 2, No. 2, pp. 63-66.

- Whiting, D., Nagi, M., Okamoto, P., Yu, T., Peshkin, D., Smith, K., Darter, M., Clifton, J., & Kaetzel, L. (1994). *Optimization of Highway Concrete Technology*. SHRP-C-373. Strategic Highway Research Program. National Research Council. Washington D.C.
- Williams, D. (2001). Past and Current Practices of Winter Maintenance at the Montana Department of Transportation (MDT). Dec. 2001.
- Winkler, E. M., & Singer, P. C. (1972). *Crystallization Pressure of Salts in Stone and Concrete*. Bull. Geol. Soc. Am., 83 [11] pp. 3509-3514
- Wolff, P.M., & Walter-Levy, M.L. (1953). *The Crystal Structure of $Mg_2(OH)_3(Cl,Br) \cdot 4H_2O$* . Acta Crystallographica, Vol. 6, pp. 40-44.
- Wolter, S. (1997). Ettringite: Cancer of Concrete. American Petrographic Laboratories, St. Paul, MN.
- Worthington, J.C., Bonner, D.G., & Nowell, D.V. (1988). *Influence of Cement Chemistry on Chloride Attack of Concrete*. Materials Science Technology, Vol. 4, pp. 305-313.
- Yehia, S.A., & Tuan, C.Y. (2003). *Conductive Concrete Can Cut Deicing Costs*. Better Roads, pp. 66 to 69.
- Yunping, X., Bazant, Z.P., & Monila, L. (1994). *Moisture Diffusion in Cementitious Materials*. Advanced Cement Based Materials, Vol. 1, pp. 258 to 266.
- Zia, P., Leming, M. L., Ahmad, S. H., Schemmel, J. J., Elliot, R. P., and Naaman, A. E. (1993). *Mechanical Behavior of High Performance Concretes, Volume 1: Summary Report*. SHRP-C-361. Strategic Highway Research Program, National Research Council, Washington DC.